The Study of Tropical Cyclone Characteristics Using Mathematical and Machine Learning Techniques

A THESIS to be Submitted by

Monu

2K21/PHDAM/04

for the award of the degree of

Doctor of Philosophy

in

Mathematics

Under the Supervision of

Prof. Laxminarayan Das

Department of Applied Mathematics

DELHI TECHNOLOGICAL UNIVERSITY

BAWANA ROAD, NEW DELHI-110042 INDIA

December 2024

DECLARATION

I declare that the research work presented in this thesis entitled "**The Study of Tropical Cyclone Characteristics Using Machine Learning Techniques**" for the attainment of the degree of ***Doctor of Philosophy in Mathematics*** has been conducted by me, under the guidance of ***Prof. Laxminarayan Das*** from the Department of Applied Mathematics, Delhi Technological University, Delhi, India. This work has not been previously submitted, either partially or in its entirety, to any other academic institution for any degree or diploma.

I declare that this thesis reflects the ideas I express in my own words. Wherever the ideas or words of others have been incorporated, appropriate citation and referencing have been provided to acknowledge the sources. I also confirm that I have upheld the principles of academic honesty and integrity and that I have not misrepresented, fabricated, or falsified any information, data, fact, or source in the content of my submission.

Mr. Monu

Enrollment No. 2K21/PHDAM/04

Department of Applied Mathematics

Delhi Technological University

CERTIFICATE

This is to certify that the thesis titled **The Study of Tropical Cyclone Characteristics Using Machine Learning Techniques**, submitted by **Mr. Monu**, to the Delhi Technological University, Delhi, for the award of the degree of **Doctor of Philosophy**, is a bonafide record of the research work done by him under our supervision and guidance. The contents of this thesis, in full or in parts, have not been submitted to any other Institute or University for the award of any degree or diploma.

Prof. Laxminarayan Das
Supervisor
Department of Applied Mathematics
Delhi Technological University

Prof. Ramesh Srivastava
Head
Department of Applied Mathematics
Delhi Technological University

New Delhi
December 2024

ACKNOWLEDGEMENTS

Initially and perhaps most significantly, I wish to extend my appreciation to my mentor, Prof. Laxminarayan Das from the Department of Applied Mathematics at Delhi Technological University (DTU), for their consistent encouragement, supportive guidance, and assistance during my research endeavors and for granting me the autonomy to pursue my ideas. Their mentorship has positively influenced my academic pursuits and greatly benefited my personal and professional growth. Undoubtedly, being under their supervision has been a delightful experience for me.

I am sincerely thankful to Prof. Aditya Kaushik (Departmental SRC Expert) and Prof. R. C. Singh (External SRC Expert, Department of Mechanical Engineering) for their invaluable feedback and steady support, which helped shape the course of my research.

My heartfelt thanks also go to Prof. Sangita Kansal (Chairperson, Departmental Research Committee), Prof. Naokant Deo (Ex-Chairperson, DRC, 2022–23), Prof. R. Srivastava (Head of Department), Dr. Satyabrata Adhikari (Ph.D. Co-ordinator), and all the esteemed faculty members of the Department of Applied Mathematics for their suggestions, encouragement, and academic support throughout my doctoral journey.

I wish to acknowledge the invaluable support and camaraderie of Vinita Khatri, Man Singh, Abhay Srivastava, Vriddhi Singh, and Dr. Shashi Kant, whose encouragement and

motivation sustained me throughout this endeavor.

I am also thankful to Dr. Kartikay Khari, Monish, Surya Giri, Yash Pathak, Kunal Madaan, Yogesh, Chandra Prakash, Rajpal Rajbhar, Deepak Kumar, Suresh Kumar Yadav, Rahul Singh, Sanyam Gupta, and all my fellow research scholars in the Department of Applied Mathematics. Your support, collaboration, and uplifting spirit have made this journey memorable.

I thank the DTU administration and academic branch for providing the infrastructure and resources essential for my research. I also deeply appreciate the assistance offered by the Department of Applied Mathematics office staff for their cooperation and timely support.

A special note of thanks to my family: my parents, Mr. Mukesh Kumar Yadav and Mrs. Babita Devi; my brother, Mr. Anuj Yadav; and my sister-in-law, for their endless love, understanding, and encouragement. Their belief in me has been my greatest strength.

I also wish to acknowledge the many individuals who, though not named here, have played a significant part in my doctoral journey through their quiet support, kind words, and encouragement.

Finally, and above all, I sincerely thank God for guiding me through every challenge and blessing me with the strength, clarity, and perseverance needed to complete my doctoral work.

(Mr. Monu)

New Delhi

December 2024

Dedicated

to

My Family

ABSTRACT

According to the 2030 Agenda for Sustainable Development, disaster risk reduction is essential to social and economic development. Storms and floods are among the most impactful natural disasters, contributing significantly to their frequency, the number of affected individuals, and economic losses. Storms and floods in coastal areas are mainly caused by tropical cyclones in tropical and subtropical parts of the globe. Approximately 0.8 million people lost their lives, and a financial loss of US$ 1407.6 billion was caused by tropical cyclones in the last 50 years. The atmospheric and oceanic causative components are multi-dimensional in nature and have a complicated non-linear connection, making any estimation effort linked to tropical cyclones (TCs) difficult. Estimating the TC's radius of maximum wind, intensity, and track is the primary focus of study on tropical cyclones. The majority of the operational models that are now in use are statistical and numerical in nature. The numerical techniques need a lot of work and time. Complex non-linear interactions between several causative elements with geographical and temporal dimensions cannot be captured by statistical approaches because they are too simplistic. Numerous deep-learning research has been published recently that successfully address several kinds of estimation issues related to tropical cyclones.

This research work tries to answer various estimation problems related to a TC. Starting from the radius of maximum wind (RMW) of a TC over the North Indian Ocean, a region with frequent and intense TC activity, the first work proposes a model to estimate the RMW

using historical data and mathematical correlations between the latitude coordinate of the TC center, estimated pressure drop at the center up to 12 hectopascals, and RMW. The accuracy of the approach is determined using statistical metrics, including error percentage, t-test, and root mean square error (RMSE) compared to existing methods. An ensemble machine learning model has been developed, further refining RMW estimation, taking input from existing methods, and targeting the data provided by the India Meteorological Department. In order to address the issue of accurately estimating the track of TC, the second work proposes a neural network method. The neural network takes the result of three traditional methods and targets the data provided by the IMD. It is trained using 56 TCs and tested on 6 TCs from 2014 to 2024. In this work, we didn't use any satellite images. The accuracy of the approach is determined using statistical metrics, including error percentage and RMSE. The third works explore the Satellite Consensus (SATCON) algorithm for estimating TC intensity using infrared and microwave sensor-based images, analyzing the performance for pre-monsoon and post-monsoon TC as well as for intensity-based TC categories. In the fourth work, we develop a neural network model to estimate the intensity of TC. As discussed in the second work, satellite images weren't used; instead, results from three state-of-the-art methods were used as the input, with the targeting of the data provided by the IMD.

The first work is a traditional method for estimating the RMW over the NIO. It achieves a mean absolute error percentage ranging from approximately 6% to 32%, whereas the other studies have a mean absolute error range of 13% to 128% concerning IMD best track data. Following this, our ensemble machine learning model has an RMSE of 10.63 nautical miles and an error percentage of 17.00 %, which are lower than other methods. In the second work, our neural network model achieves an RMSE of 0.14 knots and an error percentage of 0.41%,

lower than the alternative methods. In the third work, we demonstrate that SATCON is more effective in the post-monsoon across the West Pacific basin than in the pre-monsoon. Also, the ability of the algorithm to estimate intensity is determined to be rather excellent for mid-range TCs. In the fourth work, the RMSE of 5.71 knots and an error percentage of 10.07%, lower than existing methods.

List of publications

Journals:

Accepted Papers:

1. **Monu Yadav and Laxminarayan Das** "Analyze the SATCON algorithm's capability to estimate tropical storm intensity across the West Pacific basin", *Journal of Earth System Science*. DOI: 10.1007/s12040-024-02276-5. (**SCIE index, IF: 1.3**).

2. **Monu Yadav and Laxminarayan Das** "Formulation and evaluation of the radius of maximum wind of the tropical cyclones over the North Indian Ocean basin", *Theoretical and Applied Climatology*. DOI: 10.1007/s00704-024-04895-w. (**SCIE index, IF: 2.8**).

3. **Monu Yadav, Laxminarayan Das, and Shashi Kant** "Estimation of Tropical Cyclone's Radius of Maximum Wind using Ensemble Machine Learning Approach", *Journal of Earth System Science*. DOI: 10.1007/s12040-024-02455-4. (**SCIE index, IF: 1.3**).

4. **Monu Yadav and Laxminarayan Das** "Evaluating the intensity of Typhoons over the West Pacific basin", *Physica Scripta*. DOI: 10.1088/1402-4896/adc3d5. (**SCIE index, IF: 2.6**).

5. **Monu Yadav and Laxminarayan Das** "Detecting Tropical Cyclone from the basic overview of life cycle of Extremely Severe Cyclonic Storm, Tauktae", *Revista de Climatología*.

Communicated Papers:

1. **Monu Yadav and Laxminarayan Das** "Hybrid Activation Function-Based Neural Networks for Tropical Cyclone Intensity Estimation Over the North Indian Ocean" (Communicated).

2. **Monu Yadav and Laxminarayan Das** "A Method for Determining the Radius of Maximum Wind over the Western North Pacific Basin" (Communicated).

3. **Monu Yadav and Laxminarayan Das** "Estimating Tropical Cyclone Track with Neural Network Algorithms: A Data-Driven Approach" (Communicated).

4. **Monu Yadav and Laxminarayan Das** "Identification of storm eye from Satellite image data using fuzzy logic with machine learning" (Communicated).

List of conferences

Conference Presentations:

- **Presented** a paper entitled "**Identification of storm eye from Satellite image data using fuzzy logic with machine learning**" in Two Day International Conference on **Recent Trends in Mathematical and Computational Sciences** at Amity University Kolkata, West Bengal (India) during July 28 - 29, 2022.

- **Presented** a paper entitled "**Review of various methods for estimating the intensity of Tropical Cyclone YAAS**" in the International Conference on **Evolution in Pure and Applied Mathematics** organized by Department of Mathematics, Akal University, Talwandi Sabo, Bathinda, Punjab (India) during November 16-18, 2022.

- **Presented** a paper entitled "**Formulation and Evaluation of Radius of Maximum Wind over the North Indian Ocean basin**" in Conference on **Graph Theory and Additive Combinatorics** by the Department of Applied Sciences, IIIT Allahabad (India) during May 03 - 05, 2024.

- **Presented** a paper entitled "**Estimation of tropical cyclone intensity using machine learning technique**" in Third International Conference on **Applied Science Mathematics and Statistics (ICASMS-24)** by Department of Mathematics, Kongunadu College of Engineering and Technology (Autonomous), Trichy (India) on May 17, 2024.

Contents

DELARATION i

CERTIFICATE ii

ACKNOWLEDGEMENTS iii

ABSTRACT vi

List of publications ix

List of conferences xi

List of figures xviii

List of tables xxii

List of Abbreviations xxiii

1 Introduction 1

1.1 Introduction 2

1.2 Tropical Cyclones 4

1.3 Tropical Cyclones: A Global Overview 5

1.4 Physical Parameters favorable for the formation of Tropical cyclones 6

1.5 Life Cycle of Tropical Cyclones 8

1.5.1 Formation 8

1.5.2 Intensification 9

1.5.3 Mature 9

1.5.4 Decay 10

1.6 Naming of Tropical Cyclones 11
1.7 Physical Structure of Tropical Cyclones 11
1.8 Tropical Cyclones as a Natural Hazard 15
1.9 Classification of Tropical Cyclones: 16
1.10 Frequency of Cyclones over the Indian Ocean: 17
1.11 Tropical cyclone Forecast 19
1.12 Previous Research on Tropical Cyclones: 21
1.12.1 Global Research on cyclones: 21
1.12.2 Previous studies on Cyclones over India: 24
1.13 Scope and Outline of the Thesis: 27

2 Tropical Cyclone's Radius of Maximum Wind 30
2.1 Introduction 31
2.2 Literature Review 33
2.2.1 Graham's Empirical Formulation (1959) 33
2.2.2 Vickery's Empirical Formulation I 34
2.2.3 Vickery's Empirical Formulation II 34
2.2.4 Willoughby and Ryan's Empirical Formulation 35
2.2.5 Kato's Empirical Formulation 36
2.2.6 Powell's Empirical Formulation 36
2.2.7 Knaff's Empirical Formulation 37
2.2.8 Li's Empirical Formulation 37
2.2.9 Jiang's Empirical Formulation 38
2.2.10 Lin's Empirical Formulation 38
2.2.11 FEMA's Empirical Formulation 39
2.2.12 Zhou's Empirical Formulation 39
2.3 Data 42
2.4 Method 44
2.4.1 Method I 44
2.4.2 Method II 49
2.5 Result 55
2.5.1 Result of Method I 55

2.5.2 Result of Method II 73
2.6 Conclusion 86

3 Tropical Cyclone's Track 88
3.1 Introduction 89
3.2 Literature Review 92
3.2.1 Averaging across occurrences 92
3.2.2 Statistical forecasting techniques 93
3.2.3 Techniques based on satellite image interpretation 94
3.2.4 Techniques using artificial neural networks 94
3.3 Data and Method 95
3.3.1 Data 95
3.3.2 Method 96
3.4 Discussion of Results 102
3.5 Conclusion 118

4 Analyze the SATCON Algorithm to Estimate the Tropical Cyclone's Intensity 121
4.1 Introduction 122
4.2 Data and Methodology 124
4.3 Results and discussion 128
4.3.1 For entire year, the capability of the "SATCON" algorithm over Japan (West Pacific) 128
4.3.2 Capability of SATCON algorithm in various seasons 135
4.4 Conclusion 139

5 Tropical Cyclone's Intensity 143
5.1 Introduction 144
5.2 Data and Method 148
5.2.1 Data 148
5.2.2 Method 150
5.3 Result 155
5.3.1 SCS Asani 155

5.3.2 CS Sitrang 158
5.3.3 SCS Shaheen 160
5.3.4 ESCS Tej 161
5.3.5 SCS Remal 163
5.3.6 CS Asna 165
5.3.7 CS Dana 169
5.4 Conclusion 169

6 Conclusions, social impact and suggestions for future research 173

References 193

List of Figures

1.1 Economic and human loss caused by natural disasters globally 3

1.2 Economic and human loss caused by natural disasters in Asia 3

1.3 The Physical Structure of Tropical Cyclones with concentric eyewalls . . . 12

1.4 The schematic representation of Tropical Cyclone showing eye, eyewall, and rainbands. 14

1.5 Tropical cyclone trends in the Bay of Bengal and Arabian Sea during 1990 – 2022 18

2.1 Fitted Function vs. Observed Data Points 46

2.2 Flow-Chart of the Proposed Method for Estimating the Radius of Maximum Wind of the Tropical Cyclone 50

2.3 Architecture of Proposed Neural Network for Estimating the Radius of Maximum Wind 52

2.4 Graphical Representation of ESCS Tauktae's value of RMW by proposed method, Willoughby et al., Tan and Fang, and IMD 58

2.5 CS Gulab's value of RMW given by proposed method, Willoughby et al., Tan and Fang, and IMD is graphically represented 59

2.6 SCS Mandous's value of RMW given by proposed method, Willoughby et al., Tan and Fang, and IMD data are graphically represented 62

2.7 SCS Asani's value of RMW given by proposed method, Willoughby et al., Tan and Fang, and IMD is graphically represented 64

2.8 CS Sitrang's value of RMW given by proposed method, Willoughby et al., Tan and Fang, and IMD is graphically represented 67

2.9 CS Jawad's value of RMW given by proposed method, Willoughby et al., Tan and Fang, and IMD is graphically represented 69

2.10 VSCS Yaas's value of RMW given by proposed method, Willoughby et al., Tan and Fang, and IMD is graphically represented 71

2.11 Track of the Selected Tropical Cyclone 74

2.12 Graphical Representation of Mandous Cyclone value of RMW by our method, Yadav and Das, Willoughby et al., Tan and Fang, and IMD 75

2.13 Graphical Representation of Sitrang Cyclone value of RMW by our method, Yadav and Das, Willoughby et al., Tan and Fang, and IMD 79

2.14 Graphical Representation of Mocha Cyclone value of RMW by our method, Yadav and Das, Willoughby et al., Tan and Fang, and IMD 82

2.15 Graphical Representation of Remal Cyclone value of RMW by our method, Yadav and Das, Willoughby et al., Tan and Fang, and IMD 84

3.1 Flowchart of the proposed methodology 99

3.2 Architecture of the Proposed Neural Network, where X_1, X_2, and X_3 are input and Y is the output 100

3.3 The result of the proposed method for calculating the tropical cyclone track of the SCS Michaung with other methods is shown graphically. 104

3.4 The result of the proposed method for calculating the tropical cyclone track of the ESCS Tej with other methods is shown graphically. 106

3.5 The result of the proposed method for calculating the tropical cyclone track of the Mandous cyclone with other methods 110

3.6 The result of the proposed method for calculating the tropical cyclone track of the Biparjoy cyclone with other methods 113

3.7 The result of the proposed method for calculating the tropical cyclone track of the Mocha cyclone with other methods 114

3.8 The result of the proposed method for calculating the tropical cyclone track of the Remal cyclone with other methods 118

4.1 Compared the intensity estimation by SATCON and RSMC provided data for all typhoons (state wise) over the west pacific basin from 2017-2021. B stands for RSMC provided data, S stands for SATCON algorithm data, ViTY stands for Violent Typhoon, VSTY for Very Strong Typhoon, TY for Typhoon, STS for Severe Tropical Storm, and TS for Tropical Storm 132

4.2 Compared the intensity estimation by SATCON and RSMC provided data for pre-monsoon season. B stands for RSMC provided data, S stands for SATCON algorithm data, VSTY for Very Strong Typhoon, TY for Typhoon, STS for Severe Tropical Storm, and TS for Tropical Storm 137

4.3 Compared the intensity estimation by SATCON and RSMC provided data for the post-monsoon season. B stands for RSMC provided data, S stands for SATCON algorithm data, ViTY stands for Violent Typhoon, VSTY for Very Strong Typhoon, TY for Typhoon, STS for Severe Tropical Storm, and TS for Tropical Storm 141

5.1 Steps involved in the determination of the Intensity of a Tropical Cyclone (Source: IMD) 149
5.2 Architecture of the Proposed Neural Network 154
5.3 A representation of the research results of the SCS Asani graphically . . . 156
5.4 Representation of the results of the CS Sitrang in graphical form 160
5.5 Representation of the results of the SCS Shaheen in graphical form 161
5.6 Representation of the results of the ESCS Tej in graphical form 163
5.7 Representation of the results of the SCS Remal in graphical form 165
5.8 Representation of the results of the CS Asna in graphical form 167
5.9 Representation of the results of the CS Dana in graphical form 171

List of Tables

1.1 Classification of tropical cyclones formed over the North Indian Ocean used by the IMD New Delhi 17

2.1 Category of selected TCs and period across the NIO basin 55

2.2 Results of ESCS Tauktae, where E_1 indicates the error percentage between the proposed method and IMD, E_2 represents the error percentage between Willoughby et al.'s expression and IMD, and E_3 represents the error percentage between Tan and Fang's expression and IMD 57

2.3 Results of CS Gulab, where E_1 indicates the error percentage between our method and IMD, E_2 represents the error percentage between Willoughby et al.'s expression and IMD, and E_3 represents the error percentage between Tan and Fang's expression and IMD 59

2.4 Results of SCS Mandous over BoB during $6-10$ December 2022, where E_1 indicates the error percentage between the proposed method and IMD, E_2 represents the error percentage between Willoughby et al.'s expression and IMD, and E_3 represents the error percentage between Tan and Fang's expression and IMD 61

2.5 Results of SCS Asani over BoB during $07-12$ May 2022, where E_1 indicates the error percentage between the proposed method and IMD, E_2 represents the error percentage between Willoughby et al.'s expression and IMD, and E_3 represents the error percentage between Tan and Fang's expression and IMD 64

2.6 Results of CS Sitrang over the BoB during $22-25$ October 2022, where E_1 indicates the error percentage between the proposed method and IMD, E_2 represents the error percentage between Willoughby et al.'s expression and IMD, and E_3 represents the error percentage between Tan and Fang's expression and IMD 66

2.7 Results of CS Jawad over the BoB during $02-06$ December 2021, where E_1 indicates the error percentage between the proposed method and IMD, E_2 represents the error percentage between Willoughby et al.'s expression and IMD, and E_3 represents the error percentage between Tan and Fang's expression and IMD 68

2.8 Results of VSCS YAAS over the BoB during 23 − 28 May 2021, where E_1 indicates the error percentage between the proposed method and IMD, E_2 represents the error percentage between Willoughby et al.'s expression and IMD, and E_3 represents the error percentage between Tan and Fang's expression and IMD 71

2.9 The RMSE value of Our Method with respect to (w.r.t.) IMD, Willoughby et al. w.r.t. IMD, and Tan and Fang w.r.t. IMD 72

2.10 The Mean Absolute Error Percentage value of Our Method with respect to (w.r.t.) IMD, Willoughby et al. w.r.t. IMD, and Tan and Fang w.r.t. IMD 72

2.11 Details of Selected Tropical Cyclones for validation 73

2.12 Numerical Result of Mandous Cyclone 76

2.13 Numerical Result of Sitrang Cyclone 78

2.14 Numerical Result of Mocha Cyclone 81

2.15 Numerical Result of Remal Cyclone 83

2.16 Root Square Mean Error of all methods concerning IMD 85

2.17 Error percentage of all methods concerning IMD 85

2.18 Detail of R-squared of all cases 86

3.1 Details of Tropical Cyclone for training purpose 97

3.2 Details of Tropical Cyclone for Validation purpose 98

3.3 Whole process of proposed method 101

3.4 Layer Details of the Neural Network 102

3.5 Comparing the numerical results of the proposed method for calculating the tropical cyclone tracks of the SCS Michaung with the numerical results obtained from other methods. 105

3.6 Comparing the numerical results of the proposed method for calculating the tropical cyclone tracks of the ESCS Tej with the numerical results obtained from other methods. 107

3.7 Comparing the numerical results of the proposed method for calculating the tropical cyclone tracks of the Mandous Cyclone with the numerical results obtained from other methods 109

3.8 Comparing the numerical results of the proposed method for calculating the tropical cyclone tracks of the Biparjoy Cyclone with the numerical results obtained from other methods: Part I 111

3.9 Comparing the numerical results of the proposed method for calculating the tropical cyclone tracks of the Biparjoy Cyclone with the numerical results obtained from other methods: Part II 112

3.10 Comparing the numerical results of the proposed method for calculating the tropical cyclone tracks of the Mocha Cyclone with the numerical results obtained from other methods 115

3.11 Comparing the numerical results of the proposed method for calculating the tropical cyclone tracks of the Remal Cyclone with the numerical results obtained from other methods 117

3.12 Detail of error percentage of both cases 120

3.13 Detail of root square mean error of latitude of both cases 120

4.1 In this study, the following typhoons were considered over the West Pacific Basin 125

4.2 Different stage of typhoons with maximum sustained wind used in RSMC, Tokyo 127

4.3 Calculated different parameters (in terms of MSW and MSLP) based on SATCON and RSMC, Tokyo provided data for typhoons during the year 2017-2021 129

4.4 Compared the SATCON and RSMC, Tokyo provided data (in terms of MSW and MSLP) of typhoons (stage wise) over the West Pacific basin during the year 2017-2021 133

4.5 Compared the SATCON and RSMC, Tokyo provided data (MSW/MSLP) for typhoons over the West Pacific basin during the year 2017-2021 as pre-monsoon, post-monsoon, and annual 140

4.6 Compared the SATCON and RSMC, Tokyo provided data for typhoons (stage wise) over the West Pacific basin as pre-monsoon and post-monsoon during the year 2017-2021 142

5.1 Details of selected tropical cyclones for Training process 151

5.2 Details of selected tropical cyclones for Training process (Continue to table 5.1) 152

5.3 Details of selected tropical cyclones for Validation process 155

5.4 Numerical results of SCS Asani 157

5.5 Numerical results of CS Sitrang 159

5.6 Numerical result of SCS Shaheen 162

5.7 Numerical result of ESCS Tej 164

5.8 Numerical result of SCS Remal 166

5.9 Numerical result of CS Asna 168

5.10 Numerical result of CS Dana 170

5.11 Detail of root square mean error of both cases 172

5.12 Detail of error percentage of both cases 172

List of Abbreviations

ADT	Advanced Dvorak Technique
AiDT	Artificial Dvorak Technique
ANN	Artificial Neural Network
ARCHER	Automated Rotational Center Hurricane Eye Retrieval
AS	Arabian Sea
BoB	Bay of Bengal
CI	Current Intensity
CNN	Convolution Neural Network
ECP	Estimated Central Pressure
hPa	Hectopascals
IMD	India Meteorological Department
IR	Infrared
IST	Artificial Neural Network
ITCZ	Intertropical Convergence Zone
JTWC	Joint Typhoon Warning Center
km	Kilometer
MAD	Mean Absolute Difference
MSLP	Mean Sea Level Pressure
MSW	Maximum Sustained Wind
NIO	North Indian Ocean
NHC	National Hurricane Center
NN	Neural Network
RMW	Radius of Maximum Wind
RMSD	Root Mean Square Difference

RMSE	Root Mean Square Error
RSMC	Regional Specialized Meteorological Center
SATCON	SATellite CONsensus
SDG	Sustainable Development Goal
SST	Sea Surface Temperature
TCWC	Tropical Cyclone Warning Center
TCs	Tropical Cyclones
UTC	Artificial Neural Network
WMO	World Meteorological Organization

Chapter 1

Introduction

"Nature is written in mathematical language"

– Galileo Galilei

The introduction provides an overview of the fundamental principles related to the dynamics, structure, and impact of tropical cyclones. In this initial chapter, we summarize numerous critical concepts and observations, many of which lay the groundwork for the analyses and discussions presented in subsequent sections of this work. We also incorporate key components of meteorology, climatology, and related physical processes, ensuring a comprehensive basis for understanding these phenomena. Before starting the thesis's main body, the reader may use this chapter as a primer or review. Later on, it might be a useful reference for definitions and notation that are used in the other chapters. Finally, the chapter contains the motivation and plan of the work carried out in the thesis.

1.1 Introduction

Between 1970 and 2019, natural disasters contributed about 74% of all the economic losses, with 2.06 million reported deaths (Wallemacq and CRED, 2018; Douris and Kim, 2021). During this time, natural disasters caused US$ 3.6 trillion in financial losses.

During the 50-year period, US$ 202 million in damage occurred on average every day. Economic losses due to weather, climate, and water extremes have increased sevenfold from the 1970s to the 2010s. The reported losses from 2010 – 2019 (US$ 383 million per day on average over the decade) were seven times the amount reported from 1970 – 1979 (US$ 49 million).

According to the World Bank country classification, 82% of deaths have occurred in low and lower-middle-income countries, and most of the economic losses (88%) have occurred in upper-middle and high-income countries.

Worldwide, 44% of disasters have been associated with floods (riverine floods 24%, general floods 14%), and 17% have been associated with tropical cyclones (TCs). TCs and droughts were the most prevalent hazards with respect to human losses, accounting for 38% and 34% of disaster-related deaths from 1970 to 2019, respectively. In terms of economic losses, 38% were associated with TCs, while different types of floods account for 31%, riverine floods (20%), general floods (8%) and flash floods (3%).

Of the top 10 disasters, the hazards that led to the largest human losses during the period have been droughts (6, 50, 000 deaths), storms (5, 77, 232 deaths), floods (58, 700 deaths) and extreme temperature (55, 736 deaths). With regard to economic losses, the top 10 events include storms (US$ 521 billion) and floods (US$ 115 billion). All the storm events

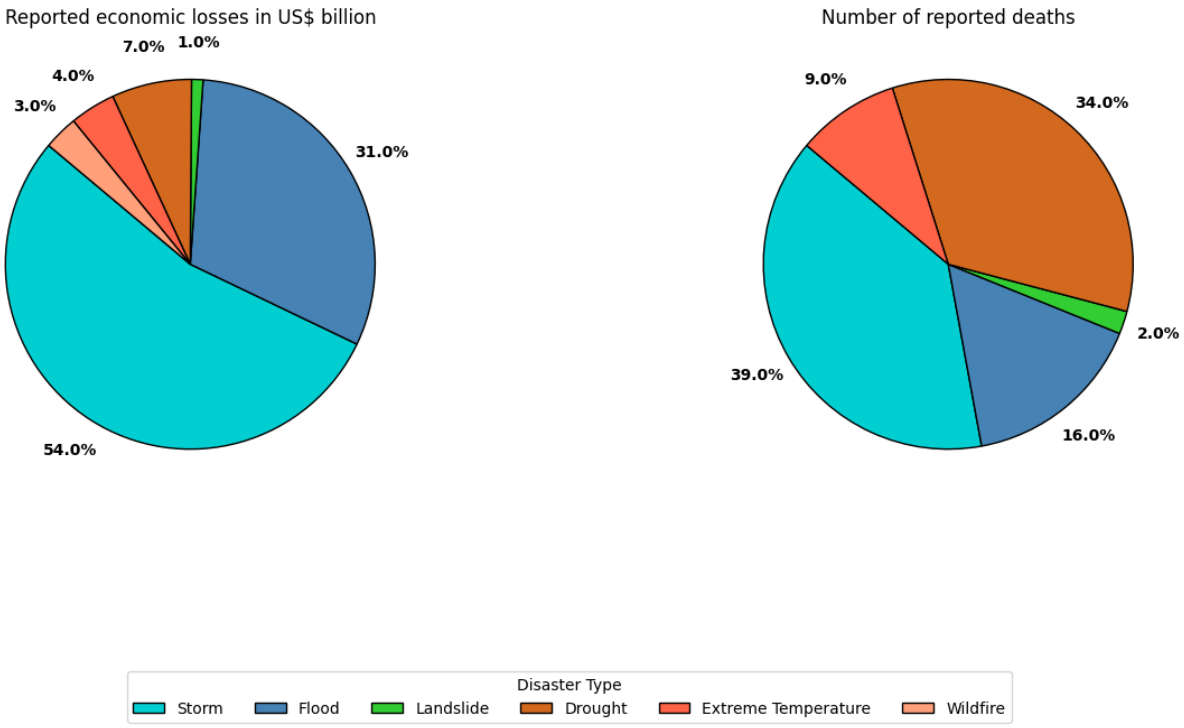

Figure 1.1: Economic and human loss caused by natural disasters globally

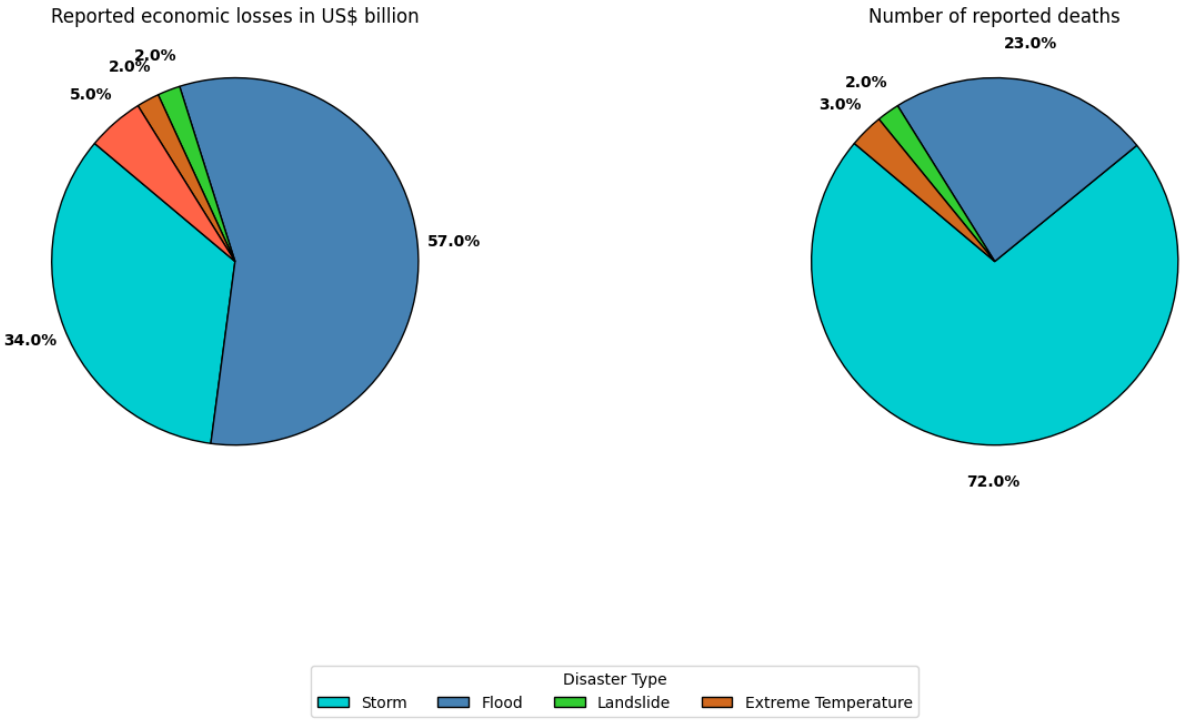

Figure 1.2: Economic and human loss caused by natural disasters in Asia

positioned in the top 10 categories in terms of both deaths and economic losses were TCs (Fig. 1.1, 1.2). Three of the top 10 disasters in terms of economic losses occurred in 2017: Hurricanes Harvey (US$ 96.9 billion), Maria (US$ 69.4 billion), and Irma (US$ 58.2 billion). These three hurricanes alone accounted for 35% of the total economic losses of the top 10 disasters worldwide from 1970 to 2019.

According to the Sendai Framework for Disaster Risk Reduction $2015-2030$, minimizing disaster losses is essential for successfully implementing the 2030 Agenda for Sustainable Development Goals (SDGs). In coastal regions worldwide, TCs are a leading cause of floods and storms. Early warning systems are crucial in reducing the economic and human losses caused by TCs. Working in this direction, in this thesis, we try to answer the TCs related to various estimation problems using mathematical and machine learning techniques.

1.2 Tropical Cyclones

The term "cyclone" is globally known for a tropical weather system with wind speeds equal to or greater than a minimum of 34 knots. The term 'cyclone' was coined by British meteorologist Henry Piddington in 1848. It is derived from the Greek word "kuklos", i.e., the snake coils that the storm's airflow resembles.

A TC is a warm-cored, intense cyclonic atmospheric vortices that develops over warm tropical oceans. It has a horizontal scale typical of hundreds of 1000 km. Its vertical extension is about 10 to 15 km. An intense mature TC generally consists of an eye with weak subsidence near its center surrounded by a rapid swirling flow where a deep convective ring slopes radially outward with height. TCs derive energy primarily from evaporation from the ocean and the associated condensation in convective clouds concentrated near their center.

TCs are significantly influenced by the underlying ocean surface over which they form and propagate. As long as the cyclone remains over warm water, highly humid Equatorial and Maritime Tropical systems evolve through a life cycle that includes the successive stages of a tropical depression and tropical storm.

TCs are seasonal phenomena. Most tropical ocean basins have a maximum frequency of cyclone formation during the late summer to early autumn. This is associated with the period of maximum sea surface temperature (SST). However, other factors are also essential, such as the seasonal variation of the Intertropical convergence zone (ITCZ) or monsoon trough location.

1.3 Tropical Cyclones: A Global Overview

There are seven main basins for TC formation: the North Atlantic Ocean, the eastern and western parts of the Pacific Ocean, the southwestern Pacific, the southwestern and southeastern Indian Ocean, and the North Indian Ocean (NIO). Worldwide, an average of 80 TCs occur each year.

- Northwest Pacific Basin:
  - It is considered to be the active basin in the globe.
  - Cyclones formation in this basin throughout the year- with a peak in frequency from July to November.
  - Cyclones in this basin generally move towards north/northwest after formation.
- Northeast Pacific Basin:
  - Second Most active basin in the globe.
  - Cyclones are formed in this basin frequently from mid-May to the end of November.

- North Atlantic Basin:
  - Cyclone formation in this basin about the beginning of June to the end of November.
  - In this basin, the movement towards west and northwest after formation.
- North Indian Basin:
  - Cyclone formation period is between April and December.
  - Basically, these are the transitional periods between seasons.
  - Cyclones in this basin tend to move northwards, and sometimes they may also recurve northeastwards
- Southwest Pacific Basin:
  - Cyclone formation peaks in late February and early March.
  - Cyclones in this basin usually move westward.
- Southwest Indian Ocean and Southeast Indian Ocean:
  - Cyclone formation period ranging from May to late October.

1.4 Physical Parameters favorable for the formation of Tropical cyclones

Numerous studies have identified environmental factors that are thought to influence TCs' formation and intensification significantly .

- Sufficient ocean thermal energy [Sea Surface Temperature $> 26.5^{\circ}$ Celsius (C) to a depth of 60 meter].
- Enhanced mid-troposphere (700 hPa) relative humidity.
- Conditional instability.
- Enhanced lower troposphere relative vorticity.

- Weak vertical shear of the horizontal winds at the genesis site.
- Displacement by at least 5° latitude away from the equator.

Gray (1968) proposed that a higher SST above a threshold of 26.5° C is strongly associated with the genesis of cyclones. However, the underlying cause of this threshold value remains uncertain. Convective instability, characterized by the vertical gradient of equivalent potential temperature between the boundary layer and the middle troposphere, is identified as another critical factor favoring TC formation. This highlights the established connection between upper tropospheric and lower tropospheric flow patterns via cumulus convection. Conversely, low relative humidity in the middle troposphere inhibits cyclone formation due to the influence of dry air, leading to reduced moisture convergence and subsequent latent heat release.

Low-level cyclonic vorticity within developing clouds is significantly correlated with TC intensification. Additionally, reduced vertical wind shear (ventilation factor) promotes more vigorous disturbance development by increasing temperature and moisture through advection.

Gray et al. (1975) hypothesized that cyclones only form when these conditions deviate from their regional climatological means, emphasizing the importance of focusing on the conditions present during individual cyclone genesis.

Charney and Eliassen (1964) introduced the Conditional Instability of the Second Kind (CISK) mechanism, which describes the interaction between cumulus convection and large-scale motion in cyclone formation. This mechanism operates in weak vertical wind shear areas, where cumulonimbus clouds warm the atmosphere through latent heat release, decreasing surface pressure and increasing horizontal convergence. This cooperative interac-

tion between the large-scale environment and cumulus convection promotes unstable system growth, potentially leading to TC formation under favorable moisture inflow conditions.

Montgomery and Enagonio (1998) and Möller and Montgomery (1999, 2000) demonstrated that small-scale vorticity patches introduced into the flow field of larger-scale vortices quickly become axisymmetrized, contributing to the energy of the vortex-scale flow. This suggests that mesoscale convective systems developing outside the eye wall may aid in intensifying the overall storm.

1.5 Life Cycle of Tropical Cyclones

Cyclones go through different stages from start to finish, which we call their "life cycle" governed by various environmental factors. This cycle usually lasts about five days but can be shorter or longer. They begin as groups of thunderstorms over warm ocean waters. When these storms become more organized, they turn into a deep depression, then a tropical storm. The conditions in the air and ocean decide how these stages happen. We have different models to explain how cyclones change over time, but they generally have four main stages: i) Formation, ii) Intensification, iii) Mature, and iv) Dissipation/Decay.

1.5.1 Formation

The formation of a TC depends upon several favorable environmental conditions, which are frequently present in the ITCZ.

- Ocean water must be warmer than 26.5° C. The heat and moisture from this warm water are ultimately the energy source for cyclones.
- High relative humidities in the lower and middle troposphere are also required for

cyclone development. These high humidities reduce the evaporation in clouds and maximize the latent heat released because there is more precipitation.

- The vertical wind shear in a TC's environment is also essential. Wind shear is the change in the wind's direction or speed with increasing altitude.

1.5.2 Intensification

Cyclone intensification is a process wherein the cyclone strengthens over time. During this phase, the central pressure of the TC decreases while the maximum surface wind speed increases. Suppose the conditions in the ocean and atmosphere remain favorable. In that case, the cyclone may continue strengthening, forming a more circular cloud system with a distinct eye at its center. The warm, moisture-laden air rising at the cyclone's core continues to ascend as long as the surrounding air remains cooler and denser, facilitating the development of deep convective clouds. Additionally, the rising air in the cyclone's core draws in air from the surrounding atmosphere at altitudes of approximately 5 kilometers (km). If this incoming air is sufficiently humid, it further fuels the intensification process. Conversely, if the incoming air is dry, it may cause some of the water droplets within the rising column to evaporate, leading to the cooling of the air compared to its surroundings. This cooling effect triggers the formation of solid downdrafts, disrupting the upward motion of air and hindering further intensification.

1.5.3 Mature

During its mature stage, a TC displays robust rotational circulation characterized by a sizeable axisymmetric component, with well-organized clouds revolving around a central area of low pressure. This phase represents the pinnacle of the cyclone's life cycle, marked

by the deepest central pressure within the eye. Maximum wind speeds reach their peak intensity during this stage. A distinct eye, typically devoid of clouds due to descending dry air, becomes evident. Surrounding the eye is an eyewall consisting of the most intense wind speeds, and convective thunderstorms are formed. Spiral rain bands, separated by areas of lighter precipitation, are commonly observed. However, they may sometimes be obscured by a dense layer of cirrus clouds aloft, resulting from upper-atmospheric air divergence. Fig. 1.3 illustrates the features of a mature hurricane. The genesis section describes the processes leading to hurricane formation and emphasizes increased convergence by rotation at the center, with intensification of the eye wall. This intensification occurs as air, unable to reach the storm's center, is compelled to concentrate around a ring encircling the center. The mature stage is typically defined as the period of maximum potential intensity, determined by the interaction between the ocean and atmosphere and the heating rate within the storm system (Emanuel, 1988).

1.5.4 Decay

The TC begins to weaken when it encounters unfavorable environmental conditions, such as a lack of moist tropical air from warm seas, dry land, strong vertical wind shear, and unfavorable large-scale atmospheric flow. These conditions are crucial for the formation of TCs.

Various physical processes occur to dissipate the cyclone, regardless of whether it's over land or water. As the cyclone moves over land or cooler water, it loses its primary energy source, latent heat released from warm water. This leads to a decrease in upper-level divergence, a drop in the mean temperature at the core, and an increase in central pressure. As a result, the pressure gradient weakens, causing the eye wall to expand outward. Meanwhile,

the cyclonic winds around the storm decrease rapidly due to the conservation of angular momentum.

Without the warm moisture source, the remaining convection within the storm dries out the surrounding air. This process continues until the pressure gradient aloft is wholly diminished, ultimately weakening and filling the cyclone's eye.

1.6 Naming of Tropical Cyclones

Various national warning centers or world meteorological organizations have named TCs and subtropical cyclones to simplify the communication between forecasters and the general public regarding forecasting, watching, and warnings. The names reduce confusion during concurrent storms in the same basin. Once storms develop, maximum sustained wind speeds of more than 33 knots (61 km/h; 38 mph), then names are generally assigned to them from predetermined lists, depending on the basin in which they originate.

1.7 Physical Structure of Tropical Cyclones

TCs are characterized by a relatively low-pressure system in the troposphere, with the most significant pressure disturbances happening at lower altitudes, closer to the Earth's surface. The area near the center of a TC is consistently warmer compared to its surrounding environment across all altitudes. The physical arrangement of a TC is depicted in the Fig. 1.3.

Center/Eye of Tropical Cyclone: The eye is a central feature of intense storms. It is a region of relatively calm weather found at the center of a TC. Winds are typically light within the eye, and skies are often clear or partly cloudy. The eye is characterized by sinking

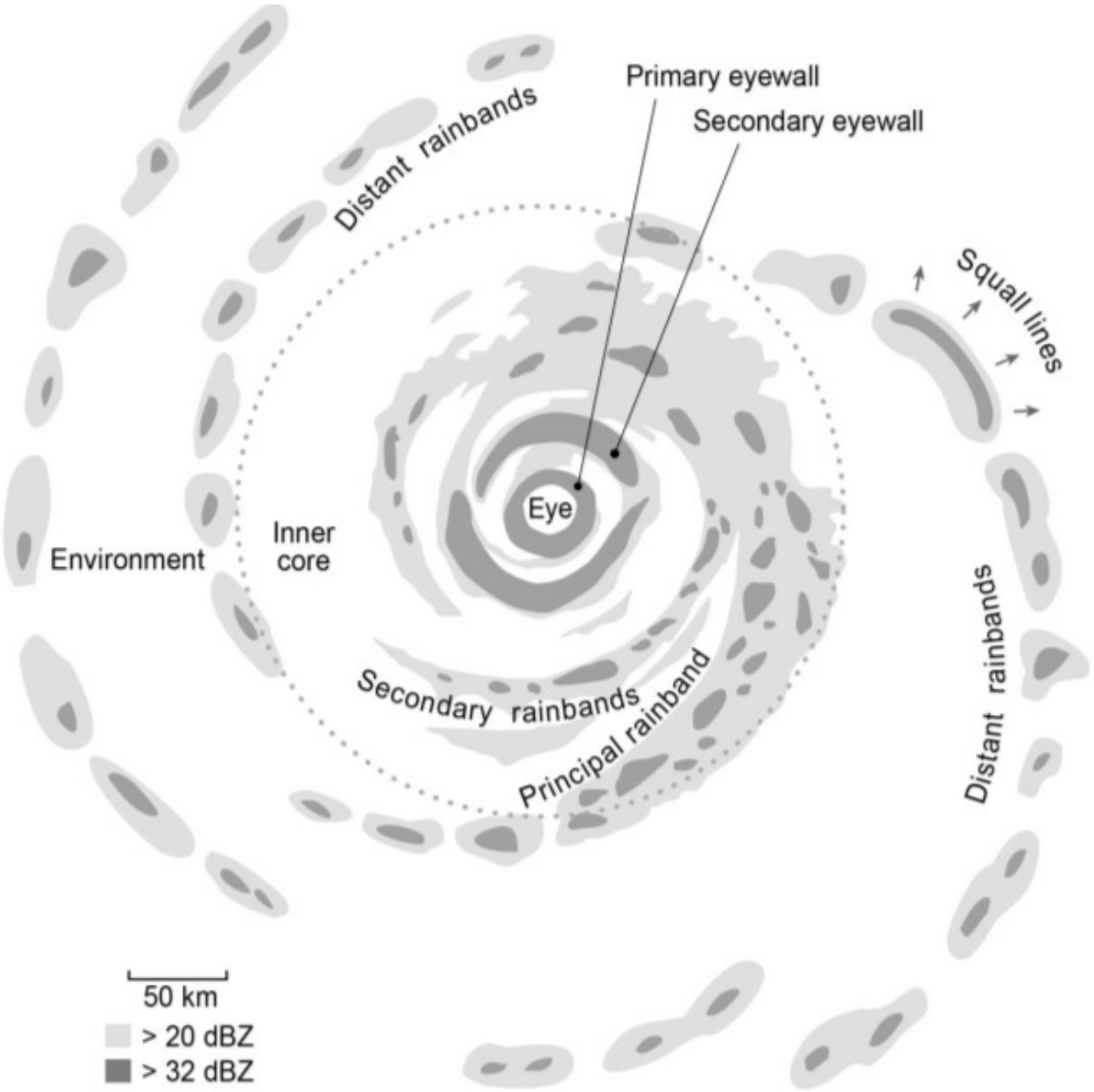

Figure 1.3: The Physical Structure of Tropical Cyclones with concentric eyewalls

air, resulting in lower atmospheric pressure and a notable absence of storm clouds. The size of the eye can vary greatly, from just a few km to over a hundred km in diameter in the largest TCs. It is surrounded by the eyewall, a ring of towering thunderstorms where the strongest winds with the heaviest rainfall occur. In intense TCs, the eyewall may vary from time to time in the eyewall replacement cycle.

Rainbands: Rainbands are a prominent feature of TCs, extending outward from the storm's center in spiral arms. These bands include intense rainfall and thunderstorms, often producing heavy precipitation and gusty winds. Rainbands play a crucial role in rainfall distribution within a TC, with the heaviest rainfall typically occurring near and within the bands.

Two primary types of rainbands are associated with TCs, namely, the outer rainbands and the inner rainbands. Outer rainbands are farther away from the storm's center and tend to be less intense, although they can still produce significant rainfall and occasionally tornadoes. Inner rainbands, also known as the eyewall or primary rainband, are located closer to the storm's center and are characterized by the most intense rainfall and strongest winds within the TC. These inner rainbands often form a ring around the eye of the storm and are responsible for much of the destructive power associated with TCs.

Rainbands are essential indicators of a TC's intensity and structure. They can also influence the storm's track and intensity as they interact with environmental factors such as wind shear and SST. Studying rainbands and their dynamics is crucial for understanding and predicting TCs' behavior and issuing accurate forecasts and warnings to potentially affected areas.

Wind Field: In the near-surface wind field of a TC, air moves swiftly in a circular

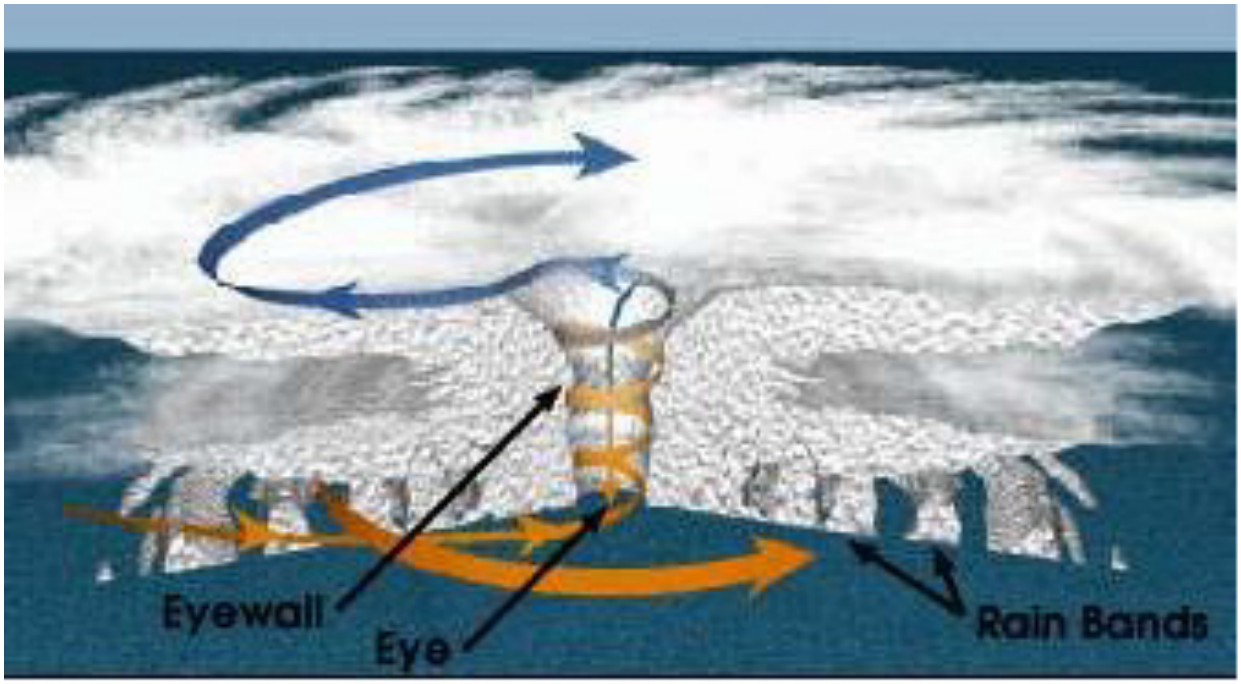

Figure 1.4: The schematic representation of Tropical Cyclone showing eye, eyewall, and rainbands.

motion around a central point of circulation while simultaneously moving inward. Towards the outer perimeter of the storm, the air may seem almost still, yet due to the Earth's rotation, it maintains some angular momentum (refer to Fig. 1.4). As the air progresses inward, it rotates cyclonically to preserve its angular momentum. At a closer distance to the center, the air begins to ascend toward the upper levels of the troposphere.

Size: The size of a TC is determined by measuring the distance from its center of circulation to the outermost closed isobar. The most commonly used method for measuring TC size is through parameters like the "Radius of Outermost Closed Isobars" (ROCI) and "the radius of vanishing wind". Size is a significant factor in influencing the damage potential of a storm. The size of a TC shows a weak correlation with storm intensity, radius of maximum wind, latitude, and maximum potential intensity.

Intensity: TC's Intensity is usually defined as the maximum wind speed or minimum sea level pressure at the center of a TC, but the specific definitions of TC intensity vary

in different oceanic zones, and there is no standard definition to date. It's measured as a 1-minute or 10-minute average at the standard reference height of 10 meters. The selection of the averaging period, along with the classification naming conventions for storms, varies among forecast centers and ocean basins.

1.8 Tropical Cyclones as a Natural Hazard

As natural hazards, TCs threaten communities due to their destructive potential. These intense storms are characterized by strong winds, heavy rainfall, and storm surges, which can cause widespread devastation. Strong winds, often exceeding 100 miles per hour (160 km per hour), can result in structural damage to buildings, uproot trees, and cause power outages. Heavy cyclone rainfall can lead to flooding, landslides, and crop damage, exacerbating humanitarian crises. Additionally, storm surges, which are elevated seawater levels driven by the cyclone's winds, can inundate coastal areas, causing coastal erosion, flooding, and displacement of populations.

Moreover, TCs' impacts extend beyond immediate physical damage. Disruption of essential services, displacement of populations, and long-term socio-economic challenges often follow these events. Environmental impacts are also profound, affecting ecosystems such as coral reefs and mangrove forests and exacerbating biodiversity loss and habitat destruction.

Furthermore, the increasing frequency and intensity of TCs due to climate change add complexity to the challenge. Rising sea levels and warmer ocean temperatures contribute to more powerful storms and higher storm surges, amplifying risks for coastal communities and ecosystems. Addressing these multifaceted risks requires a comprehensive approach integrating disaster risk reduction, climate change adaptation, and sustainable development

strategies. By investing in resilient infrastructure, promoting ecosystem-based approaches, and strengthening early warning systems, communities can build resilience and mitigate the impacts of TCs, ensuring the safety and well-being of vulnerable populations and ecosystems.

1.9 Classification of Tropical Cyclones:

The terminology used to describe different stages of TCs varies significantly. The World Meteorological Organization (WMO) convention advocates for measuring 10-minute average surface wind speeds, while the United States follows a 1-minute averaging method. In the NIO, the India Meteorological Department (IMD) employs a 3-minute averaging approach. These differences in wind averaging times contribute to confusion, as countries inconsistently use 1-minute, 3-minute, and 10-minute averages. Consequently, a tropical system may receive a name or number in one country but not another despite meeting the same wind criteria but using different averaging times.

In the Indian region, categorizing low-pressure systems relies on two primary factors: maximum sustained wind speed and the number of closed isobars associated with the system. The pressure criterion is applied when the system is over land, while the wind criterion is used over the sea.

A low-pressure system is identified if a single closed isobar is present within a 2-hectopascal (hPa) interval. If two closed isobars are observed, it is termed a depression; with three, it becomes a deep depression. The system is classified as a cyclonic storm when four or more closed isobars are present. Further classification based on wind criteria is detailed in Table 1.1.

According to wind criteria, a system with wind speeds ranging from 17 to 27 knots

Table 1.1: Classification of tropical cyclones formed over the North Indian Ocean used by the IMD New Delhi

Phases	T Number	Maximum Wind Speed
Low pressure area (WML)	T1.0	$<$ 17 kts
Depression (D)	T1.5	17-27 kts
Deep Depression (DD)	T2.0	28-33 kts
Cyclonic Storm (CS)	T2.5-T3.0	34-47 kts
Severe CS (SCS)	T3.5	48-63 kts
Very Severe CS (VSCS)	T4.0-T4.5	64-89 kts
Extremely Severe CS (ESCS)	T5.0-T6.0	90-119 kts
Super CS	T6.5-T8.0	$>$ 120 kts

(8.7-13.9 m/s) is labeled as a depression. A low-pressure system with maximum sustained 3-minute surface winds between 28 and 33 knots (14.4-17.0 m/s) is termed a deep depression. Finally, a system with maximum sustained 3-minute surface winds of 34 knots (17.4 m/s) or higher is categorized as a cyclonic storm.

1.10 Frequency of Cyclones over the Indian Ocean:

The Indian sub-continent stands as one of the world's most heavily impacted regions by TCs, with a coastline stretching approximately 7516 km (5400 km along the mainland, 132 km in Lakshadweep, and 1900 km in the Andaman and Nicobar Islands). Nearly 10% of the world's TCs affect this region. Thirteen coastal states/Union Territories, comprising 84 coastal districts, bear the brunt of cyclones. Particularly vulnerable are four states (Andhra Pradesh, Odisha, Tamil Nadu, and West Bengal) and one Union Territory (Pondicherry) along the East Coast and Gujarat along the West Coast. Approximately 40% of the total population resides within 100 km of the coastline.

The average annual frequency of TCs in the NIO, encompassing the Bay of Bengal (BoB) and the Arabian Sea (AS), accounts for about $5-6\%$ of the global annual average. Of these, approximately 35% of disturbances intensify into cyclonic storms, 16% into severe cyclonic

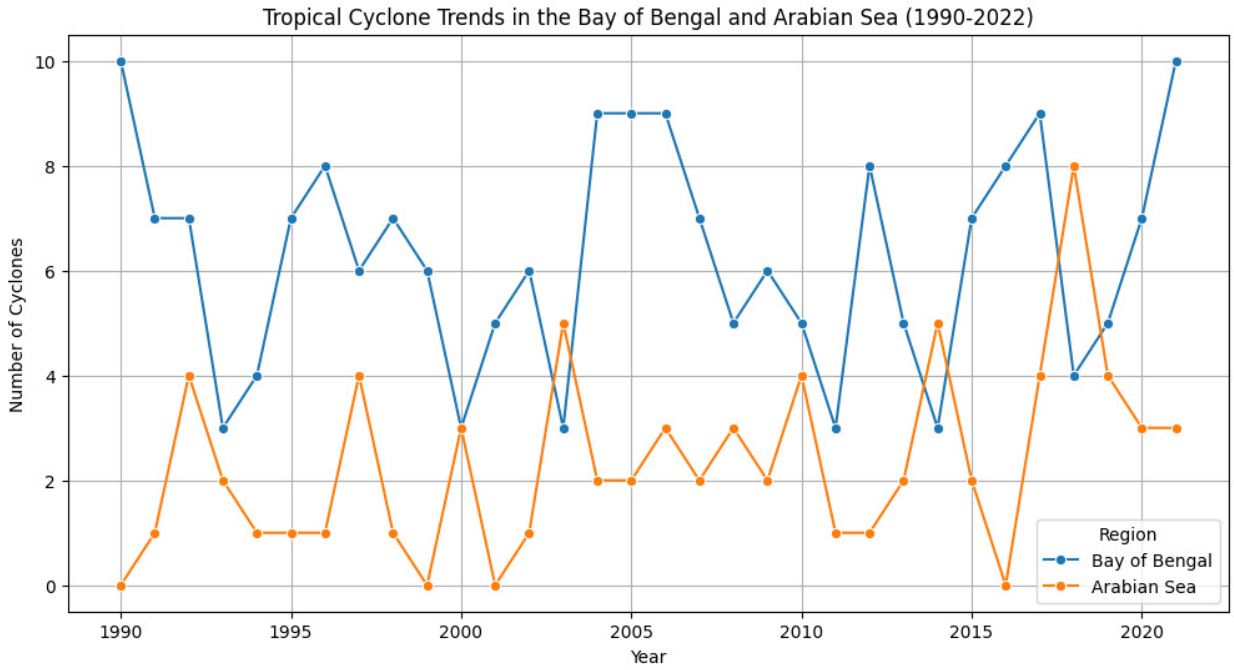

Figure 1.5: Tropical cyclone trends in the Bay of Bengal and Arabian Sea during 1990 – 2022

storms, and 7% into very severe cyclonic storms. The typical lifespan of a TC in the NIO is approximately 4 to 5 days. The monthly frequency of TCs in this region displays a bi-modal pattern, with a primary peak occurring in November and a secondary peak in May. Cyclones occurring during March-May and October-December tend to be severe, whereas those developing during the monsoon months (June to September) are generally less intense.

The BoB experiences a higher frequency of cyclones than the AS, with a ratio of approximately 4 : 1 (refer to fig. 1.5). This discrepancy is attributed to the lack of seedling disturbances and a relatively dry middle tropospheric environment in the AS. The northern part of the BoB is known for its potential to generate dangerous high storm tides when associated with cyclonic storms, making it a hotspot for TC formation. Historical data from 1891 to 2013 reveals that out of 613 cyclonic disturbances formed in the Bay of Bengal, 54% crossed India, 16% affected Bangladesh, 10% impacted Myanmar, 4% affected Sri Lanka, while 17% dissipated over the sea without making landfall on any of these countries.

1.11 Tropical cyclone Forecast

Various types of TC forecasts are available globally. Official forecasts, provided by Regional Specialized Meteorological Centers (RSMCs) and Tropical Cyclone Warning Centers (TCWCs), consist of human-generated predictions regarding TC genesis, track, intensity, and seasonal frequency. These forecasts include additional storm attributes, such as radii associated with different maximum wind speed thresholds.

Modern forecasting efforts utilize statistical methods to predict TC behavior. For example, the Climate and Persistence (CLIPER) model predicts TC tracks (Heming and Goerss, 2010; Neumann, 1972) based on climatology and persistence, while the Statistical Hurricane Intensity Forecast (SHIFOR) model (Knaff et al., 2003) forecasts intensity. Statistical-dynamical models like the Statistical Hurricane Intensity Prediction Scheme (SHIPS) (DeMaria et al., 2005) and its variants are also employed for intensity prediction. Statistical Cyclone Intensity Prediction (SCIP) (Kotal et al., 2008) models also cater specifically to TC intensity prediction in the Bay of Bengal region.

Numerical Weather Prediction (NWP) models, including global and regional systems such as the Global Forecast System (GFS), the United Kingdom Met Office model, and the European Center for Medium-Range Weather Forecasting (ECMWF) model, provide TC forecasts (Heming and Goerss, 2010). Other models from agencies like the China Meteorological Administration and the Korean Meteorological Administration contribute to global TC prediction efforts.

Mesoscale models, such as the Hurricane Weather Research and Forecasting (HWRF) model and the Coupled Ocean-Atmosphere Mesoscale Prediction System for TCs (COAMPS-

TC), offer tailored forecasts for TCs. Ongoing research focuses on developing new mesoscale and global prediction systems for TCs and improving existing ones.

In addition to forecasting, as mentioned earlier, advancements in meteorological research have led to the development of ensemble prediction systems for TCs. These systems utilize multiple simulations with slight variations in initial conditions to account for the inherent uncertainties in forecasting TC behavior. By generating a range of possible outcomes, ensemble prediction systems provide valuable information about the uncertainty associated with TC predictions, aiding decision-makers in risk assessment and disaster preparedness.

Furthermore, seasonal forecasting of TC activity has gained importance in recent years. Forecasts made before the start of the TC season offer insights into the overall expected activity, including the number of storms, their intensity, and tracks. These forecasts typically take several months and rely on various approaches, including statistical methods, dynamical General Circulation Models (GCMs), and hybrid approaches. While some seasonal forecasting methods are already in operational use, others, such as multi-season forecasts, are still in the research phase and require further validation before practical implementation.

Integrating soft computing techniques, such as neural networks and fuzzy logic, represents a promising avenue for enhancing TC forecasting capabilities. These techniques leverage the power of artificial intelligence to analyze complex meteorological data and extract patterns that may not be readily apparent using traditional statistical or dynamical methods. Research in this area aims to improve the accuracy and reliability of TC forecasts, ultimately enhancing our ability to mitigate the impacts of these devastating storms on vulnerable coastal communities.

1.12 Previous Research on Tropical Cyclones:

1.12.1 Global Research on cyclones:

Globally, numerous studies have utilized various numerical models to simulate the structure, intensity, and track of TCs (Willoughby et al., 1984; Harr and Elsberry, 1995; Braun, 2002; Atlas et al., 2005; Krishnamurti et al., 2005). High-resolution mesoscale models have been increasingly used for sensitivity studies of TCs' structure, intensification, and movement, incorporating different physical processes (Braun and Tao, 2000; Li and Pu, 2008). Fovell and Su (2007) demonstrated that altering microphysical parameterization (MP) and cumulus parameterization (CP) significantly influenced the track and landfall of Hurricane Rita using the WRF model at 30 and 12-km resolutions. Although researchers have developed several parameterization schemes, many have certain limitations for cyclone forecasts (Frank, 1983; Emanuel, 2015; Zhang et al., 1994; Kou and Bresch, 1997).

Forecasting TC intensity remains challenging for operational and research communities (Bender and Ginis, 2000; Krishnamurti et al., 2005; Rogers et al., 2006). Studies have shown that maximum TC intensity is strongly influenced by environmental factors such as sea surface temperature, moisture distribution, and vertical wind shear (Gray, 1968; Emanuel, 2015). Hill and Lackmann (2009) proposed that the structure of a TC is controlled by environmental relative humidity. This idea is supported by Kossin and Sitkowski (2009), who demonstrated the importance of relative humidity in surface entropy flux through observational studies.

The primary energy source for TCs is the exchange of moist enthalpy between the air and the sea surface through latent and sensible heat fluxes (Emanuel, 1986). The rapid

intensification of TCs is driven by ocean surface warming via these heat fluxes (Davis and Emanuel, 1988). Braun and Tao (2000) demonstrated that surface fluxes significantly influence the intensity of Hurricane Bob (1991) more than vertical mixing in the Planetary Boundary Layer (PBL).

Several studies have also shown that the heat from rainbands affects the structure and intensity of TCs (Wu et al., 2009; Moon and Nolan, 2010). Xu and Wang (2010b) investigated the relationship between surface entropy flux and the activity of spiral rainbands in simulated storms. They found that while entropy flux in the eye region minimally impacts storm intensity, it reduces the radius of maximum wind. In contrast, surface entropy fluxes under the eyewall substantially enhance storm intensity. Further outward, these fluxes are vital for the storm's inner-core size growth but can decrease storm intensity.

Xu and Wang (2010a) also found that the initial vortex and latent heat flux determine TC size. They observed that strong outer winds in storms with a larger initial size generate substantial entropy flux, promoting active spiral rainbands. However, Rozoff et al. (2012) suggested that TC size is influenced by latent heating outside the primary eyewall, which encourages secondary eyewall formation and the expansion of the outer wind field.

Stovern and Ritchie (2012) studied the impact of atmospheric temperature on TC size in an idealized framework, adjusting the atmospheric temperature profile while maintaining a constant 29° C SST. They concluded that a cooler atmosphere increases surface moisture fluxes, higher potential vorticity, outer rainband generation, and a larger wind field.

Several studies have shown that global warming significantly impacts TC track and intensity. Studies show that the western Pacific subtropical high expands as carbon emissions increase, leading to a poleward shift in TC tracks (Feng et al., 2023). Rising sea surface

temperatures also favor convections near the eyewall, increasing TC intensity (Pérez-Alarcón et al., 2023). The Hurricane Maximum Potential Intensity (HuMPI) model projects a 9.5% to 17% increase in TC intensity by the end of the twenty-first century under different climate scenarios, with a 5-7% rise in maximum potential wind speed per degree of warming (Wehner, 2021). Historical data analysis and idealized modeling indicate that observed trends in TC intensity distribution coincide with changes in the global temperature profile, with stronger storms intensifying faster than weaker ones (Done et al., 2022). These findings collectively highlight the complex interplay between global warming and TC behavior, emphasizing the need for continued research and mitigation efforts.

Many studies have found that atmospheric temperature, SST, heat from rainbands, relative humidity, climate change, and energy generated by the exchange of moist enthalpy between the air and the sea surface impact the characteristics of TCs: intensity, track, the radius of maximum wind, size, and structure but only a few are discussed above.

In the 21^{th} century, the neural network is important in researching the TC's characteristics. Neural networks (NN) can determine complex patterns and relationships from vast datasets and have become instrumental in refining our understanding of cyclone behavior. Neural Networks, particularly Deep Learning (DL) models like LSTMs and GRUs, have shown significant promise in various aspects of TC research. These models are utilized for forecasting TC tracks, classifying TC evolution, and estimating TC intensity with improved accuracy and efficiency (Hudozhnik and Windisch, 2023; Eusebi et al., 2023; Tian et al., 2023a). Physics-Informed Neural Networks have also been proposed as a valuable alternative for data assimilation in TC initial conditions, showcasing the potential for accurate reconstruction of TC wind and pressure fields (Vosper et al., 2023). Moreover, the application of Generative Adversarial Networks (GANs) and Variational Autoencoder GANs (VAEGANs)

has been explored to increase the resolution of TC rainfall measurements, demonstrating the ability to generate realistic TC rainfall fields with high accuracy, especially when trained on a comprehensive observational dataset (Tian et al., 2023b). These advancements highlight the effectiveness of neural networks in enhancing various aspects of TC research and forecasting, but there is still room for improvement.

1.12.2 Previous studies on Cyclones over India:

In India, the initial forecasting of TCs combined half persistence and half climatology (Sikka and Suryanarayana, 1972). Later, Mohanty and Gupta (1997) introduced multi-level primitive equation models with parameterization of physical processes for cyclone track prediction. Prasad and Rama Rao (2003) evaluated the Quasi-Lagrangian Model (QLM) for track forecasting. Numerous models and traditional methods have been developed to predict cyclone positions, accurately enabling timely disaster management warnings. Accurately predicting the track and intensity of TCs remains a challenging problem for the east coast of India and Bangladesh (Pattanayak and Mohanty, 2008; Paul, 2010).

Over the past decade, mesoscale models have been employed for sensitivity studies on TC structure, intensification, and movement (Trivedi et al., 2002; Mohanty et al., 2004; Rao and Prasad, 2007; Srinivas et al., 2007; Bhaskar Rao et al., 2009; Pattanaik and Rama Rao, 2009; Shen et al., 2010).

In the last few years, the rapid advancement of high-performance computing has enabled the use of high-resolution non-hydrostatic mesoscale atmospheric models, such as MM5 and WRF, for forecasting the structure, intensification, and movement of TCs (Prasad and Rama Rao, 2003; Mohanty et al., 2004; Trivedi et al., 2006; Reale et al., 2009; Pattanayak

and Mohanty, 2010; Raju et al., 2012; Osuri et al., 2013).

Prater and Evans (2002) studied TC Irene (1999) using various convective parameterization (CP) schemes in the MM5 model and concluded that the Kain-Fritsch (KF) scheme produced relatively accurate results compared to observations. Ming-Jen and Lin (2005) found that combining the MRF scheme in the Planetary Boundary Layer (PBL) and the Grell-Devenyi ensemble (GD) in CP with the Goddard Graupel scheme in cloud microphysics (MP) provided the best performance in their study of Typhoon Toraji (2001) using the MM5 model.

Kumar et al. (2011) studied the impact of lateral and boundary forcing on predicting the track and intensity of Cyclone SIDR. They found that reducing the domain size improved the accuracy of the cyclone's predicted track and intensity. Pattanayak et al. (2012) simulated Cyclone MALA using different initial conditions in the Hurricane Weather Research and Forecasting (HWRF) model. They demonstrated that a high-resolution inner nest domain produced higher cyclone intensity. Mohanty et al. (2010) conducted a sensitivity study using various initial and boundary conditions in the WRF model for five cyclones over the Bay of Bengal. They concluded that the landfall error was smaller with Final Analyses (FNL) data compared to Global Forecast System (GFS) data and National Centre for Medium-Range Weather Forecasting (NCMRWF) data. However, the NCMRWF data better simulated the cyclone's intensity than the other data sources.

Global warming significantly impacts TCs over the NIO, particularly in the Bay of Bengal and the Arabian Sea. Studies show that the warming climate influences the frequency, intensity, and landfall patterns of cyclones in this region, with projections indicating an exacerbation of storm intensity due to rising sea surface temperatures (Mukherjee and Ra-

makrishnan, 2023; Singh and Panda, 2022). The sea surface temperature anomalies in the Tropical Indian Ocean have been linked to the proportion of rapidly intensifying TCs over the western North Pacific, suggesting a global warming amplification effect on cyclone intensity (Gupta et al., 2019). Additionally, analyses of cyclonic disturbances data spanning 140 years highlight the vulnerability of coastal areas like India and Bangladesh to devastating cyclones, emphasizing the need for monitoring and disaster mitigation strategies under probable warming scenarios (Gao et al., 2020). These findings underscore the importance of understanding the relationship between global warming and TCs in the NIO for effective disaster management and preparedness efforts.

In recent years, Neural networks, particularly artificial neural networks (ANNs) and Long Short-Term Memory networks (LSTMs), have been extensively utilized in studying TCs over the NIO. These networks have been employed for various purposes, such as intensity estimation, track prediction, and parameter estimation. ANNs have been used to estimate cyclone parameters like wind speed, pressure, landfall point, and time of crossing land, showing promising results in predicting geophysical parameters (Ali et al., 2021; Kumar et al., 2021). LSTMs have been applied for accurate track prediction of cyclones using variables like central pressure, wind speed, latitude, and longitude, outperforming existing models regarding the accuracy and prediction time (Steptoe and Xirouchaki, 2022). Additionally, deep learning methods, including Generative Adversarial Neural Networks (GANs) and Recurrent Neural Networks (RNNs), have been explored for nowcasting TCs, demonstrating the potential of DL approaches in predicting cyclone development accurately (Chand et al., 2022). Moreover, machine learning algorithms have been used to estimate cyclone grade and maximum sustained surface wind speed (MSWS) with high accuracy over the NIO, showcasing the effectiveness of these models in cyclone intensity estimation.

1.13 Scope and Outline of the Thesis:

According to previous studies, the forecasting of TCs is highly complex. It includes different aspects of the TC, such as the structure, intensity, movement, associated weather, and the storm surge that may occur when the system lands at the coast. The strong winds, heavy rains, and large storm surges associated with TCs are the factors that eventually lead to loss of life and property. This loss can be minimized by reducing the forecast error and estimated error associated with the radius of the maximum wind, track, and intensity of the TCs to provide more reliable warnings for TC disaster management. So, the principal objective of the thesis is to estimate the TC's characteristics, such as the radius of maximum wind, track, and intensity, more accurately using mathematical methods and machine learning techniques to reduce the loss of life and property.

To achieve the aforesaid objective, the following studies are carried out:

- Formulation and Evaluation of radius of maximum wind.
- Estimate the radius of maximum wind using machine learning technique.
- Estimate the track of tropical cyclones using machine learning technique.
- Analyze the SATellite CONsensus (SATCON) algorithm to estimate the tropical cyclone's intensity.
- Estimate the tropical cyclone's intensity using the machine learning technique.

To attain these objectives, the present work is divided into six chapters.

Chapter 1 briefly introduces TCs, covering their formation, physical structure, life cycle, and classification. It also discusses the destruction caused by TCs. Additionally, it details

forecasting methods and includes a literature review focusing on TCs that formed over the North Indian Ocean. Finally, the scope and objectives of the current study are outlined.

We examine the radius of maximum wind over the North Indian Ocean in Chapter 2. We proposed a relationship between the estimated pressure drop, the latitude coordinate of the TC center, and the radius of maximum wind. There are four TCs for validation and twenty-five TCs for model training in the dataset used in this study. Furthermore, we point out the importance of latitude and estimated pressure drop in TC behavior and intensity, identifying them as critical criteria for calculating the radius of maximum wind. The relationship is limited to estimated pressure drops of 12 hPa or less.

Following this, we develop a neural network model to improve the estimate of the radius of maximum wind by using the output of conventional techniques: one that we first presented earlier in this chapter and the work of Willoughby et al. (2008) and Tan and Fang (2016). In this work, sixty-one TCs were used for model training, and four TCs were used for validation. We performed three statistical tests: error percentage, root square mean error, and R-squared to comment on the accuracy of the proposed model.

Chapter 3 explains a technique for estimating the track of tropical storms in the North Indian Ocean using a neural network. Instead of satellite images, the method uses results from three different approaches: the automated rotational center hurricane eye retrieval algorithm, the advanced Dvorak technique, and the satellite Consensus technique as inputs, with data from the India Meteorological Department serving as the target for the neural network.

In Chapter 4, we analyze the performance of the Satellite Consensus (SATCON) algorithm to estimate the intensity of TCs over the West Pacific basin. We compare the

SATCON algorithm's performance in pre-monsoon and post-monsoon. Further, we analyze the performance according to different categories of TCs like tropical storms, severe tropical storms, typhoons, very strong typhoons, and violent typhoons.

In Chapter 5, we develop a method for estimating the intensity of TCs in the North Indian Ocean using a neural network. As discussed in Chapter 3, satellite images weren't used; instead, results from three state-of-the-art methods: the automated rotational center hurricane eye retrieval algorithm, the advanced Dvorak technique, and the satellite Consensus technique were used as inputs, with the target being data from the India Meteorological Department.

Finally, the overall summary and conclusions, along with the future scope of the present study, are given in Chapter 6.

Chapter 2

Tropical Cyclone's Radius of Maximum Wind

"Mathematics is, in its way, the poetry of logical ideas"

– Albert Einstein

In this chapter[1], we examine the estimation of the radius of maximum wind (RMW) of TCs over the NIO, a region particularly susceptible to these storms. We propose two models; one is based on key TC parameters such as latitude and estimated pressure drop at the center, and the other uses machine learning techniques to accurately estimate the RMW, which is crucial for assessing TC intensity and impact. Using data from the India Meteorological Department and various statistical tests, we validate the proposed methods against established models (such as those by Willoughby et al. (2006) and Tan and Fang (2018)). The results show that the proposed methods significantly reduce the average error percentage and root mean square error (RMSE) compared to existing methods, especially for TCs with estimated pressure drop at the center up to 12 hPa.

[1] The content of this chapter is based on the following research papers:
Formulation and evaluation of the radius of maximum wind of the TCs over the North Indian Ocean basin, *Theoretical and Applied Climatology.* DOI: 10.1007/s00704-024-04895-w. (**SCIE index, IF: 2.8**)
Estimation of Tropical Cyclone's Radius of Maximum Wind using Ensemble Machine Learning Approach, *Journal of Earth System Science.* DOI: 10.1007/s12040-024-02455-4. (**SCIE index, IF: 1.3**)

2.1 Introduction

TCs are powerful and destructive natural disasters impacting socio-economic conditions and global human lives. (Guha-Sapir et al., 2019; Crunch, 2023). Driven by warm ocean waters, these intense storm systems can unleash a devastating combination of high winds, heavy rainfall, and storm surges, causing widespread damage to infrastructure, agriculture, and coastal communities. The study of TCs leads to more accurate predictions of their characteristics, thereby strengthening global disaster preparedness and response impacts. Additionally, scientific research on TCs contributes to a deeper understanding of how these extreme weather events are affected by climate change, helping us better adapt to the challenges they pose in a changing world.

The NIO is important in this study due to its unique geographical location, where warm sea surface temperatures provide ideal climatic conditions for TC formation. The region comprises two important basins: the AS and the BoB, both susceptible to TC formation (Rahaman et al., 2020; Jangir et al., 2021; Shenoi et al., 2002; Knutson et al., 2006). As a result, many TCs form in the NIO each year. Warm sea water continuously provides the energy needed for TCs to develop and grow rapidly. Under the increasing frequency of marine heat waves (Sen Gupta et al., 2020; Gupta et al., 2024; Rathore et al., 2022), the characteristic parameters of TCs may change and cause even more damaging impacts on the coast.

Additionally, TCs in the NIO are notorious for their ability to influence extreme rainfall. (Khouakhi et al., 2017). Among the components of a TC, wind significantly impacts the behavior, formation, and air dynamics movement of TCs.

Meteorologists and warning centers have been studying winds associated with TCs since the 19^{th} century, and there is still room for improvement in understanding and predicting dynamic wind's functionality (Tan and Fang, 2018). Accurate wind information is crucial for minimizing the human and economic losses caused by TCs (Knapp et al., 2010). One important wind-related parameter is the RMW (Hsu and Yan, 1998; Vickery and Wadhera, 2008). RMW is a crucial parameter in understanding the behavior of TCs. It is the distance from the storm's center to the location where the maximum sustained wind speed (MSW) peaks.

Additionally, RMW is closely related to a TC's size and structure. A smaller RMW indicates a more intense and well-organized storm with more rainfall, while a larger RMW may suggest a weaker or more disorganized system (Chavas and Knaff, 2022). Therefore, understanding the RMW is critical in assessing TCs' behavior and potential hazards, ultimately aiding in timely warnings and practical disaster response efforts in vulnerable regions.

Various studies have focused on predicting and estimating multiple aspects of TCs, including "intensity, sea surface temperature, moisture, precipitation, pressure systems, and cloud shapes;" only a few studies have centered on the RMW specifically over the Pacific (Tan and Fang, 2018; Gross et al., 2004) and Atlantic basin (Tan and Fang, 2018; Hsu and Yan, 1998; Quiring et al., 2011; Lajoie and Walsh, 2008). However, limited studies exist over NIO basins (Tan and Fang, 2018; Willoughby et al., 2006). All these studies have an extensive error range of -26% to 200% concerning the India Meteorological Department (IMD) best track data, which needs to be reduced further.

2.2 Literature Review

The RMW represents the radial extent from the cyclone's center to the point where the wind intensity peaks within the cyclonic circulation. This parameter serves as a primary metric for measuring the spatial dimensions of cyclonic systems. Within the $H10$ model equation framework, the RMW velocity is a critical determinant governing the pressure distribution and wind profile characteristics. Given the scarcity and difficulty in obtaining direct observational data on the RMW, empirical relationships derived from regional TC datasets have often been employed. These relationships establish the relationship between the RMW velocity and other cyclone parameters, which aid in the development of accurate estimates using numerical modeling. Each empirical formulation is briefly introduced below.

2.2.1 Graham's Empirical Formulation (1959)

In their study, Graham (1959) analyzed past TCs along the eastern coast of the United States and in the Gulf of Mexico. They examined how factors like central pressure, latitude, and the speed at which the cyclone moved affected the RMW speed. Based on their studies, a method was described to represent these relationships:

$$RMW = 28.52 \times tanh[0.0873(\theta - 28)] + 12.22 \times exp\left(\frac{P_c - 1013.2}{33.86}\right) + 0.2 \times V_t + 37.22 \quad (2.1)$$

where the symbol θ stands for geographical latitude of TC's center, V_t is the translation speed, P_n denotes the peripheral environment pressure, and P_c the central pressure of the TC. The unit for RMW is km, and the P_c unit is hectopascals (hPa).

2.2.2 Vickery's Empirical Formulation I

Vickery et al. (2000a) introduced a novel approach to evaluating hurricane risk in the United States. They utilized a storm reconstruction technique to simulate the trajectory of hurricanes from their formation over the ocean to their landfall. This method incorporates the hurricane's central pressure as dependent on the sea surface temperature. Its reliability was confirmed through on-site measurements. By comparing the modeled results with data gathered from two specific regions, one formulated in the form as:

$$RMW = exp(2.636 - 5.086 \times 10^{-5}(P_n - P_c)^2 + 3.94899 \times 10^{-2}\theta) \tag{2.2}$$

where variables follow the prior definitions.

2.2.3 Vickery's Empirical Formulation II

Vickery et al. (2000b) employed a dynamic model with a planetary boundary layer (PBL) to compute hurricane wind patterns. These computations were calibrated using data from aircraft detection and observations by the Hurricane Research Division (HRD). Following this calibration, they conducted a statistical analysis of the defining characteristics of hurricanes. Subsequently, they resolved a steady-state wind pattern across a series of nested rectangular grids utilizing a finite difference scheme.

Their study encompassed modeling 1560 hurricanes, considering various parameters such as the Holland B parameter within the range of 0.5 to 2.5, pressure differentials spanning from 1 to 150 millibars, an RMW speed ranging between 8 and 150 km/h, and translational velocities from 0 to 40 m/s. To refine their findings, they employed the Fourier fitting

method in the final stage, resulting in the proposed formulation for the RMW:

$$RMW = exp(3.015 - 6.291 \times 10^{-5}(P_n - P_c)^2 + 0.0337\theta) \tag{2.3}$$

where variables follow the prior definitions.

2.2.4 Willoughby and Ryan's Empirical Formulation

Willoughby and Rahn (2004) analyzed flight data from the U.S. NOAA Hurricane Research Division (HRD) from 1977 to 2000. They used 493 records of flight-level measurements taken during 606 instances of TC detection over the Atlantic and eastern Pacific Oceans. Their analysis focused on fitting the Holland80 ($H80$) model to these data using least squares analysis. They investigated how wind profiles correlate with various key parameter distributions.

By examining a frequency distribution histogram of the RMW, they determined that the RMW is a more suitable dependent variable for describing wind profiles. Additionally, they employed a multivariate normal distribution to establish an exponential relationship between the RMW and the maximum wind speed:

$$RMW = 51.6exp(-0.0223V_{fmax} + 0.0281\theta) \tag{2.4}$$

where the flight-level maximum wind speed V_{fmax} can be adjusted to a surface level according to Powell and Black (1990) for study in this paper.

2.2.5 Kato's Empirical Formulation

Kato (2005) examined the average and standard deviation of the radius where wind speed peaks, comparing it with past typhoon wind data. They also analyzed how this relates to storm surges along the Japanese coast. Their findings revealed that when the central pressure falls below 950 hPa, the RMW is $0.769 \times P_c - 650.55$. In contrast, when the central pressure exceeds 950 hPa, the radius is $1.633 \times P_c - 1471.55$. This relationship can be expressed more simply as follows:

$$RMW = 80 - 0.769(950 - P_c) \tag{2.5}$$

2.2.6 Powell's Empirical Formulation

Considering data archives spanning from 1900 to 2002, including NOAA HRD's surface wind real-time analysis from 1995 to 2002, HDR's aircraft observations from 1984 to 1987 along the western coast of the U.S. and Mexico, and the National Hurricane Center's best track records from 1988 to 1999, Powell et al. (2005) undertook a comprehensive analysis. They applied a multi-variable approach to investigate the logarithm of the observed RMW speed, which exhibited a normal distribution pattern. Consequently, they proposed an empirical formula linking Rm with pressure drop and latitude, expressed as:

$$RMW = exp[2.0633 + 0.0182(P_n - P_c) - 1.9008 \times 10^{-4}(P_n - P_c)^2 + 7.336 \times 10^{-4}\theta^2] \tag{2.6}$$

2.2.7 Knaff's Empirical Formulation

Knaff et al. (2007) utilized data from the U.S. National Hurricane Center (NHC) and Joint Typhoon Warning Center (JTWC) to analyze the radii of maximum wind speed observed in various TC occurrences. They adjusted parameters within the modified ranking vortex equation based on available data such as latitude, cyclone speed, maximum wind velocity, and the CLIPER model, which calculates the RMW across different latitudes. The resulting formula includes three constants that adapt according to the latitude of the cyclone's location. The specific formulation applicable to our study area is as follows:

$$RMW = m_0 + m_1 + m_2(\theta - 25) \tag{2.7}$$

where the three constants m_0, m_1, and m_2 are 38, -0.1167 and -0.004, respectively.

2.2.8 Li's Empirical Formulation

Due to the scarcity and irregularity of observational data collected along the Chinese coastline, particularly in non-standardized formats, statistical analysis is relevant in determining typhoon parameters specific to the study region. This approach is vital due to its focused and constraining nature. Li (2007) employed nonparametric statistical tests such as the Kolmogorov–Smirnov (K-S) and Chi-square tests to analyze the probability distribution of key typhoon parameters. From this analysis, Li proposed the RMW for the typhoon-vulnerable regions along the southern and eastern coasts of China.

$$RMW = exp[-0.163(P_n - P_c)^{0.555}] + 5.212 \tag{2.8}$$

2.2.9 Jiang's Empirical Formulation

Atkinson and Holliday (1977) conducted a study spanning 28 years, examining wind speed data collected from coastal and island stations across the western North Pacific. They formulated an exponential connection between the central pressure of cyclones and their maximum wind speeds. Building upon this framework, Jiang et al. (2008) explored TC occurrences between 1949 and 2002, as documented in the China National Typhoon Yearbook. Jiang proposed a comparable relationship, with modified parameters presented in a power exponential format inspired by the structure outlined by Atkinson and Holliday.

$$RMW = 1.119 \times 10^3 (P_n - P_c)^{-0.805} \tag{2.9}$$

2.2.10 Lin's Empirical Formulation

Lin and Fang (2013) analyzed data from 26 historical typhoon occurrences observed by ground-based meteorological stations in Hainan province, China. Their study aimed to establish an optimal empirical relationship for calculating the B parameter within the H80 model. Additionally, they investigated the spatial distribution characteristics of this parameter across the Northwest Pacific region, enhancing the applicability of the H80 model in China.

To facilitate the computation of the B parameter, which requires input on the RMW speed, Lin and Fang compiled a dataset comprising 6426 records of TC events occurring between 2001 and 2009. These records were sourced from the Joint Typhoon Warning Center (JTWC). Subsequently, they identified a relationship between the RMW speed and

pressure drop, expressed in a specific mathematical form:

$$RMW = -18.04 \times ln(P_n - P_c) + 110.22 \tag{2.10}$$

2.2.11 FEMA's Empirical Formulation

Vickery et al. (2000b) proposed a statistical model to utilize data on storms making landfall provided by the U.S. National Weather Service. This model aims to elucidate the correlation between the RMW speed and the storm center's central pressure and latitude. Subsequently, the U.S. Federal Emergency Management Agency (FEMA) refined this statistical model, introducing enhancements. The updated model offers a range of improvements to the understanding of maximum wind radius for specific storms in the Atlantic basin, such as Hurricane Mitch (1998), Brett (1999), Floyd (1999), and Gilbert (1988) (FEMA, 2018). The empirical relationship formulated from the revised model can be expressed as follows:

$$RMW = exp[2.556 - 5.026 \times 10^{-5}(P_n - P_c)^2 + 0.042\theta] \tag{2.11}$$

2.2.12 Zhou's Empirical Formulation

Zhou et al. (2018) aimed to predict storm surge levels along the Ningbo coast using a comprehensive numerical model. This model combines tidal patterns with storm surge effects caused by typhoons. They employed a nonlinear parameter determination technique to refine maximum wind speed radius estimates, converging iteratively from various initial values to a more accurate approximation. Their approach relied on a sparse dataset of pressure profile observations, with the empirical relationship primarily considering central

pressure, expressed as:

$$RMW = 29.178exp[0.0158(P_c - 900)] \tag{2.12}$$

Apart from the empirical formulas to calculate the RMW, some machine-learning techniques are also discussed in the literature. Those are briefly introduced below.

Lu et al. (2022) developed models using machine learning algorithms, including support vector machine and general regression neural network, to identify TC size parameters. The trained and optimized support vector machine models were proposed for the RMW and the radii of 34 (R34) knot winds, while the general regression neural network models were used for R50 and R64. The mean absolute errors for R34, R50, R64, and RMW were evaluated and verified against aircraft observations and Joint Typhoon Warning Center best track data. The mean absolute errors for R34 were 54 and 58 km, and the median errors were 39 and 46 km. The estimation accuracy for the RMW increased with the increasing intensity of the TC.

Wang and Li (2023) developed a deep learning model for estimating TC wind radii from geostationary satellite infrared imagery. It is based on a CNN architecture, specifically the VGGNet, and contains convolutional, pooling, and fully connected layers. The model takes both the original image and corresponding quadrant sub-images as input to capture the asymmetric structure of the TC. The model is trained using the backpropagation algorithm with a mean absolute error (MAE) loss function. The results show that the DL-TCR model significantly improves the estimation of TC wind radii, achieving MAEs of $18.5 - 19.1$ nautical miles for a 34 knot wind radius, $10.6 - 11.1$ nautical miles for a 50-knot wind radius, and $8.6 - 9.7$ nautical miles for 64-kt wind radius. Factors such as the TC eye,

cloud, and TC spiral structure influence the model's performance.

Xu et al. (2023) proposed a deep learning-based model for estimating the size of TCs by combining infrared and microwave satellite data. It uses a resnet-50 model as the basic framework. It incorporates a convolution layer with a 55 convolution kernel on the shortcut branch in its residual block for downsampling to avoid information loss. The model achieved a mean absolute error of 11.287 nautical miles and a Pearson correlation coefficient of 0.907.

As we focus on the NIOs, there are only two studies in the literature that centered on the RMW, which are as follows:

Willoughby et al. (2006) introduced an empirically derived model that describes the structure of the hurricane vortex. Their study also provided an expression for determining the RMW for the NIO basins.

The model's estimation equation for RMW (km^2) is:

$$RMW = 46.4 \times e^{(-0.0155V_{max}+0.0169\theta)} \tag{2.13}$$

where θ is latitude (degrees), V_{max} is the maximum wind speed (kt), and RMW is the RMW in km.

Tan and Fang (2018) focused on simulating wind fields of historical TCs using parametric models using satellite data. Their study provided an expression for determining the value of RMW for all seven basins.

[2]In this chapter, we first convert the RMW (km) into RMW (nautical miles) before using the Willoughby et al. 2006 equation.

The relation to determine the value of RMW (nautical miles) is:

$$RMW = -26.73 \times ln(1013.25 - P_c) + 142.41 \tag{2.14}$$

where P_c (hPa) is the estimated central pressure of TC

2.3 Data

This study evaluates a proposed method using the best track dataset obtained from the India Meteorological Department (IMD), the Regional Specialized Meteorological Center for TCs over the NIO. The India Meteorological Department (IMD) Best Track Data provides post-season, quality-controlled datasets documenting the life cycle of TCs over the NIO basin, encompassing the BoB and the AS. Each dataset entry includes TC center coordinates (latitude and longitude), maximum sustained surface wind speed (typically in knots), minimum central pressure (in hPa), and intensity classification following IMD's operational categories (e.g., Depression, Cyclonic Storm, Severe Cyclonic Storm). Earlier records (pre-1990s) generally offer 6-hourly observations, while more recent records are updated at 3-hour intervals. The compilation integrates diverse observational inputs, including surface synoptic observations, ship and buoy reports, coastal Doppler radar imagery, and critically, satellite-based estimates. Satellite data, essential over oceanic regions, primarily derives from geostationary satellites like the INSAT-3D and INSAT-3DR, providing high-frequency visible, infrared, and water vapor imagery. Supplementary data from polar-orbiting platforms such as NOAA's POES series, METOP, and NASA's Terra and Aqua (MODIS instruments) contribute higher spatial resolution observations, albeit at lower temporal frequency. Cyclone intensity assessments rely heavily on the Dvorak technique, which systematically interprets satellite cloud

patterns to estimate storm strength. Furthermore, scatterometer data (e.g., from ASCAT) and passive microwave imagery (e.g., AMSR2, SSMIS) provide critical insights into surface wind fields and inner-core structure. Collectively, these observation systems enable IMD to reconstruct a detailed and internally consistent best track dataset, which forms a foundational resource for climatological studies, operational forecasting validation, and long-term cyclone trend analysis across the North Indian Ocean region (India Meteorological Department (IMD), 2023; IMD, 2021).

The dataset consists of various metrics related to TCs, including the TC number, time (year, month, day, and hour), TC center locations (longitude and latitude), estimated central pressure (P_c), maximum wind speed (V_m), and estimated pressure drop at the center (P_d). These metrics are recorded at 6-hour intervals (`https://rsmcnewdelhi.imd.gov.in/report.php?internal_menu=MzQ=`). We use polynomial interpolation, i.e., Newton interpolation, to find some missing values of RMW in the best track database. For example, in the case of extremely severe cyclonic storm Tauktae, the value of RMW is available in the best track database for 14 May at 06 UTC. Next is 15 May at 00 UTC, so we find the values for 14 May at 12 and 18 UTC using Newton interpolation. To validate the proposed method, we also compared it with the RMW data from IMD bulletins.

According to the Standard Operational Procedure for Cyclone Warnings in India released by the IMD, there is no direct observation of RMW. Still, it can be calculated from the satellite and radar. In radar, the radius of maximum reflectivity is considered as RMW. In satellites, the radius of maximum reflectivity in visible imagery and the radius of the lowest cloud temperature in IR imagery is considered RMW (IMD, 2021).

2.4 Method

In this chapter, we propose two methods to estimate the RMW of the TC that formed over the NIO basin: the empirical formula and the machine learning technique.

2.4.1 Method I

We formulate a method for calculating the value of the RMW based on the characteristics of TCs, such as the latitude (Lat.) of the TC center, along with the estimated pressure drop. The choice of latitude and pressure drop as the critical parameters for RMW estimation, while excluding longitude, is grounded in empirical evidence and theoretical understanding within the field of TC research. Latitude is a fundamental indicator of TC formation and movement, with studies such as Camargo (2013) highlighting its role in determining TC genesis and tracks across different ocean basins. On the other hand, the pressure drop is closely linked to TC intensity, as discussed by Emanuel (2003). Conversely, while longitude influences TC position, its direct impact on TC intensity is less pronounced, as demonstrated by research such as Holland (1997) and Chavas et al. (2015), which emphasize the primary role of factors like sea surface temperature and atmospheric conditions in determining TC intensity. Therefore, this approach captures essential TC behavior and intensity aspects by focusing on latitude and pressure drop as crucial parameters.

The values of RMW for some TCs did not exist in most historical records until observations became available in 2001 (Knapp et al., 2010). The empirical function of RMW to the other TC variables, such as pressure drop at the center P_d and latitude, a rigorous analysis of relevant variables, and their impact of RMW over the NIO region which exists in studies of Agency (2012); Vickery and Wadhera (2008) is crucial. This analysis typically involves

collecting and analyzing observational data on TCs in the NIO, including parameters such as central pressure, wind speed, latitude, and RMW. Regression analysis is employed to identify the relationships between these variables. The analysis aims to quantify the influence of pressure drop and latitude coordinate of the TC center on RMW and drive mathematical equations that describe these relationships. Based on past studies over the NIO, the average ambient pressure was set to 1013.25 hPa (Islam and Peterson, 2008).

This relationship allows us to determine the value of RMW for estimated pressure drops (P_d) that are less than or equal to 12 hPa; it means that the atmospheric pressure at the center of the TC has decreased by 12 hPa or less compared to the surrounding environment. This pressure drop is often associated with increased cyclone intensity or strength.

Our design relationship for determining RMW (in nautical miles) is described as follows:

$$RMW = k \times e^{(a\sqrt{P_d}+b\phi)} + c \tag{2.15}$$

Here, ϕ represents the latitude coordinate of the TC center, and P_d represents the estimated pressure drop at the TC center.

These constants (k, a, b, and c) would be determined by taking a dataset of historical data of TC that includes the value of RMW, P_d, and ϕ over the NIO. By the non-linear least squares optimization method, we estimate the constants of the RMW equation (the equation of RMW is a non-linear equation). By utilizing the '$curve\_fit$' function from '*scipy.optimize*' (Virtanen et al., 2020), the code fits the experimental equation to the data, optimizing the parameters through an iterative process. The 'maxfev' parameter is increased to 10000, allowing for a higher number of function evaluations during the optimization

process, thereby enhancing the convergence of the solution. The estimated constants (k, a, b, and c) are then derived, providing insights into the underlying relationship between the variables. The least squares optimization method ensures robust parameter estimation and accurate modeling of the non-linear system. The graph visual of fitting the curve is shown in Fig. 2.1 with an R-squared of 0.92.

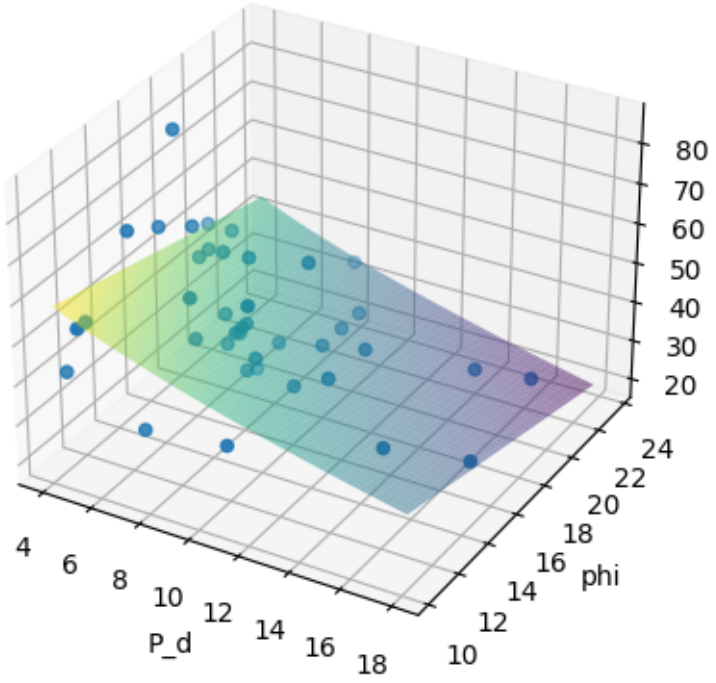

Figure 2.1: Fitted Function vs. Observed Data Points

The Final equation for determining RMW is:

$$RMW = -36640.61 \times e^{(0.00029\sqrt{P_d}+0.000029\phi)} + 36732.39 \tag{2.16}$$

This method provides a reliable means of calculating the RMW based on the given TC characteristics. The relationship established in this study allows for accurate determination of RMW as long as the value of P_d is less than or equal to 12 hPa.

To validate the accuracy of the proposed method, three evaluation techniques were employed: error percentage, statistical t-test, and root mean square error. We can confidently assert that the proposed approach outperforms alternative methods for determining RMW in the NIO region by utilizing these methods. Willoughby et al. (2006) and Tan and Fang (2018) also provided the RMW formula for the NIO region, as mentioned above in the literature. We compare our designed method with the models proposed by Willoughby et al. (2006) and Tan and Fang (2018) to fit explicitly for NIO cases.

t-test:

The t-test is a statistical test used to compare the means of two population samples to determine if there is a significant difference between them. In this paper, the t-test has been conducted to compare the proposed method with the other approaches. When the t-test indicates that one method is "statistically better" than another, the observed differences in their outcomes are unlikely to have occurred by chance. In other words, the differences are significant and not simply due to random variation. Null Hypothesis (H_o) assumes that there is no significant difference between the means of the two groups being compared. Alternative Hypothesis (H_a) is the opposite of the null hypothesis. To show that our method is statistically better, a significance level of 0.05 is utilized. For this analysis, we employed the Python language along with the numpy and scipy libraries to calculate the t-test effectively.

Error Percentage:

Error percentage, also known as error rate or relative error, measures the relative difference between predicted and actual values. It quantifies how far off the model's predictions

are from the ground truth. The error percentage can be calculated as follows:

$$\text{Error percentage} = \left(\frac{|\text{ Predicted Value} - \text{Actual Value }|}{\text{Actual value}} \right) \times 100$$

A lower error percentage indicates a more accurate model, which signifies that the model's predictions are closer to the actual values.

Root Mean Square Error (RMSE):

RMSE is a widely used metric to assess the accuracy of regression models. It measures the average magnitude of the errors between predicted and actual values. The RMSE is calculated as follows:

$$\text{RMSE} = \sqrt{\frac{1}{n} \times \sum (\text{Predicted Value} - \text{Actual Value})^2}$$

A lower RMSE indicates that the model's predictions are, on average, closer to the actual values. It represents the standard deviation of the model's errors.

In practice, the error percentage and RMSE are used to evaluate the accuracy and performance of machine learning models. While error percentage provides a relative measure of accuracy, RMSE provides an absolute measure of the model's predictive quality. Researchers and practitioners consider both metrics to assess their models' quality and make informed decisions about their performance.

2.4.2 Method II

Following this, we develop another approach for the computation of the value of the RMW through machine learning techniques, alongside the evaluation of the results obtained from the three methodologies such as Willoughby et al. (2006), Tan and Fang (2018), and resulting empirical formula of the method I.

In our model, the input is taken as the results of the three formulas in the literature: those by Willoughby et al. (2006), Tan and Fang (2018), and the resulting empirical formula of the method I. The target variable for the model is the RMW data provided by the India Meteorological Department.

Here is the whole process of our method (Flow chart of the proposed method is shown in Fig. 2.2):

Data Preprocessing:

Standardization (Ioffe and Szegedy, 2015) of the experimental data is performed to ensure that each feature follows a standard normal distribution. This is crucial for improving the convergence speed and performance of the models.

***k*-fold cross-validation:**

k-fold cross-validation is a robust technique used to evaluate machine learning models by partitioning the dataset into k equal-sized folds, training the model on $k-1$ folds, and validating it on the remaining fold, repeating this process k times. This method ensures each data point is used for training and validation, providing a comprehensive performance estimate and reducing the risk of overfitting. In this model, we use the value of k equal to 5 (Nti et al., 2021; Pohjankukka et al., 2017).

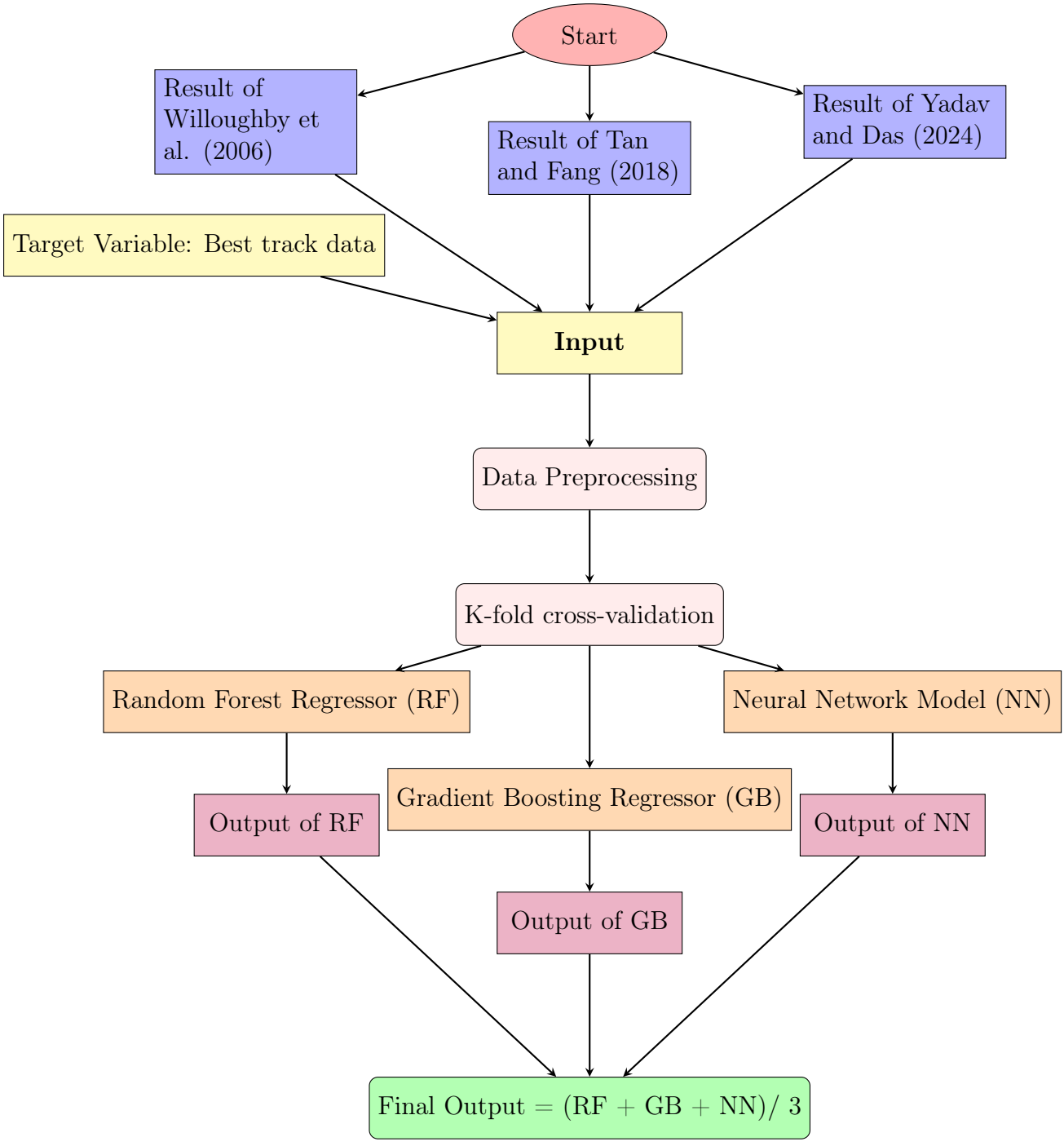

Figure 2.2: Flow-Chart of the Proposed Method for Estimating the Radius of Maximum Wind of the Tropical Cyclone

For Example, if $k = 5$, the dataset is divided into five folds. The model is trained on four folds and validated on the remaining fold. This process is repeated five times, with each fold serving as the validation set once.

- Iteration 1: Train on folds 2, 3, 4, 5; Validate on fold 1.
- Iteration 2: Train on folds 1, 3, 4, 5; Validate on fold 2.
- Iteration 3: Train on folds 1, 2, 4, 5; Validate on fold 3.
- Iteration 4: Train on folds 1, 2, 3, 5; Validate on fold 4.
- Iteration 5: Train on folds 1, 2, 3, 4; Validate on fold 5.

Model Construction:

Here is a detailed explanation of our model's architecture, component by component:

(a) Random Forest Regressor (RF):

This ensemble learning technique constructs multiple decision trees during training and outputs the average prediction of the individual trees. Random Forest (Breiman, 2001) helps to reduce overfitting and variance in the model by averaging the results from different decision trees.

(b) Gradient Boosting Regressor (GB):

Gradient Boosting (Friedman, 2001) is an ensemble technique that builds a robust model by combining multiple weak models. It sequentially adds predictors to an ensemble, and each one corrects its predecessor's errors. This method focuses on reducing bias and improving overall predictive performance.

(c) Neural Network Model (NN):

The neural network is a deep learning model inspired by the structure of the human brain. It consists of interconnected layers of nodes that process and transform input data. In this model, a deep neural network is constructed using the Keras API (Chollet

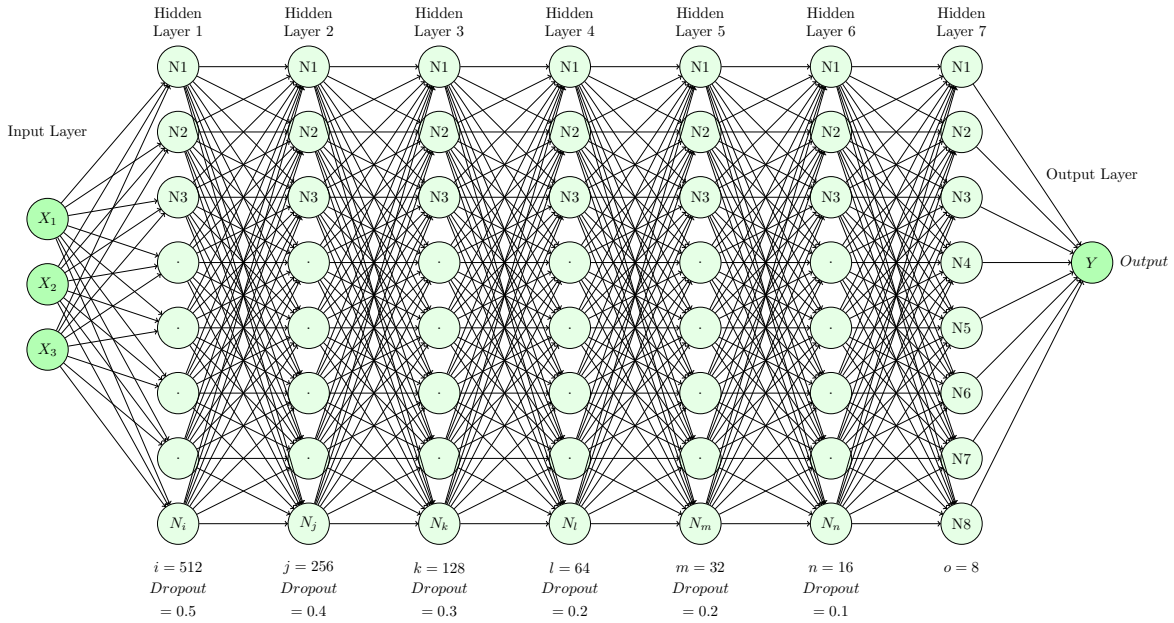

Figure 2.3: Architecture of Proposed Neural Network for Estimating the Radius of Maximum Wind

et al., 2015), consisting of multiple hidden layers with the rectified linear unit (ReLU) activation functions (Agarap, 2018). Dropout layers are included for regularization to prevent overfitting.

Here is a detailed explanation of the neural network's architecture (Fig. 2.3), layer by layer:

(i) **Input Layer:**

- The input layer has three nodes corresponding to the three features (experimental results: the results of the three methods we mentioned above) being fed into the network.

(ii) **Dense Layer** 1 **(Fully Connected Layer):**

- This layer consists of 512 neurons, each connected to all the nodes from the input layer. The ReLU activation function is applied to introduce non-linearity.
- Batch normalization is used to standardize the inputs to the next layer, which helps stabilize and accelerate the learning process.
- Dropout with a rate of 0.5 is implemented to prevent overfitting by randomly dropping half of the connections during each training step.

(iii) **Dense Layer** 2**:**

- The second dense layer comprises 256 neurons using the ReLU activation function and batch normalization.
- Dropout with a rate of 0.4 is applied.

(iv) **Dense Layer** 3**:**

- This layer consists of 128 neurons with ReLU activation and batch normalization.
- Dropout with a rate of 0.3 is applied.

(v) **Dense Layer** 4**:**

- The fourth dense layer has 64 neurons with ReLU activation and batch normalization.
- Dropout with a rate of 0.2 is applied.

(vi) **Dense Layer** 5**:**

- This layer contains 32 neurons with ReLU activation and batch normalization.
- Dropout with a rate of 0.2 is applied.

(vii) **Dense Layer** 6**:**

- The sixth layer has 16 neurons with ReLU activation and batch normalization.
- Dropout with a rate of 0.1 is applied.

(viii) **Dense Layer** 7**:**

- This layer consists of 8 neurons with ReLU activation and batch normalization.

(i) **Output:**

- The output layer has one neuron representing the predicted value.

The neural network model is trained to minimize the mean squared error (MSE) loss function using the Adam optimizer (Kingma and Ba, 2014). By configuring multiple hidden layers with different activation functions and applying batch normalization and dropout, the network can learn complex patterns in the data and generalize well to unseen examples, thereby improving the overall predictive performance.

(d) Training and Evaluation:

The models are trained using the provided experimental data (the results of the three methods mentioned above), and the performance is evaluated based on the MSE between the predicted and actual experimental results. The training process involves optimizing the model parameters through the backpropagation algorithm, minimizing the loss function, and updating the model weights iteratively.

(e) Ensemble Prediction:

The final ensemble prediction is generated by combining the predictions from the Random Forest, Gradient Boosting, and Neural Network models. This ensemble method leverages the diverse forecasts from different models to improve the overall predictive accuracy.

Combining these methodologies aims to enhance the predictive accuracy of experimental results by leveraging the strengths of ensemble learning and deep neural networks alongside traditional machine learning algorithms.

To check the accuracy of the designed model, we performed three statistical tests: error percentage, root square mean error, and R-squared. Section 2.4.1 provides a detailed discussion of error percentage and root square mean error.

R-squared (R^2):

R-squared (R^2), also known as the coefficient of determination, is a statistical measure that indicates the proportion of the variance in the dependent variable that is predictable from the independent variables in a regression model. It provides insight into the model's goodness of fit (Chicco et al., 2021). The value of R^2 ranges from 0 to 1, where:

- $R^2 = 1$ indicates that the model explains all the variability of the response data around its mean.

- $R^2 = 0$ indicates that the model explains none of the variability of the response data around its mean.
- Negative R^2 values can occur when the model is a poor fit and performs worse than a horizontal line representing the mean of the dependent variable.

2.5 Result

2.5.1 Result of Method I

The proposed method (Emiripical formula) for determining the value of RMW was evaluated using seven TC cases, namely: Extremely Severe Cyclonic Storm Tauktae (ESCS Tauktae), Cyclonic Storm Gulab (CS Gulab), Severe Cyclonic Storm Mandous (SCS Mandous), Severe Cyclonic Storm Asani (SCS Asani), Cyclonic Storm Sitrang (CS Sitrang), Cyclonic Storm Jawad (CS Jawad), and Very Severe Cyclonic Storm Yaas (VSCS Yaas). These specific cases were chosen to assess the proposed method's effectiveness accurately. Furthermore, Table 2.1 provides details regarding the category of each of these selected TCs, along with the corresponding periods.

Table 2.1: Category of selected TCs and period across the NIO basin

S. No.	Name	Category	Time Period
1	Tauktae	Extremely Severe Cyclonic Storm	14 - 19 May,2021
2	Gulab	Cyclonic Storm	24 - 28 September 2021
3	Mandous	Severe Cyclonic Storm	6 - 10 December, 2022
4	Asani	Severe Cyclonic Storm	07 - 12 May 2022
5	Sitrang	Cyclonic Storm	22 - 25 October, 2022
6	Jawad	Cyclonic Storm	02 - 06 December,2021
7	Yaas	Very Severe Cyclonic Storm	23 - 28 May, 2021

ESCS Tauktae

TC Tauktae, which formed in May 2021, was a powerful and destructive storm that primarily affected the Arabian Sea (AS) region and the western coast of India. It intensified into ESCS, boasting an MSW of $85-90$ knots with gusts reaching 100 knots. This TC was extraordinary in its path, causing widespread adverse weather conditions and damage across the entire west coast, including states, Union Territories, and Lakshadweep, as it tracked parallel to the west coast before crossing Gujarat. ESCS Tauktae experienced rapid intensification over 24 hours, from the morning of May 16^{th} (0530 IST/0000 UTC) to the morning of May 17^{th} (0530 IST/0000 UTC), with MSW increasing from 65 knots to 100 knots. The TC's peak MSW reached 100 knots, gusting to 113 knots between 0530 IST (0000 UTC) on May 17^{th} and 1130 IST (0600 UTC) on May 17^{th} over the east-central AS. During this period, the lowest estimated central pressure dropped to 950 hPa, representing a 50 hPa decrease compared to the surrounding region (Division, 2021c).

Our study, in conjunction with the methodologies proposed by Willoughby et al. (2006) and Tan and Fang (2018), as well as utilizing data sourced from the IMD, is visually presented in Fig. 2.4. This graphical illustration effectively conveys the significance of the parameter denoted as RMW. Complementing this visual representation, Table 2.2 provides a quantitative summary of the results obtained for the ESCS Tauktae.

Upon analyzing the average error across all cases concerning the IMD's average RMW of 41.28 nautical miles, our method demonstrates an error rate of 19.42%. In contrast, the approaches by Willoughby et al. (2006) and Tan and Fang (2018) exhibit error rates of 25.99% and 54.85%, respectively. Detailed root mean square error (RMSE) values are in Table 2.9.

Table 2.2: Results of ESCS Tauktae, where E_1 indicates the error percentage between the proposed method and IMD, E_2 represents the error percentage between Willoughby et al.'s expression and IMD, and E_3 represents the error percentage between Tan and Fang's expression and IMD

Date/ Time	IMD's RMW (nautical miles)	Proposed RMW (nautical miles)	Willoughby et al. RMW (nautical miles)	Tan and Fang RMW (nautical miles)	E_1 (%)	E_2 (%)	E_3 (%)
14/06	40	58.82	38.571	66.288	47.05	3.57	65.72
14/12	29	32.18	39.46	64.21	10.96	36.06	121.41
14/18	36	42.20	47.12	60.98	17.22	30.88	69.38
15/00	60	48.20	31.69	60.7136	19.66	47.18	1.18
15/06	60	44.123	29.65	58.30	26.46	50.58	2.83
15/12	32	35.92	25.785	53.10	12.25	19.42	65.93
15/18	32	31.24	24.207	50.4	2.37	24.35	57.5
Mean	41.28	41.81	33.78	59.14	19.42	25.99	54.85

Upon conducting a t-test, it is evident that our method is statistically better than the other two approaches with $\alpha = 0.05$, as the error percentage and RMSE are less.

CS Gulab

The formation of the cyclonic system known as "Gulab" occurred during the active phase of the monsoon season over the Indian subcontinent. Several favorable atmospheric conditions contributed to its development, including warm sea temperatures, the incursion of warm and moist air into the core of the system, which was a favorable Madden Julian Oscillation (MJO) phase, and relatively low to moderate vertical wind shear over the region (Division, 2021a).

Notably, the system had a shorter lifespan than the long-term average for cyclonic systems during the monsoon season over the Bay of Bengal. Specifically, its duration was approximately 90 hours, while the long-term average span of the cyclone, based on the data from 1990 to 2013, stands at 110 hours. Additionally, the peak intensity of Cyclone Gulab

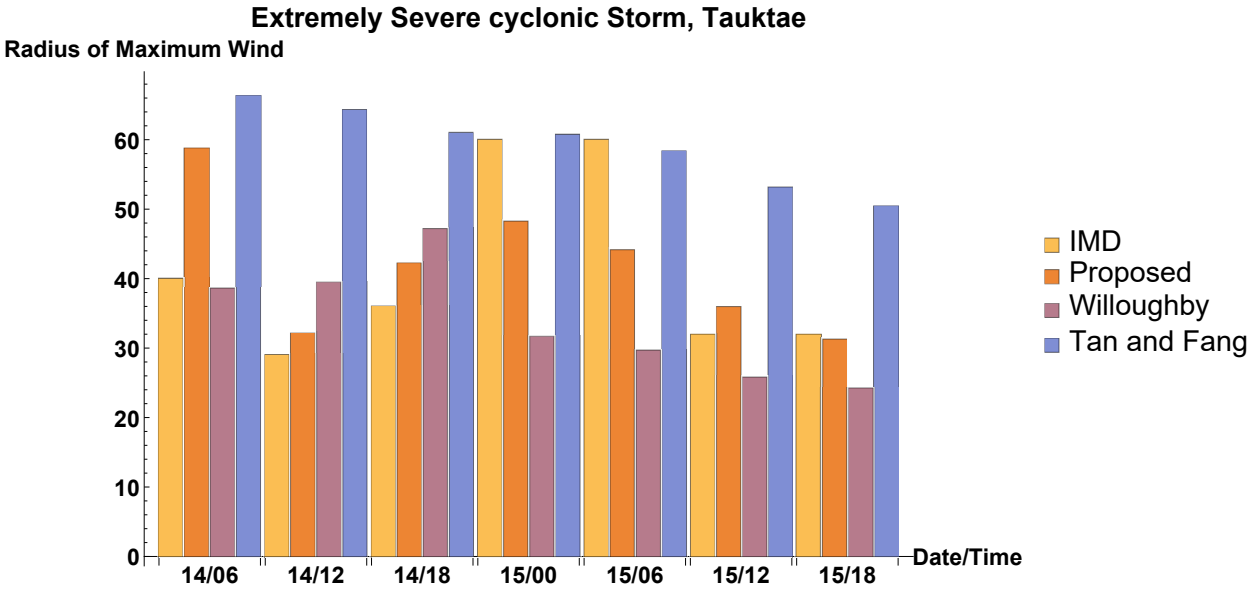

Figure 2.4: Graphical Representation of ESCS Tauktae's value of RMW by proposed method, Willoughby et al., Tan and Fang, and IMD

reached 45 knots, occurring between 0600 and 1200 UTC on the 26^{th} September.

Our methodology, in conjunction with the techniques proposed by Willoughby et al. (2006) and Tan and Fang (2018), and the utilization of data provided by the IMD, is visually illustrated in Fig. 2.5, this graphical representation effectively demonstrates the significance of the (RMW). Table 2.3 complements this visual representation by providing a quantitative summary of the results for CS Gulab.

Upon analyzing the average error across all cases concerning IMD's reference value for the RMW at 32.12 nautical miles, our methodology yields an average error of 28.49%. In contrast, Willoughby et al. (2006) and Tan and Fang (2018) methods exhibit average errors of 41.37% and 128.62%, respectively. The RMSE values are detailed in Table 2.9.

Furthermore, a t-test analysis indicates that our proposed methodology statistically outperforms the alternative methods, consistently yielding lower error percentages and RMSE values.

Table 2.3: Results of CS Gulab, where E_1 indicates the error percentage between our method and IMD, E_2 represents the error percentage between Willoughby et al.'s expression and IMD, and E_3 represents the error percentage between Tan and Fang's expression and IMD

Date/ Time	IMD's RMW (nautical miles)	Proposed RMW (nautical miles)	Willoughby et al. RMW (nautical miles)	Tan and Fang RMW (nautical miles)	E_1 (%)	E_2 (%)	E_3 (%)
25/00	55	40.85	40.55	71.39	25.72	26.27	29.8
25/06	55	39.78	40.55	71.39	27.67	26.27	29.8
25/12	24	34.84	37.55	65.28	45.16	56.45	174.5
25/18	24	34.84	37.55	66.28	45.16	56.45	176.16
26/00	30	37.78	34.84	63.35	25.93	16.13	111.16
26/06	24	30.53	32.38	60.71	27.20	34.91	152.95
26/12	24	30.53	32.38	60.71	27.20	34.91	152.95
26/18	21	28.72	37.62	63.35	36.76	79.14	201.66
Mean	32.12	34.73	31.98	65.31	32.60	41.37	128.62

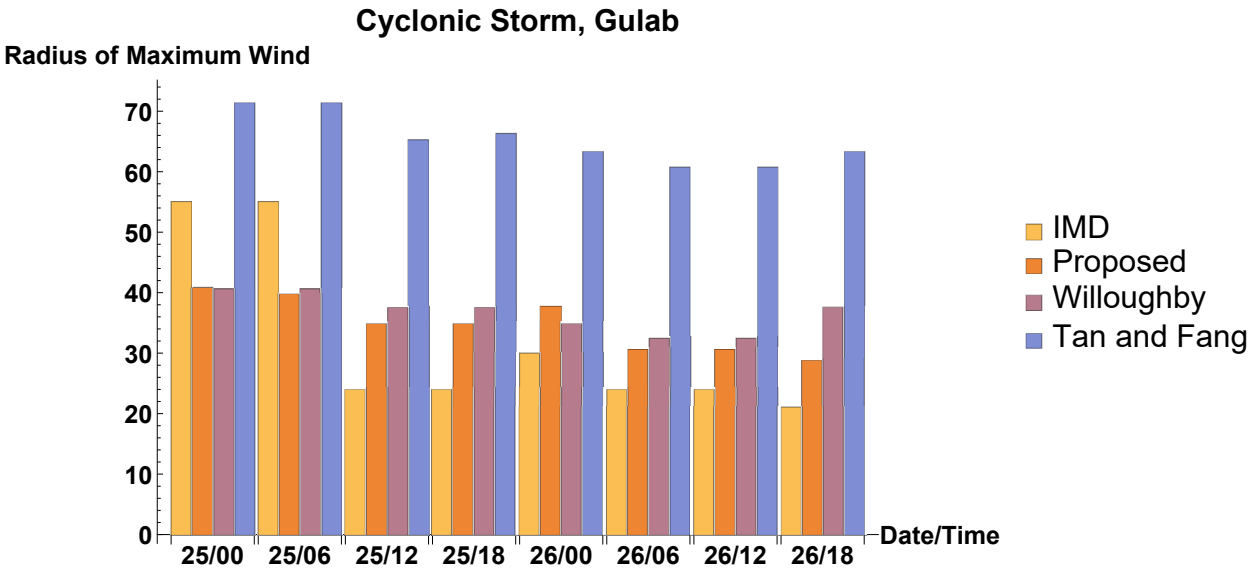

Figure 2.5: CS Gulab's value of RMW given by proposed method, Willoughby et al., Tan and Fang, and IMD is graphically represented

SCS Mandous

In December, the Bay of Bengal typically witnesses the formation of approximately 25 TCs, including 15 SCS. Nine of these 25 TCs made landfall along the Tamil Nadu coast. One of them initially started as depression, one as a CS, and the remaining seven as SCSs. Among these, Mandous was one of the SCSs that made landfall.

Mandous followed a unique track. Initially, it moved in a west-northwest direction until the evening of December 7^{th}, at 1730 hours IST. Afterward, it changed its course to the northwest until it made landfall. Following landfall, the system altered its trajectory to move west-northwest until the morning of December 10^{th} at 0530 hours IST, after which it headed west-southwest.

This distinct movement pattern can be attributed to the influence of an anticyclone storm raised in the northeast direction of the storm's center in the middle and upper tropospheric levels, which steered the system over the sea.

The duration of Mandous's existence as a storm, from its initial formation stage to its subsequent status as a depression, spanned approximately 96 hours, equivalent to 4 days. This duration is closely aligned with the long-term average $(1990-2013)$ for Severe Cyclonic Storms in the Bay of Bengal during the post-monsoon season, which also stands at about 96 hours or four days. The system did not exhibit rapid intensification or weakening during its life cycle. Mandous achieved its peak intensity of 50 knots at 1200 UTC on December 8^{th} and maintained this strength until 0000 UTC on December 9^{th} (Division, 2022c).

Our study incorporates a methodology, in conjunction with the methods proposed by Willoughby et al. (2006) and Tan and Fang (2018), and utilizing data provided by the IMD.

These approaches are visually illustrated in Fig. 2.6, presenting a graphical representation highlighting the parameter's significance (RMW). Furthermore, Table 2.4 offers a quantitative summary of the results of SCS Mandous.

Upon calculating the average error for all cases concerning the IMD's average RMW of 40.46 nautical miles, our method exhibits an error rate of 29.63 %. At the same time, Willoughby et al. (2006) and Tan and Fang (2018) methods exhibit error rates of 35.80% and 79.23%, respectively. The Root Mean Square Error (RMSE) values are presented in Table 2.9.

The t-test reveals that our proposed method demonstrates statistically superior performance compared to the alternative methods, as evidenced by its lower error percentage and RMSE.

Table 2.4: Results of SCS Mandous over BoB during $6-10$ December 2022, where E_1 indicates the error percentage between the proposed method and IMD, E_2 represents the error percentage between Willoughby et al.'s expression and IMD, and E_3 represents the error percentage between Tan and Fang's expression and IMD

Date/ Time	IMD RMW (nautical miles)	Proposed RMW (nautical miles)	Willoughby et al. RMW (nautical miles)	Tan and Fang RMW (nautical miles)	E_1 (%)	E_2 (%)	E_3 (%)
07/00	64	55.28	30.36	71.39	13.62	52.56	11.54
07/06	64	55.10	31.41	69.58	13.90	50.93	8.71
07/12	64	53.68	31.53	69.58	16.12	50.73	8.71
07/18	34	42.09	29.203	67.88	23.7	14.12	76.82
08/00	34	40.67	28.97	64.78	19.6	14.79	90.52
08/06	34	38.03	27.95	60.71	11.8	12	78.55
08/12	22	35.23	30.15	58.309	60.1	37.045	165.04
08/18	22	34.40	31.33	58.309	51.6	34.68	165.04
09/00	22	38.75	31.509	58.309	76.1	43.22	165.04
09/06	34	44.24	28.76	60.71	30.1	15.41	78.55
09/12	34	45.37	29.32	62.002	10.61	13.76	82.35
09/18	34	46.74	30.05	64.781	33.4	11.16	90.53
10/00	64	48.27	32.95	69.58	24.57	48.51	8.71
Mean	40.46	44.45	31.03	64.30	29.63	35.80	79.23

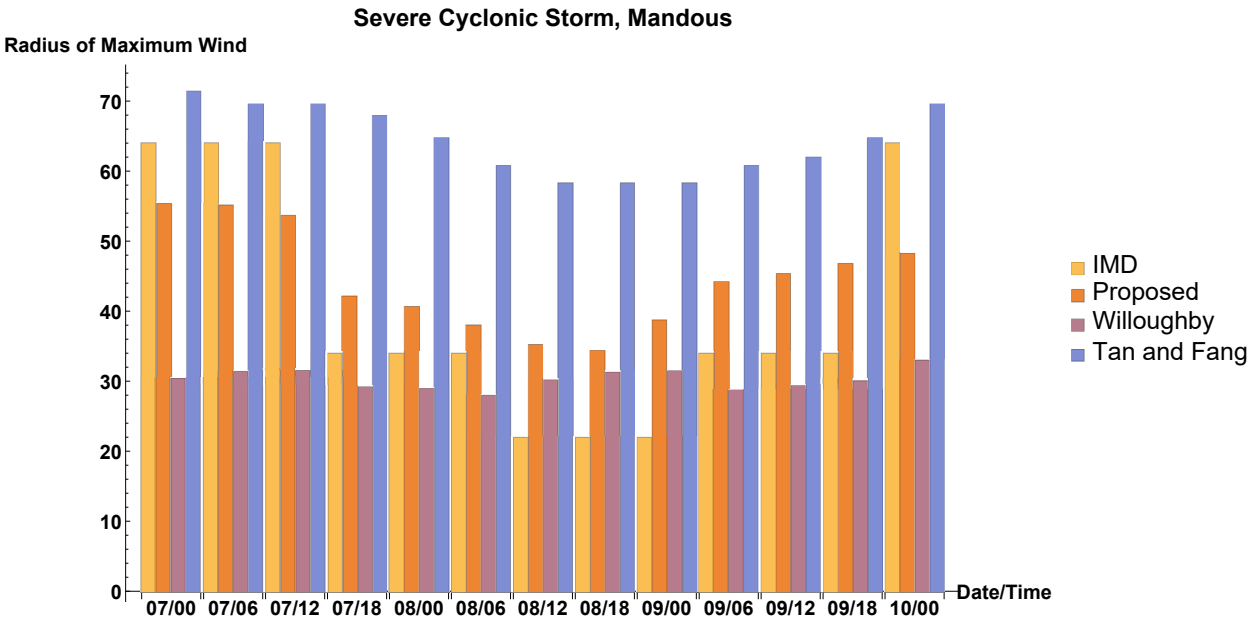

Figure 2.6: SCS Mandous's value of RMW given by proposed method, Willoughby et al., Tan and Fang, and IMD data are graphically represented

SCS Asani

On the morning of May 6^{th}, 2022, a low-pressure area began to develop over the South Andaman Sea and the adjoining Southeast Bay of Bengal (BoB). By the early morning of May 7^{th}, it had intensified into a well-marked low-pressure area over the Southeast BoB and the adjacent South Andaman Sea. Favorable environmental conditions allowed it to consolidate further, eventually becoming a depression around noon on the same day, May 7^{th}, 2022. This system, named SCS "Asani," transformed into a deep depression before making landfall. Remarkably, it exhibited an unusually slow movement, crawling at $5-6$ km per hour, significantly slower than the typical speed of 13 km per hour. This sluggish pace kept it hovering within 50 km of the coastline from morning to evening on May 11^{th}.

SCS "Asani" displayed multiple shifts in its trajectory. Most meteorological models had initially predicted a change in its direction, veering from northwest to northeast near the coast. It initially moved northward/northwestward and later shifted to a west-southwestward

direction. This unexpected change was primarily influenced by the system's response to a short amplitude westerly trough in the middle and upper tropospheric levels approaching from the west, causing it to deviate from the anticipated northeastward path near the coast (Division, 2022b).

Our study introduces a novel methodology visually presented in Fig. 2.7, alongside existing approaches proposed by Willoughby et al. (2006) and Tan and Fang (2018), and data sourced from the IMD. This graphical representation effectively illustrates the significance of the RMW. To complement this visual insight, Table 2.5 provides a quantitative summary of the results on SCS Asani.

When comparing the average error of our method to the IMD's average RMW value of 40.71 nautical miles, our method exhibits an error percentage of 15.92%. At the same time, the approaches presented by Willoughby et al. (2006) and Tan and Fang (2018) yield error percentages of 19.25% and 59.15%, respectively. Additionally, Table 2.9 presents the RMSE values for these methods. Statistical analysis using a t-test demonstrates that our proposed method performs better than the alternative methods, consistently yielding lower error percentages and RMSE values.

CS Sitrang

In the early morning of October, 20 2022, a low-pressure area developed over the North Andaman Sea and extended into the South Andaman Sea and Southeast BoB. By the evening of October 21, it had intensified into a well-marked low-pressure area, still situated over the North Andaman Sea and the adjoining Southeast BoB. As favorable environmental conditions persisted, this system gradually concentrated and formed a depression over the

Table 2.5: Results of SCS Asani over BoB during $07-12$ May 2022, where E_1 indicates the error percentage between the proposed method and IMD, E_2 represents the error percentage between Willoughby et al.'s expression and IMD, and E_3 represents the error percentage between Tan and Fang's expression and IMD

Date/ Time	IMD RMW (nautical miles)	Proposed RMW (nautical miles)	Willoughby et al. RMW (nautical miles)	Tan and Fang RMW (nautical miles)	E_1 (%)	E_2 (%)	E_3 (%)
07/12	55	57.05	35.303	64.78	3.72	35.81	17.78
07/18	55	56.52	35.66	63.35	2.76	35.16	15.18
08/00	30	41.63	33.31	60.71	38.76	11.03	102.6
08/06	30	35.61	28.86	56.10	18.70	3.8	87.01
11/00	30	33.03	30.98	56.10	10.10	3.26	87.01
11/06	30	38.18	33.51	58.30	27.26	11.7	94.36
11/12	55	49.40	36.309	60.71	10.18	33.98	10.38
Mean	40.71	44.48	32.41	60.01	15.92	19.25	59.15

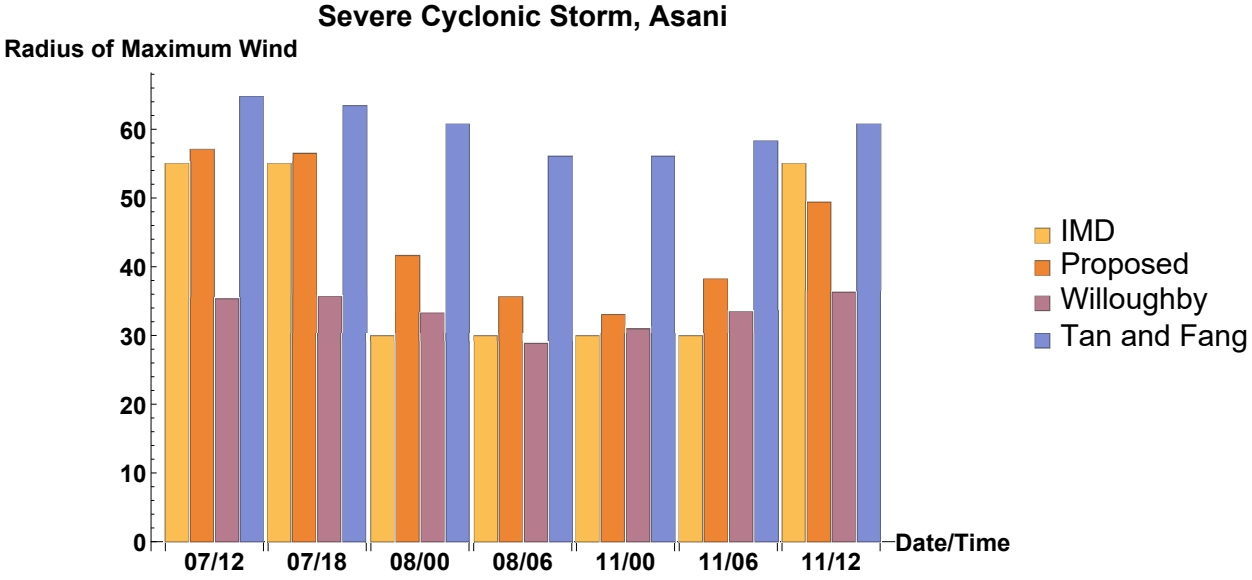

Figure 2.7: SCS Asani's value of RMW given by proposed method, Willoughby et al., Tan and Fang, and IMD is graphically represented

Southeast and the neighboring east-central BoB, near the Andaman Islands, by the forenoon of October 22, 2022.

This weather system, CS Sitrang, initially moved northwestward due to the influence of southeasterly winds in the middle and upper tropospheric levels. This pattern continued until the morning of October 23. Subsequently, a gradual change in its trajectory occurred as it started to recurve north-northeastwards from the night of October 23. This shift was attributed to a trough in the western direction and an anticyclone located to the east of Myanmar.

On the 24^{th} of October, CS Sitrang exhibited exceptionally rapid movement due to several factors, including the influence of a westerly trough, an anticyclone over Myanmar, and interactions with the land. The entire lifespan of this storm, from its formation as a depression to another depression, lasted approximately 69 hours, which equates to 2 days and 21 hours. This duration was shorter than the long-term average for cyclonic storms in the Bay of Bengal during the post-monsoon season, about 88 hours or 3 days and 16 hours, based on data from 1990 to 2013 (Division, 2022a).

Our methodology, in conjunction with the techniques introduced by Willoughby et al. (2006) and Tan and Fang (2018), and utilizing data from the IMD, its characteristics are visually presented in Fig. 2.8. This graphical illustration effectively demonstrates the significance of the (RMW). Complementing this visual representation, Table 2.6 provides a numerical summary of the results of the CS Sitrang.

Regarding the average error compared to IMD's average RMW of 40.00 nautical miles, our methodology yields an error rate of 15.21%. At the same time, the methods proposed by Willoughby et al. (2006) and Tan and Fang (2018) exhibit error rates of 18.42% and

Table 2.6: Results of CS Sitrang over the BoB during $22-25$ October 2022, where E_1 indicates the error percentage between the proposed method and IMD, E_2 represents the error percentage between Willoughby et al.'s expression and IMD, and E_3 represents the error percentage between Tan and Fang's expression and IMD

Date/ Time	IMD RMW (nautical miles)	Proposed RMW (nautical miles)	Willoughby et al. RMW (nautical miles)	Tan and Fang RMW (nautical miles)	E_1 (%)	E_2 (%)	E_3 (%)
23/00	64	44.87	36.48	75.43	29.88	43	17.85
23/06	64	43.00	36.87	73.33	32.80	42.39	14.57
23/12	34	41.14	38.55	71.39	21.01	13.38	109.97
23/18	34	40.10	36.92	69.58	17.96	8.58	104.64
24/00	34	37.09	31.66	66.28	9.10	6.88	94.94
24/06	34	34.42	30.87	66.28	1.26	9.20	94.94
24/12	34	32.99	29.55	66.28	2.95	13.08	94.94
24/18	34	31.71	30.29	66.28	6.70	10.91	94.94
Mean	41.5	38.16	27.11	55.48	15.21	18.42	62.679

62.67%, respectively. The RMSE values are detailed in Table 2.9.

Further statistical analysis using a t-test indicates that our proposed methodology significantly outperforms the other methods, as evidenced by lower error percentages and RMSE values.

CS Jawad

In 2021, TC Jawad held the distinction of being the 5^{th} TC observed over the NIO. Additionally, it marked the first TC occurrence during the post-monsoon season, which typically spans from October to December. Interestingly, December had no recorded instances of a TC making landfall in Odisha in the historical records. Instead, these cyclones typically made landfall over the northern regions of Andhra Pradesh and south of West Bengal.

Even without landfall, Odisha experienced the impact of TCs in previous years, primarily in heavy rainfall. The genesis of most TCs occurred over the southern BoB and the southern

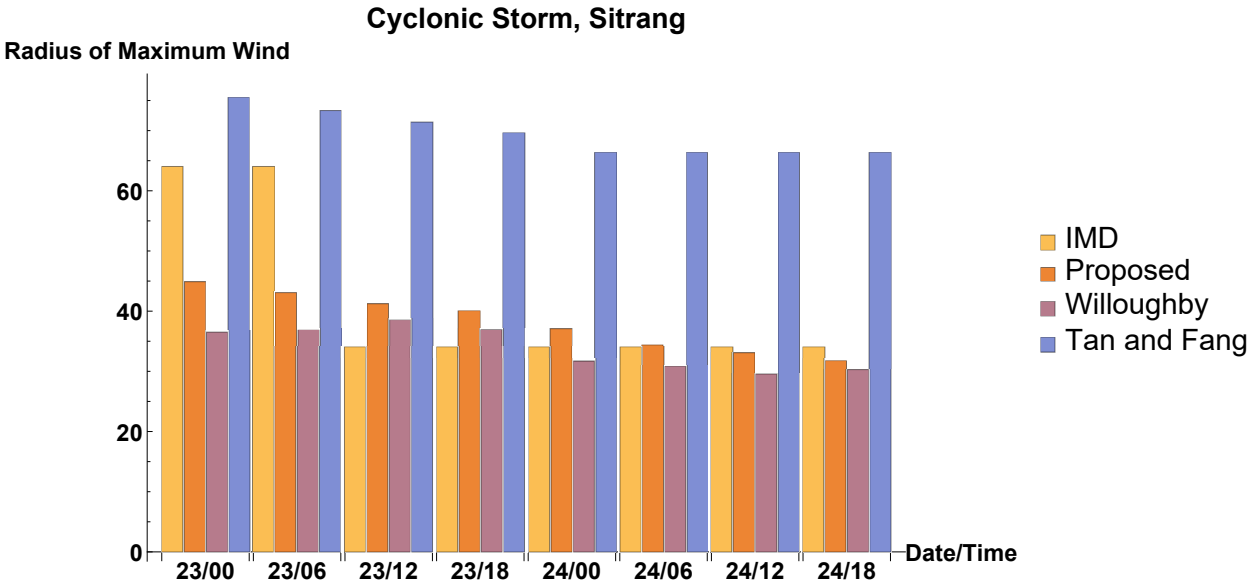

Figure 2.8: CS Sitrang's value of RMW given by proposed method, Willoughby et al., Tan and Fang, and IMD is graphically represented

Andaman Sea. When these occurrences reached a latitude beyond 15 degrees North in the Bay of Bengal, they tended to alter their course, curving north-northeastward.

This pattern of CS Jawad was similarly observed in the case of other occurred TCs, and it initially moved north-northwestward and began to recurve on the morning of the 4^{th} day (at 0530 hours IST/0000 UTC). The peak MSW of TC Jawad was recorded at 40 knots, with gusts reaching up to 50 knots between the 3^{rd} and 4^{th} days (from 1200 UTC on the 3^{rd} to 0000 UTC on the 4^{th}).

On the 4^{th} day at 0600 UTC, Dhamra Port reported south-southeastern winds with an intensity of 32 knots, gusting to 35 knots. Subsequently, the cyclonic system began to weaken due to unfavorable conditions, including enhanced wind shear, the incursion of dry air into the core of the system, lower ocean thermal energy, interactions with land, and an unfavorable Madden-Julian Oscillation index (Division, 2021b).

Our study incorporates a methodology and utilizes previously proposed approaches by Willoughby et al. (2006) and Tan and Fang (2018) in conjunction with data sourced from

Table 2.7: Results of CS Jawad over the BoB during $02-06$ December 2021, where E_1 indicates the error percentage between the proposed method and IMD, E_2 represents the error percentage between Willoughby et al.'s expression and IMD, and E_3 represents the error percentage between Tan and Fang's expression and IMD

Date/ Time	IMD RMW (nautical miles)	Proposed RMW (nautical miles)	Willoughby et al. RMW (nautical miles)	Tan and Fang RMW (nautical miles)	E_1 (%)	E_2 (%)	E_3 (%)
03/00	69	53.76	36.26	77.71	22.08	47.44	12.62
03/12	42	48.23	32.23	73.33	14.83	23.26	74.59
03/06	42	45.22	33.21	75.43	7.66	20.92	79.59
03/18	42	44.80	32.45	73.33	6.66	22.73	74.59
04/00	42	44.48	31.62	73.33	5.90	24.71	74.59
04/06	42	46.21	31.37	75.43	10.02	25.30	79.59
04/12	55	57.05	35.53	77.71	3.72	35.40	41.29
Mean	47.71	48.53	33.23	75.18	10.12	28.53	62.41

the IMD. These elements are visually represented in Fig. 2.9, highlighting the significance of the RMW. Supplementary to this visual representation, Table 2.7 provides a numerical summary of the results of the CS Jawad.

When assessing the average error across all cases in comparison to IMD's average RMW of 47.17 nautical miles, our method yields an error rate of 10.12%, whereas the methods of Willoughby et al. (2006) and Tan and Fang (2018) report error rates of 28.53% and 62.41%, respectively. Table 2.9 presents the RMSE values.

Statistical analysis, specifically the t-test, indicates that our proposed method exhibits statistically superior performance compared to the alternative methods, demonstrating lower error percentages and RMSE values.

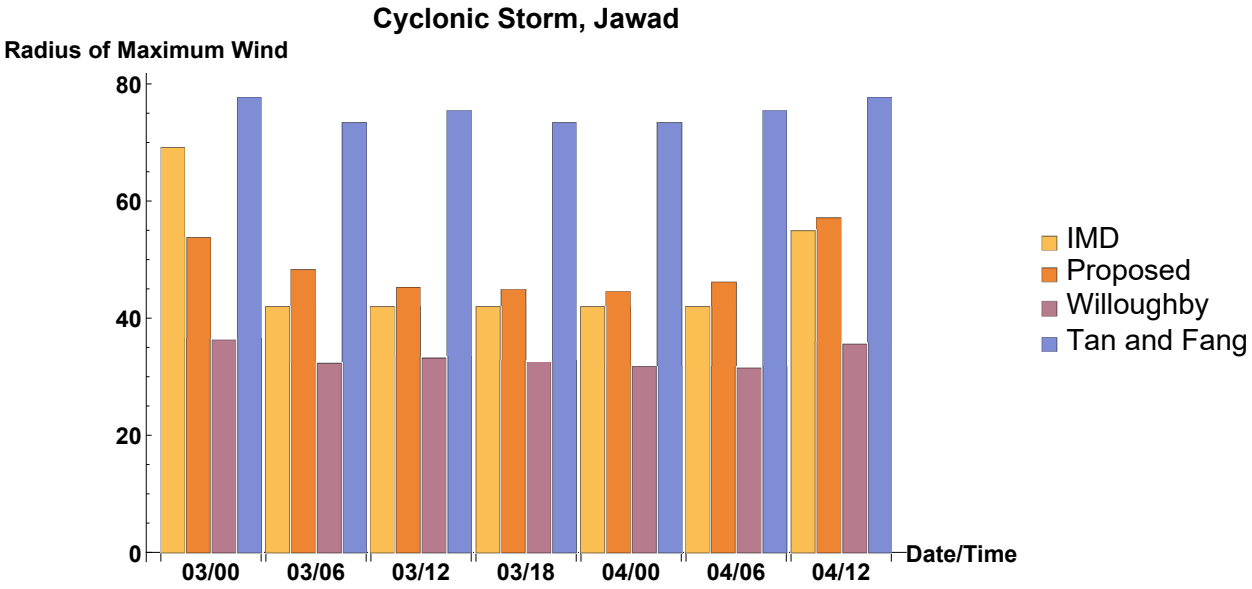

Figure 2.9: CS Jawad's value of RMW given by proposed method, Willoughby et al., Tan and Fang, and IMD is graphically represented

VSCS Yaas

Four days after the landfall of ESCS Tauktae dissipated over the Arabian Sea, TC Yaas emerged in the BoB. This occurrence of consecutive or simultaneous TCs in the BoB and the AS is not uncommon. When we examine the statistical data from the past decade $(2010 - 2020)$, we find instances of similar back-to-back or simultaneous appearances of VSCS over both the Bay of Bengal and the Arabian Sea in the years 2020, 2019, 2018, 2016, 2015, 2013, and 2010.

TC Yaas had a relatively minor impact on the affected regions compared to Tauktae. It brought adverse weather conditions to the Andaman and Nicobar Islands, Odisha, and West Bengal until the 26^{th} May, followed by cyclonic disturbances in Jharkhand, Bihar, and East Uttar Pradesh after making landfall. The TC followed a straight north-northwestward trajectory. TC Yaas exhibited MSW to 75 knots during its peak intensity period, gusting to 85 knots. This intense phase occurred from 0230 IST on the 26^{th} to 1130 IST on the

same day, situated in the northwest Bay of Bengal. At its most potent, the cyclone's central pressure reached an estimated low of 970 hPa, indicating a 28 hPa drop in pressure compared to its surrounding environment (Division, 2021e).

Interestingly, TC Yaas experienced rapid weakening after landfall, with its intensity decreasing by 35 knots in a mere nine-hour span. Remarkably, the system maintained VSCS intensity even after landfall for 12 hours, lasting from 0600 to 1800 UTC on the 26^{th}.

Our approach, in conjunction with methodologies introduced by Willoughby et al. (2006) and Tan and Fang (2018), and data sourced from the IMD, is visually represented in Fig. 2.10. This graphical representation effectively illustrates the significance of RMW. Complementing this visualization, Table 2.8 provides a numerical summary of the findings of the VSCS Yaas.

In assessing the average error across all cases concerning the IMD's average RMW at 53.28 nautical miles, our method yields an error rate of 24.45%. In contrast, the methods proposed by Willoughby et al. and Tan and Fang result in error rates of 38.17% and 29.10%, respectively. Table 2.9 presents the RMSE values.

Statistical analysis through a t-test demonstrates that our proposed method exhibits superior performance compared to the alternative methods, as evidenced by lower error percentages (Table 2.10) and RMSE values (Table 2.9).

As we discussed above, the seven selected TCs over the NIO were used to examine the accuracy of our method with other methods. We perform three tests (error percentage, t-test, and root square mean error) to support the idea that our method for determining the RMW is better than the existing methods. Our method performs significantly better than previously available; even if it still has a relatively high error rate, it may represent

Table 2.8: Results of VSCS YAAS over the BoB during $23-28$ May 2021, where E_1 indicates the error percentage between the proposed method and IMD, E_2 represents the error percentage between Willoughby et al.'s expression and IMD, and E_3 represents the error percentage between Tan and Fang's expression and IMD

Date/ Time	IMD RMW (nautical miles)	Proposed RMW (nautical miles)	Willoughby et al. RMW (nautical miles)	Tan and Fang RMW (nautical miles)	E_1 (%)	E_2 (%)	E_3 (%)
23/18	85	50.67	39.13	60.71	40.38	53.96	28.57
24/00	58	46.31	35.309	48.309	20.15	39.13	16.70
24/06	58	44.26	32.74	26.103	23.68	43.56	54.99
24/12	58	39.97	30.67	50.06	31.06	47.12	13.68
24/18	38	36.22	28.63	52.17	4.68	24.65	37.28
25/00	38	29.77	27.68	48.74	21.65	27.15	28.26
25/06	38	26.77	25.98	47.18	29.55	31.63	24.15
Mean	53.28	39.13	40.35	42.15	24.45	38.17	29.10

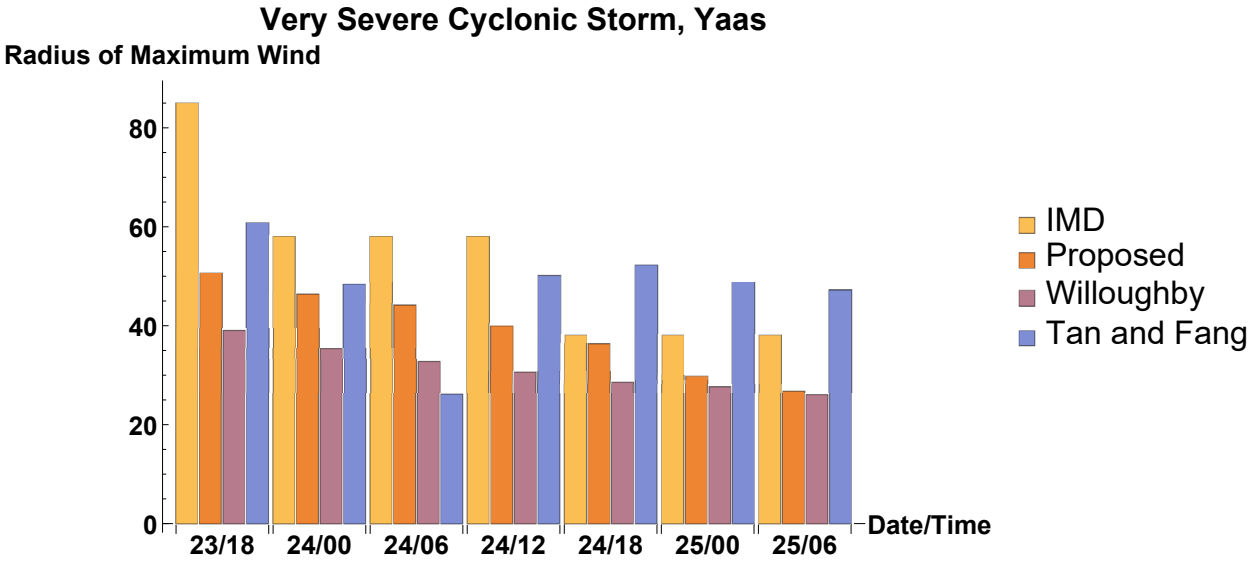

Figure 2.10: VSCS Yaas's value of RMW given by proposed method, Willoughby et al., Tan and Fang, and IMD is graphically represented

Table 2.9: The RMSE value of Our Method with respect to (w.r.t.) IMD, Willoughby et al. w.r.t. IMD, and Tan and Fang w.r.t. IMD

Name of TC	Our Method w.r.t. IMD	Willoughby et al. w.r.t. IMD	Tan and Fang w.r.t IMD
Tauktae	10.75	17.14	21.84
Gulab	10.06	12.37	34.69
Mandous	15.9	18.17	32.37
Asani	6.33	12.74	21.73
Sitrang	10.67	14.01	29.68
Jawad	6.73	16.63	28.71
Yaas	17.01	24.91	17.59

Table 2.10: The Mean Absolute Error Percentage value of Our Method with respect to (w.r.t.) IMD, Willoughby et al. w.r.t. IMD, and Tan and Fang w.r.t. IMD

Name of TC	Our Method w.r.t. IMD	Willoughby et al. w.r.t. IMD	Tan and Fang w.r.t IMD
Tauktae	19.42	25.99	54.85
Gulab	32.60	41.37	128.62
Mandous	29.63	35.80	79.23
Asani	6.33	12.74	21.73
Sitrang	15.21	18.42	62.679
Jawad	10.12	28.53	62.41
Yaas	24.45	38.17	29.10

progress. This improvement signifies a significant step in understanding and predicting TC behavior in the NIO region. Additionally, if the method is adopted, it should be viewed as a starting point, with opportunities for further enhancement and error reduction.

2.5.2 Result of Method II

We present a comprehensive analysis of the performance of various methodologies for estimating the RMW in the context of three specific TCs: Severe Cyclonic Storm Mandous (SCS Mandous), Severe Cyclonic Storm Sitrang (SCS Sitrang), and Extremely Severe Cyclonic Storm Mocha (ESCS Mocha). Our study evaluates these methods by comparing their error percentages and RMSE based on the data obtained from the IMD.

Table 2.11: Details of Selected Tropical Cyclones for validation

Name of TC	Category	Time period
Mandous	Severe Cyclonic Storm (SCS)	06^{th}˘10^{th} December, 2022
Sitrang	Severe Cyclonic Storm (SCS)	$22^{th} - 25^{th}$ October, 2022
Mocha	Extremely Severe Cyclonic Storm (ESCS)	$9^{th} - 15^{th}$ May, 2023
Remal	Severe Cyclonic Storm (SCS)	$24^{th} - 28^{th}$ May, 2024

SCS Mandous

The Mandous Cyclone (Table 2.11), a disturbing meteorological phenomenon known for its intense winds and significant impact on coastal regions, served as a primary case study for our analysis (Division, 2022c). It followed a unique track illustrated in Fig. 2.11. Employing our proposed method, we achieved an error percentage of 10.33% (refer to Table 2.12) compared to the RMW data obtained from the IMD. In contrast, the error percentages for the traditional methods, including Yadav and Das (2024c), Willoughby et al. (2006), and Tan and Fang (2018), were recorded at 31.24%, 31.13%, and 79.23%, respectively. Similarly, the RMSE values associated with our method were notably lower at 5.61 (refer

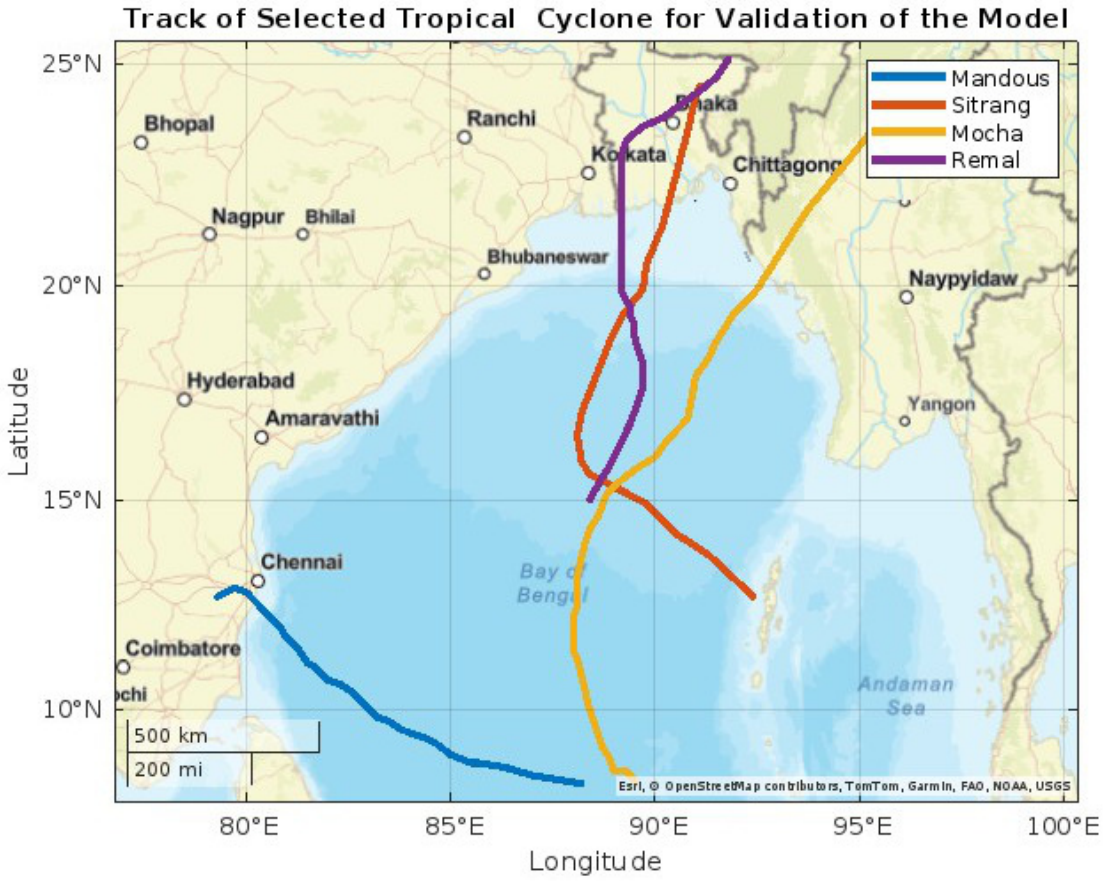

Figure 2.11: Track of the Selected Tropical Cyclone

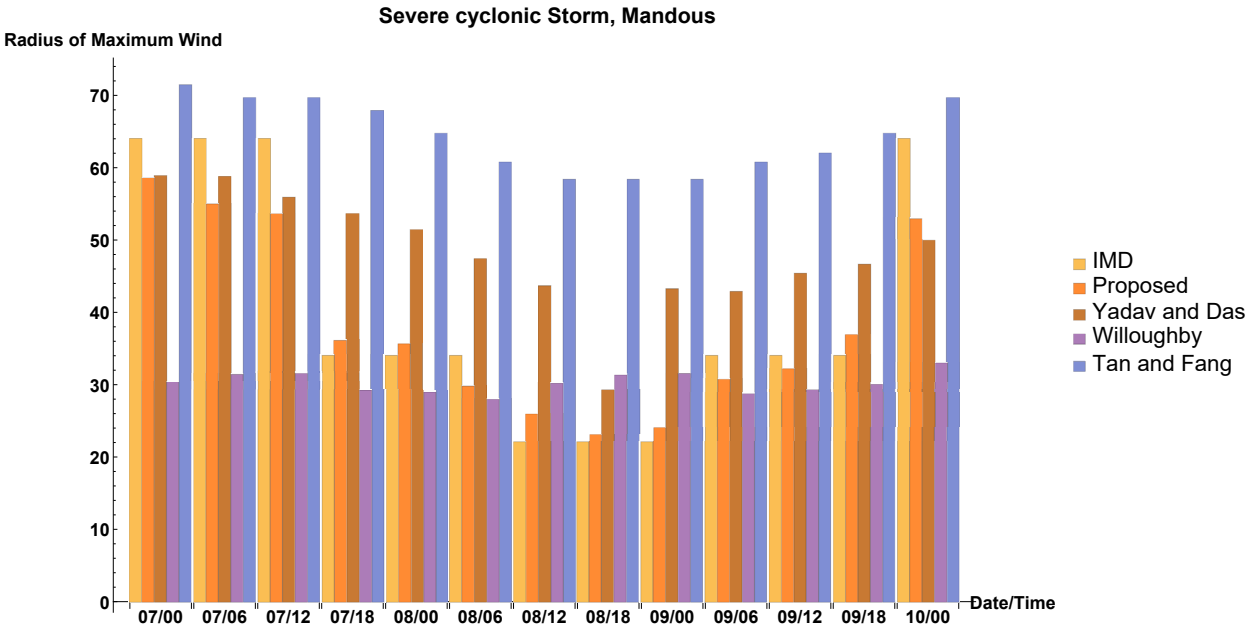

Figure 2.12: Graphical Representation of Mandous Cyclone value of RMW by our method, Yadav and Das, Willoughby et al., Tan and Fang, and IMD

to Table 2.16) compared to the respective RMSE values of 14.35, 18.82, and 26.82 derived from the traditional methods.

The graphical representation in Fig. 2.12 illustrates the comparison between the IMD and all other model's results. The relative similarity or decrease in error rates between the two datasets is apparent, indicating our model's performance compared to other methods concerning the IMD data.

The R^2 value (Table 2.18) of 0.88 suggests that the proposed model is highly effective and explains most of the variance in the data. However, the R^2 value of 0.27 indicates a weak model that only explains a small portion of the variance, with room for significant improvement. The negative R^2 values of -0.32 and -1.68 are concerning, as these models perform worse than a simple mean prediction.

Table 2.12: Numerical Result of Mandous Cyclone

Date / Time	IMD r_{max} (nautical miles)	Our Method r_{max} (nautical miles)	Yadav and Das r_{max} (nautical miles)	Willoughby et al. r_{max} (nautical miles)	Tan and Fang r_{max} (nautical miles)	$ER_{Our}{}^a$ (%)	$ER_{YD}{}^b$ (%)	$ER_W{}^c$ (%)	$ER_{TF}{}^d$ (%)
07/00	64	58.59	58.86	30.36	71.39	8.45	8.03	52.56	11.54
07/06	64	54.91	58.76	31.41	69.58	14.20	8.19	50.93	8.71
07/12	64	53.64	55.95	31.53	69.58	16.18	12.58	50.73	8.71
07/18	34	36.13	53.65	29.203	67.88	6.26	51.91	14.12	76.82
08/00	34	35.58	51.39	28.97	64.78	4.64	42.32	14.79	90.52
08/06	34	29.74	47.41	27.95	60.71	12.52	39.44	17.79	78.55
08/12	22	25.84	43.67	30.15	58.309	17.45	43.95	37.045	165.04
08/18	22	23.10	29.63	31.33	58.309	5.0	34.68	34.68	165.04
09/00	22	23.96	43.25	31.509	58.309	8.90	46.59	43.22	165.04
09/06	34	30.78	42.82	28.76	60.71	9.47	25.94	15.41	78.55
09/12	34	32.13	45.39	29.32	62.002	5.5	33.50	13.76	82.35
09/18	34	36.87	46.59	30.05	64.781	8.44	37.033	11.16	90.53
10/00	64	52.87	49.93	32.95	69.58	17.39	21.98	48.51	8.71
Mean	40.46	38.01	48.26	30.26	64.30	10.33	31.24	31.13	79.23

[a]Error Percentage of our method with respect to IMD.
[b] Error Percentage of Yadav and Das method concerning IMD.
[c] Error Percentage of Willoughby et al. method concerning IMD.
[d] Error Percentage of Tan and Fang method concerning IMD.

SCS Sitrang

The Sitrang Cyclone (Table 2.11), characterized by its complex atmospheric dynamics and profound influence on regional climate patterns, presented an equally crucial case study in our investigation (Division, 2022a). The track of the TC is illustrated in Fig. 2.11. Our method demonstrates an error percentage of 10.83% (refer to Table 2.13) compared with the RMW data from the IMD for the Sitrang Cyclone. Conversely, the error percentages associated with the Yadav and Das, Willoughby, and Tan and Fang methods were determined to be 19.62%, 18.42%, and 78.34%, respectively. Correspondingly, the RMSE values for our method were computed at 7.25 (refer to Table 2.16), highlighting its superior precision compared to the RMSE values of 9.52, 14.01, and 29.682 associated with the traditional methodologies.

Fig. 2.13 compares the IMD results to other models' outcomes. The relative similarity or decrease in error rates between the two datasets highlights our model's performance compared to other methods when considering IMD data.

The R^2 value (Table 2.18) of 0.66 suggests that the proposed model is fairly effective, explaining a substantial portion of the variance in the data. The R^2 value of 0.46 indicates a moderate model that captures less than half of the variance, implying the need for improvement. The negative R^2 values of -0.16 and -4.22 are concerning, indicating that these models perform worse than a simple mean prediction. These negative values suggest that the models are not capturing the important relationships in the data and may require significant modifications or complete reevaluation.

Table 2.13: Numerical Result of Sitrang Cyclone

Date / Time	IMD r_{max} (nautical miles)	Our Method r_{max} (nautical miles)	Yadav and Das r_{max} (nautical miles)	Willoughby et al. r_{max} (nautical miles)	Tan and Fang r_{max} (nautical miles)	ER_{Our}[a] (%)	ER_{YD}[b] (%)	ER_W[c] (%)	ER_{TF}[d] (%)
23/00	64	50.89	51.74	36.48	75.43	20.48	19.16	43	17.85
23/06	64	49.63	48.83	36.87	73.33	22.45	23.70	42.39	14.57
23/12	34	36.23	46.10	38.55	71.39	6.55	35.61	13.38	109.97
23/18	34	35.76	45.25	36.92	69.58	5.17	33.10	8.58	104.64
24/00	34	32.94	40.74	31.66	66.28	3.11	19.83	6.88	94.94
24/06	34	31.52	37.63	30.87	66.28	7.29	10.68	9.20	94.94
24/12	34	30.67	36.35	29.55	66.28	9.79	6.92	13.08	94.94
24/18	34	29.98	36.71	30.29	66.28	11.82	7.98	10.91	94.94
Mean	41.50	37.20	42.91	33.89	69.35	10.83	19.62	18.42	78.34

[a] Error Percentage of our method with respect to IMD.
[b] Error Percentage of Yadav and Das method concerning IMD.
[c] Error Percentage of Willoughby et al. method concerning IMD.
[d] Error Percentage of Tan and Fang method concerning IMD.

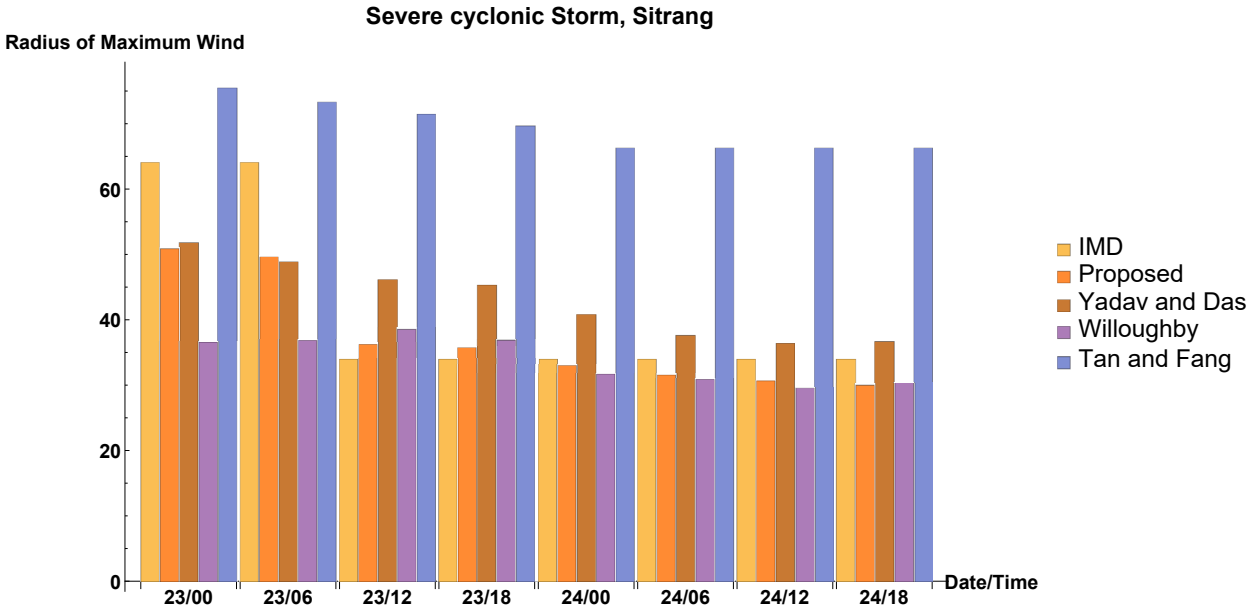

Figure 2.13: Graphical Representation of Sitrang Cyclone value of RMW by our method, Yadav and Das, Willoughby et al., Tan and Fang, and IMD

ESCS Mocha

ESCS Mocha (Table 2.11), the initial cyclonic storm of 2023, made landfall on Myanmar's coast (track of Mocha is shown in Fig. 2.11) with an MSW of 100 knots on May 14^{th}, 2023. Analyzing the climatological data from 1965 to 2022 reveals that out of approximately 200 cyclonic storms in the BoB, 61 crossed the coasts of Bangladesh and Myanmar during this period. Comparing recent events, the last Extremely Severe Cyclonic Storm (ESCS) to impact Myanmar before Mocha was "ESCS GIRI" in 2010. Historical records from the Indian Meteorological Department show that the most intense storm in the BoB was the 1999 Odisha Super Cyclone, reaching a peak MSW of 140 knots, followed by several others with peak MSWs ranging from 125 to 130 knots. Mocha Cyclone was not the most intense cyclonic storm in the Bay of Bengal based on available historical data (Agency, 2012).

Our proposed methodology for determining the RMW yielded an error percentage of 29.84% (refer to Table 2.14), as contrasted with the RMW data acquired from the IMD. In

stark divergence, traditional approaches, namely those of Yadav and Das, Willoughby, and Tan and Fang, exhibited error percentages of 38.43%, 53.79%, and 84.66%, respectively. Likewise, the RMSE values associated with our approach were markedly lower at 19.05 (refer to Table 2.16) compared to the corresponding RMSE values of 23.89, 31.28, and 35.00 derived from conventional methodologies.

The graph in Fig. 2.14 compares the results from the India Meteorological Department (IMD) with those from other models. Our model performs similarly or with less error than the others when considering the IMD data.

The R^2 value (Table 2.18) of 0.56 suggests that the proposed model is moderately effective, explaining over half of the variance in the data but still leaving a substantial portion unexplained. The R^2 value of 0.31 indicates a weak model, explaining less than one-third of the variance and pointing to the need for significant improvement. The negative R values of -0.61 and -0.46 are concerning, as they indicate that these models perform worse than simply using the mean of the dependent variable, suggesting fundamental issues with the model's ability to capture the data's underlying patterns.

SCS Remal

The Remal Cyclone, characterized by its complex atmospheric dynamics and profound influence on regional climate patterns, presents a crucial case study in our investigation (Table 2.11). The track of the TC is illustrated in Fig. 2.11.

Our method demonstrated an error percentage of 20.58% compared to the RMW data from the IMD for the Remal Cyclone (Table 3.11). In contrast, the error percentages associated with the Yadav and Das, Willoughby, and Tan and Fang methods were 28.02%,

Table 2.14: Numerical Result of Mocha Cyclone

Date / Time	IMD r_{max} (nautical miles)	Our Method r_{max} (nautical miles)	Yadav and Das r_{max} (nautical miles)	Willoughby et al. r_{max} (nautical miles)	Tan and Fang r_{max} (nautical miles)	ER_{Our}[a] (%)	ER_{YD}[b] (%)	ER_W[c] (%)	ER_{TF}[d] (%)
10/00	90	69.05	61.48	49.55	69.07	23.27	31.68	44.94	23.25
10/06	90	67.83	60.84	50.06	71.01	24.63	32.40	44.37	21.10
10/12	90	62.98	57.37	50.82	72.82	30.02	36.25	43.53	19.08
10/18	90	61.57	56.52	51.51	72.82	31.58	37.20	42.76	19.08
11/00	40	51.46	53.83	51.52	74.52	28.65	34.57	28.80	86.30
11/06	40	43.38	45.82	51.26	76.12	08.45	14.55	28.15	90.30
11/12	26	39.87	41.97	51.50	79.05	53.34	61.42	98.07	204.03
11/18	26	36.09	41.44	51.94	81.69	38.80	59.38	99.76	214.19
Mean	61.50	54.02	52.04	51.02	74.63	29.84	38.43	53.79	84.66

[a] Error Percentage of our method with respect to IMD.
[b] Error Percentage of Yadav and Das method concerning IMD.
[c] Error Percentage of Willoughby et al. method concerning IMD.
[d] Error Percentage of Tan and Fang method concerning IMD.

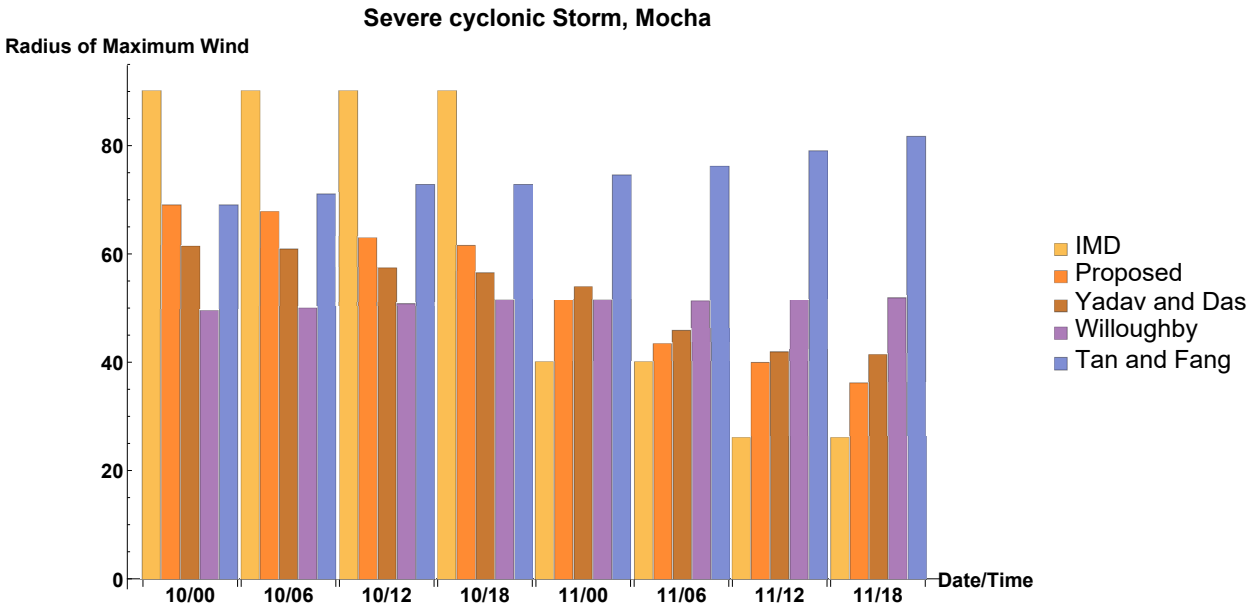

Figure 2.14: Graphical Representation of Mocha Cyclone value of RMW by our method, Yadav and Das, Willoughby et al., Tan and Fang, and IMD

35.73%, and 36.68%, respectively.

The Root Mean Square Error (RMSE) values for our method were computed at 20.75, underscoring its superior precision compared to the RMSE values of 27.56, 32.00, and 22.93 associated with the traditional methodologies (Table 2.16).

Fig. 2.15 compares the IMD results to the outcomes of other models. The relative similarity or decrease in error rates between the datasets highlights our model's improved performance compared to other methods when evaluated against IMD data.

These results bear significant scientific implications. The consistent outperformance of our machine learning technique across all the case studies: Mandous, Sitrang, Mocha, and Remal Cyclones underscores its robustness in estimating RMW in real-world TCs. Compared to traditional methods, the remarkable reduction in error percentages and RMSE values substantiates the efficacy of data-driven approaches in meteorological research.

Moreover, these findings emphasize the urgent need for modernizing the field of TC

Table 2.15: Numerical Result of Remal Cyclone

Date / Time	IMD r_{max} (nautical miles)	Our Method r_{max} (nautical miles)	Yadav and Das r_{max} (nautical miles)	Willoughby et al. r_{max} (nautical miles)	Tan and Fang r_{max} (nautical miles)	$ER_{Our}{}^a$ (%)	$ER_{YD}{}^b$ (%)	$ER_W{}^c$ (%)	$ER_{TF}{}^d$ (%)
25/00	100	61.92	51.80	40.00	62.00	38.08	48.20	60.00	38.00
25/06	92	57.62	48.65	40.41	59.48	37.37	47.12	56.08	35.35
25/12	55	50.14	45.74	37.87	58.30	08.84	16.84	31.15	06.00
25/18	55	47.28	41.18	35.43	56.10	14.04	25.13	35.58	02.00
26/00	33	35.82	34.20	30.60	52.17	08.55	03.64	07.27	58.09
27/06	35	36.27	32.05	40.66	53.10	03.63	08.43	16.17	51.71
27/12	74	47.89	34.78	41.07	55.06	35.28	53.00	44.50	25.59
27/18	33	39.23	40.21	44.57	58.30	18.88	21.85	35.06	76.67
Mean	59.62	47.02	41.07	38.82	56.81	20.58	28.02	35.73	36.68

[a]Error Percentage of our method with respect to IMD.
[b] Error Percentage of Yadav and Das method with respect to IMD.
[c] Error Percentage of Willoughby et al. method with respect to IMD.
[d] Error Percentage of Tan and Fang method with respect to IMD.

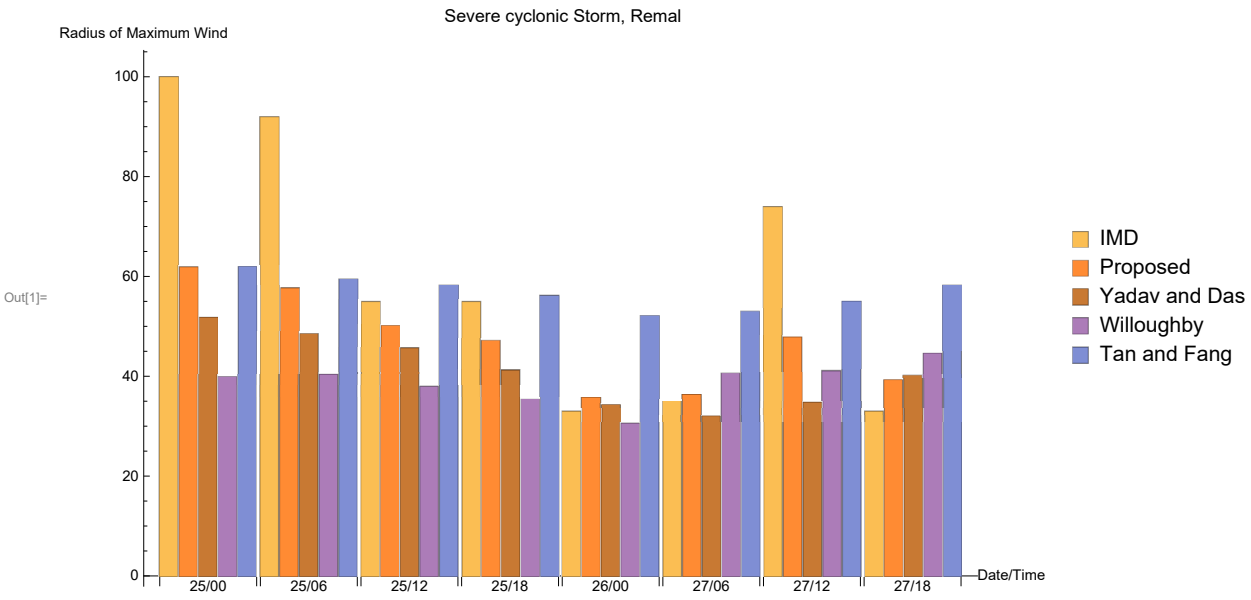

Figure 2.15: Graphical Representation of Remal Cyclone value of RMW by our method, Yadav and Das, Willoughby et al., Tan and Fang, and IMD

analysis, harnessing the potential of advanced computational techniques to enhance our understanding and predictive capabilities. Our results underscore the promise of machine learning in revolutionizing the accuracy of RMW estimation, with far-reaching implications for TC forecasting, disaster preparedness, and climate research. This study contributes to the evolving landscape of meteorological research, highlighting the potential for innovative methodologies to advance our comprehension of these dynamic and complex weather phenomena.

The R^2 values (Table 2.18) provide insight into the performance of the models. The value of 0.30 indicates a weak fit, explaining only a small portion of the variance in the data. The value of 0.15 suggests an even weaker fit, with most of the variability unexplained. The negative R^2 values of -0.22 and -0.65 are particularly concerning, indicating that these models perform worse than simply using the mean of the dependent variable.

Upon the analysis, we observe that excluding Willoughby's formula for RMW from the ensemble increases the error percentage and the root square mean error. This suggests that

Table 2.16: Root Square Mean Error of all methods concerning IMD

Name of TC	Our Method w.r.t. Best Track	ARCHER w.r.t. Best Track	ADT w.r.t Best Track	SATCON w.r.t. Best Track
Mandous	5.61	14.35	18.82	26.82
Sitrang	7.25	9.52	14.01	29.68
Mocha	19.05	23.89	31.28	35.00
Remal	20.75	27.56	32.00	22.93
Mean	13.16	18.83	24.02	28.60

Table 2.17: Error percentage of all methods concerning IMD

Name of TC	Our Method w.r.t. Best Track	ARCHER w.r.t. Best Track	ADT w.r.t Best Track	SATCON w.r.t. Best Track
Mandous	10.33	31.24	31.13	79.23
Sitrang	10.83	19.62	18.42	78.34
Mocha	29.84	38.43	53.79	84.66
Remal	20.58	28.02	35.73	36.68
Mean	17.89	29.32	34.76	69.72

despite the discrepancy in RMW value, Willoughby's formula significantly improves the accuracy of the overall model. So, we have included Willoughby's formula in the model to get a more accurate result.

The study of the RMW holds strong implications for research and operational purposes in TC forecasting and disaster management. Accurate estimation of the RMW is integral to various applications. In the interest of research, it provides invaluable insights into the dynamics of TCs, allowing for a deeper understanding of their structure, intensity, and behavior. By uncovering the complex relationships between the RMW and various meteorological parameters, researchers can refine existing models and develop new ones that better capture the complexity of these phenomena.

From an operational perspective, the RMW is a critical parameter for forecasting agencies and disaster response teams. It directly impacts the intensity and extent of wind and storm surge hazards associated with TCs, making it a key input for operational models and forecasts. Accurate RMW estimates enable improved predictions of storm tracks, intensities,

Table 2.18: Detail of R-squared of all cases

Name of TC	Our Method w.r.t. Best Track	ARCHER w.r.t. Best Track	ADT w.r.t Best Track	SATCON w.r.t. Best Track
Mandous	0.88	0.27	− 0.32	− 1.68
Sitrang	0.66	0.46	− 0.16	− 4.22
Mocha	0.56	0.31	− 0.61	− 0.46
Remal	0.30	− 0.22	− 0.65	0.15

and potential impacts, enhancing the ability to issue timely warnings and advisories. This is particularly important for vulnerable coastal regions, where even minor changes in the RMW can have significant implications for preparedness and mitigation measures.

2.6 Conclusion

This chapter focuses on determining the value of RMW across the NIO. There is a lack of literature addressing RMW in the NIO, which is globally recognized as highly susceptible to TCs. Through an analysis of historical observations, we investigate the relationship between the position of the TC's center (latitude) and the estimated pressure drop P_d to develop a relation for calculating RMW.

To evaluate the accuracy of our proposed approach, we employ three statistical methods: error percentage, t-test, and RMSE. By examining various TC cases within the NIO, we find that our method performs well compared to other methodologies: Willoughby et al. (2006); Tan and Fang (2018) as observed from reduced mean errors (Table 2.10) and RMSEs (Table 2.9), where t-test favored their method as well. However, it is important to note a limitation of our method, which is that the value of P_d must be less than or equal to 12 hPa, and no specific conditions are imposed on the latitude of the TC center within the NIO basin.

After that, we extend this to improve the accuracy using machine learning techniques

such as neural networks. We take the input as the results of three methods: Willoughby et al. (2006); Tan and Fang (2018); Yadav and Das (2024c) and target the IMD-provided RMW data. to evaluate the accuracy of the neural network model, we used two statistical methods: error percentage and root square mean error. We observed the reduction in error percentage (Table 2.17) and root square mean error (Table 2.16). So, we can say that the neural network model estimates the RMW more accurately than the other method.

Chapter 3

Tropical Cyclone's Track

"Life is a math equation. In order to gain the most, you have to know how to convert negatives into positives"

– Albert Einstein

In this chapter[1], we explain a technique for estimating the track of tropical storms in the NIO using a neural network. Instead of satellite images, the method uses results from three different approaches: the automated rotational center hurricane eye retrieval algorithm, the advanced Dvorak technique, and the satellite Consensus technique as inputs, with data from the India Meteorological Department serving as the target for the neural network.

---

[1] The content of this chapter is based on a research paper "Estimating Tropical Cyclone Track with Neural Network Algorithms: A Data-Driven Approach" (Submitted).

3.1 Introduction

TCs, formidable atmospheric phenomena characterized by low-pressure systems and organized convection, traverse vast expanses of open ocean, posing significant risks to coastal regions. These cyclones' trajectory, or track, is a fundamental aspect of their dynamics, influencing their intensity, structure, and ultimate impact upon landfall. Advancements in meteorological sciences have underscored the critical importance of accurately predicting TC tracks. These forecasts are pivotal in informing disaster management strategies, facilitating early warnings, and implementing evacuation protocols (Emanuel, 2003).

Tracking TCs is imperative for mitigating the potentially catastrophic consequences of their landfall. Authorities can strategically allocate resources, implement evacuation measures, and enhance overall disaster preparedness through precise track predictions. The track is the most important in understanding the complex interactions between the cyclone and its environment, influencing the storm's intensity, size, and evolution (Kossin et al., 2014). As a result, advancements in track prediction methodologies directly contribute to more effective risk assessment and management.

The interdependence between the TC track and its other characteristics is complicated. Changes in the track can induce alterations in the environmental conditions encountered by the storm, thus impacting its development and intensity (Emanuel, 2005). The radius of maximum wind, a key parameter defining the spatial extent of solid winds within the cyclone, is closely tied to the track as variations in trajectory influence the distribution of wind forces. Intensity, storm eye, and storm size also exhibit intricate connections with the track; for instance, shifts in the track may lead to changes in the cyclone's core structure, affecting the development and maintenance of the storm eye. Therefore, an accurate understanding

of the track is essential for comprehending and predicting the dynamics of these additional characteristics, offering a holistic view of the TC system.

While considerable progress has been made in TC track prediction, limitations persist in current methodologies. Various authors have identified challenges such as uncertainties in initial conditions, inaccuracies in modeling atmospheric processes, and the inherent complexity of the dynamic systems involved (Emanuel, 2003; Knapp et al., 2010). These limitations underscore the ongoing need for innovation in tracking methods to enhance predictive accuracy and reliability.

In the past two decades, numerous researchers have significantly contributed to advancing our understanding of TC tracks and associated characteristics. Emanuel (2003) explored the thermodynamic control of hurricane intensity, shedding light on the intricate relationship between track and intensity. Kossin et al. (2014) conducted comprehensive analyses of the poleward migration of TC maximum intensity, providing insights into how tracks influence the spatial distribution of storm intensity.

Zhang et al. (2019) explored the application of deep learning for TC intensity estimation, showcasing the potential of artificial intelligence in refining our understanding of cyclone characteristics. Chen et al. (2020) extended this work by applying deep learning approaches to hurricane track forecasting, demonstrating the ability of neural networks to capture the complexities of cyclone dynamics.

Knapp et al. (2010) contributed to improving the International Best Track Archive for Climate Stewardship (IBTrACS), enhancing our access to high-quality historical cyclone data for research and analysis. These studies collectively highlight the complicated nature of TCs and underscore the ongoing efforts to improve predictive capabilities in track

forecasting.

Recent strides in meteorological research have witnessed the increasing incorporation of artificial intelligence, particularly neural networks, to improve the accuracy of TC characteristics prediction. Neural networks (NN), with their ability to determine complex patterns and relationships from vast datasets, have become instrumental in refining our understanding of cyclone behavior. Research employing neural networks in TC tracking has shown promising results, but still room for improvement exists, indicating the potential for these technologies to enhance predictive capabilities (Zhang and et al., 2019; Chen and et al., 2020; Yadav and Das, 2022). These innovative approaches leverage neural networks' adaptability and learning capabilities, offering new avenues for more accurate and nuanced predictions of cyclone tracks and associated features.

In this chapter, we develop an NN model to estimate the TC track over the NIO. The NN model is trained with the input from experimental results of three methodologies to capture complex patterns and relationships inherent in TC movements in this region. The significance lies in its potential to enhance forecasting accuracy, aiding meteorologists and authorities in making more informed disaster preparedness and response decisions. This research contributes to advancing predictive capabilities crucial for mitigating the impact of TCs in the NIO. We emphasize the NIO as a conducive environment for forming TCs. Despite this, the NIO comprises only 7% (Mohapatra et al., 2014; Shaji et al., 2014) of the world's total TCs, approximately five per year (Mohapatra et al., 2014; Yadav and Das, 2023a). Specifically, four of these TCs occur in the Bay of Bengal (Mohapatra et al., 2014; Yadav and Das, 2023a; Vissa et al., 2013; Rajasekhar et al., 2014), while one occurs in the Arabian Sea (Mohapatra et al., 2014; Yadav and Das, 2023a; Rajasekhar et al., 2014; Rajeevan et al., 2013).

3.2 Literature Review

This section briefly explains the methods used to forecast the tracks of TCs. In the literature, many methods and groups of methods are used to determine the track of TCs, but only a few are discussed in this section. In practice, these methods often involve a combination of techniques. We have therefore chosen to group the various methods according to the main techniques. The main techniques are discussed below:

- Averaging across occurrences.
- Statistical forecasting techniques.
- Techniques based on satellite image interpretation.
- Techniques using artificial neural networks.

3.2.1 Averaging across occurrences

This technique, also called extrapolation, uses the recent movement of a cyclone (usually the last 6 to 12 hours) to predict where it will go next. It is the simplest way to forecast a cyclone's path. In this method, we assume that all factors influencing the cyclone's movement stay the same, so it continues moving as it has been (Holland, 2015). The accuracy of the forecast depends on how accurately we choose the cyclone's recent positions and direction. Extrapolation can work well for short-term forecasts (12 to 24 hours), but it's not good enough for longer forecasts (Jeffries and Miller, 1993).

Extrapolation (XTRP) is a method of averaging used by the Joint Typhoon Warning Center (JTWC) in Hawaii, USA. They used this technique from 1970 for about 20 years to predict cyclones in the Northwest Pacific region. Since each cyclone-prone area has its

distinct climate and geography, forecasting techniques may perform differently in different areas, even if similar.

3.2.2 Statistical forecasting techniques

Statistics forecasting methods primarily rely on regression analysis. Over time, various techniques for statistically predicting TCs have emerged. These methods can be categorized into five main types.

- climatologically-aware forecasting techniques
- climatology and persistence forecasting techniques (does not include synoptic data)
- statistical synoptic techniques
- steering airflow determination, and
- statistical-dynamical techniques.

Statistical techniques can create short-term (24-hour) and long-term (72-hour) forecasts by analyzing data sources such as current storms, past storm data, synoptic analysis, and numerical simulations. These methods are advantageous because they can consider different parameters from the available data and require relatively low computational resources compared to other forecasting techniques.

However, there are drawbacks to using statistical methods. Forecasts generated through statistical regression tend to represent the average behavior of storms within the data set used. They perform best when the current synoptic conditions align closely with the typical climatology of the area. Additionally, these techniques rely heavily on having sufficient and accurate data to reliably identify trends in cyclone tracks.

Statistical forecasting may produce unreliable results in sparse or poor historical track data regions. Errors can occur, especially when:

- Forecasting suggests a northward and eastward movement at low latitudes.
- Forecasting indicates a southward and eastward movement above the subtropical ridge.
- Forecasting predicts the cyclone will stall or exhibit looping motion near the northern or southern subtropical ridges.
- Major synoptic features deviate significantly from their usual positions.
- Cyclone formation occurs outside the typical cyclone season for the region.

3.2.3 Techniques based on satellite image interpretation

Cyclones usually travel long distances across tropical oceans before reaching land. Since they spend most of their time over these oceans, gathering detailed information about them using ground-based observations is hard. However, it's crucial to understand their formation and movement patterns to forecast their tracks and landfalls accurately. Satellite images are critical in providing this information (Goerss and Hogan, 2006; Goerss, 2009; Kidder et al., 2000; Le Marshall, 1998). While many forecasting techniques rely on satellite images alongside other data sources, some primarily use satellite images for cyclone track forecasts. A few examples of techniques based on satellite image interpretation are: Dvorak (1973); Weir (1982); Mautner et al. (1992); Goerss and Hogan (2006); Goerss (2009); Dvorak (1984).

3.2.4 Techniques using artificial neural networks

Satellites are one of the most important for keeping track of cyclones. They help gather info about the cyclone and its surroundings. But it's tough to spot cloud changes and analyze

all the data from different sensors. This makes it hard for traditional forecasting methods to predict cyclones accurately. These old methods are complicated, need powerful computers, and can mess up if they don't start with the right info. Plus, satellite data is big and often has a lot of noise.

Because of all this, scientists are looking into new ways to process satellite images and forecast cyclones. One promising idea is using ANNs. These are simpler and might do a better job of handling the complex data from satellites.

Artificial neural networks are relatively new in cyclone forecasting compared to other methods. They're still being developed and need significant effort to create and train, so they're not as commonly used as other techniques. A few examples of techniques based on the artificial neural networks are: Zhang and et al. (2019); Chen and et al. (2020); Chen et al. (2018, 2019); Lee et al. (2019); Combinido et al. (2018); Pradhan et al. (2017); Higa et al. (2021); Chen and Yu (2020); Zhang et al. (2021); Varalakshmi et al. (2023).

3.3 Data and Method

In this section, we have discussed the data used to train and validate the model and the technique of the proposed model in detail.

3.3.1 Data

The data for this study has been collected as results from three different modeled members (ARCHER, ADT, and SATCON), which are the input to our model, collected from their respective websites (ARCHER "`https://tropic.ssec.wisc.edu/real-time/archerOnline/cyclones/`", ADT "`https://tropic.ssec.wisc.edu/misc/adt/info.html`", and SATCON

"https://tropic.ssec.wisc.edu/real-time/satcon/") for 2014-24. The study primarily focused on the NIO regions for training and validation. To ensure comprehensive data acquisition, the best track data has been collected from the official websites of the RSMC for the NIO, which is also known as IMD (https://rsmcnewdelhi.imd.gov.in/) for 2014-24. We collected the data from 56 TCs (details of TCs are given in Table 3.1) for training purposes and 6 TCs (details of TCs are given in Table 3.2) for validation purposes.

Our study does not utilize satellite images to estimate the TC track. Instead, our approach relies on output data generated by three contemporary state-of-the-art track estimation models: ARCHER, ADT, and SATCON. The deliberate exclusion of satellite images is acknowledged, highlighting our dependence on the pre-existing outputs produced by these well-established models.

3.3.2 Method

The primary aim of this chapter is to develop a model alongside the results obtained from the three methodologies (ARCHER, ADT, and SATCON) to obtain a single result. The proposed model estimates demonstrate a remarkable improvement over individual member-provided estimates and a simple arithmetic mean of those estimates. This improvement is substantiated by rigorous scientific analyses, revealing the model's ability to discern patterns and synthesize information more effectively than individual estimators. Notably, the model's performance is on par with established traditional methodologies. The brief descriptions of the current members in our model are as follows:

- **ARCHER (Automated Rotational Center Hurricane Eye Retrieval)**:

  The ARCHER estimates TC characteristics using the ATMS-derived MSLP anomaly, TC eyewall vigour, and the inner core Tb gradient (maximum of either channel 8 or

Table 3.1: Details of Tropical Cyclone for training purpose

S. No.	Name of Tropical Cyclone	Category	Time period
1	Depression	Depression	04 - 07 January 2014
2	Depression	Depression	21 - 23 May 2014
3	Nanauk	Cyclonic Storm	10 - 14 June 2014
4	Deep Depression	Deep Depression	03 - 07 August 2014
5	Hudhud	Very Severe Cyclonic Storm	07 - 14 October 2014
6	Nilofar	Very Severe Cyclonic Storm	25 - 31 October 2014
7	Deep Depression	Deep Depression	05 - 08 November 2014
8	Ashobaa	Cyclonic Storm	07 - 12 June 2015
9	Komen	Cyclonic Storm	26 July - 02 August 2015
10	Deep Depression	Deep Depression	09 - 12 October 2015
11	Chapala	Extremely Severe Cyclonic Storm	28 October - 04 November 2015
12	Megh	Extremely Severve Cyclonic Storm	05 - 10 November 2015
13	Deep Depression	Deep Depression	08 - 10 November 2015
14	Roanu	Cyclonic Storm	17 - 22 May 2016
15	Depression	Depression	27 - 29 June 2016
16	Deep Depression	Deep Depression	09 - 12 August 2016
17	Deep Depression	Deep Depression	16 - 21 August 2016
18	Kyant	Cyclonic Storm	21 - 28 October 2016
19	Depression	Depression	02 - 06 November 2016
20	Nada	Cyclonic Storm	29 November - 02 December 2016
21	Vardhah	Very Severe Cyclonic Storm	06 - 13 December 2016
22	Marrutha	Cyclonic Storm	15 - 17 April 2017
23	Mora	Severe Cyclonic Storm	28 - 31 May 2017
24	Deep Depression	Deep Depression	11 - 13 June 2017
25	Depression	Depression	18 - 19 July 2017
26	Depression	Depression	26 - 27 July 2017
27	Deep Depression	Deep Depression	09 - 10 October 2017
28	Depression	Depression	19 - 22 October 2017
29	Ockhi	Very Severe Cyclonic Storm	29 November - 06 December 2017
30	Deep Depression	Deep Depression	06 - 09 December 2017
31	Sagar	Cyclonic Storm	16 - 21 May 2018
32	Mekunu	Extremely Severe Cyclonic Storm	21 - 27 May 2018
33	Daye	Cyclonic Storm	19 - 22 September 2018
34	Luban	Very Severe Cyclonic Storm	06 - 15 October 2018
35	Gaja	Very Severe Cyclonic Storm	10 - 19 November 2018
36	Fani	Extremely Severe Cyclonic Storm	26 April – 4 May 2019
37	Vayu	Very Severe Cyclonic Storm	10 – 17 June 2019
38	Hikka	Very Severe Cyclonic Storm	22 – 25 September 2019
39	Kyarr	Super Cyclonic Storm	24 October – 02 November 2019
40	Maha	Extremely Severe Cyclonic Storm	30 October – 07 November 2019
41	Pawan	Cyclonic Storm	02 - 07 December 2019
42	Deep Depression	Deep Depression	03 - 05 December 2019
43	Amphan	Super Cyclonic Storm	16 - 21 May 2020
44	Nisarga	Severe Cyclonic Storm	01 - 04 June 2020
45	Gati	Very Severe Cyclonic Storm	21 - 24 November 2020
46	Tauktae	Extremely Severe Cyclonic Storm	14th-19th May, 2021
47	Yaas	Very Severe Cyclonic Storm	23 – 28 May, 2021
48	Gulaab	Cyclonic Storm	24 - 28 September 2021
49	Shaheen	Severe Cyclonic Storm	30 September – 4 October 2021
50	Depression	Depression	10 - 11 November 2021
51	Deep Depression	Deep Depression	03 - 06 March 2022
52	Asani	Severe Cyclonic Storm	07 - 12 May 2022
53	Depression	Depression	12 - 13 August 2022
54	Depression	Depression	14 - 16 August 2022
55	Sitrang	Cyclonic Storm	22-25 October 2022
56	Deep Depression	Deep Depression	14-17 December 2022

Table 3.2: Details of Tropical Cyclone for Validation purpose

Name of Tropical Cyclone	Category	Time period
Michaung	Severe Cyclonic Storm	01 - 06 December 2023
Tej	Extremely Severe Cyclonic Storm	20 - 24 October 2023
Mandous	Severe Cyclonic Storm	06 - 10 December 2022
Biparjoy	Extremely Severe Cyclonic Storm	06 - 19 June 2023
Mocha	Extremely Severe Cyclonic Storm	09 - 15 May 2023
Remal	Severe Cyclonic Storm	24 - 28 May 2024

9) (Velden and Herndon, 2020).

- **ADT (Advanced Dvorak technique)**:

  The ADT is a computer-based algorithm meticulously crafted to estimate TC characteristics by analyzing geostationary satellite infrared imagery. It is widely adopted by operational TC analysis and forecasting centers across the globe to assist in gauging TC intensity, particularly in oceanic regions where direct measurements are unavailable. Originating from the earlier versions introduced by Olander and Velden (2007), the algorithm was initially designed to emulate the Dvorak technique closely. This traditional method involves a trained analyst applying pattern-matching and classification schemes to satellite imagery for TC characteristic estimation. Over time, the ADT algorithm has evolved into an operational tool endorsed and maintained by NOAA/NESDIS. It has become a reliable resource for providing real-time, objective TC characteristics guidance to operational TC centers worldwide.

- **SATCON (Satellite Consensus)**:

  The SATCON, crafted by CIMSS, integrates the ADT estimation derived from Geostationary Satellites with other estimates obtained during polar-orbiting satellite overpasses. This combination yields a comprehensive estimation of TC characteristics on a global scale, as discussed in studies by Herndon et al. (2010); Velden and Herndon (2014); Goyal et al. (2017); Velden and Herndon (2019, 2020); Ahmed et al. (2022); Yadav and Das (2024a)

In Figure 3.1, the high-level flowchart of the applied methodology is given. Each of the components depicted in Figure 3.1 is further analyzed in Table 3.3, while the architecture

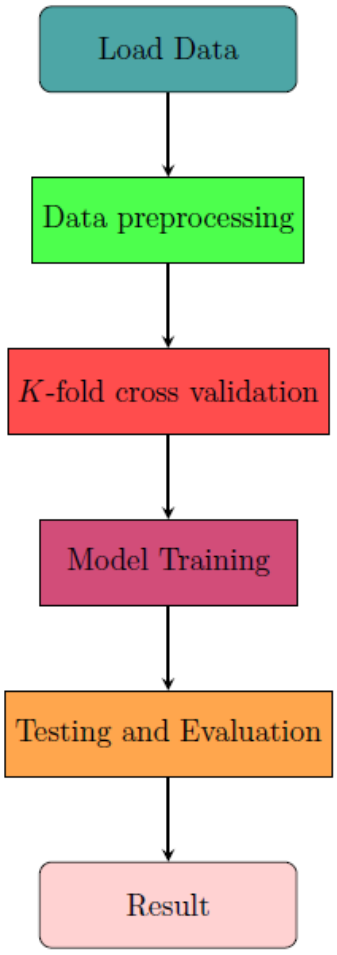

Figure 3.1: Flowchart of the proposed methodology

of our NN model is illustrated in Figure 3.2. Table 3.4 gives the NN's layer details.

Our methodology employs a Neural Network training paradigm utilizing 1-minute interval data paired with corresponding labels. For validation, we adopt 3-minute averages of the data, computed by averaging values over three consecutive 1-minute intervals. Subsequently, the trained NN generates predictions or classifications based on these 3-minute averages. Performance evaluation entails comparing these predictions with the actual 10-minute averaged data. Consistency in data preprocessing and meticulous handling of time intervals are imperative considerations maintained throughout the training and verification

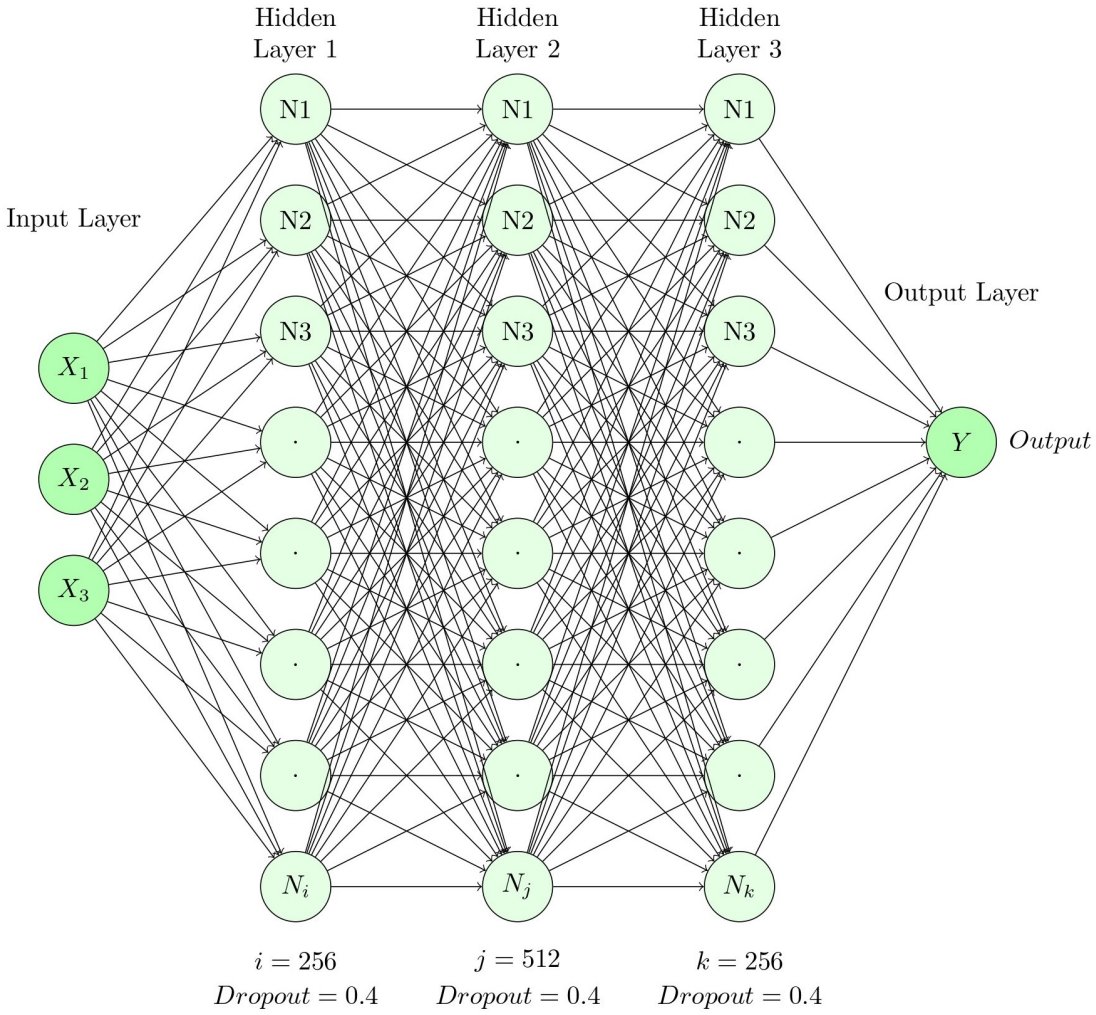

Figure 3.2: Architecture of the Proposed Neural Network, where X_1, X_2, and X_3 are input and Y is the output

Table 3.3: Whole process of proposed method

Section	**Explanation**
Import Statements	Libraries like NumPy (Harris et al., 2020), TensorFlow (Abadi et al., 2016), and Keras (Chollet et al., 2015) are imported.
Placeholder Data	Experimental and original values are defined as NumPy arrays.
Data Combination and Normalization	Experimental values are combined and normalized using StandardScaler.
K-fold cross-validation	To provide a comprehensive performance estimate and reduce the risk of overfitting (Nti et al., 2021; Pohjankukka et al., 2017).
NN Model Definition	Sequential model with three hidden layers, LeakyReLU activation, Batch Normalization, and Dropout for regularization. The output layer has one neuron for regression.
Layer Details	Refer to the Table 3.4 for details on each layer in the neural network.
Optimizer Definition	Use the Adam optimizer (Kingma and Ba, 2014) with a learning rate = 0.001.
Model Compilation	Compiles the model with mean squared error loss and mean absolute error as metrics.
Model Training	Trains the model with specified epochs=6000, batch size=64, and verbose=0.
Model Evaluation	Following training, the model is evaluated using the trained neural network to predict the experimental values. The mean absolute percentage and root mean square errors are calculated to assess the model's accuracy and performance.

phases Yadav and Das (2024b).

To check the accuracy of our model, we use three statistical methods: t-test, error percentage, and root mean square error. Using these statistical methods, we can say that our model is more efficient and accurate than the three methods: ADT, ARCHER, and SATCON. Section 2.4.1 provides a detailed discussion of the t-test, error percentage, and root square mean error.

Table 3.4: Layer Details of the Neural Network

Layer	**Details**
Input Layer	Dense(256, $input\_shape = (3,)$): Input layer with 256 neurons and input shape of $(3,)$.
Activation Layer	Leaky ReLU (alpha=0.3): Activation using Leaky ReLU with a small negative slope (alpha=0.3).
Batch Normalization Layer	BatchNormalization(): Normalizes inputs for stability.
Dropout Layer	Dropout(0.4): Dropout layer with a 40% dropout rate for regularization
Hidden Layer 2	Dense(512): The second hidden layer contains 512 neurons.
Activation Layer	LeakyReLU(alpha=0.3): Leaky ReLU activation.
Batch Normalization Layer	BatchNormalization(): Batch normalization layer.
Dropout Layer	Dropout(0.4): Dropout layer with a 40% dropout rate.
Hidden Layer 3	Dense(256): Third hidden layer with 256 neurons.
Activation Layer	LeakyReLU(alpha=0.3): Leaky ReLU activation.
Batch Normalization Layer	BatchNormalization(): Batch normalization layer.
Dropout Layer	Dropout(0.4): Dropout layer with a 40% dropout rate.
Output Layer	Dense(1): Output layer with a single neuron for regression.

3.4 Discussion of Results

In this study, we conduct a comprehensive analysis to assess the effectiveness of various methodologies for estimating the TC track within the specific TCs: Severe Cyclonic Storm Michaung (SCS Michaung), Extremely Severe Cyclonic Storm Tej (ESCS Tej), Severe Cyclonic Storm Mandous (SCS Mandous), Extremely Severe Cyclonic Storm Biparjoy (ESCS Biparjoy), Extremely Severe Cyclonic Storm Mocha, and Severe Cyclonic Storm Remal (SCS Remal) (details of the time period of selected TC is given in Table 3.2). Our evaluation encompasses a comparative study of error percentages and RMSE concerning the data obtained from the IMD. Additionally, we incorporate the t-test results to provide a statistical

measure of the significance of observed differences between the methodologies.

SCS Michaung

The sixth cyclone with a maximum sustained wind speed (MSW) of $\geq$ 34 knots ($\geq$ 62 kmph) occurred over the NIO in 2023. Over the past 33 years (1990-2022), approximately 13 cyclones formed over the Bay of Bengal (BoB) in December. Michaung did not exhibit rapid intensification or weakening throughout its life cycle. The system reached its peak intensity of 55 knots (100-110 kmph) at 1200 UTC (1730 IST) on December 4th, 2023, with an estimated central pressure of 986 hPa and a pressure drop of about 16 hPa. Subsequently, it weakened slightly at 1800 UTC on December 4th, 2023, upon entering an area with a slightly lower sea surface temperature.

The cyclone Michaung followed a track with two recurvatures during its existence. Initially, it recurved from a west-northwestward movement to northwestwards around 1730 hours IST/1200 UTC on December 2nd, 2023. Another recurvature occurred when it changed its track from northwestward to north-northwest/northward from the evening of December 4th, 2023 (Division, 2023b).

Applying the suggested methodology resulted in an error rate of 0.78% for latitude and 0.37% for longitude (refer to Table 3.5), compared to the TC track data obtained from IMD. In contrast, traditional approaches such as ARCHER, ADT, and SATCON exhibited higher error rates (see Table 3.12) with 1.34%, 1.40%, and 1.40% for latitude, and 0.79%, 0.86%, and 0.86% for longitude, respectively. Additionally, the proposed method demonstrated significantly reduced RMSE values at 0.13 and 0.38 for latitude and longitude, respectively (see Table 3.13), compared to the corresponding RMSE values of 0.23, 0.26, and 0.26 for

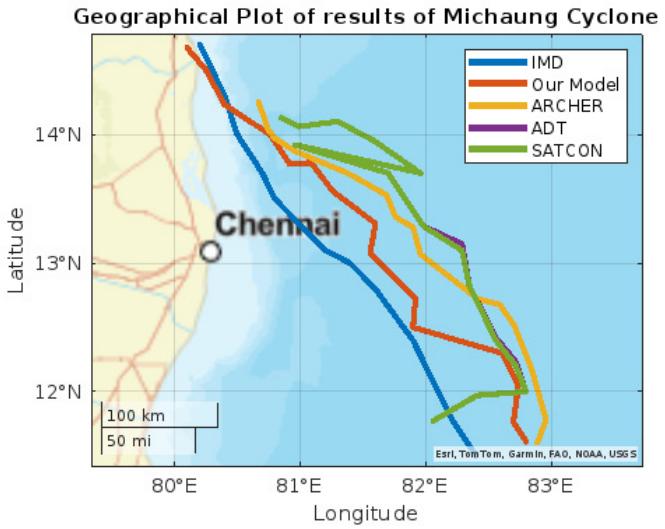

Figure 3.3: The result of the proposed method for calculating the tropical cyclone track of the SCS Michaung with other methods is shown graphically.

latitude and 0.66, 0.76, and 0.76 for longitude from conventional methods. The visual representation of these findings is presented in Fig. 3.3.

ESCS Tej

In 2023, the initial cyclone of the post-monsoon season and the second cyclone occurred over the Arabian Sea (AS). This event marked the third cyclone to land in Yemen since 1965, following Very Severe Cyclonic Storm (VSCS) Luban and Cyclonic Storm (CS) Sagar in 2018. Notably, from October 20 to October 24, 2023, two cyclones named "Tej" and "Hamoon" simultaneously developed over the Arabian Sea and the BoB.

The simultaneous formation of cyclones in both basins is considered a rare phenomenon. Climatologically, the AS witnessed the development of approximately 66 TCs with a Maximum Sustained Wind (MSW) of 62 km/h from 1965 to 2022. Tej followed a west-northwestward trajectory until the afternoon of October 21, 2023 (1430 hours IST/0900 UTC). Subsequently, it altered its course to move northwestward until 0000 UTC of October 23, 2023,

Table 3.5: Comparing the numerical results of the proposed method for calculating the tropical cyclone tracks of the SCS Michaung with the numerical results obtained from other methods.

Date/ Time	IMD		Proposed Method		ARCHER		ADT		SATCON		EP^a		EP^b		EP^c		EP^d	
	Lat.	Long.	Lat.	Long.	Lat.	Long.	Lat.	Long.	Lat.	Long.	Lat.	Long.	Lat.	Long.	lat.	Long.	lat.	Long.
03/03	11.5	82.4	11.61	82.90	11.60	82.89	11.77	82.06	11.77	82.06	0.98	0.61	0.87	0.59	2.35	0.41	2.35	0.41
03/06	11.8	82.2	11.76	82.70	11.78	82.96	11.97	82.41	11.97	82.41	0.26	0.68	0.17	0.92	1.44	0.26	1.44	0.26
03/09	12.0	82.1	12.05	82.84	12.19	82.84	12.00	82.80	12.00	82.80	0.47	0.90	1.58	0.90	0.00	0.85	0.00	0.85
03/12	12.2	82.0	12.30	82.71	12.51	82.71	12.20	82.72	12.20	82.72	0.90	0.87	2.54	0.87	0.00	0.88	0.00	0.88
03/15	12.4	81.9	12.50	81.90	12.68	82.59	12.40	82.56	12.40	82.56	0.89	0.00	2.26	0.84	0.00	0.81	0.00	0.81
03/18	12.8	81.6	12.72	81.92	12.72	82.42	12.82	82.35	12.82	82.35	0.62	0.39	0.63	1.00	0.16	0.92	0.16	0.92
03/21	13.0	81.4	13.08	81.56	13.07	81.96	13.10	82.29	13.10	82.29	0.65	0.20	0.54	0.69	0.77	1.09	0.77	1.09
04/00	13.1	81.2	13.31	81.60	13.28	81.90	13.29	81.98	13.29	81.98	1.62	0.49	1.37	0.86	1.45	0.96	1.45	0.96
04/03	13.3	81.0	13.56	81.26	13.36	81.76	13.70	81.70	13.70	81.70	1.98	0.32	0.45	0.94	3.01	0.86	3.01	0.86
04/06	13.5	80.8	13.78	81.09	13.53	81.69	13.92	80.96	13.92	80.96	2.10	0.36	0.22	1.10	3.11	0.20	3.11	0.20
04/09	13.7	80.7	13.77	80.92	13.70	81.38	13.70	81.96	13.70	81.96	0.58	0.27	0.00	0.84	0.00	1.49	0.00	1.49
04/12	14.0	80.5	14.00	80.76	13.87	80.96	13.95	81.59	13.95	81.59	0.05	0.32	0.93	0.57	0.36	1.35	0.36	1.35
04/15	14.3	80.4	14.23	80.40	13.97	80.80	14.10	81.30	14.10	81.30	0.46	0.00	2.31	0.50	1.40	1.12	1.40	1.12
04/18	14.5	80.3	14.50	80.25	14.03	80.75	14.06	80.99	14.06	80.99	0.05	0.06	3.24	0.56	3.03	0.86	3.03	0.86
04/21	14.7	80.2	14.67	80.10	14.25	80.67	14.13	80.85	14.13	80.85	0.16	0.12	3.06	0.57	3.88	0.81	3.88	0.81

[a]Error Percentage of our model with respect to Best track data provided by the IMD.
[b] Error Percentage of ARCHER method with respect to Best track data provided by the IMD.
[c] Error Percentage of ADT method with respect to Best track data provided by the IMD.
[d] Error Percentage of SATCON method concerning Best track data provided by the IMD.

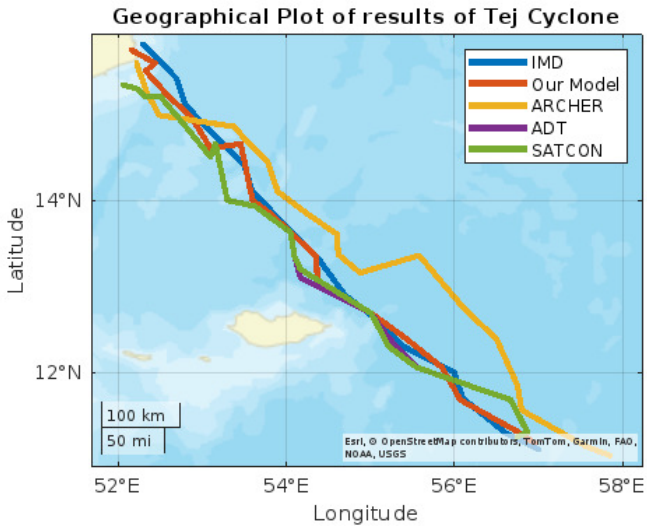

Figure 3.4: The result of the proposed method for calculating the tropical cyclone track of the ESCS Tej with other methods is shown graphically.

followed by a north-northwestward movement until landfall at 2100 UTC on October 23, 2023. After landfall, TEJ continued its trajectory, nearly moving westwards (Division, 2023a).

By implementing the proposed methodology, we achieved error percentage metrics of 0.57% and 0.20% for latitude and longitude, respectively, as detailed in Table 3.6, compared to the TC track data obtained from the IMD. In contrast, traditional approaches such as ARCHER, ADT, and SATCON exhibited higher error rates, as indicated in Table 3.12, with latitude errors of 1.67%, 1.02%, and 1.02%, and longitude errors of 1.14%, 0.51%, and 0.51%, respectively.

Furthermore, the proposed method demonstrated notably reduced RMSE values at 0.10 and 0.15 for latitude and longitude, respectively, as illustrated in Table 3.13. This contrasts sharply with the corresponding RMSE values for latitude (0.26, 0.18, and 0.18) and longitude (0.68, 0.31, and 0.31) obtained from conventional methods. The visual representation of these findings is presented in Fig. 3.4.

Table 3.6: Comparing the numerical results of the proposed method for calculating the tropical cyclone tracks of the ESCS Tej with the numerical results obtained from other methods.

Date/ Time	IMD		Proposed Method		ARCHER		ADT		SATCON		EP^a		EP^b		EP^c		EP^d	
	Lat.	Long.	Lat.	Long.	Lat.	Long.	Lat.	Long.	Lat.	Long.	Lat.	Long.	Lat.	Long.	lat.	Long.	lat.	Long.
21/15	11.1	57.0	11.18	56.95	11.03	57.85	11.25	56.75	11.25	56.75	0.72	0.44	0.62	1.49	1.35	0.44	1.35	0.44
21/18	11.3	56.6	11.30	56.77	11.14	57.56	11.30	56.87	11.30	56.87	0.00	0.48	1.42	1.70	0.00	0.48	0.00	0.48
21/21	11.7	56.1	11.68	56.07	11.56	56.80	11.68	56.67	11.68	56.67	0.17	1.02	1.20	1.25	0.17	1.02	0.17	1.02
22/00	12.0	56.0	12.06	55.85	11.85	56.75	12.06	55.55	12.06	55.55	0.50	0.80	1.25	1.34	0.50	0.80	0.50	0.80
22/03	12.3	55.4	12.40	55.42	12.39	56.50	12.40	55.22	12.40	55.22	0.81	0.32	0.73	1.99	0.81	0.32	0.81	0.32
22/06	12.6	55.1	12.69	55.01	12.75	56.11	12.69	55.01	12.69	55.01	0.71	0.16	1.19	1.83	0.71	0.16	0.71	0.16
22/09	12.9	54.7	13.06	54.37	13.36	55.58	13.10	54.17	13.10	54.17	1.24	0.97	3.57	1.61	1.55	0.97	1.55	0.97
22/12	13.3	54.4	13.35	54.36	13.16	54.88	13.35	54.10	13.35	54.10	0.38	0.55	1.05	0.88	0.38	0.55	0.38	0.55
22/15	13.6	54.1	13.63	54.05	13.37	54.62	13.63	54.05	13.63	54.05	0.22	0.09	1.69	0.96	0.22	0.09	0.22	0.09
22/18	13.8	53.9	13.83	53.83	13.61	54.60	13.93	53.63	13.93	53.63	0.22	0.50	1.38	1.30	0.94	0.50	0.94	0.50
22/21	14.1	53.6	14.00	53.60	13.85	54.24	14.00	53.30	14.00	53.30	0.71	0.56	1.77	1.19	0.71	0.56	0.71	0.56
23/00	14.4	53.5	14.65	53.46	14.10	53.90	14.65	53.16	14.65	53.16	1.74	0.64	2.08	0.75	1.74	0.64	1.74	0.64
23/03	14.7	53.2	14.60	53.10	14.45	53.78	14.50	53.10	14.50	53.10	0.63	0.19	1.70	1.09	1.36	0.19	1.36	0.19
23/06	15.0	52.9	14.95	52.88	14.65	53.56	14.88	52.78	14.88	52.78	0.33	0.23	2.33	1.25	0.80	0.23	0.80	0.23
23/09	15.1	52.8	15.20	52.60	14.85	53.38	15.20	52.50	15.20	52.50	0.66	0.57	1.66	1.10	0.66	0.57	0.66	0.57
23/12	15.4	52.7	15.49	52.33	14.98	52.49	15.19	52.33	15.19	52.33	0.58	0.70	2.73	0.40	1.36	0.70	1.36	0.70
23/15	15.6	52.5	15.58	52.44	15.25	52.34	15.28	52.24	15.28	52.24	0.12	0.50	2.24	0.30	2.05	0.50	2.05	0.50
23/18	15.8	52.3	15.73	52.16	15.58	52.22	15.33	52.06	15.33	52.06	0.44	0.46	1.39	0.15	2.97	0.46	2.97	0.46

SCS Mandous

Cyclone Mandous was a severe cyclonic storm that formed over the Bay of Bengal in December 2022. Making landfall in Tamil Nadu, India brought heavy rainfall and strong winds to the region. The cyclone caused significant damage to property and infrastructure, affecting the lives of thousands. Due to its slow movement, Mandous dumped copious amounts of rain, flooding several areas. While no major loss of life was reported, the economic impact of the cyclone was substantial, particularly for the agricultural sector (Yadav and Das, 2024c).

Our proposed methodology significantly outperformed traditional methods (ARCHER, ADT, and SATCON) in estimating TC tracks. As detailed in Table 3.7, our method achieved remarkably low error rates of 0.84% and 0.11% for latitude and longitude, respectively, compared to IMD TC track data. Conversely, traditional approaches displayed substantially higher error percentages (Table 3.12). Furthermore, our method exhibited significantly lower RMSE values for latitude and longitude (Table 3.13) than conventional methods. The graphical comparison of these results is provided in Fig. 3.5, clearly demonstrating the superiority of our approach.

A t-test analysis reveals that our model performs better than the other approaches.

ESCS Biparjoy

Cyclone Biparjoy was a powerful and erratic TC that formed over the Arabian Sea in June 2023. A significant weather event caused substantial damage in India and Pakistan. Biparjoy was notable for its long lifespan and rapid intensification. Despite causing disruptions and loss of life, extensive preparedness and evacuation efforts helped mitigate the overall impact.

Table 3.7: Comparing the numerical results of the proposed method for calculating the tropical cyclone tracks of the Mandous Cyclone with the numerical results obtained from other methods

Date/Time	IMD		Proposed Method		ARCHER		ADT		SATCON		EP^a		EP^b		EP^c		EP^d	
	Lat.	Long.	Lat.	Long.	Lat.	Long.	Lat.	Long.	Lat.	Long.	Lat.	Long.	Lat.	Long.	lat.	Long.	lat.	Long.
08/00	9.4	84.1	9.56	83.89	9.32	85.06	9.69	83.93	9.69	83.93	1.70	0.24	0.85	1.14	3.08	0.20	3.08	0.20
08/03	9.5	83.8	9.68	83.77	9.56	84.36	9.88	83.67	9.88	83.67	1.84	0.03	0.63	0.66	4.00	0.15	4.00	0.15
08/06	9.7	83.5	9.74	83.48	9.72	84.06	9.84	83.48	9.84	83.48	0.41	0.02	0.20	0.67	1.44	0.02	1.44	0.02
08/09	9.8	83.2	10.00	83.23	9.99	83.60	10.07	83.18	10.07	83.18	2.04	0.03	1.93	0.48	2.75	0.02	2.75	0.02
08/12	10.1	82.9	10.27	82.87	10.26	83.15	10.27	82.87	10.27	82.87	1.68	0.03	1.58	0.30	1.68	0.03	1.68	0.03
08/15	10.4	82.6	10.45	82.59	8.51	82.17	10.50	82.57	10.50	82.57	0.48	0.01	18.1	0.52	0.90	0.03	0.90	0.03
08/18	10.6	82.3	10.65	82.30	8.72	81.83	10.72	82.28	10.72	82.28	0.47	0.00	17.7	0.57	1.13	0.02	1.13	0.02
08/21	10.7	82.0	10.65	81.97	11.17	81.90	10.60	81.93	10.60	81.93	0.46	0.03	4.39	0.12	0.93	0.08	0.93	0.08
09/00	11.0	81.7	10.97	81.65	11.37	81.51	10.87	81.61	10.87	81.61	0.27	0.06	3.36	0.23	1.18	0.11	1.18	0.11
09/03	11.1	81.5	11.15	81.38	11.30	81.58	11.12	81.08	11.12	81.08	0.45	0.14	1.80	0.09	0.18	0.51	0.18	0.51
09/06	11.4	81.3	11.45	80.98	11.23	81.66	11.32	80.80	11.32	80.80	0.43	0.39	1.49	0.44	0.70	0.61	0.70	0.61
09/09	11.7	81.0	11.62	81.08	11.15	81.61	11.42	81.08	11.42	81.08	0.68	0.09	1.62	0.75	2.39	0.09	2.39	0.09
09/12	12.0	80.8	11.83	80.80	12.21	81.84	11.63	80.80	11.63	80.80	1.41	0.00	1.75	1.28	3.08	0.00	3.08	0.00
09/15	12.2	80.6	12.01	80.78	12.67	81.49	12.11	80.88	12.11	80.88	0.08	0.22	5.58	1.10	0.91	0.34	0.91	0.34
09/18	12.5	80.3	12.47	80.43	12.86	81.04	12.27	80.63	12.27	80.63	0.23	0.16	2.87	0.92	1.84	0.41	1.84	0.41
09/21	12.8	80.0	12.71	80.17	13.05	80.60	12.81	80.37	12.81	80.37	0.70	0.21	1.95	0.74	0.07	0.46	0.07	0.46

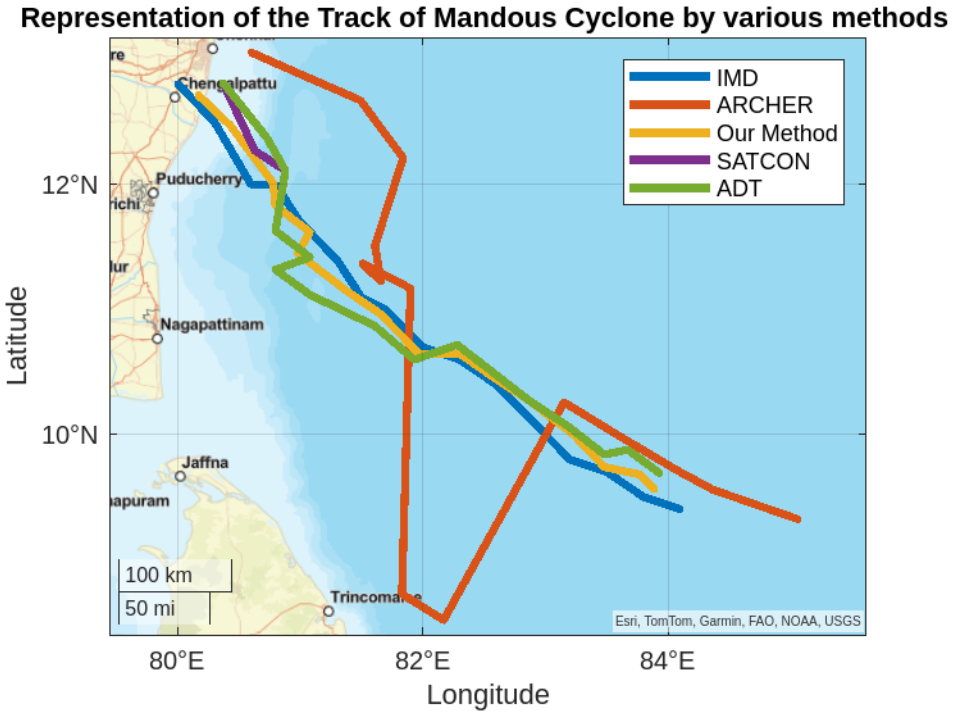

Figure 3.5: The result of the proposed method for calculating the tropical cyclone track of the Mandous cyclone with other methods

The cyclone served as a reminder of the increasing frequency and intensity of such weather events due to climate change.

Our proposed methodology significantly outperformed traditional methods (ARCHER, ADT, and SATCON) in estimating TC tracks. As detailed in Table 3.8, 3.9, our approach achieved error percentages of only 0.62% for latitude and 0.20% for longitude, compared to substantially higher error rates from conventional methods (Table 3.12). Moreover, our method yielded significantly lower Root Mean Square Error (RMSE) values of 0.16 for latitude and 0.10 for longitude (Table 3.13), underscoring its superior accuracy. These results are visually depicted in Fig. 3.6.

A t-test-based statistical analysis shows that our recommended approach betters the other approaches.

Table 3.8: Comparing the numerical results of the proposed method for calculating the tropical cyclone tracks of the Biparjoy Cyclone with the numerical results obtained from other methods: Part I

Date/Time	IMD		Proposed Method		ARCHER		ADT		SATCON		EP^a		EP^b		EP^c		EP^d	
	Lat.	Long.	Lat.	Long.	Lat.	Long.	Lat.	Long.	Lat.	Long.	Lat.	Long.	Lat.	Long.	lat.	Long.	lat.	Long.
06/21	12.5	66.0	12.35	66.15	12.25	66.20	12.40	66.30	12.40	66.30	1.20	0.22	2.00	0.30	0.79	0.45	0.79	0.45
07/00	12.6	66.1	12.59	66.19	12.49	66.29	12.47	66.38	12.47	66.38	0.07	0.13	0.87	0.28	1.03	0.42	1.03	0.42
07/03	12.7	66.2	12.65	66.25	12.65	66.35	12.60	66.30	12.60	66.30	0.39	0.07	0.39	0.22	0.78	0.15	0.78	0.15
07/06	12.8	66.3	12.88	66.27	12.88	66.27	12.69	66.33	12.69	66.33	0.62	0.04	0.62	0.04	0.85	0.04	0.85	0.04
07/09	13.1	66.3	13.11	66.29	13.11	66.19	13.00	66.40	13.00	66.40	0.07	0.01	0.07	0.16	0.76	0.15	0.76	0.15
07/12	13.3	66.3	13.37	66.19	13.47	66.19	13.27	66.19	13.27	66.19	0.52	0.01	1.27	0.01	0.22	0.01	0.22	0.01
07/15	13.4	66.0	13.46	65.96	13.37	65.91	13.70	66.40	13.70	66.40	0.22	0.06	0.22	0.13	2.23	0.60	2.23	0.60
07/18	13.6	66.0	13.56	65.99	13.36	65.99	13.85	66.38	13.85	66.38	1.02	0.01	1.76	0.01	1.83	0.57	1.83	0.57
07/21	13.7	66.0	14.00	66.06	13.36	66.06	13.90	65.80	13.90	65.80	1.02	0.09	2.48	0.09	1.45	0.30	1.45	0.30
08/00	13.9	66.0	14.10	66.25	14.00	66.35	14.05	65.72	14.05	65.72	0.71	0.37	0.71	0.53	1.07	0.42	1.07	0.42
08/03	14.0	66.0	14.15	66.12	14.16	66.32	13.55	66.81	13.55	66.81	0.71	0.18	1.14	0.48	3.21	1.22	3.21	1.22
08/06	14.1	66.0	14.34	65.86	14.19	65.76	14.05	66.16	14.05	66.16	0.35	0.21	0.63	0.36	0.35	0.24	0.35	0.24
08/09	14.3	66.0	14.73	65.90	14.34	65.70	14.60	65.69	14.60	65.69	0.27	0.15	0.27	0.45	2.09	0.46	2.09	0.46
09/00	14.7	66.2	14.83	66.32	14.73	66.32	14.78	66.35	14.78	66.35	0.20	0.18	0.20	0.18	0.54	0.22	0.54	0.22
09/03	14.8	66.4	15.05	66.43	14.93	66.43	14.80	66.70	14.80	66.70	0.20	0.04	0.87	0.04	0.00	0.45	0.00	0.45
09/06	15.0	66.6	15.26	66.71	15.08	66.81	14.97	66.77	14.97	66.77	0.33	0.16	0.53	0.31	0.19	0.25	0.19	0.25
09/09	15.3	66.9	15.45	68.09	15.22	67.19	15.30	66.90	15.30	66.90	0.26	0.28	0.52	0.43	0.00	0.00	0.00	0.00
09/12	15.5	67.1	15.80	67.26	15.42	67.46	15.47	66.98	15.47	66.98	0.32	0.23	0.51	0.53	0.19	0.17	0.19	0.17
09/15	15.7	67.3	16.06	67.31	15.88	67.31	15.70	67.30	15.70	67.30	0.63	0.01	1.14	0.01	0.00	0.00	0.00	0.00
09/18	16.0	67.4	16.30	67.35	16.26	67.35	15.87	67.35	15.87	67.35	0.37	0.07	1.62	0.07	0.81	0.07	0.81	0.07
09/21	16.3	67.4	16.36	67.34	16.35	67.24	16.40	67.40	16.40	67.40	0.00	0.08	0.30	0.23	0.61	0.00	0.61	0.00
10/00	16.5	67.4	16.66	67.35	16.26	67.30	16.58	67.45	16.58	67.45	0.84	0.07	1.45	0.14	0.48	0.07	0.48	0.07
10/03	16.7	67.4	16.75	67.30	16.54	67.30	16.80	67.40	16.80	67.40	0.23	0.14	0.95	0.14	0.59	0.00	0.59	0.00
10/06	16.8	67.4	16.84	67.38	16.69	67.28	16.94	67.42	16.94	67.42	0.29	0.02	0.65	0.17	0.83	0.02	0.83	0.02
10/09	16.9	67.4	16.90	67.32	16.84	67.26	16.68	69.34	16.68	69.34	0.35	0.11	0.35	0.20	1.30	2.87	1.30	2.87
10/12	17.1	67.3	17.28	67.24	16.99	67.24	17.57	67.45	17.57	67.45	1.16	0.08	0.64	0.08	2.74	0.22	2.74	0.22
10/15	17.3	67.3	17.41	67.44	17.18	67.44	17.50	67.40	17.50	67.40	0.11	0.20	0.69	0.20	1.15	0.14	1.15	0.14
10/18	17.4	67.3	17.73	67.46	17.51	67.49	17.67	67.45	17.67	67.45	0.05	0.23	0.63	0.28	1.55	0.22	1.55	0.22
10/21	17.6	67.3	18.05	67.45	17.83	67.55	17.51	66.67	17.51	66.67	0.73	0.22	1.30	0.37	0.51	0.49	0.51	0.49
11/00	17.9	67.4	18.27	67.50	18.15	67.60	17.42	67.41	17.42	67.41	0.83	0.14	1.39	0.29	2.68	0.01	2.68	0.01
11/03	18.0	67.6	18.27	67.70	18.37	67.68	18.13	67.61	18.13	67.61	1.49	0.14	2.05	0.11	0.72	0.01	0.72	0.01
11/06	18.2	67.7	18.47	67.69	18.27	67.69	18.27	67.69	18.27	67.69	0.38	0.01	0.38	0.01	0.38	0.01	0.38	0.01
11/09	18.4	67.7	18.51	67.80	18.37	67.80	18.38	67.65	18.38	67.65	0.38	0.14	0.16	0.14	0.10	0.07	0.10	0.07

Table 3.9: Comparing the numerical results of the proposed method for calculating the tropical cyclone tracks of the Biparjoy Cyclone with the numerical results obtained from other methods: Part II

Date/Time	IMD		Proposed Method		ARCHER		ADT		SATCON		EP^a		EP^b		EP^c		EP^d	
	Lat.	Long.	Lat.	Long.	Lat.	Long.	Lat.	Long.	Lat.	Long.	Lat.	Long.	Lat.	Long.	lat.	Long.	lat.	Long.
11/12	18.6	67.7	18.76	67.85	18.51	67.85	18.77	67.66	18.77	67.66	0.48	0.22	0.48	0.22	0.91	0.05	0.91	0.05
11/15	18.7	67.7	18.99	67.79	18.86	67.85	20.58	68.99	20.58	68.99	0.32	0.22	0.85	0.22	10.0	1.90	10.0	1.90
11/18	18.9	67.7	19.03	67.67	18.99	67.76	19.03	67.56	19.03	67.56	0.47	0.13	0.47	0.08	0.68	0.20	0.68	0.20
11/21	19.0	67.7	18.92	67.59	19.13	67.67	19.30	67.70	19.30	67.70	0.15	0.04	0.68	0.04	1.57	0.00	1.57	0.00
12/00	19.2	67.7	19.27	67.62	18.92	67.39	19.48	67.65	19.48	67.65	1.45	0.16	1.45	0.45	1.45	0.07	1.45	0.07
12/03	19.4	67.7	19.57	67.61	19.37	67.62	19.11	67.66	19.11	67.66	0.67	0.11	0.15	0.11	1.49	0.05	1.49	0.05
12/06	19.6	67.6	19.68	67.31	19.47	67.41	19.57	67.44	19.57	67.44	0.15	0.01	0.66	0.28	0.15	0.23	0.15	0.23
12/09	19.7	67.5	19.77	67.12	19.58	67.21	19.58	67.28	19.58	67.28	0.10	0.28	0.60	0.42	0.60	0.32	0.60	0.32
12/12	19.9	67.3	19.98	67.29	19.67	67.12	20.08	67.33	20.08	67.33	0.65	0.26	1.15	0.26	0.90	0.04	0.90	0.04
12/15	20.0	67.2	20.18	67.11	19.88	67.19	20.00	67.09	20.00	67.09	0.09	0.13	0.60	0.01	0.00	0.16	0.00	0.16
12/18	20.1	67.2	20.38	67.07	20.08	67.41	20.28	67.09	20.28	67.09	0.39	0.13	0.09	0.31	0.89	0.16	0.89	0.16
12/21	20.3	67.2	20.91	66.90	20.48	67.07	20.30	67.20	20.30	67.20	0.39	0.19	0.88	0.19	0.00	0.00	0.00	0.00
13/00	20.6	67.0	20.98	66.81	20.81	66.80	20.60	66.73	20.60	66.73	1.50	0.14	1.01	0.29	0.00	0.40	0.00	0.40
13/03	20.9	66.9	20.98	66.67	20.88	66.61	20.67	66.57	20.67	66.57	0.38	0.13	0.09	0.43	1.10	0.49	1.10	0.49
13/06	21.0	66.7	21.20	66.48	20.92	66.67	20.85	66.68	20.85	66.68	0.09	0.04	0.38	0.04	0.71	0.02	0.71	0.02
13/09	21.1	66.5	21.73	66.42	20.94	66.48	20.80	66.54	20.80	66.54	0.47	0.03	0.75	0.03	1.42	0.06	1.42	0.06
13/12	21.3	66.5	21.35	66.42	21.73	67.42	21.46	66.64	21.46	66.64	2.01	0.12	2.01	1.38	0.75	0.21	0.75	0.21
13/15	21.4	66.4	21.41	66.31	21.25	66.42	21.50	66.40	21.50	66.40	0.23	0.03	0.70	0.03	0.46	0.00	0.46	0.00
13/18	21.7	66.3	21.55	66.40	21.31	66.61	21.66	66.39	21.66	66.39	1.33	0.01	1.79	0.46	0.18	0.13	0.18	0.13
13/21	21.7	66.3	21.50	66.20	21.50	66.40	21.80	66.80	21.80	66.80	0.69	0.15	0.92	0.15	0.46	0.75	0.46	0.75
14/00	21.8	66.3	21.31	66.31	21.50	66.10	21.95	66.84	21.95	66.84	1.37	0.15	1.37	0.30	0.68	0.81	0.68	0.81
14/03	21.8	66.3	21.25	66.28	21.21	66.11	21.80	66.30	21.80	66.30	2.24	0.01	2.70	0.28	0.00	0.00	0.00	0.00
14/06	21.8	66.3	21.79	66.58	21.05	66.18	21.95	66.39	21.95	66.39	2.52	0.03	3.44	0.18	0.68	0.13	0.68	0.13
14/09	21.9	66.5	21.95	66.86	21.59	66.58	21.70	66.40	21.70	66.40	0.50	0.12	1.41	0.12	0.91	0.15	0.91	0.15
14/12	22.0	66.7	21.99	66.89	21.85	66.96	21.95	66.70	21.95	66.70	0.22	0.23	0.68	0.38	0.22	0.00	0.22	0.00
14/15	22.1	66.8	22.31	66.80	21.92	66.89	22.20	66.90	22.20	66.90	0.49	0.13	0.81	0.13	0.45	0.14	0.45	0.14
14/18	22.2	66.9	22.59	66.82	22.11	66.80	22.40	67.07	22.40	67.07	0.49	0.14	0.40	0.14	0.90	0.25	0.90	0.25
14/21	22.3	66.9	22.70	66.99	22.29	66.72	22.40	66.80	22.40	66.80	1.30	0.11	0.04	0.26	0.44	0.14	0.44	0.14
15/00	22.4	67.0	22.72	67.11	22.50	66.79	22.57	66.87	22.57	66.87	1.33	0.01	0.44	0.31	0.75	0.19	0.75	0.19
15/03	22.6	67.1	22.86	67.47	22.52	67.11	22.80	67.00	22.80	67.00	0.53	0.01	0.35	0.01	0.88	0.14	0.88	0.14
15/06	22.7	67.3	22.88	67.64	22.56	67.47	22.58	67.56	22.58	67.56	0.70	0.23	0.61	0.25	0.52	0.38	0.52	0.38
15/09	22.8	67.6	22.80	67.64	22.59	67.84	22.90	67.40	22.90	67.40	0.35	0.05	0.92	0.35	0.43	0.00	0.43	0.00
15/12	22.9	68.0	22.93	68.10	22.63	68.20	23.08	67.62	23.08	67.62	0.13	0.14	1.17	0.29	0.78	0.55	0.78	0.55

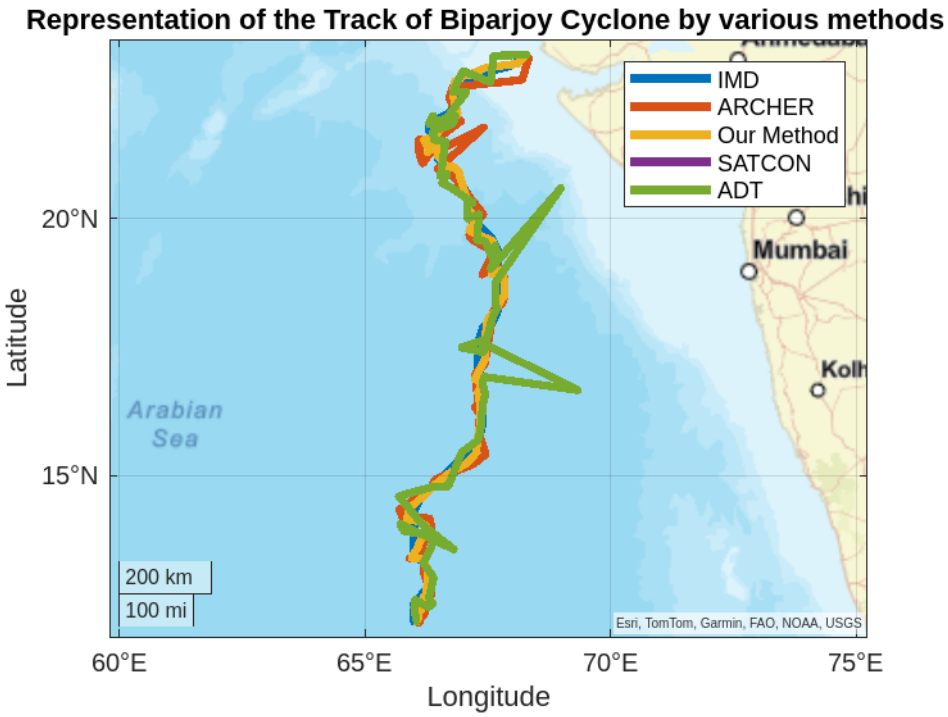

Figure 3.6: The result of the proposed method for calculating the tropical cyclone track of the Biparjoy cyclone with other methods

ESCS Mocha

Cyclone Mocha was an extremely severe cyclonic storm that wreaked havoc in the Bay of Bengal in May 2023. Originating as a low-pressure area, it rapidly intensified into a powerful cyclone and landed between Myanmar and Bangladesh. Known for its destructive winds and heavy rainfall, Mocha caused significant damage to infrastructure, agriculture, and livelihoods. The cyclone displaced thousands and resulted in numerous casualties. Despite early warnings and evacuation efforts, the storm's intensity and rapid intensification made it a challenging disaster to mitigate. Mocha is a stark reminder of the increasing threat of extreme weather events due to climate change.

Our proposed methodology significantly outperformed traditional methods (ARCHER, ADT, and SATCON) in estimating TC tracks. As detailed in Table 3.10, our method achieved remarkably low error rates of 0.62% and 0.09% for latitude and longitude, re-

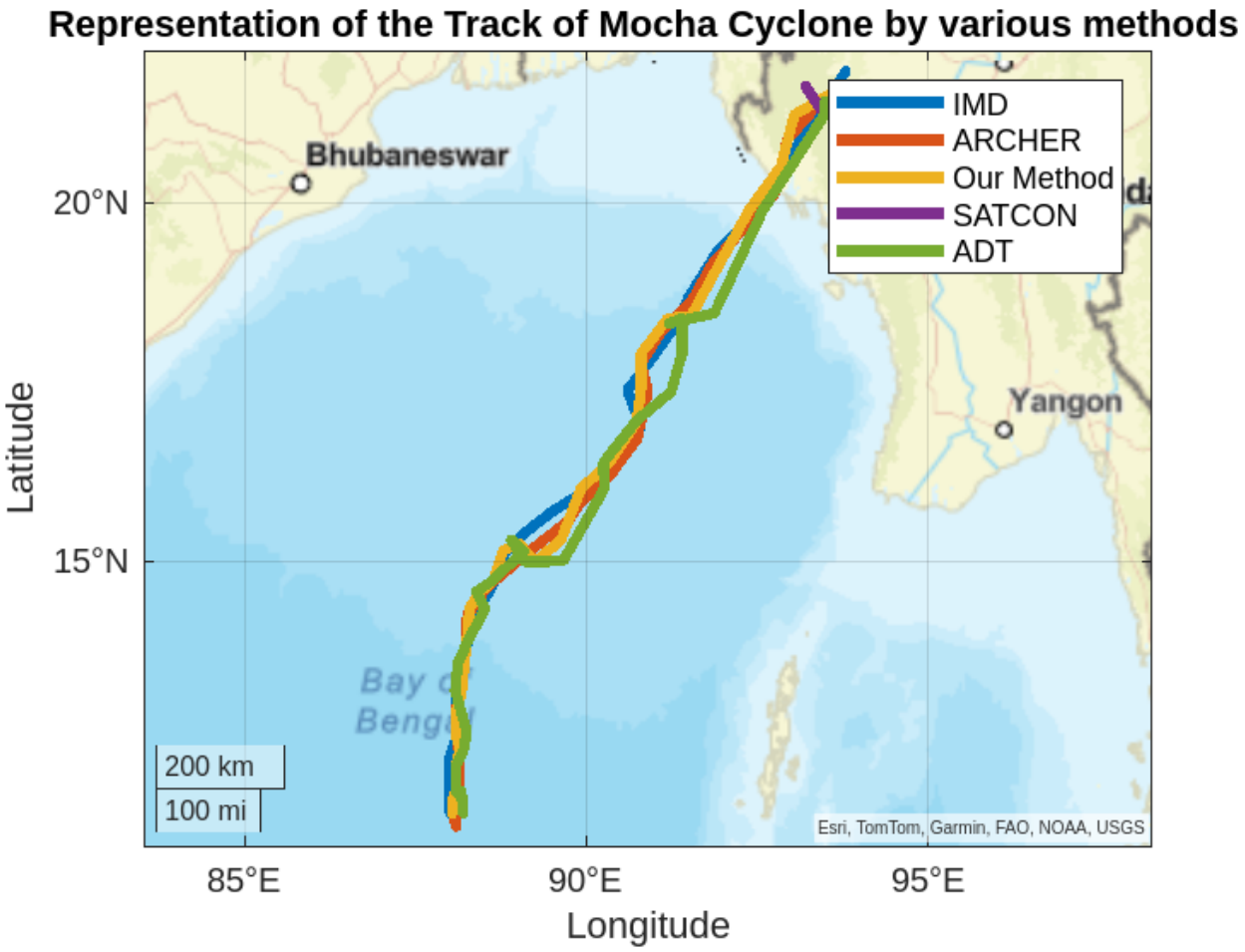

Figure 3.7: The result of the proposed method for calculating the tropical cyclone track of the Mocha cyclone with other methods

spectively, compared to IMD TC track data. In contrast, traditional methods exhibited considerably higher error rates, as shown in Table 3.12.

Furthermore, our method demonstrated superior performance in terms of RMSE, with values of 0.15 and 0.10 for latitude and longitude, respectively (Table 3.13). These results are substantially lower than those obtained from conventional approaches. Fig. 3.7 provides a graphical comparison of these findings.

The approach we propose is better than the other approaches, according to statistical analysis using a t-test.

Table 3.10: Comparing the numerical results of the proposed method for calculating the tropical cyclone tracks of the Mocha Cyclone with the numerical results obtained from other methods

Date/Time	IMD		Proposed Method		ARCHER		ADT		SATCON		EP^a		EP^b		EP^c		EP^d	
	Lat.	Long.	Lat.	Long.	Lat.	Long.	Lat.	Long.	Lat.	Long.	Lat.	Long.	Lat.	Long.	lat.	Long.	lat.	Long.
11/03	11.4	88.0	11.40	88.04	11.44	88.04	11.40	88.20	11.40	88.20	0.00	0.04	0.35	0.04	0.00	0.22	0.00	0.22
11/06	11.6	88.0	11.63	88.05	11.22	88.10	11.73	88.17	11.73	88.17	0.25	0.05	3.27	0.11	1.12	0.19	1.12	0.19
11/09	11.8	88.0	11.75	88.10	11.47	88.10	11.70	88.10	11.70	88.10	0.42	0.11	2.79	0.11	0.84	0.11	0.84	0.11
11/12	12.2	88.1	12.12	88.10	11.79	88.15	12.10	88.10	12.10	88.10	0.65	0.11	3.36	0.17	0.81	0.11	0.81	0.11
11/15	12.5	88.1	12.34	88.15	12.18	88.15	12.30	88.20	12.30	88.20	1.28	0.05	2.56	0.05	1.59	0.11	1.59	0.11
11/18	12.7	88.1	12.52	88.09	12.68	88.09	12.58	88.25	12.58	88.25	1.41	0.01	0.15	0.01	0.94	0.17	0.94	0.17
11/21	12.9	88.1	12.95	88.11	13.00	88.11	13.10	88.10	13.10	88.10	0.38	0.01	0.77	0.01	1.55	0.00	1.55	0.00
12/00	13.2	88.1	13.11	88.17	13.34	88.17	13.16	88.08	13.16	88.08	0.68	0.07	1.06	0.07	0.30	0.02	0.30	0.02
12/03	13.6	88.2	13.60	88.22	13.64	88.22	13.56	88.12	13.56	88.12	0.00	0.02	0.29	0.02	0.29	0.09	0.29	0.09
12/06	14.0	88.3	13.95	88.26	13.94	88.24	13.89	88.28	13.89	88.28	0.35	0.04	0.42	0.06	0.78	0.02	0.78	0.02
12/09	14.3	88.4	14.33	88.29	14.25	88.26	14.33	88.52	14.33	88.52	0.20	0.12	0.34	0.15	0.20	0.13	0.20	0.13
12/12	14.6	88.6	14.57	88.45	14.35	88.35	14.57	88.39	14.57	88.39	0.20	0.16	1.71	0.28	0.20	0.23	0.20	0.23
12/15	14.8	88.7	14.73	88.64	14.63	88.54	14.70	88.59	14.70	88.59	0.47	0.06	1.14	0.18	0.67	0.12	0.67	0.12
12/18	15.1	88.8	15.14	88.78	14.82	88.78	15.14	89.09	15.14	89.09	0.26	0.02	1.85	0.02	0.26	0.32	0.26	0.32
12/21	15.2	88.9	15.25	89.01	15.01	89.01	15.30	88.90	15.30	88.90	0.32	0.12	1.24	0.12	0.65	0.00	0.65	0.00
13/00	15.4	89.1	14.99	89.25	15.28	89.35	14.99	89.16	14.99	89.16	2.66	0.16	0.77	0.28	2.66	0.00	0.66	0.00
13/03	15.7	89.5	15.30	89.63	15.56	89.73	15.00	89.66	15.00	89.66	2.54	0.14	0.89	0.25	4.45	0.17	4.45	0.17
13/06	16.0	90.0	16.02	89.92	15.83	89.92	16.02	90.26	16.02	90.26	0.12	0.08	1.06	0.08	0.12	0.28	0.12	0.28
13/09	16.4	90.3	16.39	90.34	16.20	90.34	16.39	90.25	16.39	90.25	0.06	0.04	1.21	0.04	0.06	0.05	0.06	0.05
13/12	16.9	90.8	16.97	90.74	16.72	90.74	16.97	90.73	16.97	90.73	0.41	0.06	1.06	0.06	0.41	0.07	0.41	0.07
13/15	17.4	90.6	17.42	90.80	17.38	90.90	17.38	91.24	17.38	91.24	0.11	0.22	0.11	0.33	0.11	0.70	0.11	0.70
13/18	17.9	91.0	17.91	90.80	17.77	90.80	17.91	91.40	17.91	91.40	0.05	0.21	0.72	0.21	0.05	0.43	0.05	0.43
13/21	18.3	91.3	18.40	91.19	18.21	91.09	18.40	91.40	18.40	91.40	0.54	0.12	0.49	0.23	0.54	0.10	0.54	0.10
14/00	18.7	91.5	18.43	91.53	18.62	91.53	18.33	91.21	18.33	91.21	1.44	0.03	0.42	0.03	1.97	0.31	1.97	0.31
14/03	19.3	91.9	18.97	91.84	19.15	91.84	18.47	91.87	18.47	91.87	1.70	0.06	0.77	0.06	4.30	0.03	4.30	0.03
14/06	19.9	92.5	19.91	92.39	19.63	92.29	19.91	92.59	19.91	92.59	0.05	0.11	1.35	0.22	0.05	0.09	0.05	0.09
14/09	20.5	92.9	20.50	92.85	20.11	92.75	20.50	93.00	20.50	93.00	0.00	0.05	1.90	0.16	0.00	0.10	0.00	0.10
14/12	21.1	93.3	21.20	93.04	20.86	92.94	21.20	93.48	21.20	93.48	0.47	0.27	1.13	0.38	0.47	0.19	0.47	0.19
14/15	21.8	93.8	21.60	93.79	21.45	93.49	21.40	93.50	21.60	93.50	0.91	0.01	1.60	0.33	1.83	0.31	0.91	0.63

[a]Error Percentage of our model with respect to Best track data provided by the IMD.
[b] Error Percentage of ARCHER method with respect to Best track data provided by the IMD.
[c] Error Percentage of ADT method with respect to Best track data provided by the IMD.
[d] Error Percentage of SATCON method concerning Best track data provided by the IMD.

SCS Remal

Cyclone Remal was a severe cyclonic storm that struck the coastlines of West Bengal, India, and Bangladesh in May 2024. It was an early and unexpectedly strong cyclone, causing widespread damage and disruption in the region. Remal brought heavy rainfall, strong winds, and storm surges, leading to significant loss of life and property damage. The cyclone's impact was particularly severe in Bangladesh, where it was considered the costliest TC in the country's history. The rapid intensification of Remal highlighted the increasing unpredictability of extreme weather events in the region.

Our proposed methodology significantly outperformed traditional methods (ARCHER, ADT, and SATCON) in estimating TC tracks. As detailed in Table 3.11, our approach achieved error percentages of only 0.45% for latitude and 0.24% for longitude, compared to substantially higher error rates from conventional methods (Table 3.12). Moreover, our method yielded significantly lower Root Mean Square Error (RMSE) values of 0.11 for latitude and 0.25 for longitude (Table 3.13), underscoring its superior accuracy. These results are visually depicted in Fig. 3.8.

A t-test analysis reveals that our model performs better than the other approaches.

Traditional methods in TC forecasting often rely on simplistic linear or statistical models that may struggle to capture the complex, non-linear relationships inherent in TC behavior. These methods typically involve manual feature selection and may lack the adaptability to handle the sheer volume and diversity of data available in modern meteorological datasets. In contrast, an NN-based model trained on three experimental results, ARCHER, SATCON, and ADT of the TC track can provide more accurate estimation than traditional methods due to its ability to handle non-linear relationships, process large and varied datasets, adapt

Table 3.11: Comparing the numerical results of the proposed method for calculating the tropical cyclone tracks of the Remal Cyclone with the numerical results obtained from other methods

Date/Time	IMD		Proposed Method		ARCHER		ADT		SATCON		EP^a		EP^b		EP^c		EP^d	
	Lat.	Long.	Lat.	Long.	Lat.	Long.	Lat.	Long.	Lat.	Long.	Lat.	Long.	Lat.	Long.	lat.	Long.	lat.	Long.
25/18	19.3	89.4	19.55	89.30	18.55	89.08	18.87	89.10	18.87	89.10	1.29	0.11	3.88	0.35	2.22	0.33	2.22	0.33
25/21	19.4	89.4	19.46	89.30	19.46	88.83	19.20	89.10	19.20	89.10	0.30	0.11	0.30	0.63	1.03	0.33	1.03	0.33
26/00	19.5	89.4	19.58	89.25	19.88	89.22	19.34	89.01	19.34	89.01	0.41	0.16	1.94	0.20	0.82	0.43	0.82	0.43
26/03	19.8	89.3	19.90	89.20	19.90	88.89	19.70	89.00	19.70	89.00	0.50	0.00	0.50	0.34	0.50	0.22	0.50	0.22
26/06	20.2	89.2	20.27	89.10	20.37	88.84	20.53	88.61	20.53	88.61	0.34	0.11	0.84	0.40	1.63	0.66	1.63	0.66
26/09	20.6	89.2	20.56	89.01	20.56	88.54	20.70	88.90	20.70	88.90	0.19	0.21	0.19	0.73	0.48	0.33	0.48	0.33
26/12	21.1	89.2	21.11	88.92	21.11	88.81	21.02	88.89	21.02	88.89	0.04	0.31	0.04	0.43	0.37	0.34	0.37	0.34
26/15	21.4	89.2	21.47	88.88	21.47	88.65	21.20	88.80	21.20	88.80	0.32	0.35	0.32	0.61	0.93	0.44	0.93	0.44
26/18	21.7	89.2	21.77	88.86	21.87	88.72	21.53	88.84	21.53	88.84	0.32	0.38	0.78	0.53	0.78	0.40	0.78	0.40
26/21	22.0	89.2	22.16	88.71	22.26	88.80	22.00	88.51	21.90	88.47	0.72	0.54	1.81	0.44	0.00	0.77	0.45	0.81

[a]Error Percentage of our model with respect to Best track data provided by the IMD.
[b] Error Percentage of ARCHER method with respect to Best track data provided by the IMD.
[c] Error Percentage of ADT method with respect to Best track data provided by the IMD.
[d] Error Percentage of SATCON method concerning Best track data provided by the IMD.

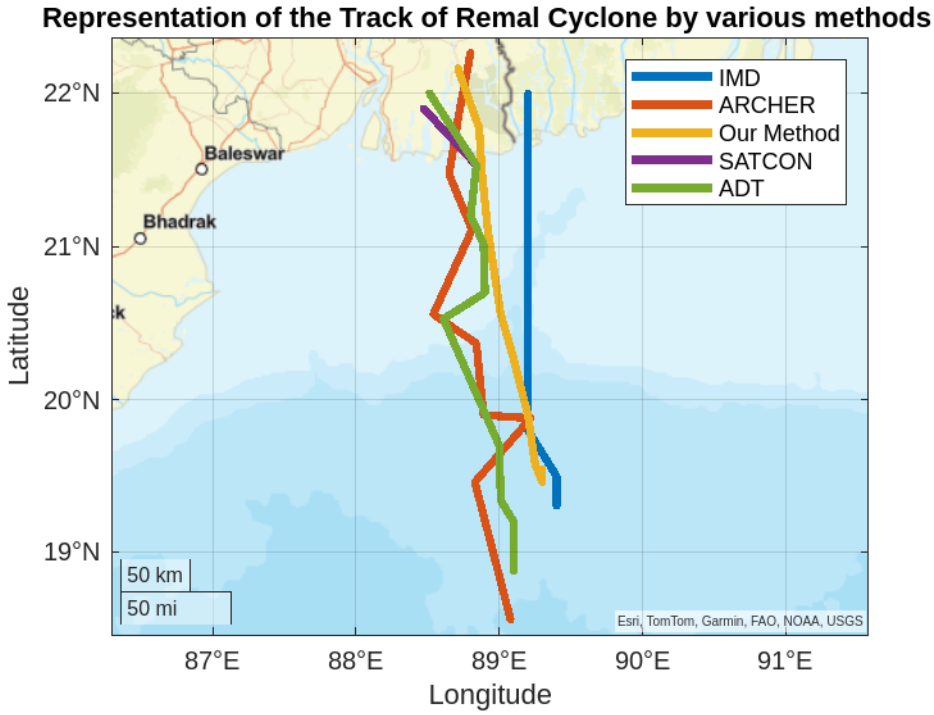

Figure 3.8: The result of the proposed method for calculating the tropical cyclone track of the Remal cyclone with other methods

to changing conditions, and generalize well to unseen data.

3.5 Conclusion

The study of the TC track represents a critical frontier in meteorological research and disaster management. The track of these powerful atmospheric phenomena is intricately linked to various characteristics, including intensity, storm eye, storm size, and the radius of maximum wind, collectively influencing the potential impact on the coastal regions. Accurate estimation of the TC track is essential for effective disaster preparedness, resource allocation, and timely evacuation measures.

Recent advancements in meteorological sciences have seen the integration of artificial intelligence, particularly neural networks, to enhance the accuracy of estimation of TC characteristics.

Our study proposes an NN-based model to estimate TC tracks, emphasizing the NIO. The methodology we employed is informed by a variety of scientifically validated practices in the field of machine learning and neural network optimization. Specifically, we employed normalization techniques, such as StandardScaler, to stabilize the learning process by ensuring all input features contribute proportionally, as discussed by Ioffe and Szegedy (2015). Including Leaky ReLU activation functions addressed issues like the vanishing gradient problem, a concern raised by Nair and Hinton (2010). Dropout layers, inspired by Srivastava et al. (2014), prevented overfitting by randomly dropping neurons during training. Considering the findings of Goodfellow et al. (2016), we optimized training parameters to balance convergence and computational efficiency. Our use of evaluation metrics, like error percentage and RMSE, was guided by statistical learning theory (Hastie et al., 2009), providing comprehensive insights into model performance. Visualization techniques outlined by Hertz et al. (1991) offered invaluable aids for interpreting and validating our model's predictions and training progress. Our adherence to these scientifically grounded principles ensures our NN-based model's robustness, accuracy, and generalization capability.

Our model exhibits superior performance compared to individual traditional methodologies. We conducted three statistical tests to show that our model was more accurate: t-test, error percentage analysis, and RMSE. The results presented in Table 3.12 demonstrate a reduced error percentage, while Table 3.13 highlights a lower RMSE, providing evidence of the model's enhanced accuracy.

Table 3.12: Detail of error percentage of both cases

Name of tropical cyclone	Component of Track	Proposed Method w.r.t. Best Track	ARCHER w.r.t. Best Track	ADT w.r.t Best Track	SATCON w.r.t. Best Track
Michaung	Latitude	0.78	1.34	1.40	1.40
Michaung	Longitude	0.37	0.79	0.86	0.86
Tej	Latitude	0.57	1.67	1.02	1.02
Tej	Longitude	0.20	1.14	0.51	0.51
Madous	Latitude	0.84	4.12	1.65	1.65
Mandous	Longitude	0.11	0.63	0.20	0.20
Biparjoy	Latitude	0.62	0.91	0.93	0.94
Biparjoy	Longitude	0.13	0.23	0.27	0.27
Mocha	Latitude	0.62	1.20	0.94	0.91
Mocha	Longitude	0.09	0.14	0.17	0.18
Remal	Latitude	0.45	1.00	0.88	0.93
Remal	Longitude	0.24	0.48	0.44	0.45
Mean	- -	0.41	1.13	0.68	0.70

Table 3.13: Detail of root square mean error of latitude of both cases

Name of tropical cyclone	Component of Track	Proposed Method w.r.t. Best Track	ARCHER w.r.t. Best Track	ADT w.r.t Best Track	SATCON w.r.t. Best Track
Michaung	Latitude	0.13	0.23	0.26	0.26
Michaung	Longitude	0.38	0.66	0.76	0.76
Tej	Latitude	0.10	0.26	0.18	0.18
Tej	Longitude	0.15	0.68	0.31	0.31
Mandous	Latitude	0.10	0.72	0.20	0.20
Mandous	Longitude	0.12	0.58	0.22	0.22
Biparjoy	Latitude	0.16	0.20	0.28	0.28
Biparjoy	Longitude	0.10	0.20	0.34	0.34
Mocha	Latitude	0.15	0.21	0.25	0.24
Mocha	Longitude	0.10	0.16	0.20	0.22
Remal	Latitude	0.11	0.29	0.21	0.21
Remal	Longitude	0.25	0.45	0.41	0.42
Mean	- -	0.14	0.38	0.30	0.31

Chapter 4

Analyze the SATCON Algorithm to Estimate the Tropical Cyclone's Intensity

"Mathematics is not about numbers, equations, computations, or algorithms: it is about understanding"

– William Paul Thurston

In this chapter[1], we analyze the performance of the Satellite Consensus (SATCON) algorithm to estimate the intensity of typhoons over the West Pacific basin. We compare the how well SATCON algorithm's performance in pre-monsoon and post-monsoon. Further, we analyze the performance according to different categories of TCs like tropical storms, severe tropical storms, typhoons, very strong typhoons, and violent typhoons.

---

[1] The content of this chapter is based on a research paper "Analyze the SATCON algorithm's capability to estimate tropical storm intensity across the West Pacific basin", *Journal of Earth System Science*, **SCIE, IF: 1.3**.

4.1 Introduction

Typhoon observation by meteorological satellites has largely reduced the challenge of detection. A constellation of geostationary (GEO) and polar-orbiting platforms regularly scans the tropics, and sensors with better spatial and spectrum sampling are used. Numerous types of multispectral photography can be used to qualitatively track and record typhoons' location, genesis, occurrence, and dissipation. Estimating the present typhoon intensity from space-based platforms is a little more complicated. It is possible to perform subjective analysis of typhoon cloud patterns using infrared (IR) images employing trained analysts and empirically supported guidelines. To analyze the CI and anchor typhoon intensity catalogs (or "best tracks") in the absence of in situ intensity observations, operational typhoon centers have depended extensively on the time-tested Dvorak technique (Dvorak, 1975, 1984) for many years. As crowdsourcing techniques demonstrate, even inexperienced analysts can accurately estimate the CI (Hennon et al., 2015). The inherent subjectivity in the interpretation of the images and restrictions on the capacity to detect structured convective structure beneath the normally massive and dense typhoon cirrus canopy, however, pose difficulties to IR-based cloud pattern recognition techniques (Velden et al., 2006; Knaff et al., 2010). Techniques that make use of cloud-penetrating microwave (MW) sensors (Brueske and Velden, 2003; Demuth et al., 2004; Bankert and Cossuth, 2016; Jiang et al., 2019) can be helpful in this area, but they also have drawbacks.

Obtaining accurate CI estimations is crucial for various reasons: The operational typhoon forecast process begins with the CI; it is one of the key input variables required to initialize both dynamical and statistical typhoon forecast models; and it is crucial for understanding typhoon climatologies and trends to have precise best-track intensities (Velden and Herndon,

2020). Forecasters (or best-track analysts) frequently struggle with the issue of competing satellite-based CI estimations with significant spread/uncertainty. Taken as a solution, a common conservative strategy is to average the estimations (simple consensus). A "smarter" consensus procedure, depending on the situational performance of each consensus attribute, is preferred since it further minimizes the CI estimate uncertainty.

Multiple satellite-fitted sensor-response data-based observation techniques are combined into an ensemble model, SATCON, created by the Cooperative Institute for Meteorological Satellite Studies (CIMSS). Below are basic explanations of SATCON's methodology.

Each attribute has situational strengths and weaknesses, represented by their separate intensity estimation error distributions, from which the individual attribute weights utilized in the SATCON process of finding a CI are created. Therefore, each attribute's performance behavior can be categorized into situational bins. For example, using the IR images of the scene type, the ADT technique (Olander and Velden, 2019) estimates the typhoon's intensity. When the eye scene is clear, it provides the best estimation; nevertheless, if it is not clear, the estimation is poor, or the outcome may be compromised. To best weight all of the available intensity estimates into a single, superior consensus estimate, SATCON uses this situational information. The typhoon intensity measurements, Mean Sea Level Pressure (MSLP), and Maximum Sustained Wind (MSW) have distinct performance traits, leading to various SATCON weighting algorithms for each metric.

Sharing information between sensors is another aspect of the SATCON process. Each SATCON attribute contains distinctive parametric data that the other coinciding attribute might use to evaluate the situational bins and modify the intensity estimates. For example, when an eye is observable in the IR, ADT generates typhoon eye size estimations (Kossin

et al., 2007).

Additional input sources to the SATCON process can come from operational TC centers via the Automated Tropical Cyclone Forecasting System (ATCF; Sampson and Schrader (2000)). These sources can include storm motion and the environmental pressure used in the pressure > wind. For storms that significantly differ from an average typhoon motion of roughly 11 kts ($1kts \approx 0.51ms^{-1}$), the methodology from (Schwerdt et al., 1979) can be used to make minor modifications to the final predicted MSW values.

4.2 Data and Methodology

We verified the "SATCON" output data by comparing it to the data provided by RSMC, Tokyo, of typhoon intensity for all typhoons between 2017 and 2021 over the West Pacific (particularly considering these storms that affect Japan). The SATCON algorithm's data collects from UW-CIMSS (`http://tropic.ssec.wisc.edu/misc/satcon`) and RSMC provided data collected from the RSMC, Tokyo (`jma.go.jp/jma/jma-eng/jma-center/rsmc-hp-pub-eg/RSMC_HP.htm`), to determine the optimal track parameters for typhoons. The number of typhoon cases included in the study is listed in Table 4.1 (Tokyo, 2017, 2018, 2019, 2020, 2021). 26 typhoons are therefore investigated in the current study. While there were additional typhoons within this timeframe, we have chosen to exclude them from our consideration.

In this paper, we examine three-hour observation data as a single case. For example, during Typhoon's lifetime, we collected eight three-hourly daily observations and considered these data as eight different cases.

Multiple satellite-fitted sensor response data-based observation techniques are combined

Table 4.1: In this study, the following typhoons were considered over the West Pacific Basin

SI. No.	Typhoon Name	Season	Date	Maximum Wind Speed (knots)	Classification
2021					
1	Surigae	Pre-Monsoon	12-30 Apr.	120 kts	Violent Typhoon
2	IN-FA	Pre-Monsoon	15-30 Jul.	85 kts	Typhoon
3	Chanthu	Post-Monsoon	05-20 Sept.	115 kts	Violent Typhoon
4	Rai	Post-Monsoon	11-21 Dec.	105 kts	Very Strong Typhoon
2020					
1	Vongfone	Pre-Monsoon	08-18 May	85 kts	Typhoon
2	Maysak	Post-Monsoon	27 Aug.-07 Sept.	95 kts	Very Strong Typhoon
3	Haishen	Post-Monsoon	30 Aug.-10 Sept.	105 kts	Very Strong Typhoon
4	Goni	Post-Monsoon	26 Oct.-06 Nov.	115 kts	Violent Typhoon
5	Molave	Post-Monsoon	22-29 Oct.	90 kts	Very Strong Typhoon
2019					
1	Nari	Pre-Monsoon	24-28 Jul.	35 kts	Tropical Storm
2	Danas	Pre-Monsoon	14-23 Jul.	45 kts	Tropical Storm
3	Lekima	Post-Monsoon	02-15 Aug.	105 kts	Very Strong Typhoon
4	Wutip	Post-Monsoon	08 Feb.-02 Mar.	105 kts	Very Strong Typhoon
5	Hagibis	Post-Monsoon	04-14 Oct.	105 kts	Very Strong Typhoon
6	Halong	Post-Monsoon	01-10 Nov.	115 kts	Violent Typhoon
2018					
1	Jelawat	Pre-Monsoon	24 Mar.-01 Apr.	105 kts	Very Strong Typhoon
2	Prapiroon	Pre-Monsoon	28 Jun.-05 Jul.	65 kts	Typhoon
3	Maria	Pre-Monsoon	03-13 Jul.	105 kts	Very Strong Typhoon
4	Shanshan	Post-Monsoon	02-11 Aug.	70 kts	Typhoon
5	Trami	Post-Monsoon	20 Sept.-03 Oct.	105 kts	Very Strong Typhoon
6	Kong-Rey	Post-Monsoon	28 Sept.-07 Oct.	115 kts	Violent Typhoon
2017					
1	Noru	Pre-Monsoon	19 July-12 Aug.	95 kts	Very Strong Typhoon
2	Talim	Post-Monsoon	08-22 Sept.	95 kts	Very Strong Typhoon
3	Sanvu	Post-Monsoon	26 Aug.-06 Sept.	80 kts	Typhoon
4	Lan	Post-Monsoon	15-23 Oct.	100 kts	Very Strong Typhoon
5	Hato	Post-Monsoon	19-24 Aug.	75 kts	Typhoon

into an ensemble model known as SATCON. The studies of the Geostationary-based Advanced Dvorak Technique and the Passive Microwave signal-based advanced sounding and imaging unit designed by the CIMSS. It provides a consensus intensity estimation of typhoons across all the basins. It uses a statistically determined weighting system that maximizes (minimizes) to evaluate consensus intensity for various typhoon structures (weaknesses). The intensity computation is built from a series of formulae dependent on the

number of attributes available, and the SATCON weights are proportional to the RMSE attribute values for the selected scenarios.

The three-part equation for SATCON (Velden and Herndon, 2020) is

$$SATCON = \frac{W_1W_2(W_1+W_2)E_3 + W_1W_3(W_1+W_3)E_2 + W_2W_3(W_3+W_2)E_1}{W_1W_2(W_1+W_2) + W_1W_3(W_1+W_3) + W_3W_2(W_3+W_2)}$$

where E_n is the attribute n's intensity estimations and W_n is the attribute n's weight (RMSE). The weights of attributes 1, 2, and 3 are W_1, W_2, and W_3, and the intensity estimations of attributes 1, 2, and 3 are E_1, E_2, and E_3.

The situational RMSE values for each attribute used to calculate the intensity estimate are known as attribute weights. The SATCON weighting structure's composition is intended to give more weight to a situational-dependent attribute with the highest efficiency (among the available attributes). For instance, the equation above shows how higher RMSEs (weights) of E_1 and E_2 are added to E_3. Thus adding greater weight to the specific estimation E_3, if E_3 is the best-performing attribute in a given context. For those more uncertain estimates, less weight (relatively smaller RMSEs) is to be allocated (E_1 and E_2) (Velden and Herndon, 2020).

One of the finest methods for estimating the typhoon intensity over the Atlantic and NIOs is the SATCON (Ahmed et al., 2022).

To evaluate the accuracy of the intensity forecasting and the effectiveness of the CIMSS-SATCON algorithm, 26 typhoons are used to validate the method (table 4.1). Comparison of RSMC, Tokyo (`jma.go.jp/jma/jma-eng/jma-center/rsmc-hp-pub-eg/RSMC_HP.htm`)

provided intensity estimation data with SATCON intensity estimates.

Between the estimation of estimated central pressure (ECP) and Vmax based on RSMC, Tokyo provided data, and SATCON calculation, various variables, which are root mean square difference (RMSD), actual mean difference (bias), and mean absolute difference (MAD), are determined. These variables are estimated for the various stages of a typhoon's "T" number, as specified in the RSMC, Tokyo-provided intensity data, inside each three-hourly observation that is at 00, 03, 06, 09, 12, 15, and 21 UTC throughout the whole period of a typhoon. The mean MAD, RMSD, and bias of intensity estimations across the West Pacific basin are estimated for various "T" numbers during the seasons and the entire year based on all typhoons considered. The student's t-test is used to determine whether there are any significant differences between the mean values over the West Pacific basin during the pre- and post-monsoon seasons.

Compared to the information provided by RSMC, Tokyo, the capability of SATCON has also been evaluated for various stages of typhoons. Table 4.2 displays the various typhoon stages used in RSMC, Tokyo.

Table 4.2: Different stage of typhoons with maximum sustained wind used in RSMC, Tokyo

Stage	Maximum Sustained Wind (knots; kts)
Tropical Storm	34-48 kts
Severe Tropical Storm	48-64 kts
Typhoon	64-85 kts
Very Strong Typhoon	85-105 kts
Violent Typhoon	105-130 kts

4.3 Results and discussion

In this section, we discuss the performance of the SATCON algorithm throughout the year, considering different time periods (pre-monsoon and post-monsoon), various typhoon categories, and a range of "T" numbers. The focus is primarily on typhoons that made landfall in Japan within the West Pacific basin.

4.3.1 For entire year, the capability of the "SATCON" algorithm over Japan (West Pacific)

This subsection discusses the year-round performance of the SATCON algorithm, considering different typhoon categories, cloud patterns defined by the Dvorak technique, and a range of "T" numbers.

Capability of the SATCON algorithm for various "T" number stages

Table 4.3 compares the capability of SATCON typhoon MSW and MSLP calculation to intensity estimation data provided by RSMC for typhoons across the West Pacific basin during 2017–2021. The bias progressively declines as the "T" number rises, but it gradually rises after T5.5, being roughly 16–10 knots (kts) for T2.0-T2.5, approximately 6–4 kts for T3.0-T5.0, and about 2 kts for T5.5. Due to the small sample size, the results for T6.0-T7.0 bias increasing with an increase in T number from roughly 8 to 21 kts may not be indicative. According to the student's t-test for the "T" numbers T2.0-T5.5 and T6.0-T7.0, the difference is significant with a 99% confidence level.

During this initial phase, accurately capturing the typhoon's traits using satellite sensors

Table 4.3: Calculated different parameters (in terms of MSW and MSLP) based on SATCON and RSMC, Tokyo provided data for typhoons during the year 2017-2021

Best track T No.	Total no. of cases	Best track intensity range	Best track intensity (MSW) (A^1)	SATCON intensity range	SATCON intensity MSW (B^1)	BIAS (A-B)	Mean absolute difference	RMSD
2.0	94	30-40	35	40-67	50.75	-15.75	15.4	17.98
2.5	99	40-50	42.68	40-70	52.97	-10.29	10.81	13.57
3.0	97	50-60	52.89	45-74	57.5	-4.61	5.13	12.18
3.5	166	60-70	62.65	46-92	82.1	-5.56	7.71	13.03
4.0	114	70-75	71.84	62-98	76.11	-4.27	10.08	12.83
5.0	123	75-80	80	69-100	83.47	-3.47	8.37	10.09
5.5	133	80-95	86.85	73-114	88.36	-1.51	6.93	11.72
6.0	98	95-105	97.5	90-122	105.04	-7.54	11.05	10.38
6.5	43	105-115	105.7	112-138	125.15	-19.45	20.18	21.76
7.0	16	115-125	115.93	122-144	136.47	-20.57	21.06	22.85
MSLP (hPa)								
Best track T No.	Total no. of cases	Best track intensity range	Best track intensity (MSLP) (A^1)	SATCON intensity range	SATCON intensity MSLP (B^1)	BIAS (A-B)	Mean absolute difference	RMSD
2.0	21	996-1003	1005.85	984-1004	1002.03	3.82	4.92	6.28
2.5	35	983-1002	972.54	981-1004	970.59	1.95	4.01	6.83
3.0	158	983-996	971.86	980-1000	969.5	2.36	5.58	7.09
3.5	116	978-991	970.58	967-999	966.34	4.24	7.16	9.43
4.0	104	975-988	964.67	957-994	959.5	5.17	9.78	11.13
5.0	82	964-982	988.18	950-980	981.43	6.75	8.16	9.72
5.5	45	955-964	962.45	939-976	956.38	6.07	9.09	10.73
6.0	36	946-956	958.57	934-970	955.36	3.21	7.89	8.29
6.5	22	932-946	898.11	922-940	891.69	6.42	8.95	8.47
7.0	17	922-930	865.35	920-935	867.83	-2.48	6.72	7.43

proves difficult due to their less distinct features and smaller size. Consequently, estimating the intensity of these weaker systems can result in more pronounced errors. As these typhoons progress and intensify into the moderate to strong category (T3.0-T5.0), their more defined structures and larger sizes facilitate the satellite sensors in acquiring pertinent data. This increased availability of reliable data and the heightened organization of these typhoons culminate in reduced intensity errors. Extremely powerful typhoons (T6.0-T7.0) are characterized by exceedingly high wind speeds and intense convective activity. These formidable systems may display swift fluctuations within their inner core and eyewall, posing challenges for satellite sensors and forecasting models to gauge their intensity precisely. The SATCON algorithm reports elevated intensity errors for these cases.

After the T3.5, the MAD is approximately 10–14 kts, and the MAD is approximately 12–16 kts for T2.0-T.3.0 . Due to the small sample size, the higher MAD value in the T6.5 range could not be indicative. The MAD values for T5.0 and above across the west Pacific (7–10 kts) are consistent with Herndon and Velden (2018); Velden and Herndon (2020) observations.

Consequently, the intensity is estimated to be overestimated (negative bias) by approximately 2 hPa for T7.0, approximately 2–5 hpa for T2.0-T3.5, and approximately 5–7 hPa for more than T3.5. For the range of T2.0-T6.5, the underestimate is statistically significant at a 99% level of confidence. For T2.0-T2.5, the MAD is approximately 5 hPa, and for T3.0-T7.0, it is approximately 5–10 hPa. For T2.0-T3.0, the RMSD is about 6–7 hPa; for T3.5-T7.0, it is approximately 8–11 hPa.

Results of the SATCON technique for the various typhoon categories

The SATCON method and the intensity estimation data provided from the RSMC, Tokyo, were used to analyze the average characteristics of tropical storms to violent typhoons over the West Pacific basin between the years 2017–2021 in terms of the MSW (knots) and MSLP (hPa). It demonstrates that as a typhoon goes to a higher category, the basis steadily reduces from 14 to 10 kts for a tropical storm to a very strong typhoon but increases for a violent typhoon, which is 12.21 kts, which may happen due to the small sample size (table 4.4). Accordingly, the bias is reduced for stronger typhoons, except violent typhoons, which is consistent with Herndon and Velden (2018); Velden and Herndon (2020) findings. Although the MAD is for typhoons, severe typhoons, and tropical storms, approximately 9–12 kts, and approximately 7–11 kts for very strong and violent typhoons (figure 4.1), the overestimation is statistically significant for all typhoon categories at a 99 % confidence level.

Intensity errors in typhoons over the Pacific Ocean are closely tied to several factors. The sensitivity of Pacific Ocean typhoons to sea surface temperatures (SST) is particularly noteworthy. If SSTs are not accurately predicted, this can significantly impact the accuracy of typhoon intensity forecasts.

Furthermore, typhoons in the Pacific Ocean frequently contact land masses, including Mexico and Central America. These land interactions can disrupt the storm's typical structure, often resulting in rapid weakening. Accurately predicting the extent and timing of these disruptions poses a considerable challenge.

In addition to these land interactions, typhoons in this region exhibit diurnal variations in intensity. Environmental factors like daytime heating and nighttime cooling drive these daily fluctuations. Accurately forecasting these intensity changes remains a complex task,

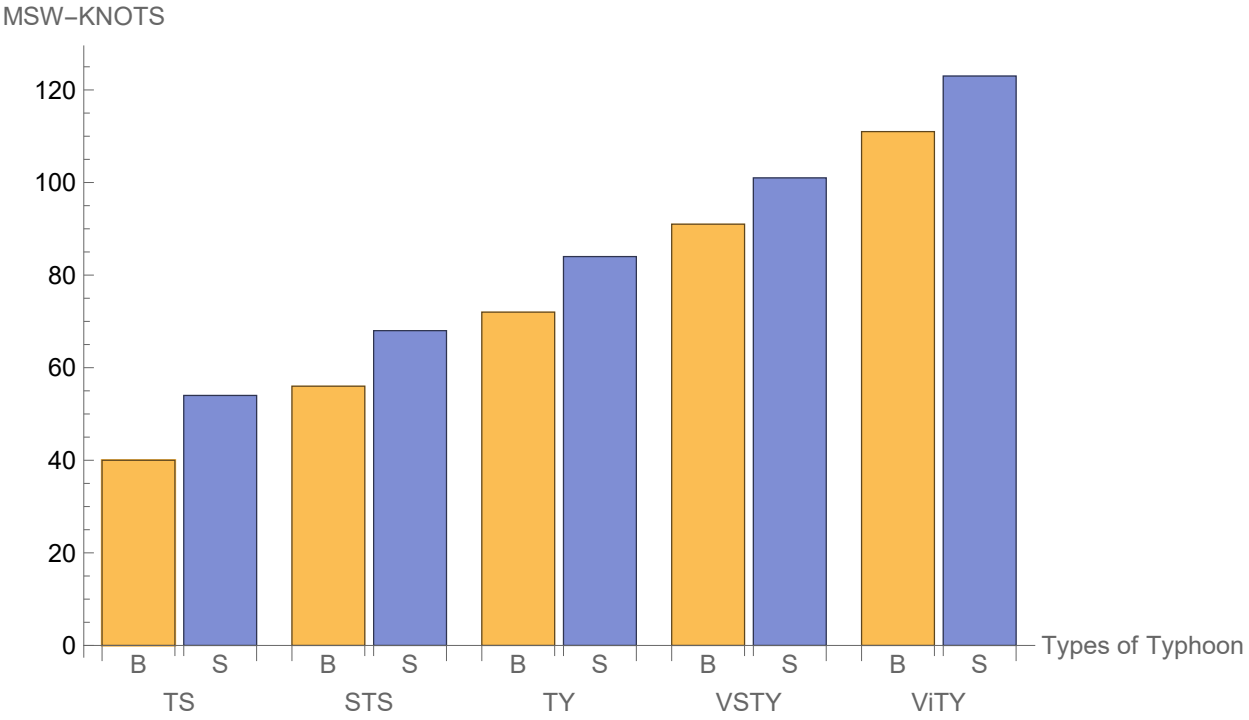

Figure 4.1: Compared the intensity estimation by SATCON and RSMC provided data for all typhoons (state wise) over the west pacific basin from 2017-2021. B stands for RSMC provided data, S stands for SATCON algorithm data, ViTY stands for Violent Typhoon, VSTY for Very Strong Typhoon, TY for Typhoon, STS for Severe Tropical Storm, and TS for Tropical Storm

further contributing to the challenge of predicting typhoon intensity in the Pacific Ocean.

The MAD value for typhoons and intense typhoons (8–10 kts) is consistent with Herndon and Velden (2018); Velden and Herndon (2020) prior findings. A slight increase in MAD intensity over the West Pacific basin is recorded for tropical storms, severe tropical storms, and very strong typhoons compared with (Herndon and Velden 2018, 2020). For tropical storms, severe tropical storms, typhoons, and very strong typhoons, the RMSD values over the West Pacific are approximately 11–14, and for violent typhoons, they are less than 10 kts. The Violent typhoon RMSD estimates across the West Pacific (<10 kts) are consistent with (Herndon and Velden 2018, 2020) earlier observations. However, compared to (Herndon and Velden, 2018; Velden and Herndon, 2020) findings, the RMSD values over the West Pacific for the tropical storm, severe tropical storm, typhoon, and very strong typhoon categories

Table 4.4: Compared the SATCON and RSMC, Tokyo provided data (in terms of MSW and MSLP) of typhoons (stage wise) over the West Pacific basin during the year 2017-2021

Category	Total no. of cases	Best track range	Best track MSW (A[1])	SATCON range	SATCON MSW (B[1])	BIAS (A-B)	Mean absolute difference	RMSD
Violent Typhoon	34	105-130	110.8	116-144	123.01	-12.21	7.43	9.24
Very Strong Typhoon	79	85-105	90.89	73-138	101.36	-10.47	10.97	12.5
Typhoon	167	64-85	72.23	62-100	84.07	-11.84	9.61	11.43
Severe Tropical Storm	108	48-64	55.73	46-92	68.21	-12.48	11.06	13.74
Tropical Storm	251	34-48	39.59	40-74	53.93	-14.34	10.89	12.96
MSLP (hPa)								
Category	Total no. of cases	Best track range	Best track MSLP (A[1])	SATCON range	SATCON MSLP (B[1])	BIAS (A-B)	Mean absolute difference	RMSD
Violent Typhoon	28	920-928	925.56	922-940	928.45	-2.89	6.94	7.24
Very Strong Typhoon	75	932-966	962.63	930-972	957.17	5.46	8.41	9.58
Typhoon	168	964-984	981.81	953-983	975.73	6.08	9.08	10.43
Severe Tropical Storm	106	983-990	980.58	965-990	976.3	4.28	7.83	9.12
Tropical Storm	267	983-1002	1003.29	984-1004	1002.03	1.26	6.14	7.01

[a]In each range, there are several cases where the mean has been calculated and represented by A and B.
In each range of the Best Track data, A represents the mean values of the number of cases.
In each range of the SATCON data, B represents the mean values of the number of cases.

are marginally greater (11–14 kts).

As a result, the intensity is understated (negative bias) in terms of MSLP by about −3 hPa for violent typhoons and 1–6 hPa for all other types of storms. The MAD is roughly 6 hPa for tropical storms, and for all other storm types, it is between 7–9 hPa. All storm types have RMSD values between 7 and 11 hPa.

The performance of SATCON algorithm estimations for various cloud patterns developed in the West Pacific Ocean as defined by the Dvorak Technique (Dvorak, 1975, 1984)

The SATCON algorithm shows the overestimation of the intensity of typhoons during the beginning stage of formation and up to T2.5; it may be seen from this. But after that, it was discovered that its performance is fairly good in measuring the intensity of stronger typhoons (more than Severe Tropical storms). The SATCON method creates a single estimate from several typhoon intensity estimations derived from objective intensity algorithms. The major component of the SATCON model, ADT 9.0, feeds continuous inputs into the model every 30 minutes, whilst the microwave sounder satellite feeds irregular intensity inputs into the model, which are then extrapolated to hourly estimations. The final SATCON estimate is produced by combining these interpolated estimates with ADT estimates. An objective method evolved from the original Dvorak Technique is used by the ADT to calculate intensity. The cloud organization pattern is not specified until T2.5 in the first development phase. Currently, the Dvorak Technique cannot comprehend the intricate details of cloud patterns. Because of this, both the ADT 9.0 technique and SATCON overstate the intensity estimations based on the methodology's pre-defined fixed cloud pattern, primarily the central dense overcast (CDO) and eye pattern, regardless of whether it is a curved band or

shear pattern. The shear pattern typhoons have a maximum strength of T3.0, and most typhoons over the West Pacific originate from shear patterns under the influence of monsoon circulation. As a result, when the intensity is T2.0 or higher, the ADT 9.0 version and SATCON are utilized globally. Additionally, the SATCON algorithm is reasonably good for T3.0 and more because typhoons whose intensity is more than T3.0 show clear cloud patterns, i.e., either eye pattern or CDO. In addition, SATCON used the new ADT 9.0 methodology, which integrates infrared sensor, short-wave infrared imaging sensor, visible imaging sensor, and microwave images to find phenomena that the original Dvorak Technique was unable to find, such as secondary eye-wall formation, double eyewall structure, the center in the presence of cirrus canopy, coiling of convective clouds (in the presence of cirrus) around the center, and eye-wall replacement cycle (Olander and Velden, 2019).

Given the foregoing, forecasters can utilize the SATCON technique to estimate intensity in the case of stronger typhoons (T3.0 or more). As cloud organization patterns are not clearly defined in the beginning stage, and the automated approach of ADT (an attribute of SATCON) selects pre-established patterns, overestimating the intensity results, it is unsuitable for cyclogenesis and the beginning phase of typhoon formation. However, forecasters can accurately estimate typhoon intensities based on SATCON data using the bias, RMSD, and MAD calculated in this study.

4.3.2 Capability of SATCON algorithm in various seasons

This subsection discusses the session-wise (pre- and post-monsoon) performance of the SATCON algorithm.

The pre-monsoon season's capabilities of the SATCON algorithm

SATCON typhoon MSW (kts) and MSLP (hPa) estimates' capability in comparison to RSMC Tokyo intensity estimate data for typhoons developed over the west Pacific during the pre-monsoon are shown in tables 4.5 and 4.6. Except for very strong typhoons, the bias value stays high during all phases of typhoons at roughly 11–18 kts. A very strong typhoon has a bias value of less than 1 kts (fig. 4.2). The smaller sample size may cause the very strong typhoon's unrepresentative value. According to the student's t-test for all types of typhoons, the difference is significant at a 99% confidence level.

For tropical storms, severe tropical storms, and typhoons, the MAD is approximately 12–19 kts; for very strong typhoons, it is approximately 4 kts. The RMSD ranges between 13 and 19 kts for tropical storms, severe tropical storms, and typhoons and between 4 and 5 kts for very strong typhoons. This contradicts (Herndon and Velden, 2018; Velden and Herndon, 2020) past findings.The average SATCON intensity, in turn, overestimates the MSW in the pre-monsoon season by around 11 kts and underestimates the average MSLP estimations by nearly 7 hPa, as demonstrated in Table 4.5.

The onset of the monsoon marks the beginning of the pre-monsoon season, characterized by shifts in atmospheric circulation patterns. These changes introduce additional uncertainty into typhoon movement predictions, diminishing their accuracy. The East Asian monsoon strongly influences the North West Pacific basin, significantly altering atmospheric circulation patterns. Consequently, the normal flow is disrupted, and predicting cyclone tracks during the pre-monsoon period becomes more intricate.

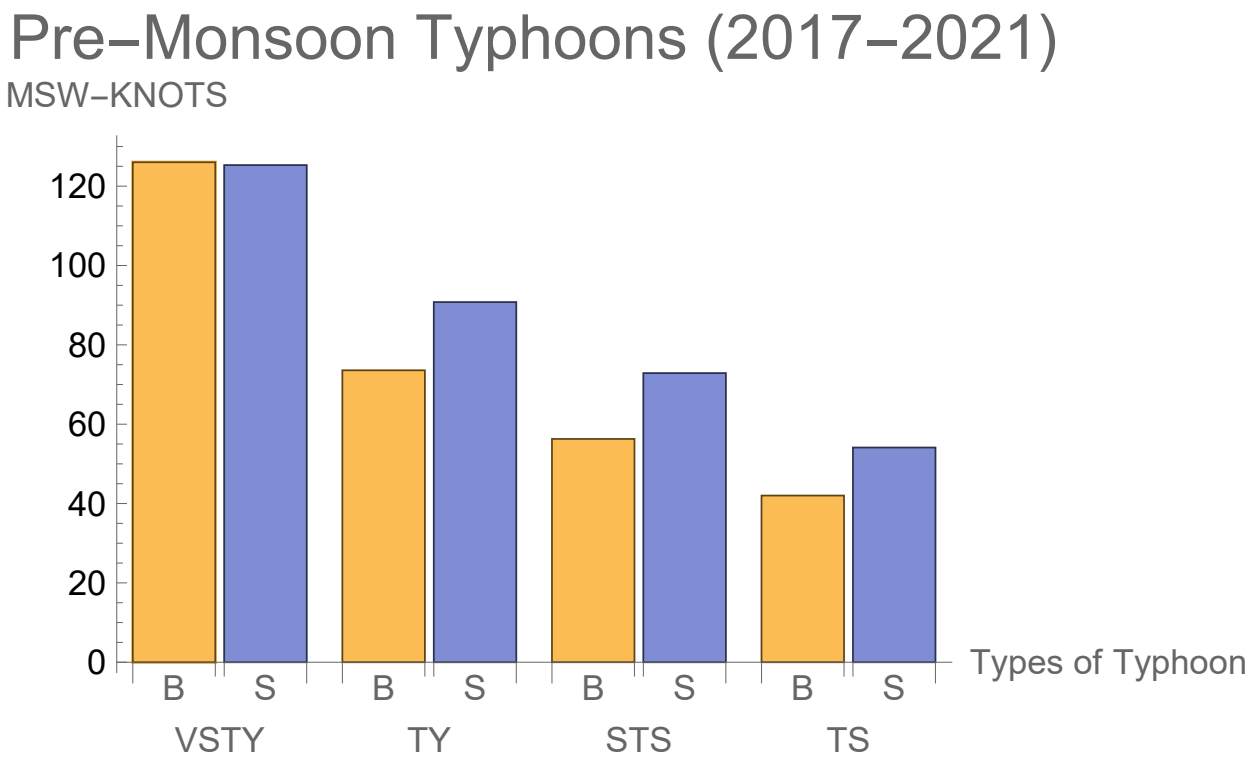

Figure 4.2: Compared the intensity estimation by SATCON and RSMC provided data for pre-monsoon season. B stands for RSMC provided data, S stands for SATCON algorithm data, VSTY for Very Strong Typhoon, TY for Typhoon, STS for Severe Tropical Storm, and TS for Tropical Storm

The post-monsoon season's capabilities of the SATCON algorithm

Tables 4.5 and 4.6 show the capability of SATCON's algorithm of typhoons MSW (kts) and MSLP (hPa) estimations compared to RSMC, Tokyo provided data of intensity estimates for typhoons developed across the west Pacific during the year 2017–2021's post-monsoon. When the strength rises, the bias steadily decreases between 2 and 7 knots for tropical storms, severe typhoons, and typhoons, and between 11 to 13 knots for extremely strong and violent typhoons (figure 4.3). The student's t-test for all forms of typhoons indicates that the difference is significant at a 99% level of confidence. The bias value for the typhoon stage is consistent with Herndon and Velden (2018); Velden and Herndon (2020) research.

The MAD for a tropical storm is approximately 11 knots. For typhoon categories such as severe tropical storms, typhoons, very strong typhoons, and violent typhoons, it is between 8 and 10 knots. The results of Herndon and Velden (2018); Velden and Herndon (2020) are supported by the MAD values throughout the west Pacific for severe tropical storms, typhoons, very strong typhoons, and violent typhoon stages (8–10 kts).

Moderate to strong typhoon intensities typically encompass tropical storms, severe typhoons, and typhoons. These typhoons exhibit well-defined structures and sufficient size for accurate data collection by satellite sensors. Enhanced data availability and improved forecasting models contribute to relatively minor intensity errors, usually between 2 to 7 knots, as these models better grasp the typhoons' dynamics. The predictability of atmospheric conditions and interactions within this intensity bracket exceeds that of more extreme typhoon categories.

On the contrary, very severe and violent typhoons are distinguished by their remarkably high wind speeds and intense convective activity. These cyclones' intricate and rapidly

shifting inner cores challenge satellite sensors and models in precisely gauging their strength. Within this category, substantial intensity errors, ranging from 11 to 13 knots, arise due to the complexities of capturing these formidable typhoons' dynamic and exceptionally variable processes. Elements like rapid oscillations in the eyewall structure interplay with the surrounding environment and abrupt shifts in atmospheric conditions all contribute to these inaccuracies.

However, compared to Herndon and Velden (2018); Velden and Herndon (2020) findings, the MAD values for the tropical storm stage are slightly higher (11 kts). The RMSD across the West Pacific is approximately 10–14 kts for all storm types. This contradicts (Herndon and Velden, 2018; Velden and Herndon, 2020) earlier research conclusions. Table 4.5 demonstrates that the average SATCON intensity underestimates the average MSLP estimates by around 5 hPa while overestimating the average MSW during the post-monsoon season by nearly 9 kts.

4.4 Conclusion

The key takeaways from the results and discussions above are listed below.

Tropical storms, severe tropical storms, typhoons, very strong typhoons, and violent typhoon types of typhoons were examined in terms of intensity ('T' number) estimates across the West Pacific basin from 2017 to 2021 using data from RSMC, Tokyo, and the SATCON algorithm. As typhoons progress through the initial development phase, the range of overestimation of SATCON intensity estimation decreases. The result for T6.0-T7.0 may not be representative due to the sample size.

When we compared the SATCON algorithm's output with the data provided by the

Table 4.5: Compared the SATCON and RSMC, Tokyo provided data (MSW/MSLP) for typhoons over the West Pacific basin during the year 2017-2021 as pre-monsoon, post-monsoon, and annual

Season	Total no. of cases	Best track MSW (A^1)	SATCON MSW (B^1)	BIAS (A-B)	Mean absolute difference	RMSD
Pre-Monsoon	158	64.85	75.59	-10.74	11.53	13.96
Post-Monsoon	308	59.51	66.26	-6.75	9.38	12.21
Annual Season	466	62.18	70.92	-8.74	10.83	13.07
MSLP (hPa)						
Season	Total no. of cases	Best track MSW (A^1)	SATCON MSW (B^1)	BIAS (A-B)	Mean absolute difference	RMSD
Pre-Monsoon	156	984.13	976.3	7.83	8.55	10.59
Post-Monsoon	359	959.39	958.16	1.23	5.34	7.24
Annual Season	515	971.76	967.23	4.53	6.86	8.79

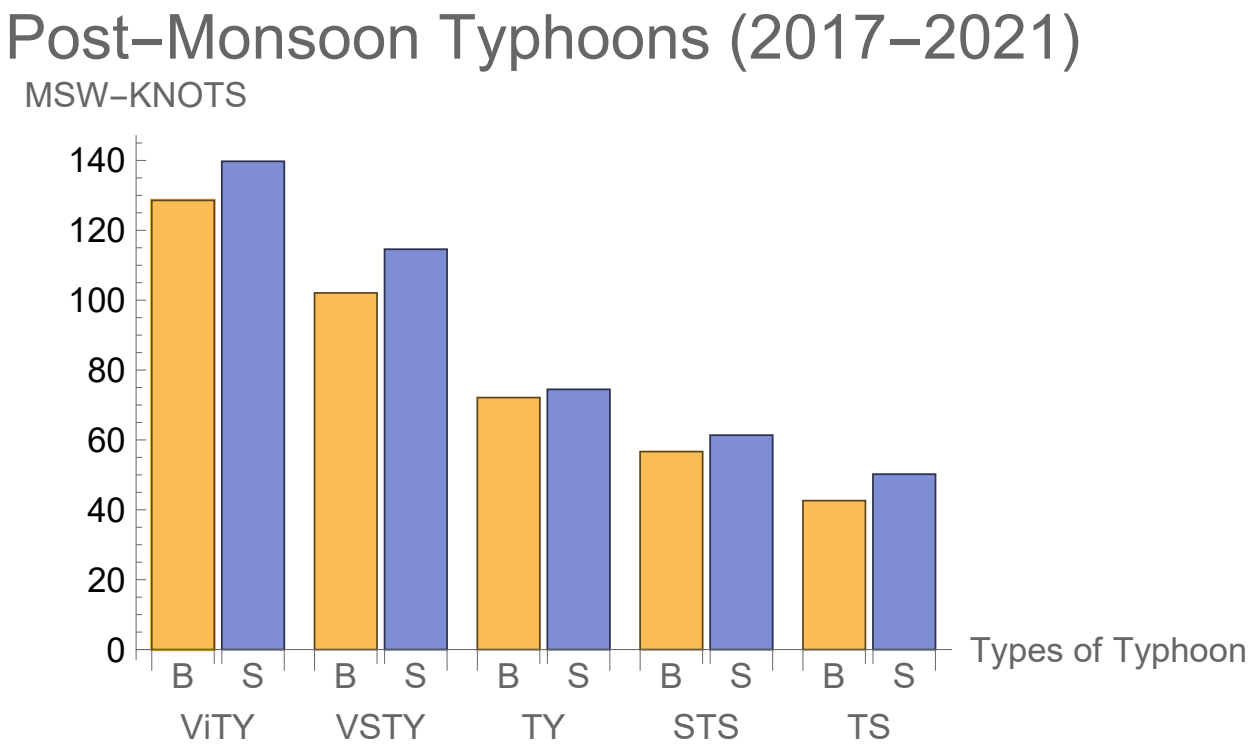

Figure 4.3: Compared the intensity estimation by SATCON and RSMC provided data for the post-monsoon season. B stands for RSMC provided data, S stands for SATCON algorithm data, ViTY stands for Violent Typhoon, VSTY for Very Strong Typhoon, TY for Typhoon, STS for Severe Tropical Storm, and TS for Tropical Storm

Table 4.6: Compared the SATCON and RSMC, Tokyo provided data for typhoons (stage wise) over the West Pacific basin as pre-monsoon and post-monsoon during the year 2017-2021

Category of typhoon	Season	Best Track interval	Best Track MSW (A^1)	SATCON interval	SATCON MSW(B^1)	BIAS (A-B)	Mean Absolute difference	RMSD
Violent	Pre-Mon	-	-	-	-	-	-	-
Typhoon	Post-Mon	105-130	128.57	120-144	139.73	-11.16	8.68	13.34
Very	Pre-Mon	80-110	126.03	90-120	125.30	0.73	4.26	4.92
strong	Post-Mon	85-105	102.08	112-132	114.57	-12.49	9.52	14.19
Typhoon								
Typhoon	Pre-Mon	64-85	73.58	79-100	90.77	-17.19	18.44	18.24
	Post-Mon	65-90	72.12	72-98	74.46	-2.34	8.24	10.18
Severe	Pre-Mon	48-64	56.25	69-81	72.87	-16.62	16.54	17.08
Tropical	Post-Mon	44-63	56.66	57-87	61.36	-4.69	9.24	12.47
Storm								
Tropical	Pre-Mon	34-48	42.01	16-70	54.11	-12.1	12.19	13.48
Storm	Post-Mon	30-50	42.62	39-74	50.19	-6.92	10.58	12.84

RSMC, we found that during the pre-monsoon, the SATCON algorithm overestimated tropical storms by about 13 kts, severe tropical storms by about 17 kts, and typhoons by about 19 kts. During the post-monsoon, the SATCON algorithm overestimated tropical storms by about 11 kts and severe tropical storms, very strong typhoons, and violent typhoons by about 9 kts.

By comparing the algorithm results, we demonstrate that SATCON is more effective in the post-monsoon across the West Pacific basin than in the pre-monsoon.

Chapter 5

Tropical Cyclone's Intensity

"Mathematics is the most beautiful and most powerful creation of the human spirit"

– Stefan Banach

In this chapter[1], we develop a method for estimating the intensity of TCs in the NIO using a neural network with a hybrid activation function. As discussed in Chapter 3, satellite images weren't used; instead, results from three state-of-the-art methods, the automated rotational center hurricane eye retrieval algorithm, the advanced Dvorak technique, and the satellite Consensus technique, were used as inputs, with the target data from the India Meteorological Department.

---

[1] The content of this chapter is based on a research paper "Estimation of Tropical Cyclone Intensity using Neural Network Approach" (Submitted).

5.1 Introduction

TCs, characterized by their spiraling winds, are recognized as severe weather phenomena accompanied by gales, rainstorms, and storm surges, substantially impacting global environmental and socio-economic aspects. Estimating TC intensity is one of the most critical steps in forecasting the TC (Chen et al., 2020; Jiang et al., 2023; Zhou et al., 2023). TC intensity typically encompasses the maximum wind speed or minimum sea level pressure at the center of a TC. However, this definition exhibits variations across different oceanic regions, lacking a standardized, universally accepted definition thus far (Chen et al., 2020). In fact, according to the definition, a TC's intensity is the maximum wind speed for achieving realistic and practical forecast results. Since the TC life cycle mainly occurs over the open ocean, satellite images become a significant source for estimating TC intensity. The meteorological satellites can observe TCs and obtain satellite cloud images containing abundant TC feature information. Although satellites cannot directly reflect the TC intensity, it is beneficial for estimating the TC intensity (Jiang et al., 2023). Traditional meteorological methods, such as Dvorak (1975), deviation-angle variance (DAV) (Piñeros et al., 2011), and Advanced Dvorak Technique (ADT) (Olander and Velden, 2019), are based on cloud patterns recognized from satellite images executed by meteorologists.

Dvorak (1973) proposed a Dvorak technique to estimate the TC intensity only based on TC cloud features observed in visible light satellite images. This technique examines the typhoon's central region, including its eye area, and analyzes the cloud-type characteristics within its eyewall and the distinctive spiral rain belt features encircling its periphery. Nevertheless, the Dvorak method heavily depends on meteorological experts' expertise and intuitive judgment. With the development of infrared imaging technology, Dvorak (1975)

introduced infrared satellite images to obtain the cloud-top brightness temperature of TCs at night, which promoted the development of the Dvorak technique. In 1984, Dvorak (1984) further improved the objectivity of the Dvorak technique. After that, Velden et al. (1998, 2006); Olander and Velden (2019); Olander et al. (2021) and others continuously optimized the Dvorak technique and successively proposed Objective Dvorak Technique (ODT), advanced objective Dvorak technique (AODT), Advanced Dvorak Technique (ADT), artificial intelligence enhanced advanced Dvorak technique (AiDT) algorithms, which further improved the accuracy of the Dvorak technique and reduced its subjectivity and achieved the automatic determination of TC intensity. In 2010, the Automated Rotational Center Hurricane Eye Retrieval (ARCHER) algorithm was proposed by (Wimmers and Velden, 2010). The algorithm can find the center of rotation using spirally oriented brightness temperature gradients in TC banding patterns in combination with gradients along the ring-shaped edge of a possible eye. The Advanced Microwave Sounding Unit (AMSU) technique (Kidder et al., 2000) uses temperature anomaly profiles associated with the TC warm core to estimate intensity. The SATCON (Velden and Herndon, 2020; Ahmed et al., 2022; Yadav and Das, 2024a) technique ensembles estimations from various methods, including ADT and Advanced Microwave Sounding Unit (AMSU), to achieve state-of-the-art estimation.

Goodfellow et al. (2016) is a foundational textbook that comprehensively covers deep learning concepts, including neural networks, optimization, and generative models. It is a key resource for researchers and practitioners in machine learning and artificial intelligence. Pradhan et al. (2017) proposes a deep CNN using satellite image classification for Typhoon intensity estimation using satellite images. This model achieves improved accuracy and lower root mean square error (RMSE) compared to traditional methods like the Dvorak and deviation-angle variance techniques. Chen et al. (2018) introduces a novel

dataset for Typhoon intensity estimation and proposes a CNN-based model incorporating domain knowledge. Combinido et al. (2018) demonstrates that a CNN-based approach can effectively estimate Typhoon intensity from infrared satellite images, achieving an RMSE of 13.23 knots (kts). The model learns critical features like cloud organization and eye formation, comparable to traditional feature-based techniques, highlighting the potential of deep learning in meteorology. Lee et al. (2019) demonstrates that multi-dimensional CNNs using multi-spectral satellite data improve intensity estimation. The optimized 2D-CNN model achieved an RMSE of 8.32 kts, outperforming previous methods and confirming the potential of deep learning in meteorological applications. Chen et al. (2019) presents a deep-learning model using CNNs for intensity estimation from satellite imagery. The optimized and smoothed CNN model demonstrates superior accuracy to traditional methods, achieving an RMSE of 8.39 kts and promising future operational applications. Higa et al. (2021) proposes a deep learning model for Typhoon intensity classification by integrating meteorological domain knowledge. By utilizing VGG-16 with fisheye-preprocessed satellite images, the model achieved a higher classification accuracy of 76.8%, outperforming previous methods. The fisheye preprocessing enhanced key Typhoon features like the eye and cloud distribution, improving interpretability. Chen and Yu (2020) introduces a novel tensor-based (TCNN) for intensity estimation using multispectral satellite images. By integrating tensor decomposition and deep learning, TCNN effectively captures typhoon structures, improving intensity categorization and wind speed estimation. The proposed models, C-TCNN and T-TCNN, outperform traditional and state-of-the-art methods in accuracy and efficiency. Experimental results confirm TCNN's potential for operational meteorological applications. Zhang et al. (2021) proposes a novel deep learning approach, TCICENet, for intensity classification and estimation using infrared satellite images. The model consists of cascading

CNN modules, achieving an RMSE of 8.60 kt and an MAE of 6.67 kt. Varalakshmi et al. (2023) proposed a deep learning model that combines CNN architectures for feature extraction and machine learning models for regression to predict the intensity of TCs. Griffin et al. (2024) presents two machine-learning methods, D-MINT and D-PRINT, utilizing infrared and microwave imagery to predict short-term intensity changes in typhoons, demonstrating improved skill over traditional methods, particularly in the North Atlantic and western North Pacific regions. Raynaud et al. (2024) introduces a CNN based on the U-Net architecture for detecting Typhoon wind structures in high-resolution numerical weather prediction (NWP) models. The model outperforms traditional heuristic methods, achieving an average intersection-over-union metric of 0.8, particularly improving detection for weaker cyclones. Additionally, it generalizes well to different domains and higher-resolution data, demonstrating its potential for operational forecasting. Yadav and Das (2024b) focuses on estimating the radius of maximum wind (RMW) in typhoons, a crucial parameter for assessing cyclone intensity and predicting impacts on climate and ecosystems. Using machine learning methods, they introduce an ensemble model combining random forests, gradient boosting, and NNs, enhancing precision in RMW estimation over traditional techniques.

The structural characteristics of TCs, such as shear-relative composites and convective cores, have not been comprehensively incorporated within NN-based models. Another crucially overlooked aspect has been the neglect of rotational symmetry in satellite images induced by TCs' rotations.

Integrating multiple techniques becomes imperative when faced with the limitation of individual methods in providing an accurate estimation of TC intensity. In this context, we consider the three distinct methodologies: ADT, ARCHER, and SATCON, each yielding less than optimal results independently and a straight average of those estimations. By

harnessing the power of a neural network, we effectively merge the outputs of these three methods into a single result. This combined approach minimizes errors and maximizes each method's strengths, attaining more accurate and reliable results than traditional approaches.

5.2 Data and Method

5.2.1 Data

We collected the 3-hourly data of the TC's Intensity from three state-of-the-art intensity estimation models, namely ARCHER "`https://tropic.ssec.wisc.edu/real-time/archerOnline/cyclones/`," ADT "`https://tropic.ssec.wisc.edu/misc/adt/info.html`," and SATCON "`https://tropic.ssec.wisc.edu/real-time/satcon/`." We collected 3-hourly data on 76 TCs, including deep and deep depressions, in which 69 TCs for training and 7 TCs were used to validate the results from 2013-2024. The input of our Neural Network model is the value of intensity from three models, and the target of our model is the best track data released by the India Meteorological Department.

According to the Standard Operational Procedure for Cyclone Warnings in India 2021, released by the India Meteorological Department (IMD), the system's intensity is measured in terms of 3-minute average MSW at the surface level (10 meters above ground level). The maximum Wind is determined from Dvoark's technique (IMD, 2021). However, the following technique is followed for better accuracy:

- Wind reported by ships and buoys.
- Wind observed by scatterometry, i.e., OCEANSAT & ASCAT.
- Radar

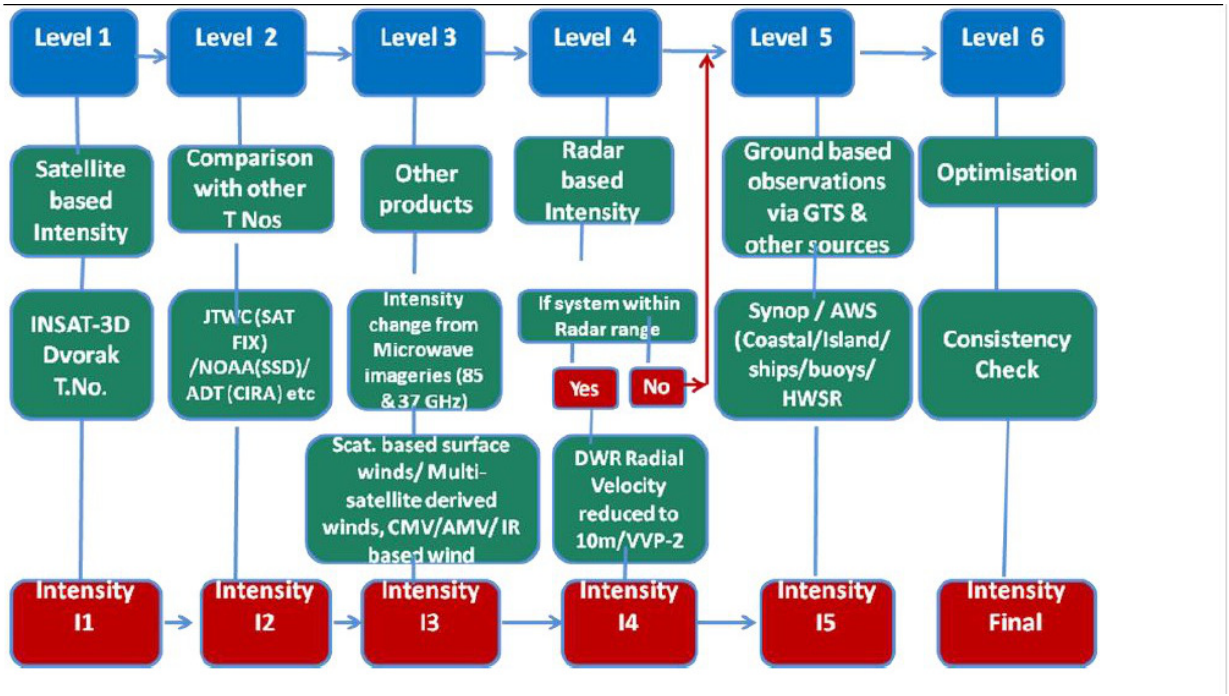

Figure 5.1: Steps involved in the determination of the Intensity of a Tropical Cyclone (Source: IMD)

- CMV/AMV reduced to 10-meter Wind

Various steps involved in determining intensity by the IMD are shown in Fig. 5.1.

The study primarily focused on the NIO regions for training and validation. To ensure comprehensive data acquisition, the Best Track data has been collected from the official websites of the Regional Specialized Meteorological Center (RSMC) for the NIO (`https://rsmcnewdelhi.imd.gov.in/`) for 2013-24. We collected the data of 69 TCs (details in Table 5.1) for training purposes and seven TCs (details in Table 5.3) for validation purposes. Our analysis also includes consideration for depressions (details of all categories of cyclonic disturbance with their respective wind speed in Table 1 of the reference paper (Yadav and Das, 2023b)) that have not attained TC intensity.

Our study does not incorporate satellite images in estimating the intensity of TCs. Instead, our methodology utilizes output data from three state-of-the-art intensity estimation

models: ARCHER, ADT, and SATCON. The absence of satellite images is a deliberate choice, and we acknowledge the reliance on the pre-existing outputs from these established models.

5.2.2 Method

The primary aim of this chapter is to develop an NN-based model alongside the results obtained from the three methodologies to get a single result.

Here is the whole process of our method:

1. **Preprocessing:**

   The three sets of experimental values are first combined and normalized using the StandardScaler from scikit-learn (Pedregosa et al., 2011) to ensure that all the input data are on a similar scale.

2. **k-fold cross-validation:** k–fold cross-validation is a robust technique used to evaluate machine learning models by partitioning the dataset into k equal-sized folds, training the model on $k-1$ folds, and validating it on the remaining fold, repeating this process k times (Nti et al., 2021; Pohjankukka et al., 2017).

   For Example, we have divided our data into 5 equal groups. To test a model, we use 4 groups for training and the remaining group to check how well the model performs. We do this 5 times, using each group to check once.

   - Iteration 1: Use folds 2, 3, 4, and 5 to train the model, then test it on fold 1.
   - Iteration 2: Use folds 1, 3, 4, and 5 to train the model, then test it on fold 2.
   - Iteration 3: Use folds 1, 2, 4, and 5 to train the model, then test it on fold 3.
   - Iteration 4: Use folds 1, 2, 3, and 5 to train the model, then test it on fold 4.
   - Iteration 5: Use folds 1, 2, 3, and 4 to train the model, then test it on fold 5.

3. **Neural Network Architecture:**

Table 5.1: Details of selected tropical cyclones for Training process

S.No.	Name	Category	Time period
1	Viyaru	Cyclonic Storm	10 - 16 May 2013
2	Depression	Depression	29 - 31 May 2013
3	Depression	Depression	30 July - 01 August 2013
4	Phailin	Very Severe Cyclonic Storm	08 - 14 October 2013
5	Depression	Depression	08 - 11 November 2013
6	Depression	Depression	13 - 17 November 2013
7	Helen	Severe Cyclonic Storm	19 - 23 November 2013
8	Lehar	Very Severe Cyclonic Storm	23 - 28 November 2013
9	Madi	Very Severe Cyclonic Storm	06 - 13 December 2013
10	Depression	Depression	04 - 07 January 2014
11	Depression	Depression	21 - 23 May 2014
12	Nanauk	Cyclonic Storm	10 - 14 June 2014
13	Deep Depression	Deep Depression	03 - 07 August 2014
14	Hudhud	Very Severe Cyclonic Storm	07 - 14 October 2014
15	Nilofar	Very Severe Cyclonic Storm	25 - 31 October 2014
16	Deep Depression	Deep Depression	05 - 08 November 2014
17	Ashobaa	Cyclonic Storm	07 - 12 June 2015
18	Komen	Cyclonic Storm	26 July - 02 August 2015
19	Deep Depression	Deep Depression	09 - 12 October 2015
20	Chapala	Extremely Severe Cyclonic Storm	28 October - 04 November 2015
21	Megh	Extremely Severve Cyclonic Storm	05 - 10 November 2015
22	Deep Depression	Deep Depression	08 - 10 November 2015
23	Roanu	Cyclonic Storm	17 - 22 May 2016
24	Depression	Depression	27 - 29 June 2016
25	Deep Depression	Deep Depression	09 - 12 August 2016
26	Deep Depression	Deep Depression	16 - 21 August 2016
27	Kyant	Cyclonic Storm	21 - 28 October 2016
28	Depression	Depression	02 - 06 November 2016
29	Nada	Cyclonic Storm	29 November - 02 December 2016
30	Vardhah	Very Severe Cyclonic Storm	06 - 13 December 2016
31	Marrutha	Cyclonic Storm	15 - 17 April 2017
32	Mora	Severe Cyclonic Storm	28 - 31 May 2017
33	Deep Depression	Deep Depression	11 - 13 June 2017
34	Depression	Depression	18 - 19 July 2017
35	Depression	Depression	26 - 27 July 2017
36	Deep Depression	Deep Depression	09 - 10 October 2017
37	Depression	Depression	19 - 22 October 2017
38	Ockhi	Very Severe Cyclonic Storm	29 November - 06 December 2017
39	Deep Depression	Deep Depression	06 - 09 December 2017
40	Sagar	Cyclonic Storm	16 - 21 May 2018
41	Mekunu	Extremely Severe Cyclonic Storm	21 - 27 May 2018
42	Daye	Cyclonic Storm	19 - 22 September 2018
43	Luban	Very Severe Cyclonic Storm	06 - 15 October 2018
44	Gaja	Very Severe Cyclonic Storm	10 - 19 November 2018
45	Pabuk	Cyclonic Storm	04 - 08 January 2019

Table 5.2: Details of selected tropical cyclones for Training process (Continue to table 5.1)

S.No.	Name	Category	Time period
46	Fani	Extremely Severe Cyclonic Storm	26 April - 04 May 2019
47	Vayu	Very Severe Cyclonic Storm	10 - 17 June 2019
48	Hikaa	Very Severe Cyclonic Storm	22 - 25 September 2019
49	Kyarr	Super Cyclonic Storm	24 October - 04 November 2019
50	Maha	Extremely Severe Cyclonic Storm	30 October - 07 November 2019
51	Bul Bul	Very Severe Cyclonic Storm	05 - 11 November 2019
52	Pawan	Cyclonic Storm	02 - 07 December 2019
53	Deep Depression	Deep Depression	03 - 05 December 2019
54	Amphan	Super Cyclonic Storm	16 - 21 May 2020
55	Nisarga	Severe Cyclonic Storm	01 - 04 June 2020
56	Gati	Very Severe Cyclonic Storm	21 - 24 November 2020
57	Tauktae	Extremely Severe Cyclonic Storm	14th-19th May, 2021
58	Yaas	Very Severe Cyclonic Storm	23 – 28 May, 2021
59	Gulab	Cyclonic Storm	24 - 28 September 2021
60	Depression	Depression	10 - 11 November 2021
61	Deep Depression	Deep Depression	3 - 6 March, 2022
62	Depression	Depression	12 - 13 August 2022
63	Deep Depression	Deep Depression	18 - 22 August 2022
64	Mandous	Severe Cyclonic Storm	6 - 10 December 2022
65	Deep Depression	Deep Depression	14 - 17 December 2022
66	Mocha	Extremely Severe Cyclonic Storm	09 - 15 May 2023
67	Biparjoy	Extremely Severe Cyclonic Storm	06 - 19 June 2023
68	Depression	Depression	09 - 10 June 2023
69	Deep Depression	Deep Depression	31 July - 01 August 2023

The model is designed using the Keras Sequential API (Chollet et al., 2015). It comprises multiple layers, including densely connected layers with different activation functions, batch normalization, and dropout layers, preventing overfitting. The model architecture (Figure 5.2) promotes deep learning using three hidden layers: 256 neurons with LeakyReLU activation function and a dropout rate of 0.4, 512 neurons with ReLU activation function and a dropout rate of 0.3, and 256 neurons with Tanh activation function and a dropout rate of 0.2.

Integrating LeakyReLU, ReLU, and Tanh activation functions across different layers of an NN demonstrates a strategic approach to enhancing model accuracy through tailored activation dynamics. By employing LeakyReLU in the initial layer, the network mitigates the "dying neuron" problem while ensuring adequate gradient flow for both positive and negative inputs, enabling robust feature extraction from diverse datasets. In subsequent layers, ReLU capitalizes on its computational simplicity and sparsity-inducing properties, focusing on the most relevant features and improving computational efficiency. Finally, adopting Tanh in later layers introduces a smooth, bounded output that is particularly effective for capturing complex nonlinear relationships and normalizing activations within a constrained range. This deliberate combination of activation functions enhances the network's ability to learn diverse patterns, stabilizes training by reducing gradient-related issues, and demonstrates superior performance on complex tasks, as evidenced by improved model accuracy in experimental results.

4. **Training the Model:**

   The compiled model is trained using the Adam optimizer (Kingma and Ba, 2014) with a reduced learning rate of 0.00001, optimizing the mean squared error loss function. To enhance the model's learning process, a substantial number of epochs, $10,000$ in this case, are executed during the training process. The batch size is set to 128, and the training progress is tracked for analysis.

5. **Model Evaluation:**

   Following training, the model is evaluated using the trained neural network to predict the experimental values. The mean absolute percentage and root mean square errors are calculated to assess the model's accuracy and performance.

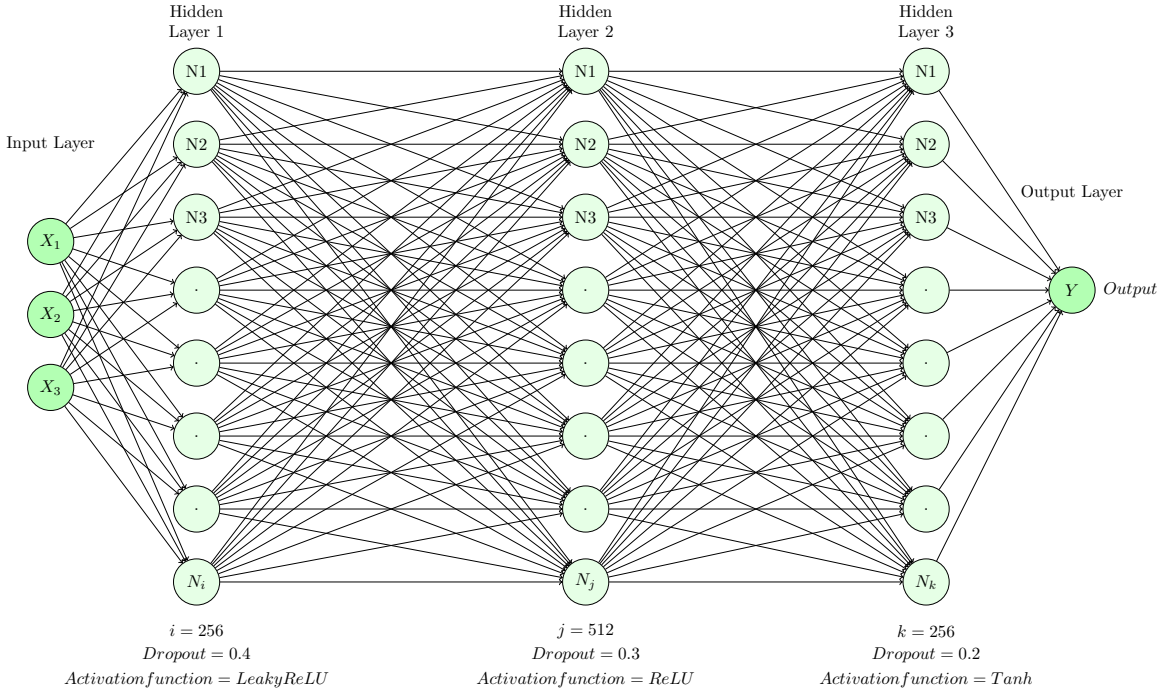

Figure 5.2: Architecture of the Proposed Neural Network

In our approach, we train the NN using 1-minute interval data and corresponding labels. We use 3-minute data averages for verification purposes, where each average is computed for three consecutive 1-minute intervals. The trained NN then makes predictions or classifications based on these 3-minute averages, and we evaluate its performance by comparing the predictions with the actual 10-minute averaged data. Maintaining consistency in data preprocessing and appropriately handling time intervals throughout the training and verification processes is essential.

To check the accuracy of our NN-based model, we use three statistical methods: t-test, error percentage, and root mean square error. Section 2.4.1 provides a detailed discussion of the t-test, error percentage, and root mean square error. Using these methods, we confidently say that our NN-based model is more efficient and accurate than the three methods: ADT, ARCHER, and SATCON.

5.3 Result

The proposed NN-based model for estimating the TC intensity has been evaluated using three cases, namely: Severe Cyclonic Storm Asani (SCS Asani), Cyclonic Storm Sitrang (CS Sitrang), Severe Cyclonic Storm Shaheen (SCS Shaheen), Extremely Severe Cyclonic Storm Tej (ESCS Tej), Severe Cyclonic Storm Remal (SCS Remal), Cyclonic Storm Asan (CS Asan), and Severe Cyclonic Storm Dana (SCS Dana). For further insight into these TCs, Table 5.3 provides details regarding the category of selected TCs, along with the corresponding periods.

Table 5.3: Details of selected tropical cyclones for Validation process

Name	Category	Basin	Time Period
Asani	Severe Cyclonic Storm	NIO	07-12 May, 2022
Sitrang	Cyclonic Storm	NIO	22-25 October, 2022
Shaheen	Severe Cyclonic Storm	NIO	30 September - 4 October, 2021
Tej	Extremely Severe Cyclonic Storm	NIO	20-24 October, 2023
Remal	Severe Cyclonic Storm	NIO	24-28 May, 2024
Asan	Cyclonic Storm	NIO	25 August - 02 September, 2024
Dana	Severe Cyclonic Storm	NIO	22-26 October, 2024

5.3.1 SCS Asani

On the morning of May 6, 2022, a region of low pressure commenced forming over the South Andaman Sea and the neighboring Southeast Bay of Bengal. By the early morning of May, 7 had strengthened into a well-defined area of low pressure located over the Southeast Bay of Bengal and the adjacent South Andaman Sea. The favorable environmental conditions facilitated its further consolidation, developing into a depression around noon on the same day, May 7, 2022. This system, dubbed SCS "Asani," progressed into a deep depression before reaching the coast. Notably, it exhibited an unusually sluggish movement, creeping

at a pace of 5-6 km per hour, considerably slower than the usual speed of 13 km per hour. This slow progression resulted in its lingering within 50 km of the coastline from morning to evening on May 11. SCS "Asani" demonstrated multiple shifts in its path. Most meteorological models had initially forecasted a change in its course, veering from northwest to northeast along the coast. It initially moved in a northward/northwestward direction and subsequently altered its course to a west-southwestward direction. This unforeseen deviation was primarily influenced by the system's response to a short-amplitude westerly trough in the middle and upper levels of the troposphere approaching from the west, leading it to veer away from the anticipated northeastward trajectory near the coast (Division, 2022b).

Our method, along with the existing methods such as ARCHER, ADT, SATCON, and Best track data provided by the respective RSMC, is graphically shown in Fig. 5.3. This graphical representation estimates the TC intensity. Table 5.4 has the numerical result of our method and other results of existing methods for SCS Asani. When comparing the mean error of our method to the Best track data provided by the RSMC's average TC intensity value of 48.16 knots, our method has an error percentage of 15.52%. On the other hand, other approaches like ARCHER, ADT, and SATCON have 20.14%, 34.53%, and 25.41%, respectively. RMSE (Table 5.11) also favors our proposed method compared to other approaches. Statistical analysis using a t-test says that our proposed method performs better than the alternative methods.

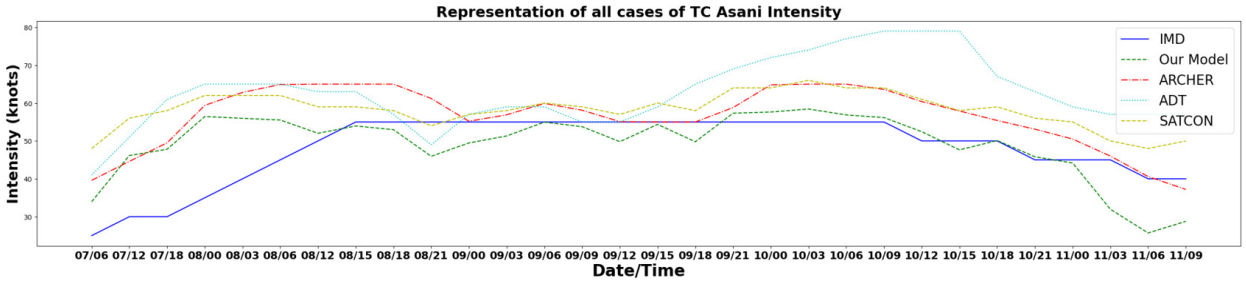

Figure 5.3: A representation of the research results of the SCS Asani graphically

Table 5.4: Numerical results of SCS Asani

Date/Time	IMD (knots)	Our Model (knots)	ARCHER (knots)	ADT (knots)	SATCON (knots)	E_1 [a]	E_2 [b]	E_3 [c]	E_4 [d]
07/06	25	33.94	39.6	41	48	35.76	58.4	64	92
07/12	30	46.15	44.6	51	56	53.83	48.6	70	86.66
07/18	30	47.80	49.5	61	58	59.3	65	103.33	93.33
08/00	35	56.44	59.4	65	62	61.25	69.7	85.71	77.14
08/03	40	55.97	62.8	65	62	39.92	57	62.5	55
08/06	45	55.52	64.9	65	62	23.37	44.2	44.4	37.77
08/12	50	52.02	65	63	59	4.04	30	26	18
08/15	55	53.95	65	63	59	1.90	18.18	14.5	7.27
08/18	55	52.97	65	57	58	3.69	18.18	3.63	5.45
08/21	55	45.95	61.2	49	54	16.45	11.27	10.90	1.81
09/00	55	49.47	55.2	57	57	10.05	0.36	3.63	3.63
09/03	55	51.31	56.9	59	58	6.70	3.45	7.27	5.45
09/06	55	54.97	59.9	59	60	0.05	8.9	7.27	9.09
09/09	55	53.76	58.1	55	59	2.25	5.63	0	7.27
09/12	55	49.81	55.1	55	57	9.43	0.18	0	3.63
09/15	55	54.37	55	59	60	1.14	0	7.27	9.09
09/18	55	49.78	55	65	58	9.49	0	18.18	5.45
09/21	55	57.32	58.8	69	64	4.21	6.90	25.45	16.36
10/00	55	57.63	64.8	72	64	4.78	17.8	30.90	16.36
10/03	55	58.43	65	74	66	6.23	18.18	34.54	20
10/06	55	56.86	65	77	64	3.38	18.18	40	16.36
10/09	55	56.16	63.6	79	64	2.10	15.63	43.6	16.36
10/12	50	52.44	60.4	79	61	4.88	20.8	58	22
10/15	50	47.64	57.9	79	58	4.72	15.8	58	16
10/18	50	50.10	55.4	67	59	0.2	10.8	34	18
10/21	45	45.82	53.1	63	56	1.82	18	40	24.44
11/00	45	44.17	50.5	59	55	1.84	12.22	31.11	22.22
11/03	45	31.96	46	57	50	28.9	2.22	26.66	11.11
Mean	48.16	49.24	56.35	62.6	58.2	15.52	20.14	34.53	25.41

[a]Error Percentage of our model with respect to Best track data.
[b] Error Percentage of ARCHER method with respect to Best track data.
[c] Error Percentage of ADT method with respect to Best track data.
[d] Error Percentage of SATCON method with respect to Best track data.

5.3.2 CS Sitrang

On October 20, 2022, a low-pressure area formed over the North Andaman Sea, extending to the South Andaman Sea and Southeast Bay of Bengal (BoB). By October 21, it developed into a well-marked low-pressure area over the north Andaman Sea and southeast BoB. Under favorable conditions, it concentrated into a depression over the southeast and adjoining east-central BoB near the Andaman Islands on October 22. Moving northwest, it intensified into a deep depression over west-central BoB on October 23 and further developed into the cyclonic storm "Sitrang" on October 23 evening. The storm shifted its course to the north-northeast, making landfall on the Bangladesh coast between Tinkona and Sandwip near Barisal on October 24. It weakened into a deep depression over northeast Bangladesh on October 25 in the early hours, followed by a depression over interior Bangladesh on the same day's early morning, and eventually regressed into a well-marked low-pressure area over northeast Bangladesh and adjoining Meghalaya by October 25 forenoon (Division, 2022a).

Our model, depicted alongside other methodologies such as ARCHER, ADT, and SATCON and complemented by Best-track data sourced from the respective RSMC, is visually illustrated in Fig. 5.4. This graphical representation provides insight into the estimated TC intensity. For a detailed quantitative summary of the CS Sitrang results, refer to Table 5.5.

When evaluating the mean error based on the TC intensity data provided by the RSMC, where the reference intensity is at 40.90 knots, our model exhibits an error rate of 4.82%, outperforming alternative approaches. Specifically, ARCHER, ADT, and SATCON demonstrate error rates of 7.46%, 6.17%, and 8.35%, respectively. The values of the RSME for this case are presented in Table 5.11.

Table 5.5: Numerical results of CS Sitrang

Date/Time	IMD (knots)	Our Model (knots)	ARCHER (knots)	ADT (knots)	SATCON (knots)	E_1[a]	E_2[b]	E_3[c]	E_4[d]
23/12	35	32.80	35.0	36	40	6.2	0.00	2.85	14.2
23/15	35	33.25	35.0	36	40	5.0	0.00	2.85	14.2
23/18	35	35.15	35.0	39	42	.04	0.00	11.4	20.0
23/21	40	36.89	35.0	39	42	7.7	12.5	2.50	5.00
24/00	40	41.23	35.0	41	44	3.0	12.5	2.50	10.0
24/03	45	47.23	36.4	46	46	4.9	19.1	2.22	2.22
24/06	45	40.97	39.6	48	46	8.9	12.0	6.66	2.22
24/09	45	45.40	42.6	47	47	0.8	5.33	4.44	4.44
24/12	45	47.80	44.9	42	46	6.2	0.22	6.66	2.22
24/15	45	45.35	41.2	39	44	0.7	8.44	13.3	2.22
24/18	40	43.50	35.2	35	46	8.7	12.0	12.5	15.0
Mean	40.9	40.87	37.71	40.72	43.90	4.82	7.46	6.17	8.35

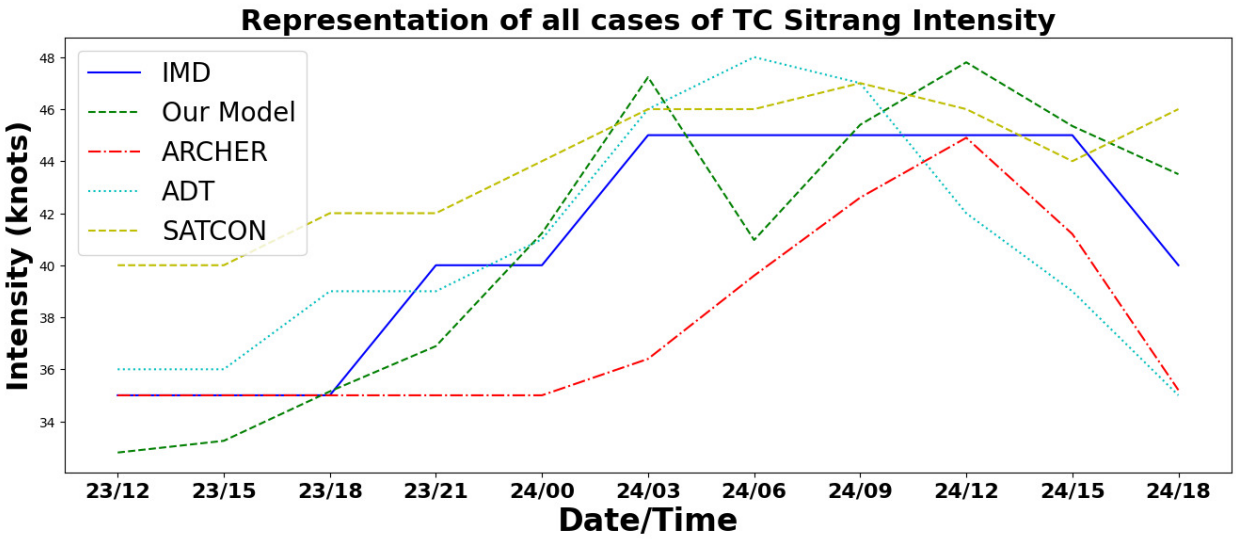

Figure 5.4: Representation of the results of the CS Sitrang in graphical form

5.3.3 SCS Shaheen

On the morning of September 29, the remnants of CS Gulab transitioned into a well-defined low-pressure area over the southern Gujarat region and the adjacent Gulf of Khambhat, confirmed by the 0830 hours IST observation. Favored by favorable environmental conditions and sea states, this system further concentrated into a depression over the northeastern Arabian Sea and adjoining Kutch by 0530 hours IST on September 30. Continuing on a west-northwest trajectory, it intensified into a deep depression over the same region by the midnight observation at 2330 hours IST on September 30. Progressing westward, the system evolved into CS "Shaheen" off the Gujarat coast by the morning of October 1. After a brief westward movement, it changed to west-northwest, reaching severe cyclonic storm status by the evening observation at 1730 hours IST on October 1. It sustained this trajectory until the evening observation at 1730 hours IST on October 2, when it shifted west-southwestward. It made landfall on the coast of Oman between 0030 and 0130 IST on October 4, exhibiting wind speeds of 95-105 kmph, with gusts reaching 115 kmph (Division, 2021d).

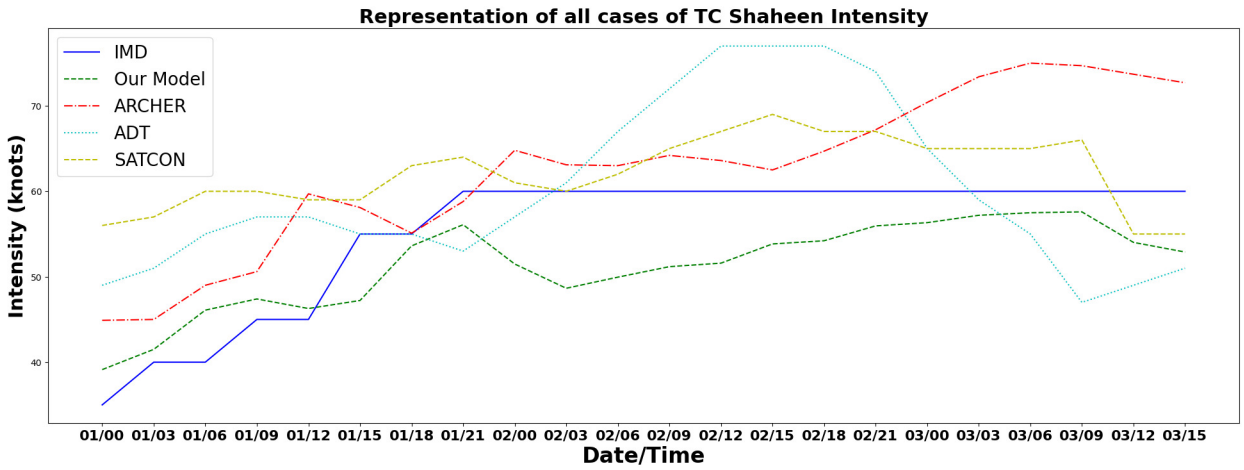

Figure 5.5: Representation of the results of the SCS Shaheen in graphical form

Our model, combined with complementary methodologies including ARCHER, ADT, SATCON, and the utilization of Best Track data from the respective RSMC, is visually depicted in Fig. 5.5. This graphical representation illustrates the estimated TC intensity. Table 5.6 offers a quantitative summary of the outcomes for SCS Shaheen.

Upon evaluating the mean error based on TC intensity data provided by RSMC, where the intensity is recorded at 55.0 knots, our model exhibits an error rate of 9.89%, surpassing other methodologies such as ARCHER, ADT, and SATCON, which exhibit error rates of 13.32%, 17.24%, and 16.53%, respectively. The corresponding values of RMSE for this scenario are presented in Table 5.11. A t-test analysis reveals that our model performs better than the other approaches.

5.3.4 ESCS Tej

Tropical Storm Tej was an extremely severe cyclonic storm that formed in the Arabian Sea in October 2023. It rapidly intensified and moved northwestward, making landfall in Yemen, causing significant damage and loss of life. This event was notable for its coexistence with another tropical storm, Hamoon, in the Bay of Bengal, a rare occurrence.

Table 5.6: Numerical result of SCS Shaheen

Date/Time	IMD (knots)	Our Model (knots)	ARCHER (knots)	ADT (knots)	SATCON (knots)	$E_1{}^a$ (knots)	$E_2{}^b$	$E_3{}^c$	$E_4{}^d$
01/00	35	39.13	44.9	49	56	11.8	28.2	40.0	60.0
01/03	40	41.50	45.0	51	57	3.75	12.5	27.5	42.5
01/06	45	46.09	49.0	55	60	2.42	8.88	22.2	33.3
01/09	45	47.40	50.6	57	60	5.33	12.4	26.6	33.3
01/12	55	46.28	59.7	57	59	15.8	8.54	3.63	7.27
01/15	55	47.22	58.1	55	59	14.1	5.63	0.00	7.27
01/18	60	53.61	55.1	55	63	10.6	8.16	8.33	5.00
01/21	60	56.09	58.8	53	64	6.51	2.00	11.6	6.66
02/00	60	51.49	64.8	57	61	14.1	8.00	5.00	1.66
02/03	60	48.65	63.1	61	60	18.9	5.16	1.66	0.00
02/06	60	49.95	63.7	67	62	16.7	6.16	11.6	3.33
02/09	60	51.18	64.2	72	65	14.7	7.00	20.2	8.33
02/12	60	51.59	63.6	77	67	14.0	6.00	28.3	11.6
02/15	60	53.84	62.5	77	69	10.2	4.16	28.3	15.0
02/18	60	54.21	64.7	77	67	9.65	7.83	28.3	11.6
02/21	60	55.95	67.2	74	67	6.75	12.0	23.3	11.6
03/00	60	56.33	70.4	65	65	6.11	17.3	8.33	8.33
03/03	60	57.19	73.4	59	65	4.68	22.3	1.66	8.33
03/06	60	57.49	75.0	55	65	4.18	25.0	8.33	8.33
03/09	60	57.59	74.7	47	66	4.01	24.5	21.6	10.0
03/12	60	54.02	73.7	49	55	9.96	22.8	18.3	8.33
03/15	60	52.89	72.7	51	55	11.8	20.3	15.0	8.33
Mean	55.0	50.5	61.4	59.1	61.6	9.89	13.32	17.24	16.53

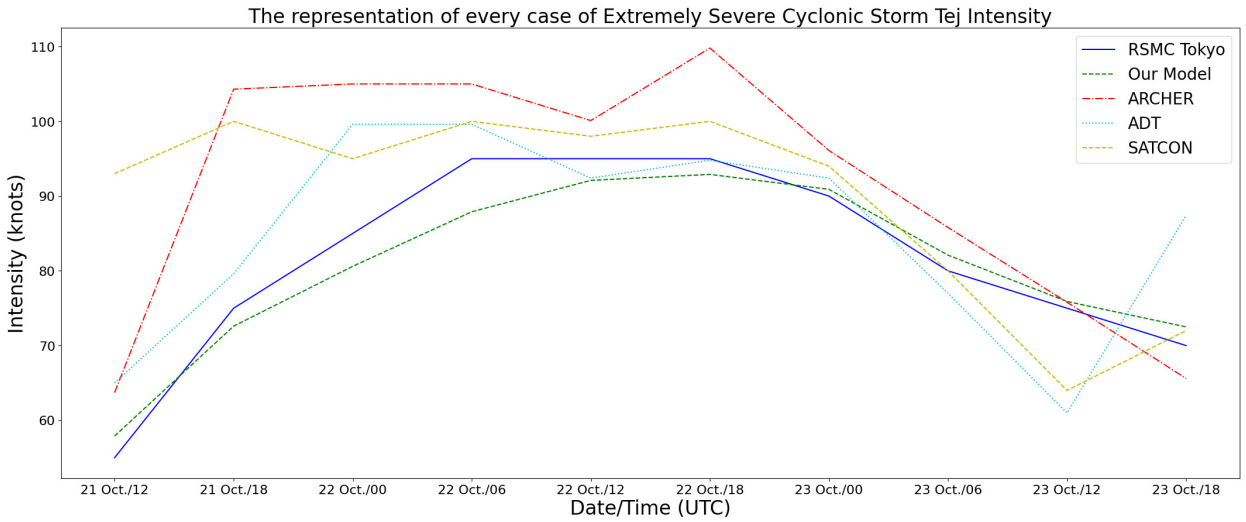

Figure 5.6: Representation of the results of the ESCS Tej in graphical form

Figure 5.6 compares the proposed typhoon intensity estimation method with ARCHER, ADT, and SATCON, based on Best Track data from IMD. Results for Tropical Storm Sanba are summarized in Table 5.7.

The proposed method shows a percentage error of 3.47%, much lower than ARCHER (13.12%), ADT (9.92%), and SATCON (14.98%). RMSE values in Table 5.11 confirm its improved accuracy, supported by a t-test analysis.

5.3.5 SCS Remal

Tropical Storm Remal, a severe cyclonic storm, struck West Bengal and Bangladesh in late May 2024. Originating in the Bay of Bengal, it made landfall near the border, bringing heavy rainfall, strong winds, and a significant tidal surge. This event resulted in widespread damage, including loss of life, destruction of homes, and infrastructure disruption. Large-scale evacuations were implemented in coastal areas to minimize casualties.

Figure 5.7 shows how our proposed method for estimating TC intensity is doing well compared to other traditional methods: ARCHER, ADT, and SATCON, concerning the

Table 5.7: Numerical result of ESCS Tej

Date/Time	IMD (knots)	Our Model (knots)	ARCHER (knots)	ADT (knots)	SATCON (knots)	$E_1{}^a$ (knots)	$E_2{}^b$	$E_3{}^c$	$E_4{}^d$
21/12	55	57.9	63.7	65.0	93	5.27	15.8	18.1	69.0
21/18	75	72.6	104.3	79.6	100	3.20	39.0	6.13	33.3
22/00	85	80.6	105.0	99.6	95	5.17	23.5	17.1	11.7
22/06	95	87.9	105.0	99.6	100	7.47	10.5	4.84	5.26
22/12	95	92.1	100.1	92.4	98	3.05	5.36	2.73	3.15
22/18	95	92.9	109.8	94.8	100	2.21	15.5	0.21	5.26
23/00	90	90.9	96.1	92.4	94	1.00	6.77	2.66	4.44
23/06	80	82.1	85.8	77.0	80	2.62	7.25	3.75	0.00
23/12	75	75.9	75.8	61.0	64	1.20	1.06	18.6	14.6
23/18	70	72.5	65.6	87.4	72	3.57	6.28	24.8	2.85

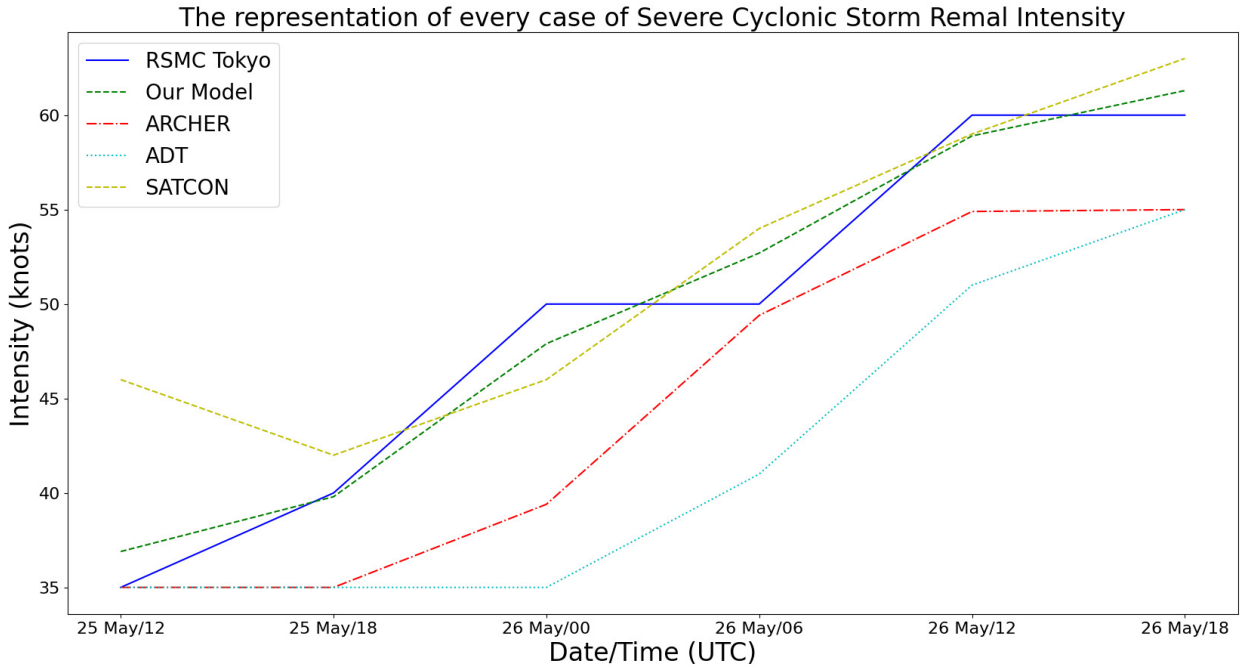

Figure 5.7: Representation of the results of the SCS Remal in graphical form

Best track data provided by the IMD. Table 5.8 provides a quantitative summary of the results for SCS Remal.

Our proposed method shows an error rate of 3.25%. This is better than the error rates of other methodologies: ARCHER (8.62%), ADT (13.97%), and SATCON (9.84%). The RMSE values for this case are listed in Table 5.11. Statistical analysis using a t-test indicates that our proposed method performs better than the other methods.

5.3.6 CS Asna

Tropical Storm Asna was a cyclonic storm that affected parts of India and Pakistan in late August and early September 2024. It formed as a deep depression over land, intensified into a cyclone, and then moved into the Arabian Sea.

It brought heavy rainfall to Gujarat, Rajasthan, Madhya Pradesh in India, and Sindh in Pakistan. This heavy rainfall led to widespread flooding, causing significant damage to

Table 5.8: Numerical result of SCS Remal

Date/Time	IMD (knots)	Our Model (knots)	ARCHER (knots)	ADT (knots)	SATCON (knots)	$E_1{}^a$ (knots)	$E_2{}^b$	$E_3{}^c$	$E_4{}^d$
25/12	35	36.9	35.0	35.0	46	5.42	0.00	0.00	31.4
25/18	40	39.8	35.0	35.0	42	0.50	12.5	12.5	5.00
26/00	50	47.9	39.4	35.0	46	4.20	21.2	30.0	8.00
26/06	50	52.7	49.4	41.0	54	5.40	1.20	18.0	8.00
26/12	60	58.9	54.9	51.0	59	1.83	8.50	15.0	1.66
26/18	60	61.3	55.0	55.0	63	2.16	8.33	8.33	5.00

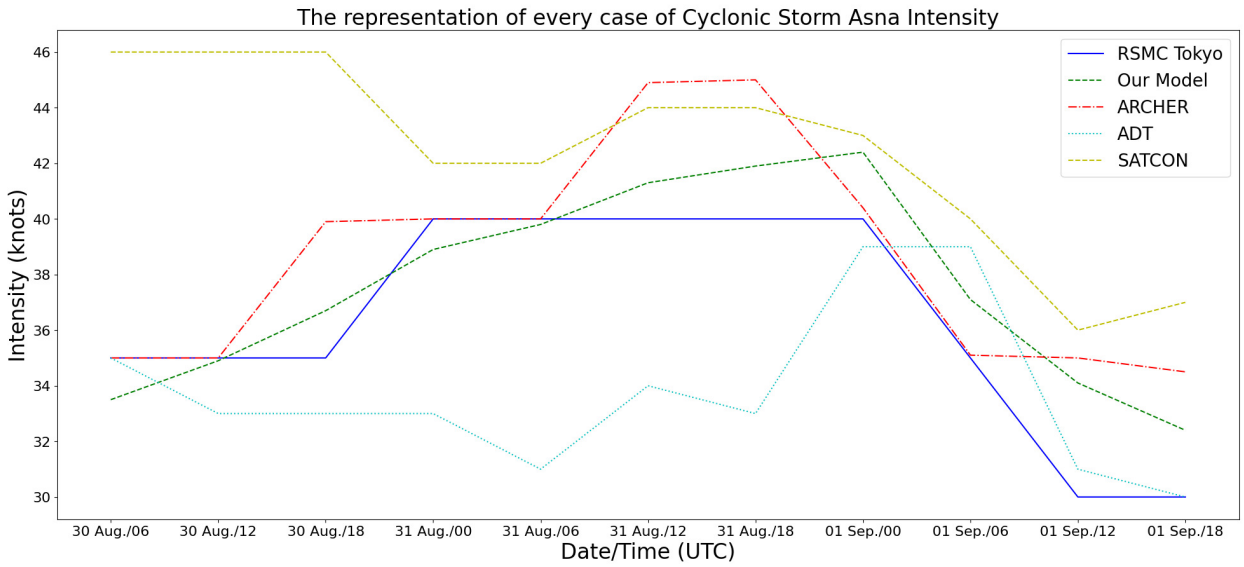

Figure 5.8: Representation of the results of the CS Asna in graphical form

infrastructure, property, and agricultural lands. The cyclone resulted in fatalities in both countries.

It is notable for its unusual formation over land before intensifying into a cyclone and moving into the Arabian Sea.

Figure 5.8 highlights the effectiveness of our proposed method in estimating TC intensity, outperforming traditional techniques such as ARCHER, ADT, and SATCON when benchmarked against Best Track data from the IMD. Table 5.9 provides a detailed quantitative analysis for CS Asna. Our method demonstrates a remarkably low error rate of 4.94%, significantly better than ARCHER (6.51%), ADT (9.19%), and SATCON (17.21%). The RMSE values associated with these results are summarized in Table 5.11. A t-test analysis further substantiates the superior performance of our method over the conventional approaches.

Table 5.9: Numerical result of CS Asna

Date/Time	IMD (knots)	Our Model (knots)	ARCHER (knots)	ADT (knots)	SATCON (knots)	$E_1{}^a$ (knots)	$E_2{}^b$	$E_3{}^c$	$E_4{}^d$
30/06	35	33.5	35.0	35	46	4.28	0.00	0.00	31.4
30/12	35	34.9	35.0	33	46	0.28	0.00	5.71	31.4
30/18	35	36.7	39.9	33	46	4.85	14.0	5.71	31.4
31/00	40	38.9	40.0	33	42	2.75	0.00	17.5	5.00
31/06	40	39.8	40.0	31	42	0.50	0.00	22.5	5.00
31/12	40	41.3	44.9	34	44	3.25	12.2	15.0	10.0
31/18	40	41.9	45.0	33	44	4.75	12.5	17.5	10.0
01/00	40	42.4	40.4	39	43	6.00	1.00	2.50	7.50
01/06	35	37.1	35.1	39	40	6.00	0.28	11.4	14.2
01/12	30	34.1	35.0	31	36	13.6	16.6	3.33	20.0
01/18	30	32.4	34.5	30	37	8.00	15.0	0.00	23.3

5.3.7 CS Dana

Tropical Storm Dana was a cyclonic storm that impacted the states of West Bengal and Odisha in India in late October 2024. It formed in the Bay of Bengal and made landfall near the border of the two states.

It brought heavy rainfall, strong winds, and a storm surge, resulting in significant damage, including loss of life, destruction of homes, and infrastructure disruption. Large-scale evacuations were conducted in vulnerable coastal areas to minimize casualties.

It highlighted the importance of preparedness and disaster relief efforts in coastal regions vulnerable to TCs.

Figure 5.9 demonstrates the better performance of our proposed method for estimating TC intensity when benchmarked against traditional techniques such as ARCHER, ADT, and SATCON, using the Best Track data provided by the IMD as a reference. Table 5.10 quantitatively summarizes the results for the case of CS Dana. Our method achieved an exceptionally low error rate of 2.69%, significantly outperforming ARCHER (13.27%), ADT (8.32%), and SATCON (5.92%). The RMSE values for these methods are reported in Table 5.11. Additionally, a rigorous statistical evaluation using a t-test confirms that the performance of the proposed method is statistically superior to the conventional approaches, further underscoring its accuracy and reliability.

5.4 Conclusion

In this chapter, we design an NN-based model to estimate TC intensity, primarily focusing on the NIO. The model demonstrates superior performance compared to traditional individual

Table 5.10: Numerical result of CS Dana

Date/Time	IMD (knots)	Our Model (knots)	ARCHER (knots)	ADT (knots)	SATCON (knots)	$E_1{}^a$ (knots)	$E_2{}^b$	$E_3{}^c$	$E_4{}^d$
23/06	40	39.6	35.1	35	46	1.00	12.2	12.5	15.0
23/12	45	43.7	39.4	43	48	2.88	12.4	4.44	6.66
23/18	50	48.3	54.2	53	52	3.40	8.40	6.00	4.00
24/00	55	52.4	59.6	63	56	4.72	8.36	14.5	1.81
24/06	55	54.8	64.9	63	57	0.36	18.0	14.5	3.63
24/12	60	57.9	65.0	61	56	3.50	8.33	1.66	6.66
24/18	55	52.1	65.0	61	53	5.27	18.1	10.9	3.63
25/00	50	49.8	60.1	51	47	0.40	20.2	2.00	6.00

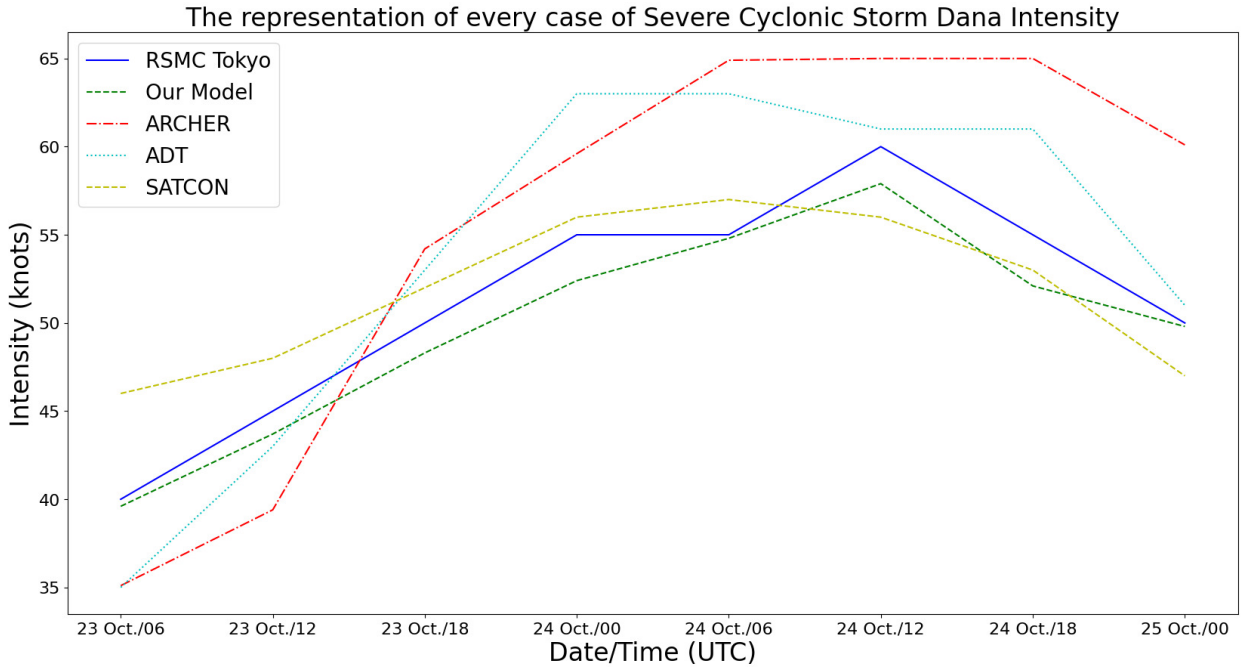

Figure 5.9: Representation of the results of the CS Dana in graphical form

methodologies. We employ three statistical tests to validate its effectiveness: t-test, error percentage, and root mean square error (RMSE), all of which show consistent improvements. Notably, our model achieves a reduction in both error percentage (Table 5.12) and RMSE (Table 5.11), confirming its enhanced predictive accuracy.

A key thing in our model is incorporating a hybrid activation function in the early layers of the neural network. Specifically, the first hidden layer uses the ReLU function to introduce nonlinearity while maintaining computational efficiency, the second layer employs Leaky ReLU to prevent the "dying ReLU" problem by allowing a slight gradient for negative inputs, and the third layer utilizes the tanh function to center activations around zero and enhance learning in later stages. This combination of diverse activation functions allows the model to capture a broader range of nonlinear patterns in the data, which contributes directly to the observed performance gains. The hybrid approach enhances the depth and representational power of the network without overfitting, as evidenced by the improved statistical metrics.

The implications of our model are significant when estimating various characteristics of tropical cyclones, including the radius of maximum winds and rapid intensification events. The core architecture and modeling strategy remain broadly consistent across these applications, requiring only training data updates and minor output configuration adjustments to adapt to new forecasting targets.

Accurate estimation of TC intensity not only aids in a deeper understanding of cyclone behavior but also plays a crucial role in risk mitigation, potentially reducing the socio-economic losses caused by severe tropical storms.

Table 5.11: Detail of root square mean error of both cases

Name of TC	Our Method w.r.t. Best Track (knots)	ARCHER w.r.t. Best Track (knots)	ADT w.r.t Best Track (knots)	SATCON w.r.t. Best Track (knots)
Asani	8.59	10.81	17.44	12.66
Sitrang	2.34	4.22	3.07	3.84
Shaheen	6.21	8.17	10.13	9.54
Tej	3.30	13.30	9.35	15.39
Remal	1.74	5.60	8.53	5.27
Asna	2.00	3.28	4.68	6.88
Dana	1.74	7.23	5.04	3.22

Table 5.12: Detail of error percentage of both cases

Name of TC	Our Method w.r.t. Best Track	ARCHER w.r.t. Best Track	ADT w.r.t Best Track	SATCON w.r.t. Best Track
Asani	15.52	20.14	34.53	25.41
Sitrang	04.82	07.46	06.17	08.35
Shaheen	09.89	13.32	17.24	16.53
Tej	3.47	13.12	9.92	14.98
Remal	3.25	8.62	13.97	9.84
Asna	4.94	6.51	9.19	17.21
Dana	2.69	13.27	8.32	5.92

Chapter 6

Conclusions, social impact and suggestions for future research

This thesis presents significant advancements in estimating TC characteristics using mathematical and machine learning techniques, addressing challenges associated with TC, and improving the accuracy of predictions. The research spans multiple aspects of TCs, including intensity, track, and radius of maximum wind (RMW), primarily focusing on the North Indian Ocean (NIO) region. The following sections provide an in-depth discussion of the findings, implications, and future directions.

Enhancing RMW Estimation

The RMW is a critical parameter in understanding the structure and impact of TCs. The NIO, encompassing the Bay of Bengal and the Arabian Sea, is particularly vulnerable to TCs, yet literature addressing RMW in this region is sparse. This research bridges this gap by developing a method to calculate RMW based on historical observations, specifically analyzing the relationship between the TC center's latitude and the estimated pressure drop (P_d).

Our proposed method performed better than existing methodologies, such as those developed by Willoughby et al. (2006) and Tan and Fang (2018). We employed three statistical methods to validate our approach: error percentage, t-test, and root mean square error (RMSE). The results indicated reduced mean errors and RMSE, highlighting the accuracy of our method. However, a notable limitation is that the P_d value must be less than or equal to 12 hPa, with no specific conditions imposed on the latitude of the TC center within the NIO basin.

Building on this, we incorporated machine learning techniques to enhance RMW estimation further. We achieved even greater accuracy by inputting results from multiple traditional methods into a neural network model. The neural network model significantly reduced error percentage and RMSE, indicating its potential for precise RMW estimation.

Advancing TC Track Estimation

Accurate TC track estimation is crucial for disaster preparedness, resource allocation, and evacuation planning. A TC's track influences its intensity, storm eye, size, and RMW, collectively affecting its potential impact on coastal regions. Our research developed a neural network-based model for TC track estimation in the NIO.

Established practices in machine learning and neural network optimization informed the model's methodology. We employed normalization techniques like StandardScaler to stabilize the learning process, ensuring proportional contributions from all input features. Leaky ReLU activation functions addressed the vanishing gradient problem, while dropout layers helped prevent overfitting. These scientifically grounded principles and evaluation metrics, like error percentage and RMSE, ensured our model's robustness, accuracy, and generalization capability.

Our model's performance was evaluated using three statistical tests: t-test, error percentage analysis, and RMSE. The results showed a reduced error percentage and lower RMSE than traditional methodologies, demonstrating the model's enhanced accuracy. This improvement is crucial for effective disaster management, as precise track predictions allow for better planning and response to TC threats.

Evaluating the Satellite Consensus (SATCON) Algorithm

In addition to developing new models, our research evaluated the performance of the SATCON algorithm, which estimates TC intensity using infrared and microwave sensor-based images. We analyzed 26 typhoons over the West Pacific basin from 2017 to 2021, comparing SATCON estimates to best track parameters provided by Tokyo's Regional Specialized Meteorological Centre (RSMC).

The findings revealed that SATCON performs well for mid-range typhoons and is more effective during the post-monsoon season than during the pre-monsoon season. This season-specific performance underscores the importance of adjusting TC estimation models based on temporal factors. By highlighting SATCON's strengths and limitations, our research contributes to the ongoing refinement of TC intensity estimation techniques.

Improving TC Intensity Estimation

Accurately estimating TC intensity is vital for understanding other TC characteristics and minimizing the damage caused by these powerful storms. Our research developed a neural network-based model with a hybrid activation function that integrates inputs from three traditional methods: the automated rotational center hurricane eye retrieval algorithm, the advanced Dvorak technique, and the satellite Consensus technique.

The model was trained using cases from the NIO and tested on additional cases from

the same region. The results indicated a significant improvement in accuracy, with a root mean square error (RMSE) of 5.71 knots and an error percentage of 10.07%. These metrics were considerably lower than those of existing methods, highlighting the effectiveness of our approach.

The implications of this model are far-reaching. Accurate intensity estimation not only aids in understanding the current state of a TC but also informs predictions of its future behavior, including potential rapid intensification. This information is critical for issuing timely warnings and mitigating the impact of TCs on affected regions.

Social Impact

This research contributes significantly to public safety and disaster preparation by advancing our understanding of tropical cyclones, namely their severity and wind structure. The research improves the accuracy of tropical cyclone forecasting via the development and assessment of advanced methods, including satellite data analysis and machine learning methodologies. Enhanced forecasting enables authorities to provide timely alerts, organize evacuations, and mitigate the danger of injury, fatalities, and property damage.

The study focuses on the radius of maximum wind, an essential element in determining the most dangerous section of a cyclone. This enhancement in estimation methods for the North Indian Ocean and West Pacific basins immediately facilitates more accurate storm impact evaluations. This is particularly advantageous in heavily populated coastal areas, where timely and accurate information may greatly enhance disaster response and recovery efforts.

This study is essential for enhancing climate resilience as both the intensity and frequency of cyclones change because of global warming. It provides enhanced protection for

individuals who are at risk, especially in developing countries, via scientifically informed planning and early warning systems. The study supports humanitarian objectives and sustainable development by mitigating the economic and social impacts of extreme weather events.

Implications and Future Directions

The advancements presented in this thesis have significant implications for meteorology and disaster management. The neural network-based models developed for RMW, track, and intensity estimation provide more accurate and reliable predictions, which are crucial for mitigating the impact of TCs. These models enable better forecasting, resource allocation, and evacuation planning, ultimately enhancing the resilience of vulnerable regions.

Future research will extend these models to other TC basins, incorporating a broader range of TC cases to improve their accuracy and generalization. Additionally, advancements in machine learning techniques, such as integrating more sophisticated neural network architectures and using real-time data, will continue to enhance the performance of TC estimation models.

Another promising direction is the exploration of ensemble learning techniques, where multiple models are combined to improve prediction accuracy. This approach could be particularly beneficial for addressing the inherent uncertainties in TC behavior and providing more robust estimates.

Moreover, integrating additional data sources, such as high-resolution satellite imagery, oceanographic data, and atmospheric conditions, could refine TC characteristic estimations. Leveraging advancements in remote sensing technologies and data assimilation techniques will enable more comprehensive and accurate models.

References

Abadi, M., Barham, P., Chen, J., Chen, Z., Davis, A., Dean, J., Devin, M., Ghemawat, S., Irving, G., Isard, M., et al. (2016). {TensorFlow}: a system for {Large-Scale} machine learning. In *12th USENIX symposium on operating systems design and implementation (OSDI 16)*, pages 265–283.

Agarap, A. F. (2018). Deep learning using rectified linear units (relu). *arXiv preprint arXiv:1803.08375*.

Agency, F. E. M. (2012). Hazus-mh 2.1 hurricane model technical manual.

Ahmed, R., Mohapatra, M., Dwivedi, S., Giri, R. K., and Kant, S. (2022). An overview of the satellite consensus (satcon) algorithm to estimate tropical cyclone intensity over the north indian ocean. *Journal of Earth System Science*, 131(3):169.

Ali, M., Tanusha, U. N., Chand, C. P., Himasri, B., Bourassa, M. A., and Zheng, Y. (2021). Impact of the madden–julian oscillation on north indian ocean cyclone intensity. *Atmosphere*, 12(12):1554.

Atkinson, G. D. and Holliday, C. R. (1977). Tropical cyclone minimum sea level pressure/-maximum sustained wind relationship for the western north pacific. *Monthly Weather Review*, 105(4):421–427.

Atlas, R., Reale, O., Shen, B.-W., Lin, S.-J., Chern, J.-D., Putman, W., Lee, T., Yeh, K.-S., Bosilovich, M., and Radakovich, J. (2005). Hurricane forecasting with the high-resolution nasa finite volume general circulation model. *Geophysical Research Letters*, 32(3).

Bankert, R. and Cossuth, J. (2016). Tropical cyclone intensity estimation via passive microwave data features. In *32nd Conf. on Hurricanes and Tropical Meteorology*.

Bender, M. A. and Ginis, I. (2000). Real-case simulations of hurricane–ocean interaction using a high-resolution coupled model: Effects on hurricane intensity. *Monthly Weather Review*, 128(4):917–946.

Bhaskar Rao, D., Hari Prasad, D., and Srinivas, D. (2009). Impact of horizontal resolution and the advantages of the nested domains approach in the prediction of tropical cyclone intensification and movement. *Journal of Geophysical Research: Atmospheres*, 114(D11).

Braun, S. A. (2002). A cloud-resolving simulation of hurricane bob (1991): Storm structure and eyewall buoyancy. *Monthly weather review*, 130(6):1573–1592.

Braun, S. A. and Tao, W.-K. (2000). Sensitivity of high-resolution simulations of hurricane bob (1991) to planetary boundary layer parameterizations. *Monthly Weather Review*, 128(12):3941–3961.

Breiman, L. (2001). Random forests. *Machine learning*, 45:5–32.

Brueske, K. F. and Velden, C. S. (2003). Satellite-based tropical cyclone intensity estimation using the noaa-klm series advanced microwave sounding unit (amsu). *Monthly Weather Review*, 131(4):687–697.

Camargo, S. J. (2013). Global and regional aspects of tropical cyclone activity in the cmip5 models. *Journal of Climate*, 26(24):9880–9902.

Chand, C. P., Ali, M., Himasri, B., Bourassa, M. A., and Zheng, Y. (2022). Predicting indian ocean cyclone parameters using an artificial intelligence technique. *Atmosphere*, 13(7):1157.

Charney, J. G. and Eliassen, A. (1964). On the growth of the hurricane depression. *Journal of the Atmospheric Sciences*, 21(1):68–75.

Chavas, D. R. and Knaff, J. A. (2022). A simple model for predicting the tropical cyclone radius of maximum wind from outer size. *Weather and Forecasting*, 37(5):563–579.

Chavas, D. R., Lin, N., and Emanuel, K. (2015). A model for the complete radial structure of the tropical cyclone wind field. part i: Comparison with observed structure. *Journal of the Atmospheric Sciences*, 72(9):3647–3662.

Chen, B., Chen, B.-F., and Lin, H.-T. (2018). Rotation-blended cnns on a new open dataset for tropical cyclone image-to-intensity regression. In *Proceedings of the 24th ACM SIGKDD International Conference on Knowledge Discovery & Data Mining*, pages 90–99.

Chen, B.-F., Chen, B., Lin, H.-T., and Elsberry, R. L. (2019). Estimating tropical cyclone intensity by satellite imagery utilizing convolutional neural networks. *Weather and Forecasting*, 34(2):447–465.

Chen, M. and et al. (2020). A deep learning approach to hurricane track forecasting. *Geophysical Research Letters*, 47(15):e2020GL087354.

Chen, R., Zhang, W., and Wang, X. (2020). Machine learning in tropical cyclone forecast modeling: A review. *Atmosphere*, 11(7):676.

Chen, Z. and Yu, X. (2020). A novel tensor network for tropical cyclone intensity estimation. *IEEE Transactions on Geoscience and Remote Sensing*, 59(4):3226–3243.

Chicco, D., Warrens, M. J., and Jurman, G. (2021). The coefficient of determination r-squared is more informative than smape, mae, mape, mse and rmse in regression analysis evaluation. *Peerj computer science*, 7:e623.

Chollet, F. et al. (2015). Keras.

Combinido, J. S., Mendoza, J. R., and Aborot, J. (2018). A convolutional neural network approach for estimating tropical cyclone intensity using satellite-based infrared images. In *2018 24th International conference on pattern recognition (ICPR)*, pages 1474–1480. IEEE.

Crunch, C. (2023). Disasters year in review 2022. *Centre for Research on the Epidemiology of Disasters*.

Davis, C. A. and Emanuel, K. A. (1988). Observational evidence for the influence of surface heat fluxes on rapid maritime cyclogenesis. *Monthly Weather Review*, 116(12):2649–2659.

DeMaria, M., Mainelli, M., Shay, L. K., Knaff, J. A., and Kaplan, J. (2005). Further improvements to the statistical hurricane intensity prediction scheme (ships). *Weather and Forecasting*, 20(4):531–543.

Demuth, J. L., DeMaria, M., Knaff, J. A., and Vonder Haar, T. H. (2004). Evaluation of advanced microwave sounding unit tropical-cyclone intensity and size estimation algorithms. *Journal of Applied Meteorology*, 43(2):282–296.

Division, C. W. (2021a). Cyclonic storm gulab over bay of bengal during 24th – 28th september 2021. *India Meteorological Department*.

Division, C. W. (2021b). Cyclonic storm, "jawad" (02nd – 06th december, 2021): A report. *India Meteorological Department*.

Division, C. W. (2021c). Extremely severe cyclonic storm, "tauktae" (14th – 19th may, 2021): A report. *India Meteorological Department*.

Division, C. W. (2021d). Severe cyclonic storm "shaheen" over northeast arabian sea adjoining kutch (30th september – 4th october 2021). *India Meteorological Department*.

Division, C. W. (2021e). Very severe cyclonic storm, "yaas" over bay of bengal (23rd – 28th may, 2021): A report. *India Meteorological Department*.

Division, C. W. (2022a). Cyclonic storm sitrang over the bob (22nd-25th october, 2022): A report. *India Meteorological Department*.

Division, C. W. (2022b). Severe cyclonic storm, "asani" (07th – 12th may, 2022): A report. *India Meteorological Department*.

Division, C. W. (2022c). Severe cyclonic storm mandous over the bob (6th-10th december, 2022): A report. *India Meteorological Department*.

Division, C. W. (2023a). Extremely severe cyclonic storm "tej"' over the arabian sea (20th-24th october, 2023): A report. *India Meteorological Department*.

Division, C. W. (2023b). Severe cyclonic storm "michaung"' over the bay of bengal (1st-6th december, 2023): A report. *India Meteorological Department*.

Done, J. M., Lackmann, G. M., and Prein, A. F. (2022). The response of tropical cyclone intensity to temperature profile change. *Weather and Climate Dynamics Discussions*, 2022:1–35.

Douris, J. and Kim, G. (2021). The atlas of mortality and economic losses from weather, climate and water extremes (1970-2019).

Dvorak, V. F. (1973). A technique for the analysis and forecasting of tropical cyclone intensities from satellite pictures.

Dvorak, V. F. (1975). Tropical cyclone intensity analysis and forecasting from satellite imagery. *Monthly Weather Review*, 103(5):420–430.

Dvorak, V. F. (1984). *Tropical cyclone intensity analysis using satellite data*, volume 11. US Department of Commerce, National Oceanic and Atmospheric Administration ....

Emanuel, K. (2003). Tropical cyclones. *Annual review of earth and planetary sciences*, 31(1):75–104.

Emanuel, K. (2005). Increasing destructiveness of tropical cyclones over the past 30 years. *Nature*, 436(7051):686–688.

Emanuel, K. (2015). *The representation of cumulus convection in numerical models*. Springer.

Emanuel, K. A. (1986). An air-sea interaction theory for tropical cyclones. part i: Steady-state maintenance. *Journal of Atmospheric Sciences*, 43(6):585–605.

Emanuel, K. A. (1988). The maximum intensity of hurricanes. *J. Atmos. Sci*, 45(7):1143–1155.

Eusebi, R., Vecchi, G., Lai, C.-Y., and Tong, M. (2023). Physics-informed neural networks for hurricane reconstruction and data assimilation.

FEMA, P. (2018). Federal emergency management agency: Washington. *DC, USA*, 1.

Feng, Z., Shi, J., Sun, Y., Zhong, W., Shen, Y., Lv, S., Yao, Y., and Zhao, L. (2023). Impact of global warming on tropical cyclone track and intensity: A numerical investigation. *Remote Sensing*, 15(11):2763.

Fovell, R. G. and Su, H. (2007). Impact of cloud microphysics on hurricane track forecasts. *Geophysical Research Letters*, 34(24).

Frank, W. M. (1983). The cumulus parameterization problem. *Monthly weather review*, 111(9):1859–1871.

Friedman, J. H. (2001). Greedy function approximation: a gradient boosting machine. *Annals of statistics*, pages 1189–1232.

Gao, J., Zhao, H., Klotzbach, P. J., Wang, C., Raga, G. B., and Chen, S. (2020). Possible influence of tropical indian ocean sea surface temperature on the proportion of rapidly intensifying western north pacific tropical cyclones during the extended boreal summer. *Journal of Climate*, 33(21):9129–9143.

Goerss, J. and Hogan, T. (2006). Impact of satellite observations and forecast model improvements on tropical cyclone track forecasts. In *Preprints, 27th Conf. on Hurricanes and Tropical Meteorology, Monterey, CA, Amer. Meteor. Soc. P*, volume 5.

Goerss, J. S. (2009). Impact of satellite observations on the tropical cyclone track forecasts of the navy operational global atmospheric prediction system. *Monthly Weather Review*, 137(1):41–50.

Goodfellow, I., Bengio, Y., and Courville, A. (2016). *Deep learning*. MIT press.

Goyal, S., Mohapatra, M., Kumari, P., Dube, S., and Rajendra, K. (2017). Validation of advanced dvorak technique (adt) over north indian ocean. *Mausam*, 68(4):689–698.

Graham, H. E. (1959). *Meteorological considerations pertinent to standard project hurricane, Atlantic and Gulf coasts of the United States*. US Department of Commerce, Weather Bureau.

Gray, W. M. (1968). Global view of the origin of tropical disturbances and storms. *Monthly Weather Review*, 96(10):669–700.

Gray, W. M. et al. (1975). Tropical cyclone genesis.

Griffin, S. M., Wimmers, A., and Velden, C. S. (2024). Predicting short-term intensity change in tropical cyclones using a convolutional neural network. *Weather and Forecasting*, 39(1):177–202.

Gross, J. M., DeMaria, M., Knaff, J. A., and Sampson, C. R. (2004). A new method for determining tropical cyclone wind forecast probabilities. In *Preprints, 26th Conf. on Hurricanes and Tropical Meteorology, Miami, FL, Amer. Meteor. Soc. A*, volume 11.

Guha-Sapir, D., Below, R., and Hoyois, P. (2019). Em-dat. international disaster database (brussels—belgium: Université catholique de louvain). Accesed on January 30, 2023.

Gupta, H., Sil, S., Gangopadhyay, A., and Gawarkiewicz, G. (2024). Observed surface and subsurface marine heat waves in the bay of bengal from in-situ and high-resolution satellite data. *Climate Dynamics*, 62(1):203–221.

Gupta, S., Jain, I., Johari, P., and Lal, M. (2019). Impact of climate change on tropical cyclones frequency and intensity on indian coasts. In *Proceedings of International Conference on Remote Sensing for Disaster Management: Issues and Challenges in Disaster Management*, pages 359–365. Springer.

Harr, P. A. and Elsberry, R. L. (1995). Large-scale circulation variability over the tropical western north pacific. part i: Spatial patterns and tropical cyclone characteristics. *Monthly Weather Review*, 123(5):1225–1246.

Harris, C. R., Millman, K. J., Van Der Walt, S. J., Gommers, R., Virtanen, P., Cournapeau, D., Wieser, E., Taylor, J., Berg, S., Smith, N. J., et al. (2020). Array programming with numpy. *Nature*, 585(7825):357–362.

Hastie, T., Tibshirani, R., Friedman, J. H., and Friedman, J. H. (2009). *The elements of statistical learning: data mining, inference, and prediction*, volume 2. Springer.

Heming, J. and Goerss, J. (2010). Track and structure forecasts of tropical cyclones. In *Global Perspectives on Tropical Cyclones: From Science to Mitigation*, pages 287–323. World Scientific.

Hennon, C. C., Knapp, K. R., Schreck III, C. J., Stevens, S. E., Kossin, J. P., Thorne, P. W., Hennon, P. A., Kruk, M. C., Rennie, J., Gadéa, J.-M., et al. (2015). Cyclone center: Can citizen scientists improve tropical cyclone intensity records? *Bulletin of the American Meteorological Society*, 96(4):591–607.

Herndon, D. and Velden, C. (2018). An update on the cimss satellite consensus (satcon) tropical cyclone intensity algorithm. 33rd conf. on hurricanes and tropical meteorology, ponte verdi, fl, amer. meteor. soc., 284.

Herndon, D., Velden, C., Hawkins, J., Olander, T., and Wimmers, A. (2010). The cimss satellite consensus (satcon) tropical cyclone intensity algorithm. In *29th Conference on Hurricanes and Tropical Meteorology D*, volume 4.

Hertz, J., Krogh, A., Palmer, R. G., and Horner, H. (1991). Introduction to the theory of neural computation.

Higa, M., Tanahara, S., Adachi, Y., Ishiki, N., Nakama, S., Yamada, H., Ito, K., Kitamoto, A., and Miyata, R. (2021). Domain knowledge integration into deep learning for typhoon intensity classification. *Scientific reports*, 11(1):12972.

Hill, K. A. and Lackmann, G. M. (2009). Influence of environmental humidity on tropical cyclone size. *Monthly Weather Review*, 137(10):3294–3315.

Holland, G. (2015). Global guide to tropical cyclone forecasting. bureau of meteorology research center, melbourne, australia. Accesed on 22 Sept. 2023.

Holland, G. J. (1997). The maximum potential intensity of tropical cyclones. *Journal of the atmospheric sciences*, 54(21):2519–2541.

Hsu, S. and Yan, Z. (1998). A note on the radius of maximum wind for hurricanes. *Journal of coastal research*, 14(2).

Hudozhnik, Y. and Windisch, A. (2023). Multivariate forecasting of tropical cyclones using combined neural networks. In *EGU General Assembly Conference Abstracts*, pages EGU–14848.

IMD (2021). *Standard Operational Procedure for Cyclone Warning in India*. INDIA METEOROLOGICAL DEPARTMENT.

India Meteorological Department (IMD) (2023). Cyclone e-Atlas for the North Indian Ocean: Best Track Data (1891–2023). Regional Specialized Meteorological Centre (RSMC), New Delhi.

Ioffe, S. and Szegedy, C. (2015). Batch normalization: Accelerating deep network training by reducing internal covariate shift. In *International conference on machine learning*, pages 448–456. pmlr.

Islam, T. and Peterson, R. E. (2008). Tropical cyclone wind characteristics for the bangladesh coast using monte carlo simulation. *Journal of Applied Sciences*, 8(9):1249–1255.

Jangir, B., Swain, D., and Ghose, S. (2021). Influence of eddies and tropical cyclone heat potential on intensity changes of tropical cyclones in the north indian ocean. *Advances in Space Research*, 68(2):773–786.

Jeffries, R. A. and Miller, R. J. (1993). Tropical cyclone forecasters reference guide, 3. tropical cyclone formation. In *Tech. Rep. No. NRL/PU/7515–93-0007*. NRL Monterey, CA.

Jiang, H., Tao, C., and Pei, Y. (2019). Estimation of tropical cyclone intensity in the north atlantic and northeastern pacific basins using trmm satellite passive microwave observations. *Journal of applied meteorology and climatology*, 58(2):185–197.

Jiang, W., Hu, G., Wu, T., Liu, L., Kim, B., Xiao, Y., and Duan, Z. (2023). Dmanet_kf: tropical cyclone intensity estimation based on deep learning and kalman filter from multi-spectral infrared images. *IEEE Journal of Selected Topics in Applied Earth Observations and Remote Sensing*.

Jiang, Z., Hua, F., and Qu, P. (2008). A new tropical cyclone parameter adjustment scheme. *Adv. Mar. Sci*, 1:1–7.

Kato, F. (2005). Study on risk assessment of storm surge flood. *Technical note of National Institute for land and infrastructure management*, 275:10.

Khouakhi, A., Villarini, G., and Vecchi, G. A. (2017). Contribution of tropical cyclones to rainfall at the global scale. *Journal of Climate*, 30(1):359–372.

Kidder, S. Q., Goldberg, M. D., Zehr, R. M., DeMaria, M., Purdom, J. F., Velden, C. S., Grody, N. C., and Kusselson, S. J. (2000). Satellite analysis of tropical cyclones using the advanced microwave sounding unit (amsu). *Bulletin of the American Meteorological Society*, 81(6):1241–1260.

Kingma, D. P. and Ba, J. (2014). Adam: A method for stochastic optimization. *arXiv preprint arXiv:1412.6980*.

Knaff, J. A., Brown, D. P., Courtney, J., Gallina, G. M., and Beven, J. L. (2010). An evaluation of dvorak technique–based tropical cyclone intensity estimates. *Weather and Forecasting*, 25(5):1362–1379.

Knaff, J. A., DeMaria, M., Sampson, C. R., and Gross, J. M. (2003). Statistical, 5-day tropical cyclone intensity forecasts derived from climatology and persistence. *Weather and Forecasting*, 18(1):80 – 92.

Knaff, J. A., Sampson, C. R., DeMaria, M., Marchok, T. P., Gross, J. M., and McAdie, C. J. (2007). Statistical tropical cyclone wind radii prediction using climatology and persistence. *Weather and Forecasting*, 22(4):781–791.

Knapp, K. R., Kruk, M. C., Levinson, D. H., Diamond, H. J., and Neumann, C. J. (2010). The international best track archive for climate stewardship (ibtracs) unifying tropical cyclone data. *Bulletin of the American Meteorological Society*, 91(3):363–376.

Knutson, T. R., Delworth, T., Dixon, K., Held, I., Lu, J., Ramaswamy, V., Schwarzkopf, M., Stenchikov, G., and Stouffer, R. (2006). Assessment of twentieth-century regional surface temperature trends using the gfdl cm2 coupled models. *Journal of Climate*, 19(9):1624–1651.

Kossin, J. P., Emanuel, K. A., and Vecchi, G. A. (2014). The poleward migration of the location of tropical cyclone maximum intensity. *Nature*, 509(7500):349–352.

Kossin, J. P., Knaff, J. A., Berger, H. I., Herndon, D. C., Cram, T. A., Velden, C. S., Murnane, R. J., and Hawkins, J. D. (2007). Estimating hurricane wind structure in the absence of aircraft reconnaissance. *Weather and Forecasting*, 22(1):89–101.

Kossin, J. P. and Sitkowski, M. (2009). An objective model for identifying secondary eyewall formation in hurricanes. *Monthly Weather Review*, 137(3):876–892.

Kotal, S., Roy Bhowmik, S., Kundu, P., and Das Kumar, A. (2008). A statistical cyclone intensity prediction (scip) model for the bay of bengal. *Journal of earth system science*, 117:157–168.

Kou, Y.-H. and Bresch, J. (1997). Summary of a mini workshop on cumulus parameterization for mesoscale models. *Bulletin of the American Meteorological Society*, 78(3).

Krishnamurti, T. N., Pattnaik, S., Stefanova, L., Kumar, T. V., Mackey, B. P., O'shay, A., and Pasch, R. J. (2005). The hurricane intensity issue. *Monthly weather review*, 133(7):1886–1912.

Kumar, A., Done, J., Dudhia, J., and Niyogi, D. (2011). Simulations of cyclone sidr in the bay of bengal with a high-resolution model: sensitivity to large-scale boundary forcing. *Meteorology and Atmospheric Physics*, 114:123–137.

Kumar, S., Biswas, K., and Pandey, A. K. (2021). Track prediction of tropical cyclones using long short-term memory network. In *2021 IEEE 11th Annual Computing and Communication Workshop and Conference (CCWC)*, pages 0251–0257. IEEE.

Lajoie, F. and Walsh, K. (2008). A technique to determine the radius of maximum wind of a tropical cyclone. *Weather and forecasting*, 23(5):1007–1015.

Le Marshall, J. (1998). Cloud and water vapour motion vectors in tropical cyclone track forecasting—a review. *Meteorology and Atmospheric Physics*, 65(3):141–151.

Lee, J., Im, J., Cha, D.-H., Park, H., and Sim, S. (2019). Tropical cyclone intensity estimation using multi-dimensional convolutional neural networks from geostationary satellite data. *Remote Sensing*, 12(1):108.

Li, R. (2007). *Prediction of typhoon extreme wind speeds based on improved typhoon key parameters*. PhD thesis, Harbin Institute of Technology Harbin, China.

Li, X. and Pu, Z. (2008). Sensitivity of numerical simulation of early rapid intensification of hurricane emily (2005) to cloud microphysical and planetary boundary layer parameterizations. *Monthly Weather Review*, 136(12):4819–4838.

Lin, W. and Fang, W. (2013). Regional characteristics of holland b parameter in typhoon wind field model for northwest pacific. *Tropical Geography*, 33(2):124–132.

Lu, X., Wong, W.-k., Yu, H., and Yang, X. (2022). Tropical cyclone size identification over the western north pacific using support vector machine and general regression neural network. *Journal of the Meteorological Society of Japan. Ser. II*, 100(6):927–941.

Mautner, D. A., Guard, C. P., and 96630, N. O. C. C. W. C. F. S. F. (1992). 1992 annual tropical cyclone report.

Ming-Jen, Y. and Lin, C. (2005). A modeling study of typhoon toraji (2001): Physical parameterization sensitivity and topographic effect. *TAO: Terrestrial, Atmospheric and Oceanic Sciences*, 16(1):177.

Mohanty, U. and Gupta, A. (1997). Deterministic methods for prediction of tropical cyclone tracks. *Mausam*, 48(2):257–272.

Mohanty, U., Mandal, M., and Raman, S. (2004). Simulation of orissa super cyclone (1999) using psu/ncar mesoscale model. *Natural Hazards*, 31:373–390.

Mohanty, U., Osuri, K. K., Routray, A., Mohapatra, M., and Pattanayak, S. (2010). Simulation of bay of bengal tropical cyclones with wrf model: Impact of initial and boundary conditions. *Marine Geodesy*, 33(4):294–314.

Mohapatra, M., Bandyopadhyay, B., and Tyagi, A. (2014). Status and plans for operational tropical cyclone forecasting and warning systems in the north indian ocean region. In *Monitoring and prediction of tropical cyclones in the Indian Ocean and climate change*, pages 149–168. Springer.

Möller, J. D. and Montgomery, M. T. (1999). Vortex rossby waves and hurricane intensification in a barotropic model. *Journal of the atmospheric sciences*, 56(11):1674–1687.

Möller, J. D. and Montgomery, M. T. (2000). Tropical cyclone evolution via potential vorticity anomalies in a three-dimensional balance model. *Journal of the atmospheric sciences*, 57(20):3366–3387.

Montgomery, M. T. and Enagonio, J. (1998). Tropical cyclogenesis via convectively forced vortex rossby waves in a three-dimensional quasigeostrophic model. *Journal of the atmospheric sciences*, 55(20):3176–3207.

Moon, Y. and Nolan, D. S. (2010). The dynamic response of the hurricane wind field to spiral rainband heating. *Journal of the atmospheric sciences*, 67(6):1779–1805.

Mukherjee, P. and Ramakrishnan, B. (2023). Tropical cyclone vayu under climate change scenario rcp 8.5. In *EGU General Assembly Conference Abstracts*, pages EGU–10.

Nair, V. and Hinton, G. E. (2010). Rectified linear units improve restricted boltzmann machines. In *Proceedings of the 27th international conference on machine learning (ICML-10)*, pages 807–814.

Neumann, C. J. (1972). An alternate to the hurran (hurricane analog) tropical cyclone forecast system.

Nti, I. K., Nyarko-Boateng, O., Aning, J., et al. (2021). Performance of machine learning algorithms with different k values in k-fold crossvalidation. *International Journal of Information Technology and Computer Science*, 13(6):61–71.

Olander, T., Wimmers, A., Velden, C., and Kossin, J. P. (2021). Investigation of machine learning using satellite-based advanced dvorak technique analysis parameters to estimate tropical cyclone intensity. *Weather and Forecasting*, 36(6):2161–2186.

Olander, T. L. and Velden, C. S. (2007). The advanced dvorak technique: Continued development of an objective scheme to estimate tropical cyclone intensity using geostationary infrared satellite imagery. *Weather and Forecasting*, 22(2):287–298.

Olander, T. L. and Velden, C. S. (2019). The advanced dvorak technique (adt) for estimating tropical cyclone intensity: Update and new capabilities. *Weather and Forecasting*, 34(4):905–922.

Osuri, K. K., Mohanty, U., Routray, A., Mohapatra, M., and Niyogi, D. (2013). Real-time track prediction of tropical cyclones over the north indian ocean using the arw model. *Journal of Applied Meteorology and Climatology*, 52(11):2476–2492.

Pattanaik, D. and Rama Rao, Y. (2009). Track prediction of very severe cyclone 'nargis' using high resolution weather research forecasting (wrf) model. *Journal of earth system science*, 118:309–329.

Pattanayak, S. and Mohanty, U. (2010). Simulation of track and intensity of gonu and sidr with wrf-nmm modeling system. *Indian ocean tropical cyclones and climate change*, pages 83–89.

Pattanayak, S., Mohanty, U., and Gopalakrishnan, S. (2012). Simulation of very severe cyclone mala over bay of bengal with hwrf modeling system. *Natural Hazards*, 63:1413–1437.

Pattanayak, S. and Mohanty, U. C. (2008). A comparative study on performance of mm5 and wrf models in simulation of tropical cyclones over indian seas. *Current Science*, pages 923–936.

Paul, B. K. (2010). Human injuries caused by bangladesh's cyclone sidr: an empirical study. *Natural hazards*, 54:483–495.

Pedregosa, F., Varoquaux, G., Gramfort, A., Michel, V., Thirion, B., Grisel, O., Blondel, M., Prettenhofer, P., Weiss, R., Dubourg, V., et al. (2011). Scikit-learn: Machine learning in python. *the Journal of machine Learning research*, 12:2825–2830.

Pérez-Alarcón, A., Fernández-Alvarez, J. C., and Coll-Hidalgo, P. (2023). Global increase of the intensity of tropical cyclones under global warming based on their maximum potential intensity and cmip6 models. *Environmental Processes*, 10(2):36.

Piñeros, M. F., Ritchie, E. A., and Tyo, J. S. (2011). Estimating tropical cyclone intensity from infrared image data. *Weather and forecasting*, 26(5):690–698.

Pohjankukka, J., Pahikkala, T., Nevalainen, P., and Heikkonen, J. (2017). Estimating the prediction performance of spatial models via spatial k-fold cross validation. *International Journal of Geographical Information Science*, 31(10):2001–2019.

Powell, M., Soukup, G., Cocke, S., Gulati, S., Morisseau-Leroy, N., Hamid, S., Dorst, N., and Axe, L. (2005). State of florida hurricane loss projection model: Atmospheric science component. *Journal of wind engineering and industrial aerodynamics*, 93(8):651–674.

Powell, M. D. and Black, P. G. (1990). The relationship of hurricane reconnaissance flight-level wind measurements to winds measured by noaa's oceanic platforms. *Journal of Wind Engineering and Industrial Aerodynamics*, 36:381–392.

Pradhan, R., Aygun, R. S., Maskey, M., Ramachandran, R., and Cecil, D. J. (2017). Tropical cyclone intensity estimation using a deep convolutional neural network. *IEEE Transactions on Image Processing*, 27(2):692–702.

Prasad, K. and Rama Rao, Y. (2003). Cyclone track prediction by a quasi-lagrangian limited area model. *Meteorology and Atmospheric Physics*, 83(3):173–185.

Prater, B. and Evans, J. (2002). Sensitivity of modeled tropical cyclone track and structure of hurricane irene (1999) to the convective parameterization scheme. *Meteorology and Atmospheric Physics*, 80(1):103–115.

Quiring, S., Schumacher, A., Labosier, C., and Zhu, L. (2011). Variations in mean annual tropical cyclone size in the atlantic. *Journal of Geophysical Research: Atmospheres*, 116(D9).

Rahaman, H., Srinivasu, U., Panickal, S., Durgadoo, J. V., Griffies, S., Ravichandran, M., Bozec, A., Cherchi, A., Voldoire, A., Sidorenko, D., et al. (2020). An assessment of the indian ocean mean state and seasonal cycle in a suite of interannual core-ii simulations. *Ocean Modelling*, 145:101503.

Rajasekhar, M., Kishtawal, C., Prasad, M., Rao, V. S., and Rajeevan, M. (2014). Extended range tropical cyclone predictions for east coast of india. In *Monitoring and prediction of tropical cyclones in the Indian Ocean and climate change*, pages 137–148. Springer.

Rajeevan, M., Srinivasan, J., Niranjan Kumar, K., Gnanaseelan, C., and Ali, M. (2013). On the epochal variation of intensity of tropical cyclones in the arabian sea. *Atmospheric Science Letters*, 14(4):249–255.

Raju, P. V., Potty, J., and Mohanty, U. (2012). Prediction of severe tropical cyclones over the bay of bengal during 2007–2010 using high-resolution mesoscale model. *Natural Hazards*, 63:1361–1374.

Rao, D. B. and Prasad, D. H. (2007). Sensitivity of tropical cyclone intensification to boundary layer and convective processes. *Natural Hazards*, 41:429–445.

Rathore, S., Goyal, R., Jangir, B., Ummenhofer, C. C., Feng, M., and Mishra, M. (2022). Interactions between a marine heatwave and tropical cyclone amphan in the bay of bengal in 2020. *Frontiers in Climate*, 4:861477.

Raynaud, L., Faure, G., Puig, M., Dauvilliers, C., Trosino, J.-N., and Béjean, P. (2024). A convolutional neural network for tropical cyclone wind structure identification in kilometer-scale forecasts. *Artificial Intelligence for the Earth Systems*, 3(2):e230059.

Reale, O., Lau, W., Susskind, J., Brin, E., Liu, E., Riishojgaard, L., Fuentes, M., and Rosenberg, R. (2009). Airs impact on the analysis and forecast track of tropical cyclone nargis in a global data assimilation and forecasting system. *Geophysical Research Letters*, 36(6).

Rogers, R., Aberson, S., Black, M., Black, P., Cione, J., Dodge, P., Dunion, J., Gamache, J., Kaplan, J., Powell, M., et al. (2006). The intensity forecasting experiment: A noaa multiyear field program for improving tropical cyclone intensity forecasts. *Bulletin of the American Meteorological Society*, 87(11):1523–1538.

Rozoff, C. M., Nolan, D. S., Kossin, J. P., Zhang, F., and Fang, J. (2012). The roles of an expanding wind field and inertial stability in tropical cyclone secondary eyewall formation. *Journal of the Atmospheric Sciences*, 69(9):2621–2643.

Sampson, C. R. and Schrader, A. J. (2000). The automated tropical cyclone forecasting system (version 3.2). *Bulletin of the American Meteorological Society*, 81(6):1231–1240.

Schwerdt, R. W., Ho, F. P., and Watkins, R. R. (1979). Meteorological criteria for standard project hurricane and probable maximum hurricane windfields, gulf and east coasts of the united states.

Sen Gupta, A., Thomsen, M., Benthuysen, J. A., Hobday, A. J., Oliver, E., Alexander, L. V., Burrows, M. T., Donat, M. G., Feng, M., Holbrook, N. J., et al. (2020). Drivers and impacts of the most extreme marine heatwave events. *Scientific reports*, 10(1):19359.

Shaji, C., Kar, S., and Vishal, T. (2014). Storm surge studies in the north indian ocean: A review.

Shen, B.-W., Tao, W.-K., Lau, W., and Atlas, R. (2010). Predicting tropical cyclogenesis with a global mesoscale model: Hierarchical multiscale interactions during the formation of tropical cyclone nargis (2008). *Journal of Geophysical Research: Atmospheres*, 115(D14).

Shenoi, S., Shankar, D., and Shetye, S. (2002). Differences in heat budgets of the near-surface arabian sea and bay of bengal: Implications for the summer monsoon. *Journal of Geophysical Research: Oceans*, 107(C6):5–1.

Sikka, D. and Suryanarayana, R. (1972). Forecasting the movement of tropical storms/depressions in the indian region by a computer oriented technique using, climatology and persistence. *MAUSAM*, 23(1):35–40.

Singh, K. and Panda, J. (2022). The variability of landfalling cyclonic disturbances over north indian ocean and consequent rainfall contribution to india in warming climate scenario. In *EGU General Assembly Conference Abstracts*, pages EGU22–2727.

Srinivas, C., Venkatesan, R., Bhaskar Rao, D., and Hari Prasad, D. (2007). Numerical simulation of andhra severe cyclone (2003): Model sensitivity to the boundary layer and convection parameterization. *Atmospheric and Oceanic: Mesoscale Processes*, pages 1465–1487.

Srivastava, N., Hinton, G., Krizhevsky, A., Sutskever, I., and Salakhutdinov, R. (2014). Dropout: a simple way to prevent neural networks from overfitting. *The journal of machine learning research*, 15(1):1929–1958.

Steptoe, H. and Xirouchaki, T. (2022). Deep learning for tropical cyclone nowcasting: Experiments with generative adversarial and recurrent neural networks. In *EGU General Assembly Conference Abstracts*, pages EGU22–1650.

Stovern, D. and Ritchie, E. (2012). The importance of atmospheric temperature on the size and structure of tropical cyclones. In *Proceedings of 30th AMS Conference on Hurricanes and Tropical Meteorology*, pages 15–20.

Tan, C. and Fang, W. (2018). Mapping the wind hazard of global tropical cyclones with parametric wind field models by considering the effects of local factors. *International Journal of Disaster Risk Science*, 9:86–99.

Tian, W., Lai, L., Niu, X., Zhou, X., Zhang, Y., and Lim Kam Sian, K. T. C. (2023a). Estimating tropical cyclone intensity using dynamic balance convolutional neural network from satellite imagery. *Journal of Applied Remote Sensing*, 17(2):024513–024513.

Tian, W., Lai, L., Niu, X., Zhou, X., Zhang, Y., and Lim Kam Sian, K. T. C. (2023b). Estimating tropical cyclone intensity using dynamic balance convolutional neural network from satellite imagery. *Journal of Applied Remote Sensing*, 17(2):024513–024513.

Tokyo, R. (2017). Annual report on activities of the rsmc tokyo- typhoon center 2017. *RSMC Tokyo*.

Tokyo, R. (2018). Annual report on activities of the rsmc tokyo- typhoon center 2018. *RSMC Tokyo*.

Tokyo, R. (2019). Annual report on activities of the rsmc tokyo- typhoon center 2019. *RSMC Tokyo*.

Tokyo, R. (2020). Annual report on activities of the rsmc tokyo- typhoon center 2020. *RSMC Tokyo*.

Tokyo, R. (2021). Annual report on activities of the rsmc tokyo- typhoon center 2021. *RSMC Tokyo*.

Trivedi, D., Mukhopadhyay, P., and Vaidya, S. (2006). Impact of physical parameterization schemes on the numerical simulation of orissa super cyclone (1999). *Mausam*, 57(1):97–110.

Trivedi, D., Sanjay, J., and Singh, S. (2002). Numerical simulation of a super cyclonic storm, orissa 1999: impact of initial conditions. *Meteorological Applications*, 9(3):367–376.

Varalakshmi, P., Vasumathi, N., and Venkatesan, R. (2023). Tropical cyclone intensity prediction based on hybrid learning techniques. *Journal of Earth System Science*, 132(1):28.

Velden, C., Harper, B., Wells, F., Beven, J. L., Zehr, R., Olander, T., Mayfield, M., Guard, C., Lander, M., Edson, R., et al. (2006). The dvorak tropical cyclone intensity estimation technique: A satellite-based method that has endured for over 30 years. *Bulletin of the American Meteorological Society*, 87(9):1195–1210.

Velden, C. and Herndon, D. (2014). Update on the satellite consensus (satcon) algorithm for estimating tc intensity; 31st conf. on hurricanes and tropical meteorology, san diego, ca. *Amer. Meteor. Soc*, 30.

Velden, C. and Herndon, D. (2019). An update on the cimss satellite consensus (satcon) tropical cyclone intensity algorithm. In *2019 Joint Satellite Conference*. AMS.

Velden, C. S. and Herndon, D. (2020). A consensus approach for estimating tropical cyclone intensity from meteorological satellites: Satcon. *Weather and Forecasting*, 35(4):1645–1662.

Velden, C. S., Olander, T. L., and Zehr, R. M. (1998). Development of an objective scheme to estimate tropical cyclone intensity from digital geostationary satellite infrared imagery. *Weather and Forecasting*, 13(1):172–186.

Vickery, P., Skerlj, P., and Twisdale, L. (2000a). Simulation of hurricane risk in the us using empirical track model. *Journal of structural engineering*, 126(10):1222–1237.

Vickery, P. J., Skerlj, P., Steckley, A., and Twisdale, L. (2000b). Hurricane wind field model for use in hurricane simulations. *Journal of Structural Engineering*, 126(10):1203–1221.

Vickery, P. J. and Wadhera, D. (2008). Statistical models of holland pressure profile parameter and radius to maximum winds of hurricanes from flight-level pressure and h* wind data. *Journal of Applied Meteorology and climatology*, 47(10):2497–2517.

Virtanen, P., Gommers, R., Oliphant, T. E., Haberland, M., Reddy, T., Cournapeau, D., Burovski, E., Peterson, P., Weckesser, W., Bright, J., van der Walt, S. J., Brett, M., Wilson, J., Millman, K. J., Mayorov, N., Nelson, A. R. J., Jones, E., Kern, R., Larson, E., Carey, C. J., Polat, İ., Feng, Y., Moore, E. W., VanderPlas, J., Laxalde, D., Perktold, J., Cimrman, R., Henriksen, I., Quintero, E. A., Harris, C. R., Archibald, A. M., Ribeiro, A. H., Pedregosa, F., van Mulbregt, P., and SciPy 1.0 Contributors (2020). SciPy 1.0: Fundamental Algorithms for Scientific Computing in Python. *Nature Methods*, 17:261–272.

Vissa, N. K., Satyanarayana, A., and Prasad Kumar, B. (2013). Intensity of tropical cyclones during pre-and post-monsoon seasons in relation to accumulated tropical cyclone heat potential over bay of bengal. *Natural Hazards*, 68:351–371.

Vosper, E., Watson, P., Harris, L., McRae, A., Santos-Rodriguez, R., Aitchison, L., and Mitchell, D. (2023). Deep learning for downscaling tropical cyclone rainfall to hazard-relevant spatial scales. *Journal of Geophysical Research: Atmospheres*, 128(10):e2022JD038163.

Wallemacq, P., U. and CRED (2018). Economic losses, poverty and disasters: 1998-2017.

Wang, C. and Li, X. (2023). A deep learning model for estimating tropical cyclone wind radius from geostationary satellite infrared imagery. *Monthly Weather Review*, 151(2):403–417.

Wehner, M. (2021). Simulated changes in tropical cyclone size, accumulated cyclone energy and power dissipation index in a warmer climate. In *Oceans*, volume 2, pages 688–699. MDPI.

Weir, R. C. (1982). *Predicting the acceleration of northward-moving tropical cyclones using upper-tropospheric winds*. US Naval Oceanography Command Center, Joint Typhoon Warning Center.

Willoughby, H. and Rahn, M. (2004). Parametric representation of the primary hurricane vortex. part i: Observations and evaluation of the holland (1980) model. *Monthly Weather Review*, 132(12):3033–3048.

Willoughby, H. E., Darling, R., and Rahn, M. (2006). Parametric representation of the primary hurricane vortex. part ii: A new family of sectionally continuous profiles. *Monthly weather review*, 134(4):1102–1120.

Willoughby, H. E., Jin, H.-L., Lord, S. J., and Piotrowicz, J. M. (1984). Hurricane structure and evolution as simulated by an axisymmetric, nonhydrostatic numerical model. *Journal of the atmospheric sciences*, 41(7):1169–1186.

Wimmers, A. J. and Velden, C. S. (2010). Objectively determining the rotational center of tropical cyclones in passive microwave satellite imagery. *Journal of Applied Meteorology and Climatology*, 49(9):2013–2034.

Wu, C.-C., Cheng, H.-J., Wang, Y., and Chou, K.-H. (2009). A numerical investigation of the eyewall evolution in a landfalling typhoon. *Monthly Weather Review*, 137(1):21–40.

Xu, J., Wang, X., Wang, H., Zhao, C., Wang, H., and Zhu, J. (2023). Tropical cyclone size estimation based on deep learning using infrared and microwave satellite data. *Frontiers in Marine Science*, 9:1077901.

Xu, J. and Wang, Y. (2010a). Sensitivity of the simulated tropical cyclone inner-core size to the initial vortex size. *Monthly Weather Review*, 138(11):4135–4157.

Xu, J. and Wang, Y. (2010b). Sensitivity of tropical cyclone inner-core size and intensity to the radial distribution of surface entropy flux. *Journal of the Atmospheric Sciences*, 67(6):1831–1852.

Yadav, M. and Das, L. (2022). Identification of storm eye from satellite image data using fuzzy logic with machine learning. *arXiv preprint arXiv:2206.14050*.

Yadav, M. and Das, L. (2023a). Characteristics of cyclonic disturbance on india and their impact analysis on human and economic losses.

Yadav, M. and Das, L. (2023b). Detecting tropical cyclone from the basic overview of life cycle of extremely severe cyclonic storm, tauktae. *Revista de Climatología*, 23:149–156.

Yadav, M. and Das, L. (2024a). Analyze the satcon algorithm's capability to estimate tropical storm intensity across the west pacific basin. *Journal of Earth System Science*.

Yadav, M. and Das, L. (2024b). Estimation of tropical cyclone intensity using neural network approach.

Yadav, M. and Das, L. (2024c). Formulation and evaluation of the radius of maximum wind of the tropical cyclones over the north indian ocean basin. *Theoretical and Applied Climatology*, pages 1–14.

Zhang, C.-J., Wang, X.-J., Ma, L.-M., and Lu, X.-Q. (2021). Tropical cyclone intensity classification and estimation using infrared satellite images with deep learning. *IEEE Journal of Selected Topics in Applied Earth Observations and Remote Sensing*, 14:2070–2086.

Zhang, D.-L., Kain, J. S., Fritsch, J. M., and Gao, K. (1994). Comments on" parameterization of convective precipitation in mesoscale numerical models: A critical review". *Monthly weather review*, 122(9):2222–2231.

Zhang, J. and et al. (2019). Deep learning for tropical cyclone intensity estimation from microwave satellite observations. *Geophysical Research Letters*, 46(7):3945–3952.

Zhou, T., Tan, Y., Chu, A., and Zhang, C. (2018). Integrated model for astronomic tide and storm surge induced by typhoon for ningbo coast. In *ISOPE International Ocean and Polar Engineering Conference*, pages ISOPE–I. ISOPE.

Zhou, Z., Zhao, Y., Qing, Y., Jiang, W., Wu, Y., and Chen, W. (2023). A physics-guided nn-based approach for tropical cyclone intensity estimation. In *Proceedings of the 2023 SIAM International Conference on Data Mining (SDM)*, pages 388–396. SIAM.